



**University of
Nottingham**
UK | CHINA | MALAYSIA

**Development of a topical therapeutic
strategy using corneal derived mesenchymal
stromal cells for the treatment of ocular
surface disorders**

Lydia Beeken, MRes

School of Medicine

Thesis submitted to the University of Nottingham for
the degree of Doctor of Philosophy

January 2023

Abstract

Ocular surface inflammatory disorders can lead to serious complications, including vision loss. Current treatments, including eye drops and steroids, are not always effective and can have negative side effects. Mesenchymal stromal cells (MSCs) have shown potential as a regenerative medicine strategy due to their ability to suppress inflammation and promote wound healing. While bone marrow derived MSCs (BM-MSCs) are considered the "gold standard" for MSC therapies, they have limited availability and require invasive harvesting. Alternatively, MSCs from the corneal limbus (CMSCs) can be obtained from corneal transplant surgery waste tissue or eye banks. However, these cells lack necessary characterisation data for clinical translation. This research aimed to extensively characterise CMSCs and assess methods for topical administration of the cells for ocular surface disorders, through functionalisation of the contact lens material poly(HEMA-co-EGDMA).

Changes in CMSCs over passages were assessed to determine the effects of cell culture over time. Flow cytometry with the BD Human Cell Surface Lyoplate was used to assess donor-to-donor variation. Markers homogeneously expressed (low Median Fluorescent Intensity (MFI) variation and > 95% of CMSCs) included CD59, CD81, CD13, CD90, CD63, HLA-A,B,C, CD9, CD147, CD140b, CD47, CD73, CD105, CD49b, B2-MG, CD26, CD55, CD46, and CD49e which could be used to identify CMSCs. Markers heterogeneously expressed across donors may be linked to differences in cell safety and efficacy, and could be used for donor screening.

The CMSC phenotypic results were compared to BM-MSCs, identifying CD49b, CD49e, CD81, CD9, CD151, CD140b, CD99, CD47, CD147, CD63, CD95 and CD98 as homogeneously expressed (low MFI variation and > 85% expression in CMSCs and BM-MSCs). Significant differences in expression were observed for CD40, CD121a, CD108, CD49d, CD142 and HPC. Medium throughput genotypic profiling was performed using the Qiagen RT² Profiler PCR Array, finding significantly higher gene expression in BM-MSCs for multiple markers including those associated with angiogenesis and coagulation and growth factors. Differentially expressed markers

provide a reference point for future directions investigating safety and efficacy of CMSCs.

CMSCs were then exposed to inflammatory conditions to mimic the toxic environment of an inflamed ocular surface. Surviving CMSCs secreted an increase in multiple factors, including growth factors HGF, FGF2 and TGF β , which were not secreted by corneal epithelial cells, highlighting a higher specificity to CMSCs. Gene expression of extracellular matrix (ECM) structural constituents and cytoskeleton regulators were significantly reduced in cytokine exposed cells, potentially beneficial to avoid fibrosis. Phenotypic and genotypic profiles of CMSCs with a three-day recovery period following cytokine exposure provided an insight into the response of CMSCs to priming, with an increase in the expression of MIC A/B highlighting a risk of increased immunogenicity.

Finally, topical administration options were investigated, using techniques including rheology and equilibrium water content assessment. Successful cell attachment was observed through immunocytochemistry (ICC) and confocal imaging of CMSCs seeded on poly(HEMA-co-EGDMA) hydrogels functionalised for the first time with a resilin like polypeptide layer.

Overall, CMSC characterisation data identified a group of markers that can be used as a template for selecting directions for future functional investigations. This robust characterisation has advanced the biological understanding of CMSCs, in addition to being a substantial basis to aid successful translation of the cells to the clinic. Furthermore, this research demonstrated a novel method for topical administration of CMSCs to the ocular surface, through the development of a topical cell therapy for ocular surface disorders.

Acknowledgements

Firstly, I would like to express my sincere gratitude to my wonderful team of supervisors. I was given the opportunity to learn from Laura Sidney, Felicity Rose and Cameron Alexander, who provided non-stop guidance and cared for my wellbeing in addition to the science. Thank you to Cameron, for introducing me to polymer chemistry and your amazing group, in particular Pratik Gurnani, whose extensive knowledge was pivotal for the direction of this project. Thank you to Fliss, for her insight and for stepping up to play a key role in overseeing the thesis writing- I am so appreciative of her time and encouragement. Finally, this endeavour would not have been possible without Laura, who was there to talk me through any issues throughout the entirety of the project, and went above and beyond to provide opportunities, guidance, and motivation. Thank you for trusting me despite the chaos, and for being a great role model.

A special thank you goes to Kristi Kiick for giving me the incredible opportunity to visit her lab at the University of Delaware. Kristi and the whole group, including Luisa Palmese, Cristobal Garcia, Sai Patkar and Ramadan Abouomar were extremely welcoming, supportive, and made me feel at home all the way over the pond. The knowledge, skills, and material they shared were fundamental to the success of the project.

Thank you to everyone in Academic Ophthalmology, for creating a great work environment. In particular, thank you to Imran Mohammed, Darren Ting, Perla Filippini, Daryl Bower, Owen Mckintosh and Ruk Akhtar. I am grateful to have been surrounded by such caring and interesting people. Additionally, I would like to acknowledge the help I received from Caitlin Adkins during her BMedSci.

Thank you to David Onion and Nicola Croxall from the University of Nottingham Flow Cytometry Facility, who were quick to help me with any concerns and queries throughout the project. A big thank you to Graziela Figueredo, for your timely help and guidance with the statistics. Also, to Tim Self and Robert Markus from the University of Nottingham SLIM facility, and Timothy Chaya from the University of

Delaware Biotechnology Institute, for your guidance and training using the microscopes.

I would like to acknowledge the EPSRC CDT in Regenerative Medicine, who gave me the opportunity to pursue a PhD in cell therapies. This helped me to build confidence, knowledge, and lifelong friendships, and I believe truly enhanced my PhD experience. In particular, I'd like to mention Mitchell Day, who has been key to my journey right from the start.

I have been lucky enough to meet a lot of fabulous people throughout my project, both from Nottingham Triathlon Club and the PhD community. I would like to thank my dearest friends; Lydia Ogradzinski, Michaela Brown, Fiona Barnes and George Budden for your support, laughter, cooking and words of wisdom. The last 4 years would not have been the same without you.

To the Cook family- thank you for letting me use your stable as an office, your house as a second home, and for welcoming me into your family. You have been central to my thesis writing, and I will never forget your kindness and generosity. Thank you also to John Lewis, for his indispensable support during the final stages.

Finally, I would like to thank my family for always believing in me and encouraging me to pursue goals that I believed were out of my reach. Thank you to my brothers and grandma for always making me smile, regardless of how work was going. Thank you to my granddad, Frank, who has always been my number one cheerleader. I truly appreciate your excitement and interest in every piece of my work despite not understanding science, and I'm glad I could make you proud. Thank you to Mum and Dad, who I wholeheartedly could not have achieved any of this without. I am forever grateful for your generosity, patience, and encouragement.

Abbreviations

ABCG2	ATP Binding Cassette Subfamily G Member 2
ACTA2	Actin Alpha 2, Smooth Muscle
AD-MSC	Adipose Derived Mesenchymal Stromal Cell
AEMA	2-Aminoethyl Methacrylate
ALDH3A1	Aldehyde dehydrogenase
AM	Amniotic Membrane
AMD	Age-Related Macular Disorder
ATRP	Atom Transfer Radical Polymerisation
BM-MSC	Bone Marrow Derived Mesenchymal Stromal Cell
CCE	Cultivated Corneal Epithelial
cDNA	Complementary DNA
CMSC	Corneal Derived Mesenchymal Stromal Cell
CNTF	Ciliary Neurotrophic Factor
COX-2	Cyclooxygenase-2
Ct	Fractional Cycle Number at Threshold
CV	Coefficient of Variation
DAPI	4',6-Diamidino-2-Phenylindole
DC	Dendritic Cell
DED	Dry Eye Disease
DMHA	N,O-Dimethacryloyl Hydroxylamine
DMPA	Dimethoxy-2-Phenylacetophenone
DNA	Deoxyribonucleic Acid
DP-MSC	Dental Pulp Derived Mesenchymal Stromal Cell
ECM	Extracellular Matrix
EGDMA	Ethylene Glycol Dimethacrylate
EGF	Epidermal Growth Factor
ELISA	Enzyme Linked Immunosorbent Assay
ENG	Endogolin
ERK	Extracellular Signal-Regulated Kinase
EV	Extracellular Vesicle
EWC	Equilibrium Water Content
FBS	Foetal Bovine Serum
FGF	Fibroblast Growth Factor
FI	Fold Increase
GAPDH	Glyceraldehyde-3-Phosphate Dehydrogenase
GAS	Interferon Gamma Activated Site
GDNF	Glial Cell-Line Derived Neurotrophic Factor

GF	Growth Factor
GMP	Good Manufacturing Practice
GVHD	Graft Versus Host Disease
HCEC2	Immortalised Human Corneal Epithelial Cells
HEMA	2-Hydroxyethyl Methacrylate
HGF	Hepatocyte Growth Factor
HRP	Horse Radish Peroxidase
Hya	Hyaluronic Acid
IBMIR	Instant Blood-Mediated Inflammatory Reaction
ICAM-1	Intercellular Adhesion Molecule 1
ICC	Immunocytochemistry
IDO	Indoleamine 2,3-Dioxygenase
IFN-γ	Interferon Gamma
IFN-γ R1	Interferon Gamma Receptor 1
IL-1R1	Interleukin 1 Receptor 1
IL-1ra	Interleukin 1 Receptor Antagonist
IL-1β	Interleukin 1 Beta
iPSCs	Induced Pluripotent Stem Cells
IRF-1	Interferon Regulatory Factor 1
ISCT	International Society for Cellular Therapy
ITGB3	Integrin Beta 3
JAK	Janus Kinase
JNK	c-Jun N-Terminal Kinase
Ki67	Marker of Proliferation Ki67
LAP	Lithium Phenyl-2,4,6-Trimethylbenzoylphosphinate
LPB	LPS- Binding Protein Subunit
LPS	Lipopolysaccharides
LSCD	Limbal Epithelial Stem Cell Deficiency
LSCT	Limbal Epithelial Stem Cell Transplantation
MFI	Median Fluorescence Intensity
MGD	Meibomian Gland Dysfunction
MHC	Major Histocompatibility Complex
MMEP	Mono(2-Methacryloyloxyethyl) Phosphate
MMP	Matrix Metalloproteinase
MSC	Mesenchymal Stromal Cell
MyD88	Myeloid Differentiation Primary Response Gene 88
NFκB	Nuclear Factor Kappa B
NKT	Natural Killer T Cell
NO	Nitric Oxide

NT5E	5'-Nucleotidase Ecto
OCT4A	Octamer-Binding Protein 4
OSIDs	Ocular Surface Inflammatory Disorders
PBS	Phosphate Buffered Saline
PEDF	Pigment Epithelium-Derived Factor
PFA	Paraformaldehyde
PG	Prostaglandin
PGE2	Prostaglandin E2
PTX-3	Pentraxin 3
RLP	Resilin Like Polypeptide
RNA	Ribonucleic Acid
RT-qPCR	Quantitative Reverse Transcription Polymerase Chain Reaction
SCL	Soft Contact Lenses
SCM	Stem Cell Medium
SSEA4	Stage-Specific Embryonic Antigen-4
STAT	Signal Transducer and Activator of Transcription
STAT	Signal Transducer and Activator of Transcription
TGF-β	Transforming Growth Factor Beta
THY1	Thy-1 cell surface antigen
TLR4	Toll-Like Receptor 4
TMB	3, 3', 5, 5'-Tetramethylbenzidine
TNFR1	Tumor Necrosis Factor Receptor 1
TNF-α	Tumour Necrosis Factor Alpha
TSG-6	TNF- α Stimulated Gene/ Protein
TSP-1	Thrombospondin-1
UC-MSC	Umbilical Cord Derived Mesenchymal Stromal Cell
VA-044	2,2'-azobis[2-(2-imidazolin-2-yl)propane] dihydrochloride
VEGF	Vascular Endothelial Growth Factor
αSMA	Alpha Smooth Muscle Actin

All abbreviations of antigens in the BD Human Cell Surface Marker Panel, and genes in the RT² Profiler PCR Array are defined in the Appendix (Table A1.1. and A1.2).

Table of Contents

Abstract	i
Acknowledgements	iii
Abbreviations	v
Table of Contents	viii
List of Figures	xv
List of Tables	xviii
CHAPTER 1: Introduction	1
1.1. The cornea	1
1.2. Potential therapeutic cells for immunomodulation of the injured ocular surface	5
1.3. Direct communication of MSCs and target cells	6
1.4. Paracrine signalling of MSCs and potential effect on corneal immunomodulation	6
1.5. MSC Source	9
1.5.1. Bone-marrow derived MSCs (BM-MSCs).....	10
1.5.2. Adipose derived MSCs (AD-MSCs).....	10
1.5.3. Dental Pulp (DP) and Umbilical Cord (UC) Derived MSCs.....	11
1.5.4. Corneal Derived MSCs (CMSCs)	12
1.6. Effect of culture, passage and priming of MSCs	13
1.7. Application of MSCs to the ocular surface: Topical vs. alternative methods	14
1.8. Potential substrates and scaffolds for topical application of MSCs to the ocular surface	15
1.9. Soft Contact Lenses for Topical Application of Stem Cells	17
1.10. SCL Composition	18
1.11. Therapeutic applications of SCLs	20
1.11.1. Biological Bandage.....	21

1.11.2. Drug Delivery.....	21
1.11.3. Regenerative medicine potential	21
1.12. Functionalisation of hydrogels with surface peptides for cell adhesion	22
1.12.1. Functionalisation of poly(HEMA) hydrogels	22
1.12.2. Functionalisation of Siloxane Hydrogels.....	24
1.13. MSC Therapy Limitations	25
1.14. Conclusion	26
1.15. Thesis hypotheses, aims and objectives	34
CHAPTER 2: Materials and Methods	36
2.1. Materials	36
2.1.1. Cells.....	36
2.1.1.i. Human Corneal Mesenchymal Stromal Cells	36
2.1.1.ii. Human Bone Marrow Stromal Cells	36
2.1.1.iii. Immortalised Human Corneal Epithelial Cells.....	36
2.1.2. General Chemicals.....	37
2.1.2.i. Knockout Serum Replacement	37
2.1.2.ii. Antibodies.....	37
2.1.3. Quantitative Reverse Transcription Polymerase Chain Reaction (RT-qPCR) Reagents.....	41
2.1.4. RT ² Profiler PCR Array – Human Wound Healing.....	41
2.1.5. Enzyme Linked Immunosorbent Assay (ELISA) Reagents	44
2.1.6. Cytokines	46
2.1.7. Polymer Reagents.....	46
2.1.8. Resillin-Like Polypeptides (RLPs).....	49
2.2. Methods	49
2.2.1. Cell Culture.....	49
2.2.1.i. CMSC Isolation from Corneoscleral Rims.....	49
2.2.1.ii. CMSC Culture	50
2.2.1.iii. BM-MSK Culture	51
2.2.1.iv. HCEC2 Culture.....	51

2.2.1.v. Cell cryopreservation and reanimation	51
2.2.2. PrestoBlue Viability Assay.....	52
2.2.3. Live/Dead Fluorescence Assay.....	52
2.2.4. Immunocytochemistry	53
2.2.4.i. Cell Fixation	53
2.2.4.ii. Cell Permeabilization	53
2.2.4.iii. Immunocytochemistry	54
2.2.5. Flow Cytometry.....	55
2.2.5.i. Sample Preparation	55
2.2.5.ii. Cell Surface Staining.....	55
2.2.5.iii. Nuclear Staining.....	55
2.2.5.iv. BD Lyoplate™ Human Cell Surface Marker Screening Panel.....	56
2.2.5.v. Cytometer Analysis	56
2.2.6. Growth Rate and Population Doubling Calculations	57
2.2.7. Reverse Transcription Quantitative Polymerase Chain Reaction (RT-qPCR) ..	57
2.2.7.i. General RNA Isolation.....	57
2.2.7.ii. General cDNA Synthesis.....	58
2.2.7.iii. General PCR	58
2.2.7.iv. General Analysis	59
2.2.8. Enzyme-linked Immunosorbent Assays (ELISAs)	60
2.2.9. Polymer Synthesis and Preparation	62
2.2.9.i. Free Radical Mechanism	62
2.2.9.ii. Poly(HEMA-co-EGDMA) synthesis	65
2.2.10. Polymer Functionalisation	65
2.2.10.i. AEMA.....	65
2.10.ii. GGGRGD and GGGYIGSR	67
2.2.10.iii. Resilin-like polypeptides (RLPs).....	67
2.2.11. Polymer Analytical Techniques	68
2.2.11.i. Mechanical Testing	68
2.2.11.ii. Oscillatory Rheology	69
2.2.11.iii. Equilibrium Water Content	70
2.2.11.iv. Opacity Assay	70

2.2.11.v. Cell attachment to hydrogels	71
2.2.12. Statistical Analysis	71
CHAPTER 3: Analysis of corneal mesenchymal stromal cell phenotype	73
over increasing passages	73
3.1. Introduction	73
3.2. Experimental Design.....	78
3.2.1. CMSC Culture	78
3.2.2. Immunocytochemistry (ICC)	78
3.2.3. Flow Cytometry.....	79
3.2.4. PrestoBlue Viability Assay	79
3.2.5. Growth Rate and Population Doublings.....	79
3.2.6. RT-qPCR	79
3.2.7. Statistical Analysis	79
3.2.8. BD Lyoplate Cell Surface Marker Panel	80
3.2.9. Lyoplate Data Analysis.....	80
3.3. Results	83
3.3.1. MSC Marker Expression.....	83
3.3.2. Stem Cell and Myofibroblast Marker Expression.....	87
3.3.4. Cell growth assessment	91
3.3.4. Structural marker analysis	93
3.3.5. CMSC Phenotyping	93
3.4. Discussion.....	99
CHAPTER 4: Medium throughput immunophenotypic and genotypic comparison of CMSCs with BM-MSCs to identify common and differentially expressed markers 108	
4.1. Introduction	108
4.2. Methods	112
4.2.1. CMSC Culture	113
4.2.2. BM-MSC Culture.....	113
4.2.3. BD Lyoplate™ Human Cell Surface Marker Screening Panel	113

4.2.4. Hierarchical Clustering	113
4.2.5. Wound Healing Gene Array Panel	114
4.2.6. Statistical Analysis	114
4.3. Results	114
4.3.1. Phenotypic differences were observed between CMSCs and BM-MSCs.....	114
4.3.2. Identification of cell surface markers specific to CMSCs and BM-MSCs.....	117
4.3.3. Identification of cell surface markers commonly expressed between CMSCs and BM-MSCs	119
4.3.4. Comparison of MFI FI against percentage of cell population expressing markers of interest.	122
4.3.5. Genotypic differences were observed between BM-MSCs and CMSCs	122
4.4. Discussion.....	125
CHAPTER 5: Analysis of corneal mesenchymal stromal cells in an <i>in vitro</i>, proinflammatory environment	132
5.1. Introduction	132
5.1.1. Receptors	137
5.1.1.i. Toll-like receptor 4 (TLR4)	137
5.1.1.ii. Tumor necrosis factor receptor 1 (TNFR1).....	137
5.1.1.iii. Interferon gamma receptor 1 (IFN- γ R1).....	137
5.1.1.iv. Interleukin 1 receptor type 1 (IL-1 R1).....	138
5.1.2. Chapter Hypotheses	138
5.2. Methods	140
5.2.1. Inflammatory Cocktail	141
5.2.2. CMSC Culture	141
5.2.3. HCEC2 Culture	141
5.2.4. PrestoBlue Viability Assay	142
5.2.5. Live/Dead Staining	142
5.2.6. BD Lyoplate™ Human Cell Surface Marker Screening Panel.....	142
5.2.7. Wound Healing Gene Array Panel	142
5.2.8. ELISAs.....	143
5.2.9. Statical Analysis.....	143

5.3. Results	144
5.3.1. A subset of CMSCs survived the cytokine cocktail, with inhibited proliferation. 144	
5.3.2. Phenotypic differences were observed between CMSCs in different conditions.	146
5.3.3. Genotypic differences were observed between CMSCs in different conditions. 151	
5.3.4. The cytokine cocktail altered the secretome of CMSCs.....	154
5.3.5. Comparison of the CMSC secretome to corneal epithelial cells demonstrated factors more specific to CMSCs.	157
5.4. Discussion	160
5.4.1. Pro-inflammatory Factors.....	164
5.4.2. Growth Factors	165
5.4.3. Anti-angiogenic Factors	166
5.4.4. Anti-inflammatory Factors.....	168
5.4.5. Wound Healing Factors.....	170
5.5. Conclusion.....	173
CHAPTER 6: Optimisation steps for the functionalisation of poly(HEMA-co-EGDMA) hydrogels for corneal mesenchymal stromal cell attachment	174
6.1. Introduction	174
6.2. Methods	178
6.2.1. Experimental Plan	179
6.2.2. Optimisation of HEMA concentration	179
6.2.3. Manufacture optimisation.....	180
6.2.4. Optimisation of EGDMA concentration	180
6.2.5. Synthesis of poly(HEMA-co-EGDMA-co-AEMA) with increasing AEMA concentration	180
6.2.6. Functionalisation with peptides.....	181
6.2.7 Functionalisation with RLP	181
6.2.8. Cell Culture and Seeding on Hydrogels	183
6.2.8.i. BM-MSCs	183
6.2.8.ii. CMSCs.....	183

6.2.9. Confocal imaging of MSC seeded hydrogels.....	183
6.3. Results	184
6.3.1. Analysis of optimal HEMA concentration.....	184
6.3.2. Methods of manufacture to achieve consistently well formed, clear hydrogels 187	
6.3.3. Effect of different EGDMA densities on properties of poly(HEMA-co-EGDMA) hydrogels	187
6.3.4. Effect of different AEMA concentrations on properties of poly(HEMA-co- EGDMA-co-AEMA) hydrogels	189
6.3.5 Transparency of hydrogels with varied EGDMA and AEMA concentrations .	191
6.3.6. CMSC attachment to hydrogels functionalised through bulk synthesis.	192
6.3.7. Gelation time of poly-HEMA-co-EGDMA) hydrogels	194
6.3.8. Optimisation of RLP layer addition	196
6.3.9. Attachment of BM-MSCs to HEMA/RLP hydrogels.....	197
6.3.10. Attachment of CMSCs to HEMA/RLP hydrogels	198
6.3.11. Overconfluence of CMSCs on RLP/HEMA hydrogels	200
6.4. Discussion.....	201
CHAPTER 7: Summary	208
7.1. Summary	208
7.2. Discussion and Future Directions	212
7.3. Limitations	217
CHAPTER 8: References	218
Appendix	235

List of Figures

Chapter 1

Figure 1. 1. The structure of the cornea. Working from the ocular surface exterior to interior.....	1
Figure 1. 2. Corneal wound healing cascade..	4
Figure 1. 3. Immunomodulation by mesenchymal stromal cells (MSCs)..	8
Figure 1. 4. Isolation of corneal derived MSCs (CMSCs) from the corneal limbal stroma..	12
Figure 1. 5. Schematic of a hydrogel..	16
Figure 1. 6. Parameters for consideration when developing a therapeutic contact lens...	18
Figure 1. 7. Factors affecting the heterogeneity and clinical outcomes of MSC therapy to the eye.....	27

Chapter 2

Figure 2. 1. Free radical initiation mechanism, depicting initiation, propagation and termination, using VA-044 as an example initiator.	63
Figure 2. 2. Suggested mechanism for the crosslinking of HEMA with EGDMA to produce poly(HEMA-co-EGDMA), with VA-044 as an example initiator.	64
Figure 2. 3. Copolymerisation of HEMA and EGDMA with AEMA..	66

Chapter 3

Figure 3. 1. Advantages and limitations of allogeneic and autologous Mesenchymal stem cell therapy.	75
Figure 3. 2. Balance between increasing cell number during cell therapy manufacture and cell changes.	76
Figure 3. 3. Schematic overview of experiments investigating changes in phenotype, genotype and growth kinetics in CMSCs as passage increases.	81
Figure 3. 4. Schematic overview of experiments investigating phenotype of CMSCs to assess donor-donor variation.....	82
Figure 3. 5. Flow cytometry analysis of MSC markers (CD105, CD90 and CD73) and negative marker (CD34) on CMSCs between passage 4 and 10.	84
Figure 3. 6. ICC analysis of MSC markers (CD105, CD90 and CD73) and negative marker (CD34) on CMSCs between passage 4 and 10..	85
Figure 3. 7. Genotypic analysis using RT-qPCR found no significant difference in gene expression of classical MSC markers (<i>ENG</i> , <i>THY1</i> , and <i>NT5E</i>) and negative MSC marker (<i>CD34</i>) in CMSCs between passage 4 and 10.	86
Figure 3. 8. Flow cytometry analysis of stem cell marker expression (SSEA-4 and ABCG2) on CMSCs between passage 4 and 10.....	88
Figure 3. 9. ICC staining of stem cell (SSEA4, ABCG2, ALDH3A1 and OCT4) and fibrotic markers (α SMA) in CMSCs over increasing passages.....	89
Figure 3. 10. CMSC genotypic analysis of stemness and fibrosis.....	90
Figure 3. 11. Growth capacity of CMSCs..	92

Figure 3. 12. Vimentin and phalloidin staining to assess structure of CMSCs between passages 4 and 10..	93
Figure 3. 13. Heat maps showing median fluorescent fold increase in expression of different markers on CMSCs compared to the isotype control..	94
Figure 3. 14. Identification of CMSC markers with lowest variation between cell donors..	96
Figure 3. 15. Clusters of markers expressed by CMSCs.....	97
Figure 3. 16. Comparison of MFI FI and percentage of CMSCs expressing each antigen..	98

Chapter 4

Figure 4. 1. Harvesting of CMSCs from waste tissue in eye banks.....	111
Figure 4. 2. Schematic of experimental procedure, investigating similarities and differences in phenotype and genotype of CMSCs and BM-MSCs.	112
Figure 4. 3. Heat maps showing percentage of positive cells expressing different markers on CMSCs compared to BM-MSCs.....	116
Figure 4. 4. Identification of markers expressed by significantly different proportions of the CMSC and BM-MSC heterogenous populations based on percentage of cells expressing the marker.....	117
Figure 4. 5. Venn diagram of markers expressed in CMSCs, BM-MSCs and both	118
Figure 4. 6. Identification of phenotypic markers with the lowest variation between CMSCs and BM-MSCs.	120
Figure 4. 7. Clusters of markers positively expressed by both CMSCs and BM-MSCs.	121
Figure 4. 8. Comparison of MFI FI and percentage of cells expressing each antigen homogeneously expressed by both CMSCs and BM-MSCs.....	122
Figure 4. 9. RT ² Profiler array to detect the expression of genes associated with wound healing and fibrosis in CMSCs and BM-MSCs	124

Chapter 5

Figure 5. 1. Potential inflammatory signalling pathways following exposure of CMSCs to the inflammatory cocktail (IFN- γ , IL-1 β , TNF- α and LPS).....	136
Figure 5. 2. Schematic overview of the inflammatory investigation experimental setup and timeline.....	140
Figure 5. 3. Viability of CMSCs to the inflammatory cytokine cocktail..	145
Figure 5. 4. Heat maps showing percentage of positive cells expressing different markers on CMSCs compared to the isotype control.	148
Figure 5. 5. Heat maps showing median fluorescent fold increase (MFI FI) in expression of different markers on CMSCs compared to the isotype control.....	149
Figure 5. 6. Diagram summarising markers displaying significant differences between untreated vs treated and recovered groups..	150
Figure 5. 7. RT ² Profiler PCR array to detect the expression of genes associated with wound healing and fibrosis..	152
Figure 5. 8. Summary schematic of genes showing significantly lower (pink) and higher (green) expression in the treated and/or recovered group compared to the control, collected using the RT ² Profiler.....	153
Figure 5. 9. Factors secreted by control vs activated and recovered CMSCs.....	155

Figure 5. 10. Summary schematic of proteins showing significantly lower and higher secretion from CMSCs for control cells (no cytokines) compared to cells treated with cytokines for 3 days, and control cells compared to the recovered group (exposure and removal of cytokines).	156
Figure 5. 11. Factors secreted by CMSCs vs HCEC2s stimulated with the inflammatory cocktail for 3 days..	158
Figure 5. 12. Summary schematic of proteins showing significantly higher secretion from CMSCs or HCEC2s for cells treated with cytokines for 3 days.	159

Chapter 6

Figure 6. 1. Workflow for development of a functionalised contact lens for cell adhesion.	178
Figure 6. 2. Schematic illustration of methods for functionalising 60% poly(HEMA-co-EGDMA) with 20% RLP hydrogel using free radical polymerisation.	182
Figure 6. 3. Poly-HEMA-co-EGDMA hydrogels with increasing vol/vol % water.	185
Figure 6. 4. Frequency sweeps from <i>in situ</i> rheology to demonstrate changes in storage (G') and loss (G'') modulus of Poly-HEMA-co-EGDMA hydrogels with increasing vol/vol % water	186
Figure 6. 5. Manufacture of poly-HEMA-co-EGDMA hydrogels in cell culture plates.	187
Figure 6. 6. Equilibrium water content (%) and Young Modulus of varying EGDMA densities (mol %) in poly-HEMA-co-EGDMA hydrogels	188
Figure 6. 7. Equilibrium water content (%), Young Modulus, max stress and max strain of varying AEMA densities in poly(HEMA-co-EGDMA-co-AEMA) hydrogels.	190
Figure 6. 8. Opacity assay demonstrating fold change in absorbance compared to PBS control.	191
Figure 6. 9. (a) Phalloidin and DAPI staining of CMSCs seeded on poly-HEMA-co-EGDMA hydrogels functionalised with 0.4% (Mw) YIGSR and RGD.....	193
Figure 6. 10. <i>In situ</i> rheology of poly(HEMA-co-EGDMA) hydrogels.....	195
Figure 6. 11. Optimisation of poly(HEMA-co-EGDMA) hydrogels with RLP. 2uL of 10 wt% RLP-FM monomer solution with 10 μ L of 60 wt% HEMA monomer solution.	196
Figure 6. 12. Confocal imaging of BM-MS-C cell attachment to RLP functionalised poly(HEMA-co-EGDMA) hydrogels compared to no functionalisation.	197
Figure 6. 13. Confocal images of CMSCs adhered to RLP functionalised poly(HEMA-co-EGDMA) hydrogels.....	199
Figure 6. 14. Confocal images of CMSCs adhered to RLP functionalised poly(HEMA-co-EGDMA) hydrogels) in serum containing media.....	200

List of Tables

Chapter 1

Table 1. 1. Advantages and limitations of poly(HEMA) vs siloxane hydrogels for contact lens materials	20
Table 1. 2. Details on in vivo studies using MSCs, demonstrating study variability within the literature.....	28

Chapter 2

Table 2. 1. Primary antibodies used for immunocytochemistry (ICC) including antigen, source, species and working dilution.....	38
Table 2. 2. Secondary antibodies used for immunocytochemistry (ICC) including Alexa Fluor, source and working dilution.....	38
Table 2. 3. Conjugated antibodies used for flow cytometry including antigen target, source, conjugated fluorophore and working dilution.....	39
Table 2. 4. Specificity, clone and isotype of antibodies in the BD Human Cell Surface Marker Screening Panel.....	40
Table 2. 5. Kits used for RNA Isolation, cDNA synthesis and RT-qPCR.....	41
Table 2. 6. Table of primers used for RT-qPCR.....	41
Table 2. 7. Table of primers used in the RT2 Profiler PCR Array, with gene description from the handbook provided by Qiagen (Cat. No. 330231 PAHS-121ZA).....	42
Table 2. 8. Kits used for RNA isolation, cDNA synthesis and RT-PCR for the RT2 Profiler Array.....	44
Table 2. 9. Reagent diluents utilised for ELISAs, including a description of the relative diluent and working concentrations.....	45
Table 2. 10. Reagent concentrations with relative diluents utilised during ELISAs.....	45
Table 2. 11. Inflammatory investigations cytokine, source and working concentration.....	46
Table 2. 12. Name, structure, molecular weight and source of materials used in polymer investigations.....	47
Table 2. 13. Cycles for gene amplification for general PCR including duration, temperature, and number of cycles.....	59

Chapter 6

Table 6. 1. Volumetric percentages of monomer and water used for optimisation of water solvent in initial solution.....	179
Table 6. 2. Molar percentages of HEMA and EGDMA used for optimisation of crosslinker concentration.....	180
Table 6. 3. Molar percentage of HEMA, EGDMA and AEMA utilised for initial functionalisation of the hydrogels.....	181
Table 6. 4. Optimisation strategy for functionalisation of poly(HEMA-co-EGDMA) with RLP.....	182

CHAPTER 1: Introduction

1.1. The cornea

The cornea is the highly organized, transparent tissue at the ocular surface. It is comprised of three main cellular layers; the epithelium, the stroma containing the keratocytes, and the endothelium, separated by the Bowman's membrane and Descemet's membrane respectively [1] (Figure 1.1). Coating the outer mucosal surface of the cornea is the tear film; a thin, liquid layer [2], mainly constituted of mucin and lipid. As the cornea is avascular, the tear film plays a vital role in the supplementation of nutrients and oxygen, as well as the expulsion of waste such as epithelial debris, foreign bodies, and toxins. Interactions between the ocular surface and the tear film allows for a smooth optical surface, correct functioning of limbal epithelial cells and protection from mechanical and microbial insults [3]. Additionally, healthy corneal tissue is maintained through tight immunoregulatory mechanisms at the ocular surface, modulated by both the innate and adaptive immune systems.

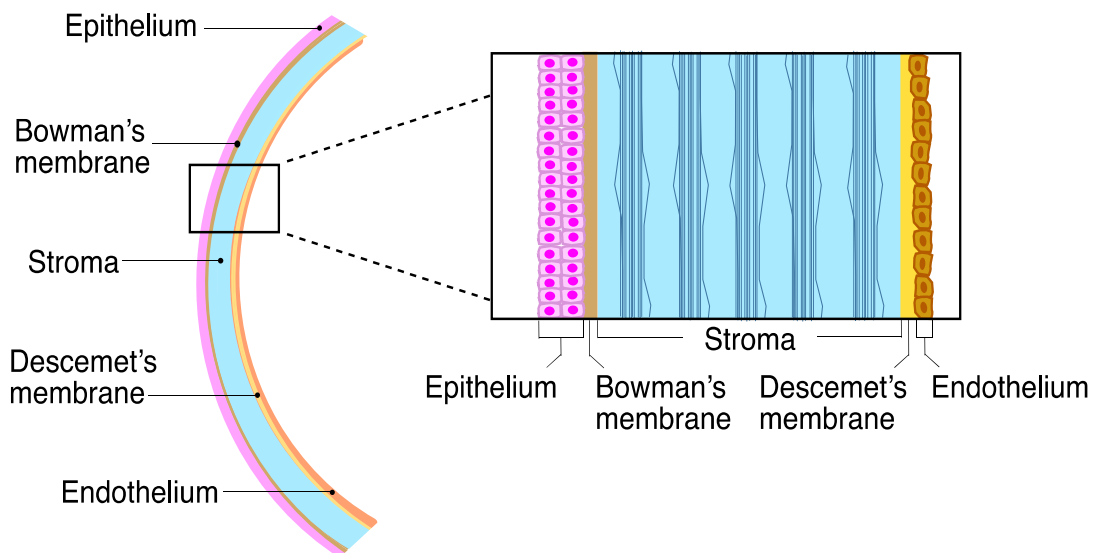


Figure 1. 1. The structure of the cornea. Working from the ocular surface exterior to interior, the cornea is made up of an epithelium; Bowman's membrane; stroma; Descemet's membrane and endothelium. Based on image from National Eye Institute, National Institutes of Health (nei.nih.gov).

Ocular surface inflammatory disorders (OSIDs) occur when the tightly regulated homeostasis at the ocular surface is disturbed, and encompass a range of heterogeneous diseases with a variety of aetiologies and symptoms, where inflammation plays a critical role in pathogenesis [4]. Dry eye disease (DED), meibomian gland dysfunction (MGD), allergic eye diseases, cicatricial conjunctivitis, chemical eye burn, trauma, iatrogenic insult following corneal and/or refractive surgery, and contact lens-related complications are the common examples of OSIDs that are frequently encountered and managed in clinical practice.

OSIDs are highly prevalent in the general population. For example, the global prevalence of DED has been estimated at around 5-50% depending on the diagnostic criteria and study population [5]. MGD is a major contributor to evaporative DED, and has been shown to cause a myriad of negative impacts on the ocular surface including heightened inflammation, oxidative stress, tear hyperosmolarity and increased corneal epitheliopathy [6]. These diseases often serve as an important risk factor for major ocular surface complications including infectious keratitis, corneal vascularisation, corneal melt and perforation, and opacity and visual impairment predominantly caused by scarring [7-9]. In addition to disease, scarring can occur through chemical or physical abrasion to the cornea (Figure 1.2) Following corneal injury, growth factors, cytokines and prostaglandins released from injured cells induces the apoptosis of usually quiescent, proximal stromal cells [10]. This in turn, prompts the shift in phenotype of distal keratocytes to fibroblasts, enhancing cell migration to the wound. Here, the fibroblasts spread, and differentiate into myofibroblasts and secrete cytokines causing inflammatory cell infiltration, and collagenase and matrix metalloproteinase (MMP) production. These factors help to clear matrix debris, leading to stromal remodelling. Following the cascade, myofibroblasts and inflammatory cells undergo apoptosis or necrosis. Although keratocytes return to their normal state, the remaining extracellular matrix (ECM) can be crosslinked, displaying as corneal haze or opacity for the patient. OSIDs and injuries are regularly associated with pain and irritation, causing a considerable reduction in the patient's quality of life, activities in daily living and work productivity [11]. Irrespective of their source, insult to the cornea ultimately

results in a vicious cycle, where chronic irritation activates an immune response, augmenting the irritation and scarring [4].

Currently, treatments include over-the-counter lubricating eye-drops to alleviate disease symptoms, and corticosteroids to ameliorate the inflammation. However, these treatments require long-term topical application, multiple times a day (every hour), placing high demand on patient compliance and interfering with their day-to-day life. Furthermore, corticosteroids have been linked to severe adverse effects including increased risk of infectious keratitis, inhibition of corneal wound healing, raised intraocular pressure, and cataracts [12, 13]. Cyclosporin serves as a valuable steroid-sparing immunomodulatory agent for managing a range of OSIDs, though side effects are common [14]. Lifitegrast, a recent FDA approved drug, represents another useful topical anti-inflammatory treatment for DED. However, both cyclosporin and lifitegrast are associated with a high rate, up to 70%, of side effects, including burning sensation, itching, and blurred vision, amongst others [15].

Due to the abundance of therapeutic factors possessed by human stem cells, regenerative medicine may hold the key to developing a superior treatment to alleviate OSIDs. This chapter outlines the process required for the application of cell therapy for OSIDs, through assessing optimum cell type and delivery method to the ocular surface. This project has focused on the use of mesenchymal stromal cells (MSCs) due to their well-accepted immunomodulatory properties and suggest that applying the cells topically, via a removable substrate or scaffold, may offer the most convenient and efficacious therapy.

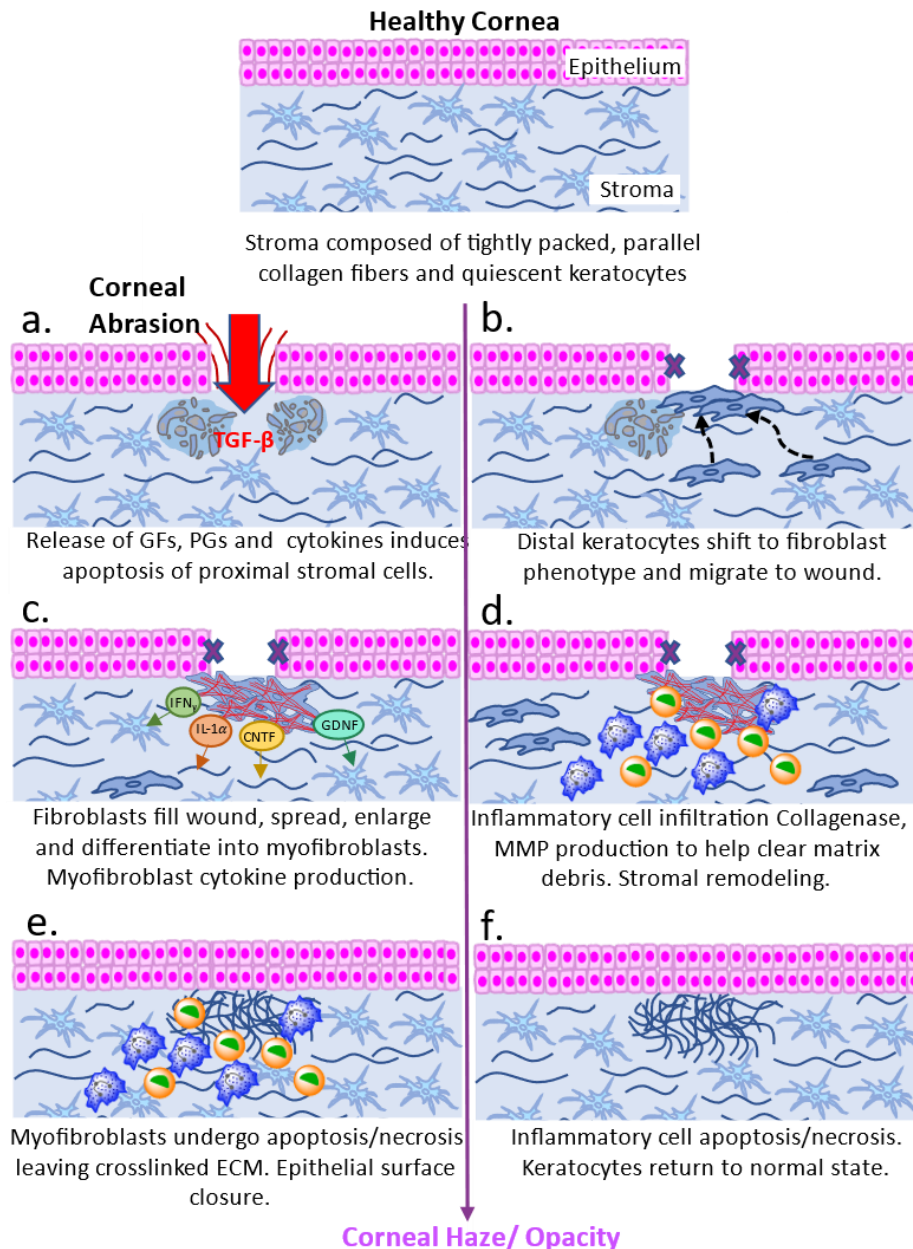


Figure 1. 2. Corneal wound healing cascade. Corneal trauma causing abrasion to the epithelia and stroma result in the secretion of growth factors (GFs), prostaglandins (PGs) and cytokines from injured cells, resulting in proximal keratocyte apoptosis (a). In turn, distal keratocytes adopt a fibroblast phenotype and migrate to the wound (b) where they sequentially shift to a myofibroblast phenotype (c). Myofibroblasts produce pro-inflammatory cytokines which induce inflammatory cells infiltration, including neutrophils (blue) and macrophages (yellow), in addition to producing collagenase and matrix metalloproteinases (MMPs) to help clear matrix debris whilst undergoing stromal remodeling (d). Myofibroblasts undergo apoptosis and necrosis and re-epithelialization occurs (e). Inflammatory cells undergo apoptosis and necrosis and the keratocytes return to a normal state (f). Corneal haze/opacity occurs due to the remodeled, crosslinked extracellular matrix (ECM) in the stroma. Figure based on Wilson *et al.*, 2001 [16].

1.2. Potential therapeutic cells for immunomodulation of the injured ocular surface

Inflammation is recognised as a significant feature in the etiopathophysiology of OSIDs, therefore stem cells with efficacious anti-inflammatory properties would be optimal for successful treatment. Limbal epithelial stem cell transplantation (LSCT) and cultivated corneal epithelial (CCE) sheets have shown promising therapeutic results for restoring a normal corneal epithelial phenotype in patients with severe chemical injury and dry eye [17, 18]. However, the primary utilization of LSCT and CCE is to generate an entire new epithelial layer *in situ* or *in vitro* respectively, rather than for their immunosuppressive capacity, used predominantly in cases where injury has resulted in a limbal epithelial stem cell deficiency (LSCD). Their incapacity to suppress inflammation is supported by data demonstrating contraindications of LSCT in the presence of active inflammation in bilateral diseases, including Stevens-Johnson syndrome, ocular cicatricial pemphigoid and graft versus host disease (GVHD). In fact, failure of LSCT is often accredited to sites of active inflammation creating a toxic microenvironment at the ocular surface [19]. Although these techniques have proven, in some cases, successful to treat injuries such as chemical burn, which are associated with high levels of inflammation, it is likely that some of the immunosuppression was governed and achieved by the immune-modulating, amniotic membrane scaffold the cells were applied with [17, 18]. The aim of this introduction was to highlight alternative sources of stem cells that could be considered for novel regenerative medicine therapies.

Differentiating induced pluripotent stem cells (iPSCs) into immune-mediating cells such as regulatory T cells [20], holds the potential to improve the inflammatory symptoms of OSIDs. However, this therapeutic strategy is limited by the high tumorigenic potential, cost and regulation associated with the generation and application of iPSCs [21].

MSCs are best known in regenerative medicine for their ability to modulate both the innate and adaptive immune systems [22], suggesting a potential use for the treatment of inflammation in OSIDs. Their capacity to reduce inflammation has

been assessed *in vitro* and *in vivo* on multiple tissues, including the kidney, heart, cartilage, liver, brain, skin and cornea [23], with preclinical success demonstrated by their current use in clinical trials [24]. MSCs encompass a group of fibroblast-like, multipotent progenitor stromal cells, defined initially by their capacity to differentiate into osteoblasts, adipocytes and chondrocytes [25], however MSCs are now utilised primarily for the ability to elicit a therapeutic response through communication with target tissue cells.

1.3. Direct communication of MSCs and target cells

Limited evidence has demonstrated that MSCs can interact with the target tissue directly via cell-cell contacts such as gap junctions and tunnelling nanotubes [26]. This has been demonstrated in cardiac tissue, where the respiratory chain in myocytes was salvaged through mitochondrial transfer. Although not investigated in the literature, hypothetically this mechanism could restore cells at the ocular surface and is therefore an area with potential for future exploration. The external anatomical location of the ocular surface means topical application could easily be achieved. Topical methods of administration are explored further in Section 1.7. Attaching the MSC to the surface of a scaffold for direct interaction with the injured epithelium would allow the cell to work through paracrine mechanisms in addition to any potential benefits of cell-to-cell contact, which was explored in this thesis. However, alternative applications could involve cell encapsulation into the hydrogel scaffold, relying entirely on paracrine mechanism for cell rescue. This may offer protection of the cells from the toxic microenvironment of the injured ocular surface, in addition to ensuring the cells maintain in the scaffold, which is difficult to achieve for surface attached cells.

1.4. Paracrine signalling of MSCs and potential effect on corneal immunomodulation

The main interest surrounding MSCs has shifted to their paracrine function, as a positive therapeutic response can be achieved irrespective of whether the cells reach the target organ [27]. There is an abundance of data demonstrating MSC

secretion of anti-inflammatory factors, cell-mobilization factors and growth factors in response to inflammatory mediators [28].

Stimulation of MSCs with interferon- γ (IFN- γ) has been studied abundantly in the literature, demonstrating activation of the IFN- γ -Janus kinase (JAK)-signal transducer and activator of transcription (STAT) 1 pathway [29] leading to the secretion of indoleamine 2,3-dioxygenase (IDO), a tryptophan catabolizing enzyme commonly directly correlated with the immunomodulatory potency of MSCs [30]. MSC activation has also been investigated with pro-inflammatory cytokines tumour necrosis factor- α (TNF- α) and interleukins (IL)-1 α /-1 β , leading to upregulation of transcription factors including Nuclear factor kappa B (NF κ B), and the secretion of several factors including transforming growth factor- β , ciliary neurotrophic factor, glial cell line-derived neurotrophic factor, interleukins -1 β , -6, -8 and -10, nitric oxide (NO), hepatocyte growth factor (HGF) and vascular endothelial growth factor (VEGF) (Figure 1.3) [31].

Using paracrine signalling, MSCs can ultimately suppress the activation and function of various cells within the adaptive and innate immune systems, including T and B lymphocytes, macrophages, natural killer cells, neutrophils and dendritic cells. Multiple corneal and ocular surface studies have demonstrated the reduction of inflammatory factors following MSC administration *in vitro* and *in vivo*, [32, 33], in addition to their capacity to inhibit allergy driven disease, such as allergic conjunctivitis, through cyclooxygenase-2 (COX-2)-dependent antiallergic mechanisms [34].

An initial consideration regarding the use of MSCs for OSIDs is the relationship between secreted growth factors and angiogenesis. In ischemic cardiac tissue, MSCs promote neovascularization through the upregulation of VEGF [35]. Ocular angiogenesis is a lead factor of blinding eye diseases including retinal disease, such as age-related macular disorder (AMD), stimulated by an increase in, VEGF [36]. Conversely, MSCs have shown the opposite effect on neovascularisation when applied to corneal injury induced by chemical burn. One study demonstrated downregulation of VEGF and significant reduction of neovascularisation in the MSC-

treated cornea [37]. This could be attributed to MSC induced up-regulation of thrombospondin-1 (TSP1), a VEGF inhibitor [38] and signifies the importance of the microenvironment on MSC behaviour.

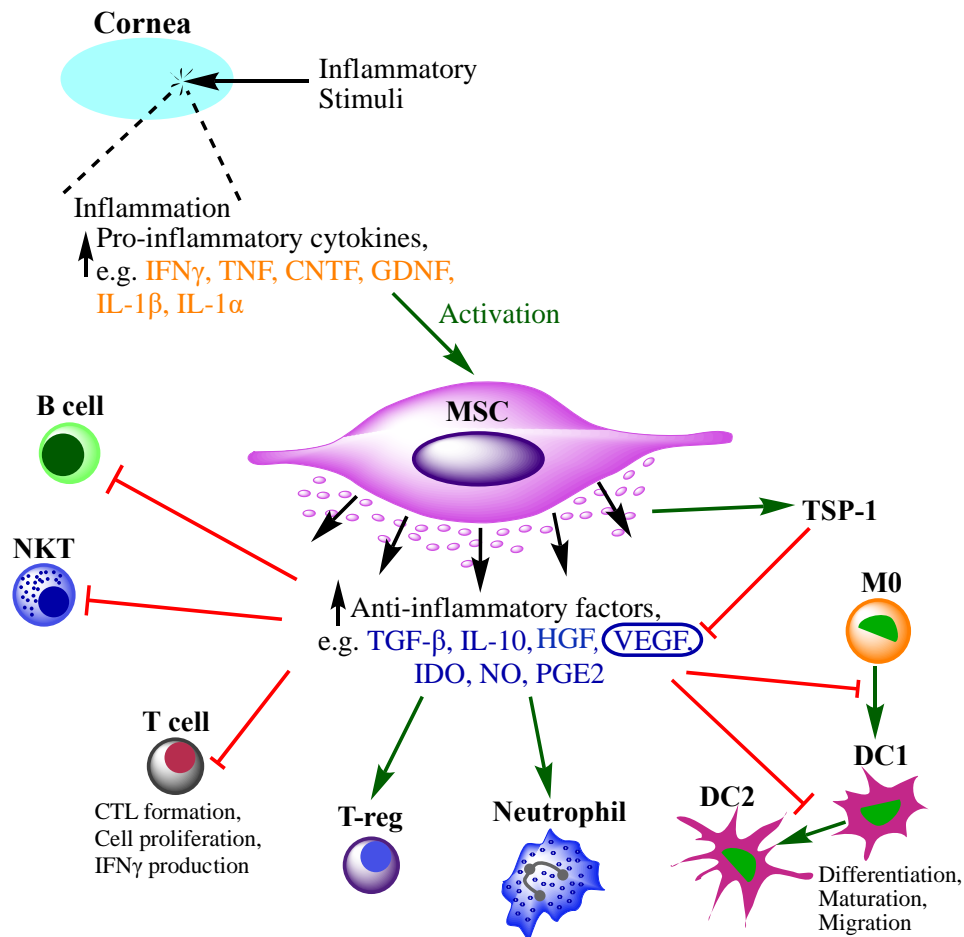


Figure 1. 3. Immunomodulation by mesenchymal stromal cells (MSCs). Inflammatory stimuli at the ocular surface results in an increase in pro-inflammatory factors, for example interferon- γ (IFN- γ), tumour necrosis factor (TNF), ciliary neurotrophic factor (CNTF), glial cell-line derived neurotrophic factor (GDNF) and interleukins (IL) 1 β and 1 α . These factors can activate and stimulate any applied MSCs to secrete immunomodulatory factors including transforming growth factor β (TGF- β), IL-10, hepatocyte growth factor (HGF), indoleamine 2,3-dioxygenase (IDO), nitric oxide (NO), prostaglandin E2 (PGE2) and vascular endothelial growth factor (VEGF). This can result in the inhibition (red line) of proliferation and function of T and B lymphocytes, natural killer T cells (NKTs) and dendritic cells (DCs), however can preserve neutrophil viability through apoptosis inhibition. MSCs also stimulate (green arrow) the upregulation of thrombospondin-1 (TSP-1) in the cornea, which inhibits VEGF and prevents angiogenesis. Diagram based on Zhao *et al.* [39].

HGF has also been implicated as a fundamental factor in immunomodulation, secreted by MSCs stimulated with IL-1 β [40]. HGF alone is powerful enough to suppress antigen presenting cell activation and to limit the generation of T helper (Th) 1 cells in the lymphoid tissue. Topical HGF application significantly reduced the rejection of corneal grafts in a murine model of GVHD, through suppression of immune cell infiltration, and has the potential to maintain and restore corneal transparency through the inhibition of α -smooth muscle actin (α SMA) and its inducer TGF- β [32, 41].

Other key anti-angiogenic molecules secreted by MSCs include TNF- α stimulated gene/ protein (TSG-6), demonstrated as vital in the inhibition of neovascularisation, and suggested to function through the inhibition of macrophage infiltration and the induction of apoptosis of vascular endothelial cells [42]. As well as macrophages, TSG-6 has been demonstrated to suppress activation and infiltration of neutrophils following chemical and mechanical corneal injuries [43], making it a potent modulator of both angiogenesis and inflammation.

An alternative method to exploit this paracrine signalling mechanism of MSC to treat OSIDs would be through harvesting extracellular vesicles (EVs) from the MSC for therapeutic application [44]. The potent therapeutic factors of MSCs packaged in small vesicles could help to overcome the safety and regulatory hurdles of cell application and have shown potential in corneal wound healing and immunomodulation *in vivo* [45].

Fully elucidating the pathways and interactions of different MSCs and the corneal microenvironment will help to increase the safety profile and therapeutic value of these cells for both tissue regeneration and inflammation suppression, highlighting the necessity to explore different MSC sources.

1.5. MSC Source

It is of utmost importance to consider MSC source, both tissue and donor (autologous or allogeneic). Although MSCs have previously been claimed as immune-privileged due to their lack of expression of Major Histocompatibility Class

(MHC) II proteins and co-stimulatory molecules B7 and CD40 ligand [46], immune rejection of MSCs derived from allogeneic sources has proven a major therapeutic challenge for application to a wide variety of conditions [47]. Similarly, the ocular microenvironment has been claimed to be immune-privileged, with original accounts demonstrating placement of a foreign antigen in the eye did not elicit an immune response [48]. Although GVHD is a contraindication of an ocular allogeneic stem cell transplant in approximately 40-60% of patients [49], the immunomodulatory properties of MSCs may give them additional protection, even if from an allogeneic source, with reports of multiple clinical trials using MSCs to both prevent and treat GVHD [50]. Although allogeneic cell therapy is beneficial for the manufacturing of the therapy, potential adverse effects of foreign cells are vital to consider.

MSCs can be isolated from most tissues in the body and cultured *in vitro*, however they do not all possess the same properties. For example, literature demonstrating MSC secretion of the anti-inflammatory cytokine, IL-10, is highly contradictory, and could be due to the source of the cells [51]. For successful translation to clinic, it is important that multiple sources of MSCs are explored, to develop the most efficacious and cost-effective treatment for OSIDs.

1.5.1. Bone-marrow derived MSCs (BM-MSCs)

Bone marrow is the most investigated source of MSCs in OSID cell therapy research. BM-MSCs have demonstrated efficacy for immunoregulation and disease amelioration in multiple *in vivo* OSID models with different administration routes. These include animal models of chemical burns [37, 52] and inflammation-induced dry eye [53]. However, a major limitation includes the invasive, and painful procedure to isolate the bone marrow, where only 0.001- 0.01% of the cells will constitute MSCs.

1.5.2. Adipose derived MSCs (AD-MSCs)

AD-MSCs have similar levels of surface antigen expression, differentiation ability and immunosuppressive activity as BM-MSCs [54], and can be isolated in abundance due to plentiful, accessible sources, which can generate a higher yield of

100 to 1,000 cells per gram of adipose tissue. However, data demonstrating their efficacy for corneal regeneration is scarce and conflicting. Fuentes-Julián *et al.* [55] found that application of AD-MSCs to a rabbit model of corneal allograft rejection increased inflammation levels. In contrast, AD-MSCs have shown efficacious effects on numerous other organs including the liver and brain [56, 57], achieved through suppression of the immune response. A recent study which compared them directly to BM-MSCs found a reduced capacity for corneal wound healing *in vitro* [58]. Further research is required to determine whether AD-MSCs have translational properties across tissues, or to understand their differential behaviour in the corneal allograft rejection model. Additionally, although Møller-Hansen *et al.* [59] found no adverse effects in a clinical trial where allogeneic AD-MSCs were injected into the lacrimal gland as a therapy for aqueous deficient dry eye disease, major safety concerns were uncovered following intravitreal injection of autologous AD-MSCs in a clinical trial for non-vascular AMD. Although a retinal disorder, it is important to note the trial induced vision loss due to retinal detachment and increased intraocular pressure following MSC administration [60].

1.5.3. Dental Pulp (DP) and Umbilical Cord (UC) Derived MSCs

Dental pulp (DP) and umbilical cord (UC) are alternative sources of MSCs. DP-MSCs display similar marker characteristics and differentiation potential to the aforementioned MSCs, in comparison to UC-MSCs which show higher levels of proliferation, more potent levels of immunomodulation and lower levels of senescence [54]. Although limited research applies these cells to the cornea, an *ex vivo* study has demonstrated the capacity of DP-MSCs to enhance repair and regeneration of human corneal epithelium, immature DP-MSCs have shown efficacy *in vivo* for LSCD, resulting in decreased corneal opacity and neovascularization [61], in addition to both directly and indirectly inducing corneal epithelial wound healing *in vitro* [62, 63], highlighting their potential as a therapeutic agent.

1.5.4. Corneal Derived MSCs (CMSCs)

Each MSC niche is different, leading to a risk of cells exhibiting unexpected behaviour when transplanted into a separate tissue. Therefore, there may be therapeutic benefits to transplanting MSCs already accustomed to the corneal microenvironment, back onto the ocular surface. It has been demonstrated that when isolated and expanded *in vitro*, keratocytes from the corneal limbal stroma assume an MSC phenotype (Figure 1.4) [64-66]. Furthermore, these CMSCs show anti-inflammatory potential when co-cultured with injured corneal epithelial cells [33], can reduce corneal scarring after wounding [67], and express specific markers of the cornea when other MSC types do not [68, 69]. CMSC secreted exosomes have also demonstrated the capacity to accelerate corneal epithelial wound healing [45]. In addition to therapeutic benefits, CMSCs can be isolated from corneoscleral disks, where the centre of donor cornea tissue is used for corneal transplant, and the rest of the tissue would usually be discarded. With the surplus of corneal tissue available due to the established eye banking infrastructure in the UK, corneal waste tissue offers great promise as a therapeutic MSC source for OSIDs.

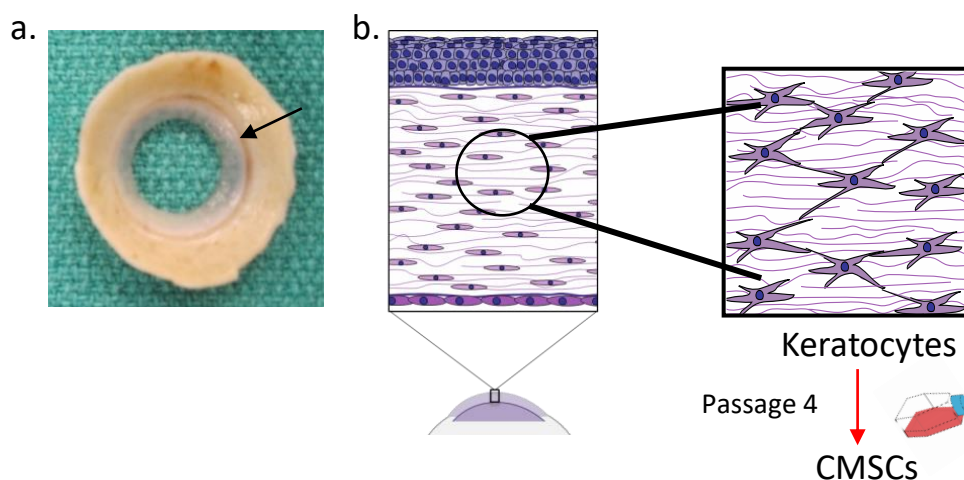


Figure 1. 4. Isolation of corneal derived MSCs (CMSCs) from the corneal limbal stroma. (a) Corneoscleral disk with centre punched out for use as a corneal transplant. Keratocytes are isolated from the limbus, depicted with an arrow. (b) Keratocytes are isolated from the central layer of the limbus called the stroma, and shift phenotype to a CMSC by passage 4 on tissue culture plastic.

1.6. Effect of culture, passage and priming of MSCs

The effect of culture and passage must be balanced when considering MSCs as a therapeutic agent. Optimally, the maintenance of MSC phenotype and behaviour is vital, however the ability to culture cells to high passage numbers allows greater opportunity for allogeneic scale-up. *In vitro* passage investigations have shown that ageing MSCs are subject to morphological changes and reduced immunomodulatory capacity with a significant reduction in release of trophic factors such as VEGF [70, 71]. This has led to the use of innovative culture techniques such as the Quantum[®] holo fibre bioreactor, to culture a greater number of cells without adverse changes [72]. Optimisation of culture medium should also be performed as different media have been shown to affect the phenotype of initially identical cell populations [68].

Priming, or 'licensing' of the cells, with *in vitro* application of cytokines such as IFN- γ has been shown to improve immunosuppressive capacity and pharmaceutical utility [73]. Although the mechanisms are not fully elucidated, suggested explanations include the upregulation of IDO, the clustering of MHC and co-inhibitory molecules, and epigenetic changes [74, 75]. Additionally, preconditioning of MSCs with the bacterial mitogen, lipopolysaccharide (LPS), enhances the paracrine protective effects and regenerative capacity of the cells [76], through interaction with toll-like receptor 4 (TLR4), leading to increased release of the regenerative factors, vascular endothelial growth factor (VEGF) and hepatocyte growth factor (HGF) [77]. These regenerative features have been associated with high levels of immunoplasticity in MSCs based on TLR4 activation, with 24 hour stimulation demonstrating reduced cellular anti-inflammatory properties, compared to 48 hour exposure to lipopolysaccharides (LPS), where MSCs increased their immunosuppressive capacity on T cell proliferation [78]. Additionally, priming the cells through hypoxia treatment and activation of the MSC nucleotide binding domain, as well as techniques including gene modification, have been shown to improve therapeutic potential [79].

1.7. Application of MSCs to the ocular surface: Topical vs. alternative methods

In contrast to developing stem cell therapies for internal organs, the location of the ocular surface makes it an ideal candidate for the non-invasive topical application of stem cells. The advantages of topical application of MSCs, in a similar manner to that discussed for skin healing [80, 81], include: the ability to deliver a concentrated population of cells to a small area without relying on cell homing mechanisms; the immediate delivery of paracrine signalling molecules to the target area, allowing for more rapid healing; the potential to remove the cells after healing if adhered to a delivery vehicle, potentially avoiding allogeneic rejection; and the less invasive nature of the treatment, delivered within a clinic setting rather than surgically.

Topical delivery of MSCs has potential for enhanced therapeutic capacity, supported by *in vitro* studies showing increased suppression of T-lymphocytes and corneal wound healing with direct MSC contact, compared to MSC paracrine factors alone in culture medium [82, 83]. When applied systemically, MSCs often become entrapped in the pulmonary circulation, and although still able to generate ameliorating effects on distant organs through paracrine signalling [27], may be more efficacious at the site of healing.

For the eye, subconjunctival injection has demonstrated success at alleviating disease in multiple ocular surface disorder models, including GVHD [84] and in corneal injury [85], where sub-conjunctival injection was deemed more effective than systemic and topical application. However, it is important to note that in this study the cells applied topically were not incorporated into a scaffold to hold them in place and would likely have been expelled through lachrymation and blinking. Consequently, for topical application of MSCs at the site of injury to be efficacious, a cell carrying scaffold is required to ensure persistence of cells placed directly into the toxic microenvironment of an injured ocular surface.

Although potentially overlooked, the choice of delivery substrate/scaffold may have a significant impact on the eventual therapy, with evidence demonstrating a 5-fold increase of factors such as HGF and Intercellular Adhesion Molecule 1 (ICAM-1)

when MSCs were cultured on 3D fibre matrices compared to 2D culture dishes, promoting faster epithelialisation and reduced scarring [86].

1.8. Potential substrates and scaffolds for topical application of MSCs to the ocular surface

Amniotic membrane (AM) is often the substrate of choice for any delivery of cells to the ocular surface, due to its long history of use within the field. AM is the translucent, inner foetal layer, lining the amniotic cavity with demonstrated low immunogenic, anti-scarring and anti-inflammatory properties [87]. For example, AM alone has the potential to induce rapid apoptosis in adhered, inflammatory cells, including T-lymphocytes and macrophages in corneas of herpetic stromal keratitis mouse models [88]. AM can be optimally preserved through freezing or drying to maintain the structural and biochemical properties [89], before cells are seeded and the structure glued or sutured into place [90]. Alternative, sutureless methods have been investigated, such as application via ProKera [91], or application using bandage contact lenses [92]. AM in combination with MSCs has been shown to provide a beneficial, additive effect, demonstrated in a chemical burn rat model where injury was significantly improved [93]. However, inter and intra donor variation, and risk of disease transmission represent a lack of standardization.

Alternative to AM, the use of both natural and synthetic hydrogels may offer more consistency, easier manufacturing, cost effectiveness and potentially simpler application, as they can be manufactured as soft contact lenses (SCL). Hydrogels are three-dimensional, polymer networks, with elastic properties and open systems for substance exchange (Figure 1.5) [94]. By definition, at least 10% water must constitute the weight or volume of the hydrogel, with the network hydrophilicity due to hydrophilic groups including $-NH_2$, $-COOH$, $-OH$, $-CONH_2$, $-CONH-$ and $-SO_3H$ [95]. Most research investigating stem cell-hydrogel applications are designed with the primary intention to bioengineer an entire new epithelial layer for transplantation to treat LSCD. Lace *et al.* (2021) [96] developed a tunable poly ϵ -lysine hydrogel, with the capacity for corneal epithelial and stromal cell growth and

integration, which could be used as an alternative material for a corneal transplant. Furthermore, poly- ϵ -lysine and functionalised poly- ϵ -lysine hydrogels, have demonstrated cell adhesion [97] and amoebicidal activity against *Escherichia coli*, *Staphylococcus aureus*, *Pseudomonas aeruginosa* and *Acanthamoeba castellanii* [98, 99]. This demonstrates great translational potential for regenerative medicine strategies, due to the dual behaviour displayed, of cell scaffold and amoebicidal agent. Alternatively, Gu *et al.* [100] incorporated MSCs within a fibrin hydrogel for ocular surface transplantation and demonstrated improvement of corneal injury. It is likely the therapeutic effect seen in this study was a result of MSC immunomodulation, supported by data demonstrating that MSCs have the capacity to secrete paracrine signals when incorporated into a hydrogel [101]. It has also been shown that the combination of a topical polysaccharide hydrogel and sub-conjunctival injection of BM-MSCs performed additively to enhance corneal epithelial cell recovery and corneal clarity in a rat model of alkali burn, reinforcing the idea that the choice of substrate is as important as the stem cell [102].

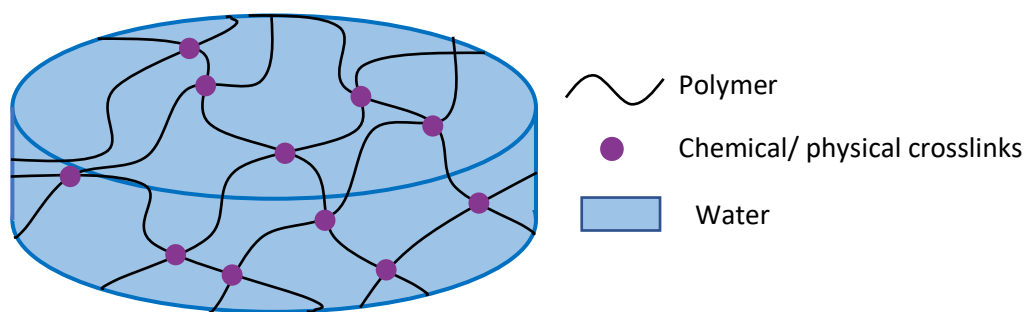


Figure 1. 5. Schematic of a hydrogel. Three dimensional network of hydrophilic polymer chains with chemical or physical crosslinks for structural integrity, with water constituting at least 10% of weight or volume [95].

Synthetic hydrogel bandage SCLs are currently used to protect the corneal surface in combination with the delivery of pharmacological or biological therapeutics [103]. Most are composed of a siloxane hydrogel [104], and hold desirable qualities, whilst the absence of protein reduces the risk of allogeneic rejection or disease

transmission [105], and their shape allows self-maintenance on the cornea. To avoid the undesirable effects of corneal epithelial cell attachment and protein fouling when placed on the ocular surface, SCL materials rarely contain cell adhesion motifs, and consequently must be functionalized to behave as a cell delivery device; these can be provided by integrin binding sites from serum, NIH/3T3 feeder layers and surface plasma polymerization with acid groups [106-108].

Three-dimensional scaffolds produced via electrospinning have a large surface area, with the nanofibers arranged to imitate extracellular matrix proteins. MSCs have been demonstrated to attach and proliferate effectively on these scaffolds, and when applied to the cornea aid healing and regeneration [52, 109]. Melt electro writing has also been applied for corneal applications, which is an innovative technique combining electrospinning and 3D printing [110]. Data demonstrated improved collagen deposition of CMSCs in an orthogonal, 3D arrangement, more akin to the corneal stroma than other electrospinning methods. Further modification of the polymers to allow for the possibility of cell detachment has also been explored with thermoresponsive, electrospun scaffolds for the culture of CMSCs [111, 112]. However, the invasive procedure of suturing the scaffold to the ocular surface seems unfavourable compared to non-surgical alternatives.

1.9. Soft Contact Lenses for Topical Application of Stem Cells

Critical components for consideration in the manufacture of therapeutic SCLs include oxygen permeability, mechanical strength for ease of handling, comfort, optical clarity, and resistance to tear film component deposition [113]. To address these points from a material perspective, wettability, lens thickness, water content, oxygen permeability, mechanical properties, and finally potential for functionalisation of the chosen polymer hydrogel material need to be considered [113] (Figure 1.6). Stronger emphasis on specific parameters may be required, dependent on the therapeutic use of the lens.

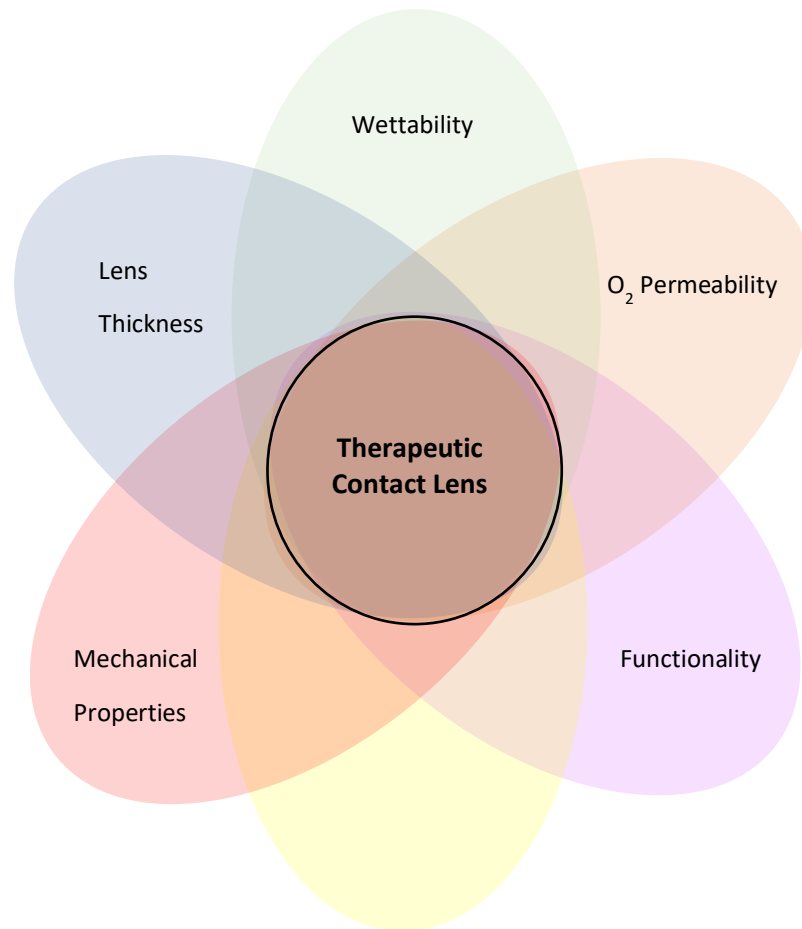


Figure 1. 6. Parameters for consideration when developing a therapeutic contact lens. From a material perspective, wettability, lens thickness, mechanical properties, H₂O content, O₂ permeability and functionality must be considered for development of the optimal therapeutic lens. Figure adapted from Musgrave and Fang (2019) [113].

1.10. SCL Composition

Current SCLs are predominantly constructed from either poly(2-hydroxyethyl methacrylate) (poly(HEMA)) hydrogels or silicone containing products. Poly(HEMA) SCLs are highly biocompatible, flexible hydrogels, with slight crosslinking and the capacity to retain large volumes of water [114]. The high water volume allows oxygen to dissolve and diffuse to the ocular surface. These were the first SCLs produced, providing an excellent starting material as interest in SCLs for therapeutic use began to rise. One limitation with poly(HEMA) as a hydrogel is the hypoxia linked adverse effects resulting from extended wear. Consequently, SCLs have been produced based on the highly oxygen permeable silicone group (-Si(CH₃)₂-O-) [104].

Although oxygen permeability was increased with these lenses, other factors including lubricity were compromised due to the highly hydrophobic nature of the polymer. Silicone-based lenses were then combined with more hydrophilic compounds and wettable agents, such as hydroxyethyl methacrylate (HEMA), N-vinylpyrrolidone, and methacrylic acid. These copolymer hydrogels encompass the high oxygen permeability provided by the silicone elastomer and the ion and water permeability of the hydrophilic component. This has formed the basis for the composition of siloxane and fluorosiloxane SCLs which were approved by the FDA for extended wear of up to 30 days in 2001 [115].

Available SCLs possess certain advantages and limitations highlighted in Table 1.1., however differing SCL materials may be better suited to specific therapeutic options of SCLs. In addition to consideration of treatment time and increased comfort for avoidance of further irritation to an injured cornea, it may be important to consider the optimal material for functionalisation for drug delivery or cell attachment and interaction for regenerative medicine strategies.

Table 1. 1. Advantages and limitations of poly(HEMA) vs siloxane hydrogels for contact lens materials [113].

	Advantages	Limitations
Poly(HEMA) Hydrogel	Increased water content increases oxygen transmission	Increased water content decreases comfort
	Lower modulus	More difficult to handle
	Good biocompatibility	Low oxygen transmission- too low for continuous wear
	Reduced bacterial adherence	Increased incidence of wear related complications including corneal neovascularization, corneal edema, and limbal hyperemia
	Inexpensive	Reduced comfort
Siloxane Hydrogel	Increased oxygen permeability	Hydrophobia
	Reduction in wear related complications including corneal neovascularization, corneal edema, and limbal hyperemia	Like other lenses, subepithelial infiltrates, limbal redness, conjunctivitis, keratitis and corneal ulcers can occur with these lenses, just like any other lens
	More resistant to protein deposits	Increased protein absorption
	Easier to handle due to more rigid structure	More rigid structure
	Less prone to drying	Increased lipid deposition
	Less susceptible to degradation over time	Increased bacterial adherence
	Improved comfort	More expensive
	Preferred mode of therapeutic contact lens wear	Requires surfactants to lower surface tension and increase wettability
Been used therapeutically for complications including recurrent epithelial erosions, abrasions, bullous keratopathy		

1.11. Therapeutic applications of SCLs

The main uses for therapeutic SCLs are for reduction in ocular pain, maintenance of corneal epithelial hydration, mechanical protection, drug delivery and for the promotion of corneal healing [52].

1.11.1. Biological Bandage

Applying a bandage to an injury is a well-accepted and utilised method to promote wound healing and to create a barrier to external complications. This strategy can be applied to the ocular surface with the use of SCLs, which can provide mechanical protection, provide structural support, control corneal hydration, and relieve pain through protection of free nerve endings [53]. In clinical trials, these have been proven efficacious for a plethora of corneal complications, including corneal ulcers, bullous keratopathy, corneal perforation and filamentary keratitis [54]. This biological bandage therapeutic effect can be augmented through its manipulation for drug delivery or regenerative medicine strategies.

1.11.2. Drug Delivery

Bioavailability at the ocular surface is extremely poor, predominantly due to the primary function of the tear fluid and blink response to create a barrier to external exogenous agents [55]. Consequently, research into scaffolds for the controlled delivery of drugs is common, with SCLs used in a variety of cases. This includes both lenses made up from silicone or poly(HEMA), loaded with drugs including timolol and betaxolol [56], [57] and modified for improved drug retention and release through strategies such as vitamin loading [58], nanoparticle embedding [59] and molecular imprinting [60]. Furthermore, functionalisation of hydrogels has been utilised to improve the therapeutic capacity of the lens. For example, copolymerisation of glycidyl methacrylate with HEMA and grafted with β -cyclodextrin improved drug loading by 1300%, with sustained drug delivery of up to two weeks [61].

Overall, SCLs offer a successful approach for drug elution at the ocular surface, with the potential for improved efficacy through material modification.

1.11.3. Regenerative medicine potential

The main aim to increase bioavailability and therefore efficacy of drugs using SCLs is mirrored with regard to topical stem cell application, where the increased cell to cell contact time could improve the therapeutic outcome.

Although the extreme hydrophilicity of poly(HEMA) and therefore its prevention of protein fouling and cell adhesion is optimal for a normal contact lens, these properties add complexity to its potential as a therapeutic cell scaffold. Not only is it used as a lens, but also regularly used to coat biomedical implants to prevent cell attachment, including ventricular catheters [62]. Consequently, strategies must be taken to increase the potential of a device to facilitate cell growth. For example, Kushnerev *et al.* (2016) [34], [35] soaked the undefined lens material in fetal bovine serum (FBS) for three hours prior to cell seeding, with the addition of ECM proteins providing adhesion motifs for integrin binding and cell attachment [63]. Although effective, this method has major drawbacks for clinical application due to the concerns surrounding use of FBS including batch-to-batch variability and risk of disease transmission.

Siloxane hydrogels may provide easier cell attachment due to the hydrophobic silicone monomer, supported by a significant increase in cell surface adhesion and spreading when HEMA was copolymerised with hydrophobic methyl methacrylate groups [64]. This is due to the increased hydrophobicity increasing the adsorption of fibronectin to the copolymer surface, providing a peptide motif for cell adhesion. However, copolymerisation with hydrophobic units can have effects on the bulk properties of the gel, including reduced swelling. Therefore, other functionalisation methods for cell attachment to hydrogels have been investigated, which would likely be translatable to hydrogel contact lenses.

1.12. Functionalisation of hydrogels with surface peptides for cell adhesion

To provide biofunctionality to synthetic materials, such as SCLs, ECM proteins and their derived synthetic peptide motifs are regularly utilised to create a more bioactive hydrogel surface [65].

1.12.1. Functionalisation of poly(HEMA) hydrogels

Poly(HEMA) hydrogels possess a high capacity for further modification, predominantly due to the hydroxyl functional groups at the polymer surface that can be used for further functionalisation. For example, Zainuddin *et al.* [66]

activated these hydroxyl groups by bromination, before using atom transfer radical polymerisation (ATRP) to covalently bind phosphate groups in the form of mono(2-methacryloyloxyethyl) phosphate (MMEP) to the hydrogel surface. This significantly increased corneal epithelial cell adhesion, proliferation and viability to a comparable level to tissue culture plastic.

As well as the hydroxyl groups of HEMA providing hydrophilicity and a potential for functionalisation, the methacrylate groups in the monomer structure allow for relatively easy free radical reactions [116]. Free radical initiation allows for chemical modification of poly(HEMA) for multiple applications, including co-polymerisation with 2-chloroquinyl methacrylate to create a drug carrier [117]; crosslinked using N,O-dimethacryloyl hydroxylamine (DMHA) to permit biodegradability [118]; and co-polymerisation with sulphated and methacrylate-modified hyaluronic acid macromers, with potential for applications including wound healing therapies [119] [120].

Poly(HEMA) has also been modified to promote cell adhesion, with laminin-derived Ac-CGGASIKVAVS-OH (SIKVAV) peptide sequences [67]. This was achieved through the copolymerisation of HEMA with the primary amine monomer, 2-aminoethyl methacrylate (AEMA), and further reacted with gamma-thiobutyrolactone to yield 2-(4-sulfanylbutanamido)ethyl methacrylate (P(HEMA-AEMA)-SH) units. SIKVAV could then be immobilised to the sulfhydryl group, which allowed for a significant increase of rat MSC attachment to the poly(HEMA) surface.

In a follow up study, MSC adhesion properties of SIKVAV were compared to fibronectin (Fn) subunits, immobilised on superporous poly(HEMA-co-AEMA) hydrogels via the maleimide-thiol coupling reaction outlined above [65]. They found significantly higher cell proliferation on the Fn-modified hydrogels, with cells spreading into a homogeneous monolayer, compared to the clustered growth on the SIKVAV-modified gel. This potentially suggests advantageous properties for Fn compared to laminin derived peptides.

IKVAV is a popular peptide, particularly because of its capacity to promote MSC differentiation into neuronal cells, however this data demonstrates it may not be a suitable substrate for the primary function of behaving as a cell adhesion motif. One of the most extensively studied cell adhesion motifs, Arg-Gly-Asp (RGD), was exposed on the Fn for cell surface integrin binding, likely contributing to the increased adhesive properties of the gel. In multiple cases of tissue engineering, incorporation of RGD has been shown to increase cell adhesion and proliferation of corneal stromal fibroblasts, which can also be defined as CMSCs [68]–[70]. However, the laminin derived Tyr-Ile-Gly-Ser-Arg (YIGSR) ligand has recently been gaining popularity in corneal tissue engineering, with both *in vitro* and *in vivo* comparative studies demonstrating enhanced CMSC proliferation, keratocyte migration and collagen 1 synthesis compared to RGD [71].

Overall, these studies demonstrate that poly(HEMA) can be readily modified for increased cell attachment, demonstrating a high potential for its use as a scaffold for the treatment of OSIDs.

1.12.2. Functionalisation of Siloxane Hydrogels

The surface chemistry of siloxane hydrogel lenses contains stable methyl groups and therefore surface modification is challenging. Consequently, plasma polymerising the surface of the lenses for activation or prior to further optimisation is likely to hold the great potential for SCL functionalisation. Plasma polymerisation utilises electrical plasma to fragment chemical vapours into highly charged compounds, which can adhere to materials, ultimately changing the material surface chemistry [72]. This method is currently used on siloxane hydrogels and silicone contact lenses to improve the wettability of the surface, however also can be utilised for the addition of functional, cell adhesion groups.

Brown *et al.* [72] found that plasma-polymerised siloxane hydrogel lenses with acid functionality (-COOH) increased rabbit epithelial cell adhesion, with higher concentrations of functional groups resulting in a greater *in vivo* transfer of the epithelial cells to the wounded corneal bed in a rabbit model of limbal stem cell deficiency. Although not explored in the literature, the acid groups are also ideal for

N-terminal peptide binding, showing that the surface chemistry of siloxane hydrogels may not be as optimal for bioactivation in comparison to poly(HEMA), however steps can be taken to increase bioconjugation potential.

1.13. MSC Therapy Limitations

MSCs from different sources, with different application routes, have shown great promise as a therapeutic cell type, with use of MSCs in 209 clinical trials since 2015 according to the US National Institute of Health–ClinicalTrials database (<http://clinicaltrials.gov>). However, only 57 of these have been classified as completed, with an additional 5 trials terminated, 7 trials suspended and 7 trials withdrawn. Of these, only 5 included results, leading to a knowledge gap, with reduced prevention of inefficacious and unnecessary clinical trials [121]. Limitations surrounding safety, efficacy and reliability of the therapies highlight the necessity for robust characterisation throughout the entirety of the therapy development, with identity, genomic integrity, sterility and purity noted by Sebastiao *et al.* as key considerations.

Limitations with characterisation exist in regenerative medicine therapies due to the vast variability at every step of the development process. Donor-to-donor variation, including age, gender, genetics, and health status all have implications on the potency of the cell (Figure 1.7), highlighting the need for robust cell screening methods [122]. The tissue source of the MSC, in addition to the cell isolation techniques, for example, enzymatic or mechanical dissociation, leads to variability, and the culture and processing have significant impact on the heterogeneity of the product. Considerations include media and reagents, confluence, culture surface, passage number, cell surface modifications in addition to cell storage including cryopreservation methods and thawing protocols. Administration causes major variation, with intravenous, subconjunctival, periorbital infections, topical administration via eye drops or variable scaffolds, and different cell buffers and therapeutic cell dosage impacting therapeutic potency. Finally, variation can also be caused by the recipient, with considerations including disease severity. The variability in cell source, application, cell dosage, cell passage, animal model, study

length and experimental findings can be found in Table 1.2. These major factors all have potential to impact the clinical outcome of the therapy, and therefore it is vital that each step is fully elucidated.

1.14. Conclusion

This introduction highlights important factors that must be considered when developing topical MSC therapies for OSIDs, including stem cell type and source; cell culture; and the choice of substrate for topical application. There are existing data demonstrating the key role of inflammation in the pathogenesis of ocular surface disorders, the awareness of MSC potent immunomodulatory capacity, and the advancements in bioengineering of scaffolds/materials for application to the ocular surface. However, there is limited research which incorporates all this information together to treat ocular surface disorders. There is scope therefore for further research into the development of a topical, anti-inflammatory, cell therapy for ocular surface disorders.

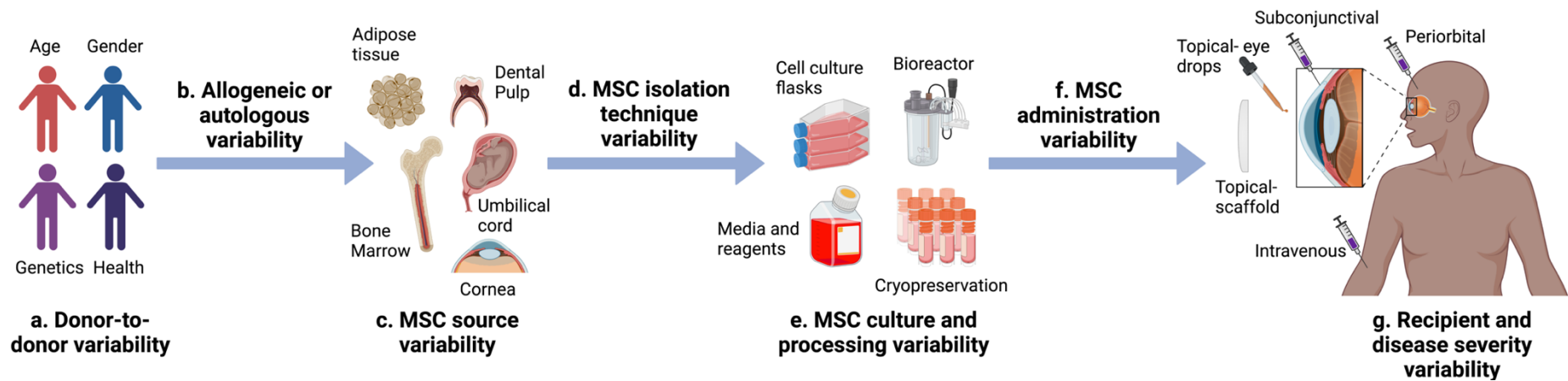


Figure 1. 7. Factors affecting the heterogeneity and clinical outcomes of MSC therapy to the eye. (a) Donor-to-donor variability caused by age, gender, genetics and health status. (b) Allogeneic or autologous therapeutic choice will impact clinical outcomes. (c) MSCs isolated from different tissues display different characteristics, impacting potency. (d) Isolation of MSCs can occur through enzymatic or mechanical debridement. (e) Variation exists in methods for MSC processing, culture and storage, including cell culture vesicles and reagents, and cryopreservation protocols. (f) MSC product can be administered at different doses, in various buffers, through different methods including topical and injections. (g) Recipient disease stage can also cause variable clinical outcomes. Figure adapted from Levy *et al.* (2020) [122].

Table 1. 2. Details on in vivo studies using MSCs, demonstrating study variability within the literature. Colour coded based on cell administration method, with topical (red), transplantation (purple), intravenous injection (teal), subconjunctival injection (green), periorbital injection (pink) and multiple administration routes (blue).

MSC Source	MSC Application	Procedure	Cell Passage	Animal Model	Study length*	Key Findings	Reference
Human AD-MSCs	Topical	2.5E+05 cells seeded on amniotic membrane, eyelids sutures	3 to 4	Rabbit partial and total LSCD	11 weeks	MSCs migrated to inflamed tissues, reduced inflammation, inhibited neovascularisation and corneal opacification, and expressed CK3 in the corneal epithelium, demonstrating partial restoration of epithelial phenotypes.	[123]
Human AD-MSCs	Topical	1.25E+05/mm(2) cells seeded on a scleral contact lens	3	Rabbit severe acute alkaline burn	4 weeks	MSCs prevented corneal melting and symblepharon, reduced the inflammatory and fibroblastic response, and significantly reduced epithelial defects.	[124]
Human BM-MSCs	Topical	1E+05 cells/cm2 seeded on amniotic membrane and cultured to 90% confluence. Eyelids sutured for 10 day	1	Rat corneal chemical burn	4 weeks	MSCs enhanced repairment of injured ocular surface and epithelial integrity. They inhibited inflammation and inflammation-induced neovascularisation, decreasing levels of IL-2 and CD45, therefore improving transparency.	[93]

Mouse BM-MSCs	Topical	4E+04 cells on polyamide 6/12 nanofiber scaffold. Eyelids sutured closed. Also seeded with LSCs.	Unknown	Mouse corneal mechanical injury	2 weeks	MSCs significantly reduced immune response, through suppression of IFN- γ , iNOS and IL-2 gene expression in local corneal cells.	[109]
Rabbit BM-MSCs	Topical	Unknown cell dose seeded in a fibrin gel, sutured to corneal surface. Eyelids sutured for 7 days	Unknown	Rabbit corneal alkali burn	4 weeks	MSCs did not improve corneal epithelium integrity, neovascularisation or corneal opacity. They expressed CK3, demonstrating differentiation into corneal-like cells.	[100]
Rabbit BM-MSCs and AD-MSCs	Topical	3E+05 cells seeded on PLA nanofiber scaffold, sutured to the conjunctiva. Eyelids closed.	3	Rabbit corneal alkali burn	15 days	MSCs caused suppression of MMP9 and iNOS, reduced levels of α SMA, TGF-B and VEGF, leading to reduced corneal opacification, neovascularisation and corneal thickness.	[52]
Rat MSC line. Source unknown.	Topical	2E+06 cells in media applied for 2 hours a day for 3 consecutive days. Eyelids sutured.	Unknown	Rat corneal chemical burn	3 weeks	MSCs- anti-inflammatory potency through IL-6 suppressing maturation of DCs, and anti-angiogenic through upregulation of TSP-1.	[38]
Human and mouse CMSCs	Topical	5E+03 cells in a fibrinogen (Ethicon) gel, eyelids sutured	3	Mouse pathologic corneal vascularisation	3 days	Inhibition of corneal neovascularisation, likely through secreted sFLT-1 and PEDF	[125]
Rabbit CMSCs	Topical	0.5E+05 cells/cm ² on human AM. Also seeded with LSCs. AM sutured into place.	3/4	Rabbit epithelial debridement and limbal keratectomy	12 weeks	MSCs promoted epithelialisation, however neovascularisation was seen when L-MSCs were applied without LESC. Cell did not migrate into the healing epithelium.	[126]

Human immature DPSCs	Topical	Cell sheet held in place with sutured amniotic membrane	6 to 7	Rabbit mild and severe chemical induced LSCD	3 months	MSCs lead to reconstruction of the corneal epithelia in the mild model, but not severe. Cells in both models adopted an epithelial-like phenotype.	[61]
Rabbit BM-MSCs	Transplantation	Confluent monolayer-temperature responsive membrane or fibrin glue 2E+05 cells/ml with fibrin glue	2	Rabbit chemically damaged cornea	60 days	MSCs transplanted with membrane and fibrin glue enhanced reepithelialisation and restored corneal homeostasis, compared to corneal damage alone.	[127]
Human BM-MSCs	Intravenous injection	1E+06 cells in balanced salt solution	2	Mouse suture induced corneal neovascularisation	1 week	MSCs reduced neovascularisation, through a TSG-6 dependent mechanism. They reduced inflammation through reduction of IL-1B, IL-6 and TNF-a and suppression of infiltrating immune cells.	[42]
Mouse BM-MSCs	Intravenous injection	5E+05 cells in saline.	2	Mouse corneal mechanical injury	3 days	MSCs lead to increased levels of HGF at the ocular surface, which helped to restore corneal transparency and suppress TGF-B-induced α SMA expression.	[41]
Mouse BM-MSCs	Intravenous injection	1E+06 cells	5 to 6	Mouse corneal transplant model	2 weeks	MSCs homed directly to the inflamed ocular surface, inhibited APC maturation, suppress allosensitization and promote allograft survival.	[32]
Mouse BM-MSCs	Intravenous	0.5 E+06 cells in 100 μ L sterile saline	2/3	Mouse corneal transplant model	8 weeks	MSCs regulate adaptive immunity through promoting Treg suppressive function during allogeneic transplantation, and MSC CD80 expression improves corneal allograft	[128]

						survival.	
Rat BM-MSCs	Intravenous injection	1E+06 cells in PBS	2	Rat high-risk corneal transplant model	37 days	MSCs increased rejection-free survival, reducing inflammation through increasing regulatory T cells and release of immunomodulatory mediators including PGE2.	[129]
Rabbit AD-MSCs	Intravenous injection	2E+06 cells in HBSS. 4 injections; D-7, D0, D3 and D14-15	3 to 4	Rabbit high-risk corneal allograft rejection model	19 days	MSCs did not home to cornea or engraft. MSCs increased oedema and neovascularisation and had no effect on infiltration of immune cells.	[55]
Rat activated omental cells (AOCs) and AD-MSCs	Subconjunctival Injection	0.5E+06 cells in saline	AOCs- 0 AD-MSCs- 3	Rat corneal alkali burn	90 days	AOC and AD-MSc groups showed significantly lower neovascularisation than the control group, however no difference was observed between the 2 cell types.	[130]
Human BM-MSCs	Subconjunctival injection	2E+05 cells in PBS	3	Mouse GVHD	18 days	MSCs did not engraft but prevented T lymphocyte infiltration and reduced inflammatory gene markers <i>TNFα</i> , <i>PAX6</i> and <i>Spr1b</i> and reduced keratinization of the cornea.	[84]
Mouse BM-MSCs	Subconjunctival injection	5E+04 cells in PBS	3 to 5	Diabetic mouse model of corneal epithelial injury	3 days	Homing of MSCs to wound edge of cornea, with TSG-6 secretion responsible for enhanced wound healing, increased epithelial stem cell proliferation, and reduction of inflammatory infiltrates and inflammatory markers; MPO, TNF- α	[106]

						and IL-1 β .	
Rat BM-MSCs	Subconjunctival injection	2E+06 cells in PBS	2 to 6	Rat corneal alkali burn	1 week	MSCs accelerated corneal epithelial recovery, inhibited neovascularisation, and demonstrated ant-inflammatory properties through inhibition of MIP-1a in local corneal cells, reduced macrophage infiltration and reduced TNF-a.	[40]
Rat BM-MSCs	Subconjunctival injection	2E+06 cells in PBS. Used polysaccharide hydrogel as bandage.	3	Rat corneal alkali burn	4 weeks	MSCs promoted epithelial recovery, corneal clarity, reduced neovascularisation, and reduced MIP-1a and MCP-1. All results were enhanced with hydrogel.	[102]
Rat BM-MSCs	Subconjunctival Injection	2E+06 cells in 0.1 ml	3	Rat ocular alkali burn	14 days	MSCs pre-stimulated with TNF- α showed enhanced anti-inflammatory and anti-fibrotic effect, compared to unstimulated MSCs.	[131]
Human and mouse BM-MSCs	Periorbital injection	1E+03 or 1E+05 cells in balanced salt solution	2	Mouse inflammation-induced dry eye	1 week	MSCs did not engraft, but increased tear production, reduced CD4+ IFN γ secreting cell infiltration and restored goblet cells in the conjunctiva.	[53]
Rabbit AD-MSCs	Multiple	2E+06 cells in 0.5 ml PBS	3/4	Rabbit corneal alkali burn	28 days	MSC treated groups showed increased central corneal sensitivity and reduced pathological vascularisation, compared to PBS only controls.	[132]

Mouse BM-MSCs	Multiple	5E+05 cells in PBS	3	Mouse corneal mechanical injury	4 days	MSCs administered through intravenous and subconjunctival injection significantly reduced inflammation, corneal opacity, and fibrosis, and restored epithelial integrity and tissue architecture. No significant difference observed for topical and intraperitoneal administration.	[85]
Human UC-MSC	Multiple	2E+04 cells in alphaMEM (intrastromal injection) 2E+04 cells in a fibrin gel carrier	Unknown (after P4)	Mouse keratectomy wound	2 weeks	MSCs increased corneal transparency and increase collagen fibre organisation.	[133]
Human UC-MSCs	Multiple	2E+06 cells in PBS	5	Rabbit corneal alkali burn	4 weeks	MSCs lead to reduced neovascularisation, corneal opacification, and VEGF and α SMA in the cornea. They also resulted in increased re-epithelialisation and proliferation of keratocytes.	[134]

1.15. Thesis hypotheses, aims and objectives

Overarching aim:

Contribute towards the development of a topical cell therapy for ocular surface disorders, utilising CMSCs as a therapeutic agent, adhered to a contact lens for administration.

The project's hypotheses and main objectives may be summarised as:

1. Hypothesis: CMSCs in *in vitro* culture will show signs of aging which would have a detrimental impact on their potency and scale up potential as a therapeutic.
 - Aim: To determine an optimal therapeutic passage of CMSCs. This was assessed through phenotypic, genotypic and secretomic analysis, in addition to investigating cell growth over increasing passages.
2. Hypothesis: Donor-to-donor variations exist for CMSCs, which will impact the final cell product.
 - Aim: To expand on the phenotypic analysis of CMSCs, to identify key donor-to-donor variations, and identify key markers homogeneously expressed across markers. This was achieved using the BD Human Cell Surface Lyoplate.
3. Hypothesis: CMSCs and BM-MSCs will have common and differentially expressed phenotypic and genotypic markers.
 - To compare both phenotype and genotype of CMSCs with BM-MSCs- the current 'gold-standard' source for MSC therapy, in order to deduce the feasibility of CMSC use. This was achieved using the BD Human Cell Surface Lyoplate and the Qiagen RT² Profiler PCR Array for wound healing markers.

4. Hypothesis: Properties and behaviour of CMSCs will change in an *in vitro* inflammatory environment compared to normal cell culture.

- Aim: To determine the potential of CMSCs as a therapeutic tool in an *in vitro* inflammatory environment, mimicking an injured ocular surface. This was achieved through assessment of the survival, secretome, and genotypic and phenotypic changes of CMSCs when exposed to a cocktail of a bacterial mitogen. and inflammatory factors.

5. Hypothesis: CMSCs will adhere to a contact lens functionalised with cell adhesive motifs.

- Aim: To develop a peptide-functionalised poly(HEMA) soft contact lens for CMSC attachment, for future use as a cell delivery vehicle to an injured ocular surface. This was primarily assessed through confocal imaging of cells seeded on different hydrogels.

CHAPTER 2: Materials and Methods

2.1. Materials

This section describes the source of the cells, chemicals and materials used throughout the thesis.

2.1.1. Cells

2.1.1.i. Human Corneal Mesenchymal Stromal Cells

Human corneal stromal mesenchymal stromal cells (CMSCs) are primary stromal cells isolated from human corneoscleral rims; defined as a ring from the corneoscleral disc, with previous dissection of 8 mm of the central cornea for corneal grafting [64]. All human corneas were obtained anonymised from Nottingham University Hospitals and all tissue handling was performed under the tenets of the Human Tissue Act, under research licence held by the University of Nottingham. Details on gender, and age of donors was not obtained. The extracted cells originally express a quiescent, keratocyte phenotype, which shifts to a mesenchymal stromal cell phenotype by passage 4 on tissue culture plastic in certain media [64]. These properties have increased the interest in the cells for research over the past 10 years, expanding the body of cell characterisation data [68, 125, 135, 136].

2.1.1.ii. Human Bone Marrow Stromal Cells

Human bone marrow stromal cells (BM-MSCs) are primary stromal cells isolated from bone marrow. Cells were isolated from healthy donors and purchased from Lonza (PT-2501). Bone marrow was the first tissue source for mesenchymal stromal cell isolation, making them the 'gold standard' regarding cell characterisation and potential for use in therapies.

2.1.1.iii. Immortalised Human Corneal Epithelial Cells

Human corneal epithelial HCEC2 cells are a cell line generated through immortalisation of normal human corneal epithelial cells with Adenovirus 12 - SV40 virus hybrid (Ad12-SV40). In culture, they demonstrate a cobblestone like

appearance, similar to normal corneal epithelial cells, with maintenance of corneal, epithelial features, including desmosome formation and development of microvilli [137]. Cells were kindly gifted from Imran Mohammad at the University of Nottingham, originally purchased from ATCC (CRL-11135).

2.1.2. General Chemicals

This section outlines the general chemicals used throughout the project. All chemicals were purchased from Merck (Sigma-Aldrich) unless otherwise stated. Sterility of cell culture medium and chemicals was achieved through use of 0.22 µm filters or by autoclaving for 1 hour at 121°C.

2.1.2.i. Knockout Serum Replacement

Medium for CMSC culture was supplemented with knockout serum replacement (KSR), purchased from Gibco, ThermoFisher Scientific. This was chosen to reduce the risk of batch-to-batch variation resulting from serum, in addition to moving towards a xenofree cell culture protocol for easier translation to clinic.

2.1.2.ii. Antibodies

Primary antibodies and the fluorescently tagged Alexa Fluor secondary antibodies utilised for immunocytochemistry (ICC) are included in Table 2.1 and 2.2 respectively. Fluorescently conjugated antibodies utilised for flow cytometry are listed in Table 2.3. Antibodies in the BD Human Cell Surface Marker Screening Panel are listed in Table 2.4.

Table 2. 1. Primary antibodies used for immunocytochemistry (ICC) including antigen, source, species and working dilution.

Primary Antibodies for ICC			
Antigen	Source	Species	Working Dilution
CD105	R&D Systems	Goat	1:200
CD90	Thermo Fisher Scientific	Mouse	1:200
CD73	Thermo Fisher Scientific	Rabbit	1:200
CD34	Sigma Aldrich	Mouse	1:200
SSEA-4	R&D Systems	Mouse	1:100
ABCG2	R&D Systems	Mouse	1:200
α -SMA	LSBio	Mouse	1:200
Oct-4A	R&D Systems	Mouse	1:100
ALDH3A1	Sigma Aldrich	Rabbit	1:200
Vimentin	Vector	Mouse	1:100

Table 2. 2. Secondary antibodies used for immunocytochemistry (ICC) including Alexa Fluor, source and working dilution.

Secondary Antibodies for ICC			
Antibody	Alexa Fluor	Source	Working Dilution
Anti-Mouse IgG	488	Life Technologies, ThermoFisher Scientific	1:300
	594	Life Technologies, ThermoFisher Scientific	1:300
Anti-Rabbit IgG	488	Life Technologies, ThermoFisher Scientific	1:300
	546	Life Technologies, ThermoFisher Scientific	1:300
Anti-Goat IgG	546	Life Technologies, ThermoFisher Scientific	1:300

Table 2. 3. Conjugated antibodies used for flow cytometry including antigen target, source, conjugated fluorophore and working dilution.

Fluorescently Conjugated Antibodies for Flow Cytometry			
Antigen	Source	Conjugated Fluorophore	Working Dilution
CD105	ThermoFisher Scientific	PE	1:20
CD90	ThermoFisher Scientific	PE-Cy5	1:20
CD73	ThermoFisher Scientific	PE	1:20
CD34	ThermoFisher Scientific	FITC	1:20
SSEA-4	ThermoFisher Scientific	PE	1:20
CD338	ThermoFisher Scientific	PE	1:20
Ki67	ThermoFisher Scientific	FITC	1:20

Table 2. 4. Specificity, clone and isotype of antibodies in the BD Human Cell Surface Marker Screening Panel. Table from the BD Lyoplate Technical Data Sheet.

Plate 1								
Specificity	Clone	Isotype	Specificity	Clone	Isotype	Specificity	Clone	Isotype
CD1a	HI149	Ms IgG 1, k	CD28	L293	Ms IgG 1, k	CD51/61	23C6	Ms IgG 1, k
CD1b	M-T101	Ms IgG 1, k	CD29	HUTS-21	Ms IgG 2a, k	CD53	HI29	Ms IgG 1, k
CD1d	CD1d42	Ms IgG 1, k	CD30	BerH8	Ms IgG 1, k	CD54	LB-2	Ms IgG 2b, k
CD2	RPA-2.10	Ms IgG 1, k	CD31	WM59	Ms IgG 1, k	CD55	JA10	Ms IgG 2a, k
CD3	HIT3a	Ms IgG 2a, k	CD32	FL18.26	Ms IgG 2b, k	CD56	B159	Ms IgG1, k
CD4	RPA-T4	Ms IgG 1, k	CD33	HIM3-4	Ms IgG 1, k	CD57	NK-1	Ms IgM, k
CD4v4	L120	Ms IgG 1, k	CD34	5B1	Ms IgG 1, k	CD58	1C3	Ms IgG 2a, k
CD5	L17F12	Ms IgG 2a, k	CD35	E11	Ms IgG 1, k	CD59	p282 (H19)	Ms IgG 2a, k
CD6	M-T605	Ms IgG 1, k	CD36	CB38 (NL07)	Ms IgM, k	CD61	VI-PL2	Ms IgG 1, k
CD7	M-T701	Ms IgG 1, k	CD37	M-B371	Ms IgG 1, k	CD62E	68-5H11	Ms IgG 1, k
CD8a	SK1	Ms IgG 1, k	CD38	HIT2	Ms IgG 1, k	CD62L	Dreg 56	Ms IgG 1, k
CD8b	25T8.5H7	Ms IgG2a, k	CD39	TU66	Ms IgG2b, k	CD62P	AK-4	Ms IgG 1, k
CD9	M-L13	Ms IgG 1, k	CD40	5C3	Ms IgG 1, k	CD63	H5C6	Ms IgG 1, k
CD10	HI10a	Ms IgG 2a, k	CD41a	HIP8	Ms IgG 1, k	CD64	10.1	Ms IgG 1, k
CD11a	G43-25B	Ms IgG 2a, k	CD41b	HIP2	Ms IgG 3, k	CD66 (a,c,d,e)	B1.1/CD66	Ms IgG 2a, k
CD11b	D12	Ms IgG 2a, k	CD42a	ALMA.16	Ms IgG 1, k	CD66b	G10F5	Ms IgM, k
CD11c	B-ly6	Ms IgG 1, k	CD42b	HIP1	Ms IgG 1, k	CD66f	IND10	Ms IgG 1, k
CD13	WM15	Ms IgG 1, k	CD43	1G10	Ms IgG 1, k	CD69	FN50	Ms IgG 1, k
CD14	M5E2	Ms IgG 2a, k	CD44	G44-26	Ms IgG 2b, k	CD70	Ki-24	Ms IgG 3, k
CD15	HI98	Ms IgM, k	CD45	HI30	Ms IgG 1, k	CD71	M-A712	Ms IgG 2a, k
CD15s	CSLEX1	Ms IgM, k	CD45RA	HI100	Ms IgG 2b, k	CD72	J4-117	Ms IgG 2b, k
CD16	3G8	Ms IgG 1, k	CD45RB	MT4	Ms IgG 1, k	CD73	AD2	Ms IgG 1, k
CD18	6.7	Ms IgG 1, k	CD45RO	UCHL1	Ms IgG 2a, k	CD74	M-B741	Ms IgG 2a, k
CD19	HIB19	Ms IgG 1, k	CD46	E4.3	Ms IgG 2a, k	CD75	LN1	Ms IgM, k
CD20	2H7	Ms IgG 2b, k	CD47	B6H12	Ms IgG 1, k	CD77	5B5	Ms IgM, k
CD21	B-ly4	Ms IgG 1, k	CD48	TU145	Ms IgM, k	CD79b	CB3-1	Ms IgG 1, k
CD22	HIB22	Ms IgG 1, k	CD49a	SR84	Ms IgG 1, k	CD80	L307.4	Ms IgG 1, k
CD23	EBVCS-5	Ms IgG 1, k	CD49b	AK-7	Ms IgG 1, k	CD81	JS-81	Ms IgG 1, k
CD24	ML5	Ms IgG 2a, k	CD49c	C3 II.1	Ms IgG 1, k	CD83	HB15e	Ms IgG 1, k
CD25	M-A251	Ms IgG 1, k	CD49d	9F10	Ms IgG 1, k	CD84	2G7	Ms IgG 1, k
CD26	M-A261	Ms IgG 1, k	CD49e	VC5	Ms IgG 1, k	CD85	GHI/75	Ms IgG 2b, k
CD27	M-T271	Ms IgG 1, k	CD50	TU41	Ms IgG 2b, k			

Plate 2								
Specificity	Clone	Isotype	Specificity	Clone	Isotype	Specificity	Clone	Isotype
CD86	2331 (FUN-1)	Ms IgG 1, k	CD123	9F5	Ms IgG 1, k	CD172b	B4B6	Ms IgG 1, k
CD87	VIM5	Ms IgG 1, k	CD124	hIL4R-M57	Ms IgG 1, k	CD177	MEM-166	Ms IgG 1, k
CD88	D53-1473	Ms IgG 1, k	CD126	M5	Ms IgG1, k	CD178	NOK-1	Ms IgG 1, k
CD89	A59	Ms IgG 1, k	CD127	hIL-7R-M21	Ms IgG 1, k	CD180	G28-8	Ms IgG 1, k
CD90	5E10	Ms IgG 1, k	CD128b	6C6	Ms IgG 1, λ	CD181	5A12	Ms IgG 2b, k
CD91	A2MR-alpha 2	Ms IgG 1, k	CD130	AM64	Ms IgG 1, k	CD183	1C6/CXCR3	Ms IgG 1, k
CDw93	R139	Ms IgG 2b, k	CD134	ACT35	Ms IgG 1, k	CD184	12G5	Ms IgG 2a, k
CD94	HP-3D9	Ms IgG 1, k	CD135	4G8	Ms IgG 1, k	CD193	5E8	Ms IgG 2b, k
CD95	DX2	Ms IgG 1, k	CD137	4B4-1	Ms IgG 1, k	CD195	2D7/CCR5	Ms IgG 2a, k
CD97	VIM3b	Ms IgG 1, k	CD137 Ligand	C65-485	Ms IgG 1, k	CD196	11A9	Ms IgG 1, k
CD98	UM7F8	Ms IgG 1, k	CD138	Mi15	Ms IgG 1, k	CD197	2H4	Ms IgM, k
CD99	TU12	Ms IgG 2a, k	CD140a	alpha R1	Ms IgG 2a, k	CD200	MRC OX-104	Ms IgG 1, k
CD99R	HIT4	Ms IgM, k	CD140b	28D4	Ms IgG 2a, k	CD205	MG38	Ms IgG 2b
CD100	A8	Ms IgG 1, k	CD141	1A4	Ms IgG 1, k	CD206	19.2	Ms IgG 1, k
CD102	CBR-1C2/2.1	Ms IgG 2a, k	CD142	HTF-1	Ms IgG 1, k	CD209	DCN46	Ms IgG 2b, k
CD103	Ber-ACT8	Ms IgG 1, k	CD144	55-7H1	Ms IgG 1, k	CD220	3B6/IR	Ms IgG 1, k
CD105	266	Ms IgG 1, k	CD146	P1H12	Ms IgG 1, k	CD221	3B7	Ms IgG 1, k
CD106	51-10C9	Ms IgG 1, k	CD147	HIM6	Ms IgG 1, k	CD226	DX11	Ms IgG 1, k
CD107a	H4A3	Ms IgG 1, k	CD150	A12	Ms IgG 1, k	CD227	HMPV	Ms IgG 1, k
CD107b	H4B4	Ms IgG 1, k	CD151	14A2.H1	Ms IgG 1, k	CD229	Hly9.1.25	Ms IgG 1, k
CD108	KS-2	Ms IgG 2a, k	CD152	BN13	Ms IgG 2a, k	CD231	M3-3D9 (SN1a)	Ms IgG 1, k
CD109	TEA 2/16	Ms IgG 1, k	CD153	D2-1173	Ms IgG 1, k	CD235a	GA-R2 (HIR2)	Ms IgG 2b, k
CD112	R2.525	Ms IgG 1, k	CD154	TRAP1	Ms IgG 1, k	CD243	17F9	Ms IgG 2b, k
CD114	LMM741	Ms IgG 1, k	CD158a	HP-3E4	Ms IgM, k	CD244	2-69	Ms IgG 2a, k
CD116	M5D12	Ms IgM, k	CD158b	CH-L	Ms IgG 2b, k	CD255	CARL-1	Ms IgG3
CD117	YB5.B8	Ms IgG 1, k	CD161	DX12	Ms IgG 1, k	CD268	11C1	Ms IgG 1, k
CD118	12D3	Ms IgG1, k	CD162	KPL-1	Ms IgG 1, k	CD271	C40-1457	Ms IgG 1, k
CD119	GIR-208	Ms IgG 1, k	CD163	GHI/61	Ms IgG 1, k	CD273	MIH18	Ms IgG 1, k
CD120a	MABTNFR1-A1	Ms IgG 1	CD164	N6B6	Ms IgG 2a, k	CD274	MIH1	Ms IgG 1, k
CD121a	HIL1R-M1	Ms IgG1, k	CD165	SN2	Ms IgG 1, k	CD275	2D3/B7-H2	Ms IgG 2b, k
CD121b	MNC2	Ms IgG 1, k	CD166	3A6	Ms IgG 1, k	CD278	DX29	Ms IgG 1
CD122	Mik-beta 3	Ms IgG 1, k	CD171	5G3	Ms IgG2 a			

Plate 3								
Specificity	Clone	Isotype	Specificity	Clone	Isotype	Specificity	Clone	Isotype
CD279	MIH	Ms IgG 1, k	TMLP receptor	5F1	Ms IgG 1, k	Ms IgG2a IC	G155-178	Ms IgG2a
CD282	11G7	Ms IgG 1, k	v87TCR	B1	Ms IgG 1, k	Ms IgG2b IC	27-35	Ms IgG2b
CD305	DX26	Ms IgG 1, k	HPC	B89	Ms IgG1	Ms IgG3 IC	1606	Ms IgG3
CD309	89106	Ms IgG 1, k	HLA-A,B,C	G16-2.6	Ms IgG 1, k	CD19f	GoH3	Rt IgG2a, k
CD314	1D11	Ms IgG 1, k	HLA-A2	BB7-2	Ms IgG 2b, k	CD104	139-9B	Rt IgG2b, k
CD321	M.AB.F11	Ms IgG 1, k	HLA-DQ	TU169	Ms IgG 2a, k	CD120b	ITNFR-M1	Rt IgG 2b, k
CDw327	E20-1232	Ms IgG1, k	HLA-DR	G46-6 (L243)	Ms IgG 2a, k	CD132	TUGh4	Rt IgG 2b, k
CDw328	F023-420	Ms IgG 1, k	HLA-DR, DP, DQ	TU39	Ms IgG 2a, k	CD201	RCR-252	Rt IgG 1, k
CD329	E10-286	Ms IgG1, k	Invariant NK T	6B11	Ms IgG 1, k	CD210	3F9	Rt IgG 2a, k
CD335	9E2/Nkp46	Ms IgG 1, k	Disialoganglioside GD2	14.G2a	Ms IgG2a	CD212	2B6/12beta 2	Rt IgG 2a, k
CD336	P44.8.1	Ms IgG1, k	MIC A/B	64.C4	Ms IgG2a	CD267	1A1 K21 M22	Rt IgG2a, k
CD337	P30-15	Ms IgG1, k	NKBL	DX9	Ms IgG 1, k	CD294	BM16	Rt IgG 2a, k
CD338	5D3	Ms IgG 2b, k	SSFA-1	MC480	Ms IgM, k	SSFA-3	MC631	Rt IgM
CD304	Neu24.7	Ms IgG1	SSFA-4	MC813-7D	Ms IgG3	CLA	HECA-452	Rt IgM, k
gBTR	T1080.1A 31	Ms IgM, k	TRA-1-60	TRA-1-60	Ms IgM	Integrin β7	F1B504	Rt IgG 2a, k
β2-microglobulin	TU99	Ms IgM, k	TRA-1-81	TRA-1-81	Ms IgM, k	Rt IgM IC	R4-22	Rt IgM
HLTR-1	203/14F11	Ms IgG1, k	V9 23	AHUT 7	Ms IgG 1, k	Rt IgG1 IC	R3-34	Rt IgG1
CLIP	CerCLIP	Ms IgG 1, k	V9 8	JR2	Ms IgG 2b, k	Rt IgG2a IC	R35-95	Rt IgG2a
CMRF-44	CMRF44	Ms IgM, k	CD326	EBA-1	Ms IgG 1, λ	Rt IgG2b IC	A95-1	Rt IgG2b
CMRF-56	CMRF56	Ms IgG1, k	Ms IgM IC	G155-228	Ms IgM			
EGF Receptor	EGFR1	Ms IgG 2b, k	Ms IgG1 IC	MOPC-21	Ms IgG1			

2.1.3. Quantitative Reverse Transcription Polymerase Chain Reaction (RT-qPCR) Reagents

RT-qPCR was carried out throughout this thesis using multiple kits, defined in Table 2.4., allowing for increased reliability and efficiency. Table 2.5. and 2.6. outline the kits and primers utilised respectively.

Table 2. 5. Kits used for RNA Isolation, cDNA synthesis and RT-qPCR.

Kit	Method	Source
RNEasy Mini Kit	RNA Isolation	Qiagen (ID: 74104)
Superscript III First Strand Synthesis Kit	cDNA synthesis	Invitrogen, ThermoFisher (ID: 18080051)
TaqMan Real-Time PCR Master Mixes	PCR	Fisher Scientific (ID: 10733457)

Table 2. 6. Table of primers used for RT-qPCR.

Gene Symbol	Protein	Source	Assay ID
ENG	CD105	ThermoFisher Scientific	Hs00923996_m1
THY1	CD90	ThermoFisher Scientific	Hs00174816_m1
NT5E	CD73	ThermoFisher Scientific	Hs01573922_m1
CD34	CD34	ThermoFisher Scientific	Hs500990732_m1
ALDH3A1	Aldehyde Dehydrogenase	ThermoFisher Scientific	Hs04464407_cn
ACTA2	α -Smooth Muscle Actin	ThermoFisher Scientific	Hs00426835_g1
GAPDH	Glyceraldehyde-3-phosphate Dehydrogenase	ThermoFisher Scientific	Hs99999905_m1

2.1.4. RT² Profiler PCR Array – Human Wound Healing

The RT² Profiler PCR Array for wound healing markers (Qiagen, Cat. No. 330231 PAHS-121ZA) was utilised for genotypic assessment of 84 key genes central to wound healing, with reference genes and controls (Table 2.7). The kits used for RNA isolation, purification, complementary DNA (cDNA) synthesis and RT-PCR are outlined in Table 2.8.

Table 2. 7. Table of primers used in the RT2 Profiler PCR Array, with gene description from the handbook provided by Qiagen (Cat. No. 330231 PAHS-121ZA).

Gene Symbol	Description
ACTA2	Actin, alpha 2, smooth muscle, aorta
ACTC1	Actin, alpha, cardiac muscle 1
ANGPT1	Angiopoietin 1
CCL2	Chemokine (C-C motif) ligand 2
CCL7	Chemokine (C-C motif) ligand 7
CD40LG	CD40 ligand
CDH1	Cadherin 1, type 1, E-cadherin (epithelial)
COL14A1	Collagen, type XIV, alpha 1
COL1A1	Collagen, type I, alpha 1
COL1A2	Collagen, type I, alpha 2
COL3A1	Collagen, type III, alpha 1
COL4A1	Collagen, type IV, alpha 1
COL4A3	Collagen, type IV, alpha 3 (Goodpasture antigen)
COL5A1	Collagen, type V, alpha 1
COL5A2	Collagen, type V, alpha 2
COL5A3	Collagen, type V, alpha 3
CSF2	Colony stimulating factor 2 (granulocyte-macrophage)
CSF3	Colony stimulating factor 3 (granulocyte)
CTGF	Connective tissue growth factor
CTNNB1	Catenin (cadherin-associated protein), beta 1, 88kDa
CTSG	Cathepsin G
CTSK	Cathepsin K
CTSL2	Cathepsin L2
CXCL1	Chemokine (C-X-C motif) ligand 1 (melanoma growth stimulating activity, alpha)
CXCL11	Chemokine (C-X-C motif) ligand 11
CXCL2	Chemokine (C-X-C motif) ligand 2
CXCL5	Chemokine (C-X-C motif) ligand 5
EGF	Epidermal growth factor
EGFR	Epidermal growth factor receptor
F13A1	Coagulation factor XIII, A1 polypeptide
F3	Coagulation factor III (thromboplastin, tissue factor)
FGA	Fibrinogen alpha chain
FGF10	Fibroblast growth factor 10
FGF2	Fibroblast growth factor 2 (basic)
FGF7	Fibroblast growth factor 7
HBEGF	Heparin-binding EGF-like growth factor
HGF	Hepatocyte growth factor (hepapoietin A; scatter factor)
IFNG	Interferon, gamma
IGF1	Insulin-like growth factor 1 (somatomedin C)
IL10	Interleukin 10
IL1B	Interleukin 1, beta
IL2	Interleukin 2

IL4	Interleukin 4
IL6	Interleukin 6 (interferon, beta 2)
IL6ST	Interleukin 6 signal transducer (gp130, oncostatin M receptor)
ITGA1	Integrin, alpha 1
ITGA2	Integrin, alpha 2 (CD49B, alpha 2 subunit of VLA-2 receptor)
ITGA3	Integrin, alpha 3 (antigen CD49C, alpha 3 subunit of VLA-3 receptor)
ITGA4	Integrin, alpha 4 (antigen CD49D, alpha 4 subunit of VLA-4 receptor)
ITGA5	Integrin, alpha 5 (fibronectin receptor, alpha polypeptide)
ITGA6	Integrin, alpha 6
ITGAV	Integrin, alpha V (vitronectin receptor, alpha polypeptide, antigen CD51)
ITGB1	Integrin, beta 1 (fibronectin receptor, beta polypeptide, antigen CD29 includes MDF2, MSK12)
ITGB3	Integrin, beta 3 (platelet glycoprotein IIIa, antigen CD61)
ITGB5	Integrin, beta 5
ITGB6	Integrin, beta 6
MAPK1	Mitogen-activated protein kinase 1
MAPK3	MAPK3 Mitogen-activated protein kinase 3
MIF	MIF Macrophage migration inhibitory factor (glycosylation-inhibiting factor)
MMP1	Matrix metalloproteinase 1 (interstitial collagenase)
MMP2	Matrix metalloproteinase 2 (gelatinase A, 72kDa gelatinase, 72kDa type IV collagenase)
MMP7	Matrix metalloproteinase 7 (matrilysin, uterine)
MMP9	Matrix metalloproteinase 9 (gelatinase B, 92kDa gelatinase, 92kDa type IV collagenase)
PDGFA	Platelet-derived growth factor alpha polypeptide
PLAT	Plasminogen activator, tissue
PLAU	Plasminogen activator, urokinase
PLAUR	Plasminogen activator, urokinase receptor
PLG	Plasminogen
PTEN	Phosphatase and tensin homolog
PTGS2	Prostaglandin-endoperoxide synthase 2 (prostaglandin G/H synthase and cyclooxygenase)
RAC1	Ras-related C3 botulinum toxin substrate 1 (rho family, small GTP binding protein Rac1)
RHOA	Ras homolog gene family, member A
SERPINE1	Serpin peptidase inhibitor, clade E (nexin, plasminogen activator inhibitor type 1), member 1
STAT3	Signal transducer and activator of transcription 3 (acute-phase response factor)
TAGLN	Transgelin
TGFA	Transforming growth factor, alpha
TGFB1	Transforming growth factor, beta 1
TGFBR3	Transforming growth factor, beta receptor III
TIMP1	TIMP metalloproteinase inhibitor 1
TNF	Tumor necrosis factor
VEGFA	Vascular endothelial growth factor A
VTN	Vitronectin
WISP1	WNT1 inducible signaling pathway protein 1

WNT5A	Wingless-type MMTV integration site family, member 5A
ACTB	Actin, beta
B2M	Beta-2-microglobulin
GAPDH	Glyceraldehyde-3-phosphate dehydrogenase
HPRT1	Hypoxanthine phosphoribosyltransferase 1
RPLP0	Ribosomal protein, large, P0
HGDC	Human Genomic DNA Contamination
RTC	RTC Reverse Transcription Control
RTC	Reverse Transcription Control
RTC	Reverse Transcription Control
PPC	Positive PCR Control
PPC	Positive PCR Control
PPC	Positive PCR Control

Table 2. 8. Kits used for RNA isolation, cdNA synthesis and RT-PCR for the RT2 Profiler Array.

Kit	Method	Source
RNEasy Mini Kit	RNA Isolation	Qiagen (ID: 74104)
RT ² First Strand Kit	cDNA synthesis	Qiagen (ID: 330401)
RT ² SYBR Green qPCR Mastermix	PCR	Qiagen (ID: 330500)
RT ² Profiler PCR Array for Wound Healing	RT-qPCR	Qiagen (ID: 330231)

2.1.5. Enzyme Linked Immunosorbent Assay (ELISA) Reagents

All reagents utilised for ELISAs were purchased from R&D systems, including the DuoSet antibodies, and the DuoSet ELISA Ancillary Reagent Kit 1 (Catalogue number: DY007), DuoSet ELISA Ancillary Reagent Kit 2 (Catalogue number: DY008) and DuoSet ELISA Ancillary Reagent Kit 3 (DY009). The contents of each kit are displayed in the Table 2.9. Table 2.10. outlines the corresponding reagent diluent (RD)- 1,2 and 3 from each kit used to make the capture antibody, detection antibody, standards and HRP solution for each antibody, in addition to the concentrations used throughout this thesis.

Table 2. 9. Reagent diluents utilised for ELISAs, including a description of the relative diluent and working concentrations.

Reagent Diluents (RDs) for ELISAs					
Name	Ancillary Duoset #	Part	Description	Diluent	Working Dilution
RD1	1	Reagent Diluent Concentrate 1	21 mL of a buffered protein base	1 x Wash Buffer	1.4:98.6
RD2	2	Reagent Diluent Concentrate 2 (10X)	2 vials (21 mL/vial) of a 10% BSA solution	Deionised Water	1:10
RD3	3	Reagent Diluent Concentrate 3 (5X)	2 vials (21 mL/vial) of a 25% Tween® 20 solution in PBS	1 x PBS	1:5
RD4	3	Reagent Diluent Concentrate 2 (10X)	2 vials (21 mL/vial) of a 10% BSA solution	Tris buffer + 0.05% Tween® 20, pH 7.2-7.4	1:100

Table 2. 10. Reagent concentrations with relative diluents utilised during ELISAs. Information provided on initial sample, capture antibodies, detection antibodies, standards, HRP and enzyme – substrate reaction time.

Reagent Concentrations and Diluents for ELISAs							
Antigen	Sample Dilution Factor	Capture Antibody Working Conc. (µg / ml)	Blocking Buffer Reagent Diluent	Detection Antibody Working Conc. in corresponding Reagent Diluent (ng / ml)	Top Standard Conc. (pg / ml)	HRP Reagent Diluent	Optimised time between colour reagent and stop solution
EGF Epithelial Growth Factor	1	4 (Coating Buffer)	RD2	50 (RD2)	250 (RD2)	RD2	20 min
FGF Fibroblast Growth Factor	1	2 (Coating Buffer)	RD2	250 (RD2)	1000 (RD2)	RD2	20 min
HGF Hepatocyte Growth Factor	4	1 (Coating Buffer)	RD2	200 (RD2)	8000 (RD2)	RD2	10 min
Hya Hyaluronan	2	0.5 (Coating Buffer)	RD3	400 (RD3)	90000 (RD3)	RD3	10 min
IDO Indoleamine 2,3-dioxygenase	2	2 (Coating Buffer)	RD2	500 (RD2)	30 (RD2)	RD2	20 min
IL-1ra Interleukin-1 Receptor Antagonist	2	10 (Coating Buffer)	RD2	100 (RD2)	2500 (RD2)	RD2	20 min
IL-6 Interleukin-6	10	2 (Coating Buffer)	RD2	50 (RD2)	600 (RD2)	RD2	20 min
IL-8 Interleukin-8	10	4 (Coating Buffer)	RD2	20 (RD4)	2000 (RD4)	RD3	5 min
PEDF Pigment Epithelium Derived	10	0.8 (Coating Buffer)	RD2	37.5 (RD2)	5000 (RD2)	RD2	10 min

Factor							
PTX-3 Pentraxin 3	2	2 (Coating Buffer)	RD2	60 (RD2)	14000 (RD2)	RD2	5 min
TGF-β1 Transforming Growth Factor Beta 1	1.4	2 (Coating Buffer)	RD3	50 (RD1)	2000 (RD1)	RD1	10 min
TSP-1 Thrombospondin 1	1	1 (Coating Buffer)	RD2	100 (RD2)	1000 (RD2)	RD2	20 min

2.1.6. Cytokines

The proinflammatory cytokines IL-1 β , TNF- α and IFN- γ , as well as the bacterial mitogen, LPS, were used throughout this study, forming the basis of the inflammatory signalling, outlined in table 2.11.

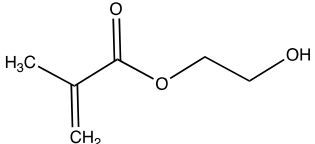
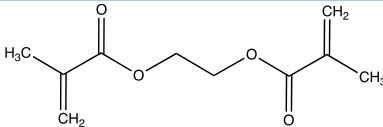
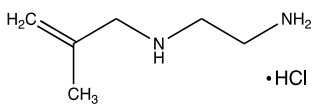
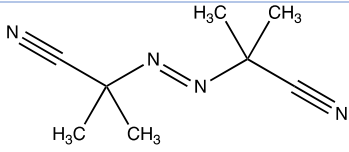
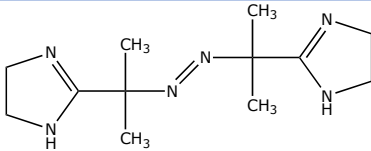
Table 2. 11. Inflammatory investigations cytokine, source and working concentration.

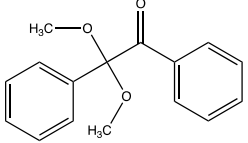
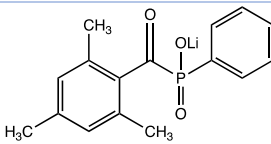
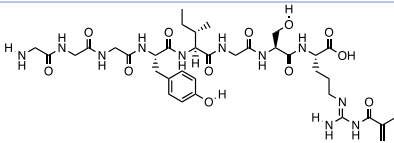
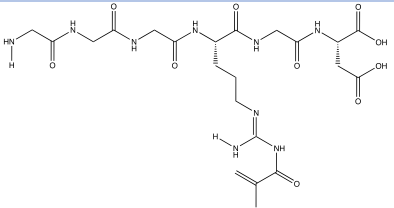
Factor	Source	Working Concentration
IL-1β Interleukin1 beta	R&D Systems (ID: 201-LB)	1 ng/mL
TNF-α Tumour Necrosis Factor Alpha	R&D Systems (ID: 10291-TA)	10 ng/mL
IFN-γ Interferon gamma	R&D Systems (ID: 10067-IF)	10 ng/mL
LPS Lipopolysaccharide	Merck (ID: 8257-67-8)	1 μ g/mL

2.1.7. Polymer Reagents

All polymer reagents are defined in Table 2.12. (Hydroxyethyl)methacrylate (HEMA) and Ethylene glycol dimethacrylate (EGDMA) were utilised due to their capacity to form a poly(HEMA-co-EGDMA) hydrogel, which has previously been well characterised as a soft contact lens [138]. The water thermal initiator, 2,2'-azobis[2-(2-imidazolin-2-yl)propane] dihydrochloride (VA-044) and the photo initiator, 2,2-dimethoxy-2-phenylacetophenone (DMPA), triggered polymerisation by free radical initiation. Functionalisation of the poly(HEMA-co-EGDMA) hydrogel was attempted with the primary amine, 2-aminoethyl methacrylate hydrochloride (AEMA); cell adherence peptide sequences with a glycine spacer and methacrylamide end group, GGGYIGSR and GGGRGD. Further detail can be found in Table 2.12.

Table 2. 12. Name, structure, molecular weight and source of materials used in polymer investigations.

Name	Acronym	Material	Structure	Mw	Source
(Hydroxyethyl)methacrylate	HEMA	Monomer		130.14 g/mol	Merck (Sigma- Aldrich) CAS: 868-77-9
Ethylene glycol dimethacrylate	EGDMA	Cross-linker		198.22 g/mol	Merck (Sigma- Aldrich) CAS: 97-90-5
2-Aminoethyl methacrylate hydrochloride	AEMA	Primary amine		164.63 g/mol	Merck (Sigma- Aldrich) CAS: 76259-32-0
Azobisisobutyronitrile	AIBN	Thermal initiator		164.21g/mol	Merck (Sigma- Aldrich) CAS: 78-67-1
2,2'-Azobis[2-(2-imidazolin-2-yl)propane]dihydrochloride	VA-044	Thermal initiator		323.27 g/mol	Merck (Sigma- Aldrich) CAS: 27776-21-2

2,2-Dimethoxy-2-phenylacetophenone	DMPA	Photo initiator		256.30 g/mol	Fisher Scientific CAS: 24650-42-8
Lithium phenyl-2,4,6-trimethylbenzoylphosphinate	LAP	Photo initiator		294.21 g/mol	Merck (Sigma- Aldrich) CAS: 85073-19-4
GGGYIGSR with N-terminal methacrylic acid	GGGYIGSR	Peptide		833.90 g/mol	Synthesised by GenScript
GGGRGD with N-terminal methacrylic acid	GGGRGD	Peptide		585/85 g/mol	Synthesised by GenScript
Resilin-like polypeptide	RLP-F/M	Peptide	Detailed in Chapter 6		Synthesised by Sai Shreedhar Patkar and Cristo Garcia from the University of Delaware

2.1.8. Resillin-Like Polypeptides (RLPs)

RLPs were synthesised by Cristobal Garcia and Sai Shreedhar Patkar from Prof. Kristi Kiick's group at the University of Delaware, USA. The RLP sequence was a 24 kDa polypeptide with 12 repeats of the amino acid sequence (GGRPSDSF/MGAPGGGN) five repeats of lysine-rich domains (GGKGGKGGKGG) for RLP functionalization, an MMP-sensitive domain (GPQGIWGQG) derived from α (I) collagen to enable cell remodelling in hydrogels, and an integrin-binding domain (GRGDSPG), derived from fibronectin, to promote cell adhesion. In this study, RLP was used to functionalise poly(HEMA-co-EGDMA) hydrogels, polymerised through photo free radical initiation using lithium phenyl-2,4,6-trimethylbenzoylphosphinate (LAP) to aid cell surface attachment.

2.2. Methods

2.2.1. Cell Culture

All cell culture was carried out using aseptic technique in a class II microbiological safety cabinet, fitted with high efficiency particulate air (HEPA) filters. Cell cultures were stored in an incubator at 37°C in a humidified atmosphere containing 5% CO₂. During culture, full media change occurred every 3 – 4 days, and cells were passaged at 90 % confluence unless stated otherwise.

2.2.1.i. CMSC Isolation from Corneoscleral Rims

Stromal cells were isolated from human corneoscleral rims using a collagenase digestion technique, obtaining a single cell suspension through the breakdown of collagen in the extracellular matrix (Figure 2.1).

Corneal rims were transferred from the organ culture bottle, into a petri dish, and washed in 1% (v/v) Gibco antibiotic-antimycotic (AbAm) (ThermoFisher Scientific), composed of 10,000 units/mL of penicillin, 10,000 µg/mL of streptomycin, and 25 µg/mL of Gibco Amphotericin B, in Dulbecco's phosphate buffered saline (PBS). Excess sclera was trimmed with approximately 1 mm left around the limbus to ensure tactility. The remaining tissue was cut into approximately 16 smaller pieces and digested in 1 mg/ml collagenase type IA (Sigma; G2674) diluted in serum free

medium. The tissue was incubated at 37°C, 5% CO₂, 95% humidity under turning rotation of RPM 60 for between 5 to 7 hours, or until all of the tissue appeared digested. M199 medium (Sigma; M4530) supplemented with 20% (v/v) foetal bovine serum (FBS) (Sigma Aldrich), 2 mmol/L L-glutamine (Sigma Aldrich) and 1% (v/v) AbAm was added to the digests (1:1) to inhibit the collagenase, and cells were filtered through a 40 µm cell strainer to remove any remaining undigested tissue. The filtrate was centrifuged at 200 *xg* for 4 minutes, the supernatant discarded, and the cell pellet resuspended in 1 ml Stem Cell Medium (SCM), consisting of Dulbecco's Modified Eagle's Medium (ThermoFisher Scientific), supplemented with 20% (v/v) Knock Out Serum, (ThermoFisher Scientific), 1% (v/v) MEM Non-Essential Amino Acids (ThermoFisher Scientific), 4 ng/ml FGF-basic (ThermoFisher Scientific), 5 ng/ml Human Leukaemia Inhibitory Factor (Cell Signalling Technologies) and 1% (v/v) AbAm. Cells were seeded following methods described below.

2.2.1.ii. CMSC Culture

Gelatin coating of all tissue culture plastic was necessary for C-MSC adhesion and proliferation in the serum free medium. 0.1% (v/v) bovine gelatin in PBS was incubated at roughly 25 µL / cm² for a minimum of 2 hours at 37°C prior to cell seeding. Gelatin was removed at the end of the incubation.

Following 1x PBS wash, CMSCs were dissociated at each cell passage by incubation with TrypLE Express Dissociation Reagent (Gibco Life Technologies) for 10 minutes at 37°C. This reagent is a recombinant fungal, serine protease, which works through cleavage of arginine and lysine bonds. Although TrypLE Express follows a similar dissociation mechanism to porcine trypsin, it is preferable due to its improved capacity to maintain cell surface antigen expression more effectively [139].

The single cell suspension was neutralised using the serum containing M199 culture media (Section 2.2.1.i) and centrifuged at 250 *xg* for 5 min for pellet formation. The supernatant was discarded, and cells were resuspended in 1 ml SCM. Cell number was measured and calculated using the Countess II FL (Invitrogen, ThermoFisher Scientific) via Trypan blue uptake, and cells were consistently reseeded at 5x10³ cells/cm².

2.2.1.iii. BM-MSC Culture

The majority of BM-MSC culture was similar to CMSCs, where all culture plates and flasks were coated with 0.1% (v/v) bovine gelatine in PBS for a minimum of 2 hours at 37°C, prior to cell seeding. The pellet was resuspended in SCM (Section 2.2.1.i) and plated into a T75 cm² cell culture flask. The majority of cell culture was carried out with this media, with passaging using reagents previously defined (Section 2.2.1.i. and 2.2.1.ii), including TrypLe Express and M199 supplemented media for enzyme quenching.

For culture of BM-MSCs in Chapter 6, flasks were not coated prior to cell seeding as MSCGM™ Mesenchymal Stem Cell Growth Medium BulletKit™ (Lonza, PT-3001) was used for cell culture, and TrypLe Express was substituted for Accutase solution (Sigma-Aldrich) and incubated for 10-20 min at 37°C, with regular checks of cell detachment to determine suitability. Cells were consistently reseeded at 5x10³ cells/cm².

2.2.1.iv. HCEC2 Culture

HCEC2s were cultured in Keratinocyte serum free media (KSF) (Gibco, ThermoFisher), supplemented with human recombinant epidermal growth factor and bovine pituitary extract, supplied with the media. Additional supplementation of 500 ng/mL hydrocortisone, 0.05% (v/v) insulin from bovine pancreas (Sigma-Aldrich) and 1% AbAm. Cells were consistently seeded at 5x10⁴ cells/cm². All future cell culture was carried out with this media, with passaging using reagents including TrypLe Express and M199 supplemented media for enzyme quenching (Section 2.2.1.i. and 2.2.1.ii).

2.2.1.v. Cell cryopreservation and reanimation

For cryopreservation, all cells were detached using TrypLe Express, as previously defined. Following centrifugation, cells were resuspended in 1 mL FBS supplemented with 10% (v/v) dimethyl sulfoxide (DMSO) (ThermoFisher Scientific) for cryoprotection, and transferred to cryogenic storage vials. Cells were placed in a -80°C freezer inside a CoolCell (Corning), allowing for controlled freezing of -1°C / minute. This ensures sufficient efflux of water throughout freezing, minimizing the

chance of intracellular ice formation and cellular damage. Cells were stored at –80°C until further use.

For reanimation, cells were rapidly thawed at 37°C, and added to 5 mL serum-containing medium. The cell suspension was centrifuged to form a pellet at 250 *xg* for 5 min, and resuspended and seeded in conditions defined previously, specific for the cell.

2.2.2. PrestoBlue Viability Assay

PrestoBlue Cell Viability Reagent (Invitrogen, ThermoFisherScientific) quantitatively measures cell metabolism through determination of the reducing ability of the cells. Viable cells reduce PrestoBlue resazurin, which is blue in colour and non-fluorescent, to the red and highly fluorescent compound, resorufin. This change is therefore proportional to cell metabolism and can be detected by a plate reader using fluorescence and absorbance measurements.

CMSCs were seeded in 6 wells of a 96 well plate and viability was assessed at day 1, 3 and 7 post passage. PrestoBlue solution was diluted 10-fold in the respective cell culture medium. Cells were washed with PBS and incubated with 200 µl PrestoBlue solution at 37°C for 20 min. Blank controls were included for each reading, where PrestoBlue solution was added to wells with no cells. 100 µl of PrestoBlue solution from each well was then transferred to a clear bottom, black plate and fluorescence was measured at excitation 535 nm (25 nm bandwidth) and emission 615 nm (10 nm bandwidth). Gain was adjusted depending on the first sample fluorescence. CLARIOstar (BMG LABTECH) plate reader was utilised to obtain measurement data. If cells were required for further timepoints, the corresponding fresh media were added for continued culture.

2.2.3. Live/Dead Fluorescence Assay

The Live/Dead Viability/Cytotoxicity kit for mammalian cells (ThermoFisher Scientific) was utilised to assess the proportion of viable cells following incubation with cytotoxic agents. The ubiquitous, intracellular esterase is active within living cells, and can be detected through the enzymatic conversion of the cell permanent

Calcein-AM from emitting very low levels of fluorescence to an intense green fluorescence. In contrast, Ethidium Homodimer works through penetrating damaged cell membranes, before undergoing a 25-fold enhancement of red fluorescence upon binding to nucleic acids. This is specific to dead cells, as the intact cell membrane of living cells excludes the dye.

To assess cell viability, cell culture medium was removed, and cells were incubated with Live/Dead stain diluted in PBS, consisting of 2 μ M calcein-AM and 4 μ M EthD-1 for 30 min at room temperature. Imaging was then immediately performed in the Live/Dead solution with Leica DFC3000 G microscope, at excitation/emission wavelengths of 495/515 nm and 495/635 nm for calcein-AM and EthD-1, respectively. Images were compiled using Fiji/ImageJ.

2.2.4. Immunocytochemistry

2.2.4.i. Cell Fixation

Cell fixation is necessary to preserve and stabilise the cell morphology, inactivate proteolytic enzymes with the potential to degrade the sample, and to protect the cells against microbial contamination. Formaldehyde is a reactive electrophilic species, which works by intra- and intermolecular crosslinking of functional groups of biological macromolecules, including proteins, glycoproteins, nucleic acids and polysaccharides.

Samples were immersed in 4% (w/v) formaldehyde (10% (w/v) neutral buffered formalin) and incubated for 10 min at room temperature. All samples were washed 3 times with PBS before and after fixation and left submerged in PBS until further processing.

2.2.4.ii. Cell Permeabilization

For the target of intracellular markers, cell membranes must be permeabilized prior to staining. This was achieved with the non-ionic surfactant, Triton X-100. The polar head of the reagent has the capacity to insert into the lipid bilayer of the cell membrane, disrupting the hydrogen bonding and therefore the integrity and

compactness of the lipid membrane. Consequently, antibodies can permeate the cell to reach the target epitope.

Samples were incubated with 0.1% (v/v) Triton X-100 (Sigma Aldrich) for 10 min at room temperature, with 3 PBS washes before and after.

2.2.4.iii. Immunocytochemistry

Immunocytochemistry uses a specific combination of antibodies and target molecules to detect the expression and location of target proteins. The indirect immunocytochemistry assay utilised throughout this project involves the tagging of target cell antigens with primary antibodies, which are sequentially bound to fluorescently labelled secondary antibodies raised against the primary antibody host species. Blocking steps are required to avoid non-specific binding of antibody to Fc receptors. In this project, serum from the secondary antibody host species was utilised, as it contains antibodies which bind to the non-specific sites, ultimately reducing background staining.

For immunocytochemistry, samples were cultured on Greiner Bio-One CELLview Cell Culture Slides, and following cell fixation and permeabilization, were incubated for 1 h in blocking buffer consisting of PBS supplemented with 1% (v/v) bovine serum albumin (BSA; Sigma, A3856), 0.3M glycine (Sigma, G7126), and 3% (v/v) donkey serum (Sigma, D9663). Samples were then incubated overnight at 4°C with primary antibodies (Table 2.1) diluted in wash buffer containing 1% (v/v) BSA and 0.3M glycine. Samples underwent 3 PBS washes, prior to incubation with secondary antibodies (Table 2.2) for 1 h at room temperature. Required samples were washed 3 times with PBS, counterstained with Alexa Fluor 488 phalloidin (Life Technologies, A12379) unless otherwise stated, by incubation for 20 min at room temperature, and washed again. Phalloidin is a stain that binds to all variants of actin filaments, utilised in this study to provide information on cell morphology. All samples were then counterstained and incubated for 10 min at room temp with 0.5 µg/mL of the nuclear stain, 4',6-diamidino-2-phenylindole (DAPI; Life Technologies, D1306), unless otherwise stated. Chambers were removed, slides were mounted in permafluor aqueous mounting medium (ThermoFisher Scientific), and samples

were imaged using a Leica DFC3000 G microscope. Images were edited using Image J (Fiji) (version 1.53v), where contrast and brightness were modified to achieve a representative image.

2.2.5. Flow Cytometry

Flow cytometry was used for phenotypic analysis of the cells, measuring the expression of cell surface and intracellular markers through detection of specifically bound fluorescent antibodies, identified using a series of lasers.

2.2.5.i. Sample Preparation

CMSCs were detached from the flask (Section 2.2.1.ii), and the cell suspension diluted in ice cold flow buffer, consisting of PBS with 10% (v/v) FBS to reduce cell aggregation and non-specific antibody binding, and 0.1% (w/v) sodium azide to prevent the internalisation of the antibody-antigen complex following staining.

2.2.5.ii. Cell Surface Staining

For cell surface staining, 95 μ l of cell suspension was added to individual flow tubes with 5 μ l of conjugated antibody (Table 2.3) and incubated at 4°C for 30 min. Additionally, 2 tubes of cells were identically prepared containing no stain, or 5 μ l of FIT-C, PE or PE-Cy5 isotype for controls. Following incubation, 1 mL PBS buffer was added to each sample, and the cells were centrifuged at 250 xg for 5 min. Supernatant was aspirated, and following another wash in 1ml PBS buffer, cells were resuspended in 400 μ l 4% (v/v) paraformaldehyde (PFA). PFA is a polymer of formaldehyde, and was utilised for flow cytometry due to its increased stability and reduced risk of epitope degradation. Samples were left in the solution at 4°C until ready for analysis.

2.2.5.iii. Nuclear Staining

Comparatively, cells stained with the nuclear marker Ki67 (conjugated with FITC) were first incubated with 4% PFA for 10 min at room temp, followed by the addition of 1mL flow buffer for dilution. The cell solution was centrifuged for 5 min at 250 xg and the supernatant discarded. Cells were permeabilised with 0.1% (v/v) Triton X-

100 (Sigma, T8787) and incubated for 10 min at room temperature. Flow buffer (1 mL) was added for dilution, samples were centrifuged and supernatant discarded. Samples were then stained with 100 μ L Ki67 antibody solution, diluted 20 fold in flow buffer, through 30 min incubation at 4°C. Following incubation, 1ml PBS buffer was added to each sample, and the cells were centrifuged at 250 xg for 5 min. Supernatant was aspirated and the cells were resuspended in 500 μ L flow buffer, and stored at 4°C until analysis.

2.2.5.iv. BD Lyoplate™ Human Cell Surface Marker Screening Panel

The BD Lyoplate™ Human Cell Surface Marker Screening Panel (BD Biosciences) was used to characterise CMSCs and BM-MSCs. The kit consists of 242 purified, lyophilised, unconjugated, monoclonal antibodies for cell surface proteins. Mouse and rat isotype controls were included. Before use, plates containing antibodies were centrifuged for 5 min at 300 xg and reconstituted in 110 μ L PBS, and then aliquoted into additional U- bottomed 96 well plates and stored at -20°C until use. The methods carried out were similar to those recommended by the manufacturer, with modification to allow for increased tests. After defrosting the plates and sample preparation, 30 μ L of cell suspension was transferred to each well containing primary antibodies, and incubated at 4°C for 30 min. Cells were then washed in flow buffer and incubated for 30 min at 4°C with Alexa Fluor 647-labeled anti-mouse or anti-rat secondary antibody (1 : 200 dilution in flow buffer). Cells were washed and fixed with 4% (v/v) paraformaldehyde (PFA). Samples were left in the solution at 4°C until ready for analysis.

2.2.5.v. Cytometer Analysis

10×10^4 cells per sample were measured using the BD FACSCanto II. David Onion and Nicola Croxall from the Flow Cytometry Facility, University of Nottingham, ran compensation beads to set voltages and gating parameters to obtain accurate fluorescence signal. Beckman Coulter Kaluza Analysis Software was utilised for cell gating, analysis and figure production. For cell gating, the cell population was first identified through assessment of a forward scatter vs side scatter density plot, which provided information on size and granularity, respectively. Single cells were

then identified through gating for doublet exclusion, through assessment of forward scatter area vs forward scatter height. Finally, a percentage of positive cells from the population of single cells, and the median fluorescent intensity (MFI) of the sample was determined through histograms and dot plots, and normalised to the antibody corresponding isotype which was used as a negative control.

2.2.6. Growth Rate and Population Doubling Calculations

As previously described, cells were counted at each passage using the Countess II (ThermoFisher Scientific). Calculations defined below, from Heathman *et al.* [73] were used to calculate growth rate and population doubling, in order to determine any differences in cell growth behaviour over the passages.

$$\text{Growth Rate } (\mu) = \frac{Cx(t)/Cx(0)}{\Delta t}$$

Equation 2.1. Where μ is the net specific growth rate (h^{-3}), and $Cx(t)$ is the final cell number, $Cx(0)$ is the seeded number of cells, and t is time (h).

$$\text{Population Doubling } (Pd) = \frac{1}{\log(2)} * \log \frac{Cx(t)}{Cx(0)}$$

Equation 2.2. Where Pd describes the number of times the cells in the population have doubled since the previous passage. $Cx(0)$ and $Cx(t)$ represent the initial and final cell numbers respectively.

2.2.7. Reverse Transcription Quantitative Polymerase Chain Reaction (RT-qPCR)

Quantitative reverse transcription PCR (RT-qPCR) is used to detect gene expression based on RNA isolation from the initial cell culture. This works through the measurement of RNA levels by utilizing complementary DNA (cDNA), which can be quantified through rapid detection of gene expression changes, performed in qPCR. In this thesis, 'general' methods refer to all PCR not carried out using the RT² Profiler PCR Array.

2.2.7.i. General RNA Isolation

CMSC and BM-MSC expression of genes in were analyzed at time points of interest. RNA was extracted using the RNEasy mini kit (Qiagen, Manchester), with reagents

provided for guanidine-isothiocyanate mediated cell lysis and homogenization, followed by RNA isolation using an RNeasy mini spin column. The spin column contains a silica membrane which the RNA in the lysate binds to, simultaneous to other contaminants being washed away. The final RNA was eluted in water, and the RNA quantity assessed on an LVis-plate in a CLARIOstar plate reader.

2.2.7.ii. General cDNA Synthesis

Complementary DNA (cDNA) was transcribed by reverse transcription from total RNA, which is used as a template for the qPCR reaction. First strand DNA (cDNA) was synthesised from 1 µg total RNA using The Script III First Strand Synthesis Kit (Invitrogen, ThermoFisher). This kit uses the RNA-dependent DNA polymerase, Moloney murine leukaemia virus reverse transcriptase (M-MLV RT), synthesising cDNA based on random hexamer primers, used to account for all RNA species (rRNA and mRNA) in the sample. Random hexamers are primers of 6 to 9 bases long, and can anneal at several points on the RNA transcript. 8 µL of total RNA mixed with water to form 8 µL, 1 µL of random hexamers (50 ng / µL), and 1 µL of 10 mM dNTP mix.

2.2.7.iii. General PCR

For PCR, 1 µL cDNA was used as a template with inventoried TaqMan assays (Applied Biosystems, ThermoFisher) to detect *GAPDH*, *ENG*, *Thy1*, *NT5E*, *CD34*, *ACTA2* and *ALDH3A1* in Chapter 3. TaqMan probes work through hydrolysis, and bind downstream of the qPCR primers. The probes contain a fluorescent reporter moiety at the 5' end, and a quencher molecule at the 3' end, meaning as the DNA polymerase extends the primer, the probe is cleaved, leading to the emission of a fluorescent signal. An Mx3005P multi-colour 96-well PCR-system (Stratagene, Agilent Technologies) was utilised for gene amplification. Thermocycling consisted of 2 subsequent holding cycles of 50°C and 95°C for 2 min and 10 min respectively, followed by 50 cycles of 15 s at 95°C and 1 min at 60°C. Amplification of DNA is achieved through the repeated PCR steps of denaturation, annealing and extension.

Table 2. 13. Cycles for gene amplification for general PCR including duration, temperature, and number of cycles.

Cycling Conditions for General PCR Reaction			
Cycles	Duration	Temperature	Comments
1	2 min	50 °C	
1	10 min	95 °C	DNA Taq Polymerase is activated by this heating step.
50	15 s	95 °C	
	1 min	60 °C	Fluorescent data collection here.

2.2.7.iv. General Analysis

Detection produces an amplification curve consisting of initiation, exponential and plateau phases. A fractional cycle number at threshold (Ct) value can be set where the fluorescence level of the exponential phase is significantly higher than the baseline or initiation value. Data analysis was performed using freely available online software based on a four parameter simple exponent model [140]. This calculates efficiency (E) and threshold cycle (CT). RNA expression levels were calculated using an efficiency corrected comparative threshold cycle method (E $\Delta\Delta$ CT). All values were normalised to GAPDH. Fold changes were calculated by The RT-qPCR Miner algorithm, with all readings normalised to the endogenous reference gene GAPDH.

2.2.7.v. Wound Healing Gene Array Panel

The RT² Profiler PCR Array for wound healing was utilised to assess differences in genotype between control and cytokine treated CMSCs, and BM-MSCs in Chapters 4 and 5. This assay utilises RT-PCR and the multigene profiling capabilities of a 96 well array to allow for medium throughput detection of multiple genes simultaneously.

RNA isolation and purification was carried out as described in 2.2.7.i. cDNA was synthesised from 150 ng RNA using the RT² First Strand Kit. As per the manufacturer's instructions, a genomic DNA elimination mix was formed using the RNA, 2 µl Buffer GE and RNase-free water, and incubated at 42°C for 5 mins. 10 µl of the reverse transcription mix was combined with 10 µl of the DNA elimination mix and incubated at 42°C for 15 mins, with the reaction terminated through 5 min incubation at 95°C. Samples were combined with 91 µl RNase free water and stored at -20°C until the subsequent step.

RT-PCR was carried out using the manufacturer's instructions for array format A. The PCR components mix was prepared, and 25 µl added to each well of the RT² Profiler Array 96 well plate. The plate was centrifuged for 1 min to remove bubbles. PCR was run on the Mx3005P multi-colour 96-well PCR-system (Stratagene, Agilent Technologies), with 10 min at 95°C to activate the HotStart DNA *Taq* Polymerase, and 40 subsequent cycles of 15 secs at 95°C and 1 min at 60°C (Table 2.14).

Table 2.14. Cycles for gene amplification utilised with the RT² Profiler PCR assay, including duration, temperature and number of cycles.

Cycling Conditions for RT ² Profiler PCR Array Reaction			
Cycles	Duration	Temperature	Comments
1	10 min	95 °C	DNA <i>Taq</i> Polymerase is activated by this heating step.
40	15 s	95 °C	
	1 min	60 °C	Fluorescent data collection here.

Analysis was performed using the PCR Miner analysis, outlined in 2.2.7.iv. HPRT1 was used as the endogenous reference gene as GAPDH was not stable when the cells were treated with cytokines.

2.2.8. Enzyme-linked Immunosorbent Assays (ELISAs)

Sandwich ELISAs were performed to assess the presence and relative quantity of secreted soluble factors from CMSCs and BM-MSCs following exposure to inflammatory stimuli. A sandwich ELISA is a plate-based assay technique which works through the immobilisation of the antigen onto the well surface using a

capture antibody which was previously attached to the plate. Subsequently, an additional primary antibody, termed the 'detection antibody' can bind to a second epitope on the antigen, therefore increasing the sensitivity and specificity of the assay, and 'sandwiching' the protein of interest. This antibody is also conjugated to the enzyme, horse radish peroxidase (HRP), which reacts with the chromogenic, enzyme substrate, TMB (3, 3', 5, 5'-tetramethylbenzidine), which forms a soluble, coloured product that accumulates over time, relative to the amount of HRP present in each well. Originally displaying as blue upon oxidation, there is a colour change to yellow following addition of sulphuric acid at the stop point of the reaction.

To analyse the production and quantity of various soluble factors (outlined in Table 2.5, Section 2.1.4) cell media supernatant was collected at a number of time points throughout the investigations (expanded in relevant chapters). Human antibody DuoSet ELISAs were used in combination with the appropriate DuoSet Ancillary Reagent Kit (R&D Systems; outlined in Table 2.4, Section 2.1.4).

Capture antibody (100 μ L diluted in ELISA plate coating buffer was added to each well and incubated at room temperature, overnight, to allow the antibody to attach to the plate. Wash buffer and reagent diluents were made up according to manufacturer's instructions (Table 2.4, Section 2.1.3). The plates were washed in wash buffer, using a plate washer, to remove any excess primary antibody. Blocking buffer (300 μ L) was then added to the plate and incubated for 2 h at room temperature, to help prevent non-specific binding. During this incubation, samples were diluted based on previous optimisation experiments, and standards were prepared. Following the incubation, plates were washed to remove the blocking buffer, and samples and standards were added to the necessary wells and incubated for 2 h at room temperature to allow for binding to the capture antibody. Each technical repeat was performed in triplicate, and standards in duplicate. Plates were washed and 100 μ L of detection antibody was added and incubated for 2 hours at room temperature, allowing for binding to the second epitope on the antigen. Plates were washed, and samples were incubated with 100 μ L HRP solution for 20 mins at room temperature, in order to conjugate to the secondary antibody.

Plates were washed, and the colour reagents A (stabilised hydrogen peroxidase) and B (stabilised TMB) were mixed to activate the TMB. 100 μ L of the colour reagent solution was added to each well and incubated for the times outlined in Section 2.1.4. Stop solution was added and the colourimetric change was read immediately on a CLARIOStar plate reader, by optical density measurements at 450 nm and background correction at 540 nm. The concentration of soluble factors was determined using a 4-parameter fit standard, and the data was corrected for using the cell viability data obtained from PrestoBlue analysis (Section 2.2.2).

2.2.9. Polymer Synthesis and Preparation

2.2.9.i. Free Radical Mechanism

Poly(HEMA-co-EGDMA) hydrogels were prepared via either thermal and photo free radical initiation. Free radical initiation polymerises through three major phases; initiation, propagation and termination (Figure 2.1). Thermal and photo initiation occurs through the decomposition of the initiator, where the radiant energy results in the haemolytic cleavage of the initiator to form 2 free radical species and a stable molecule of nitrogen (Fig 2.1.A). Subsequently, the radical initiator can attack the double bond of an alkene monomer to create a monomer radical. The radical can be transferred as the polymer chain grows in a process defined as propagation (Fig 2.1.B). This continues until termination, where either there is no monomer remaining, or two radicals combine to form a covalent bond, leaving a stable polymer (Fig 2.1.C).

2,2'-Azobis, dihydrochloride (VA-044) was initially used for thermal initiation due to its water solubility, and 2,2-dimethoxy-2-phenylacetophenone (DMPA) was utilised for efficient photo polymerisation, with fast reactions and low concentrations obtained at very low concentrations. Photo initiation was later selected over thermal initiation, to allow functionalisation of the hydrogel without peptide degradation. Various UV curing times were assessed (Chapter 6) and a concentration of 1% (w/v) was consistently used to ensure optimal polymerisation without early chain termination. Dissolution of DMPA was achieved in HEMA, omitting the need for extra solvent. It is suggested that HEMA and EGDMA form

repeating units in a randomised order and can crosslink through hydrogen bonds (Figure 2.2).

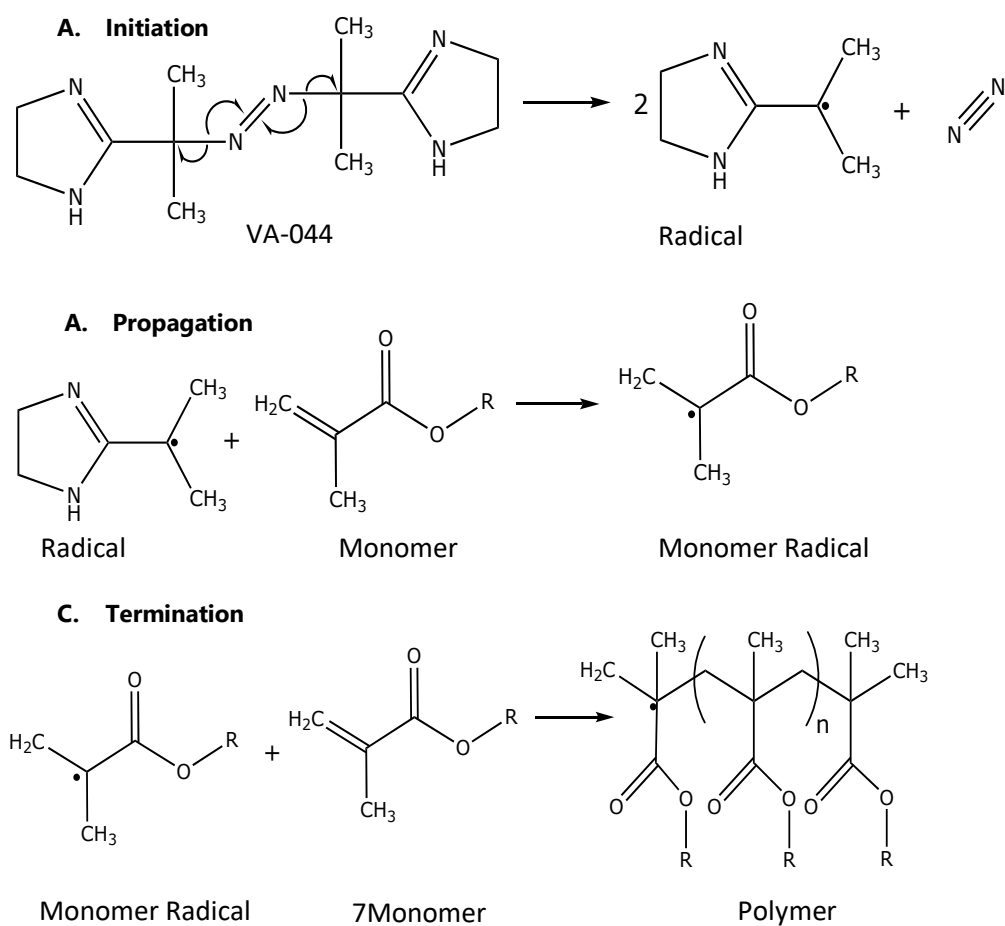


Figure 2. 1. Free radical initiation mechanism, depicting initiation, propagation and termination, using VA-044 as an example initiator.

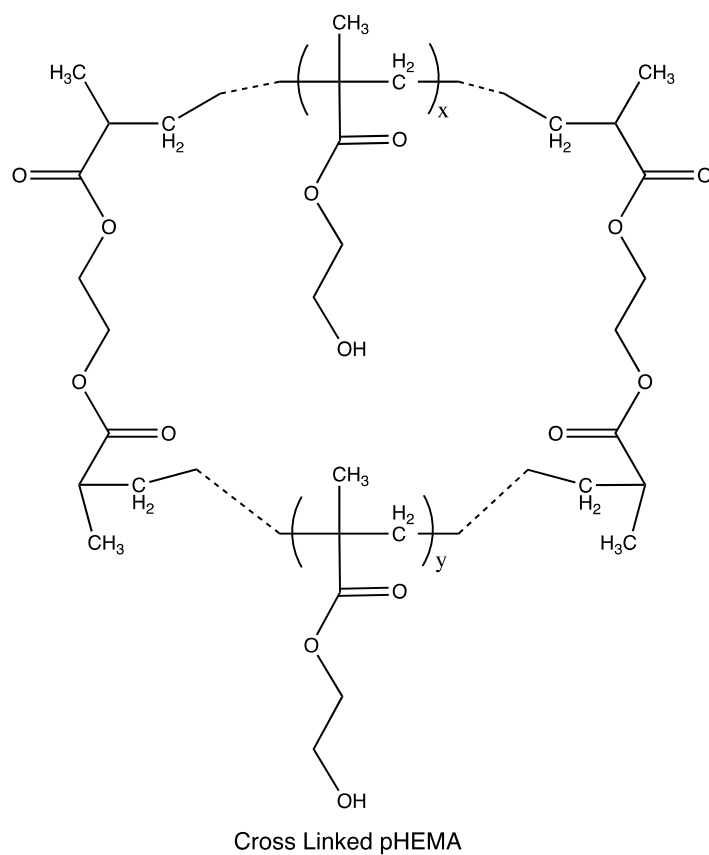
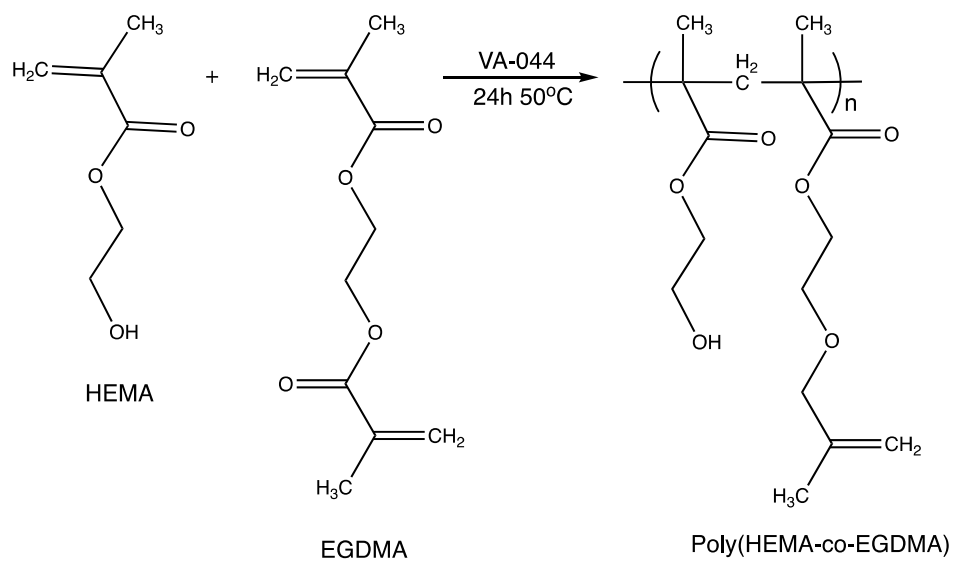


Figure 2. 2. Suggested mechanism for the crosslinking of HEMA with EGDMA to produce poly(HEMA-co-EGDMA), with VA-044 as an example initiator.

2.2.9.ii. Poly(HEMA-co-EGDMA) synthesis

For thermal initiation the following methods were undertaken. VA-044 initiator was weighed out and dissolved in water. HEMA was mixed with 1 Mw % EGDMA to form a homogeneous solution, before addition of the VA-044 dissolved in water. The overall mixture consisted of 79% (v/v) HEMA, 1% (v/v) EGDMA, 19% (v/v) water and 1% (w/v) VA-044. Monomer solution was injected between the slides separated with a silicone spacer and held together with bulldog clips. Samples were then placed in the oven at 50°C for 24h for polymerisation.

For photoinitiation using DMPA, an initial mixture of HEMA with 1 Mw % EGDMA was mixed together. An aliquot of this mixture was dispensed into a different tube, and DMPA was added to make a 10 wt % solution. The HEMA/EGDMA/DMPA solution was then added to the initial HEMA/EGDMA solution at a ratio of 1:10 to create a final DMPA concentration of 1 wt %. Water was then added to make up 20 wt % of the overall solution. If sterility was required for cell culture, the solution was filtered through a 0.22 µm filter and subsequent steps were taken in the microbiological safety cabinet (MSC). 10 µL of the final solution was pipetted onto a slide with a silicone spacer, before an additional slide was placed on top. Samples were irradiated with UV light (365 nm, ≈5 mW/cm²) for 10 min.

Due to the high adhesion of poly(HEMA) to glass, slides were coated with RainX Rain/Water Glass Repellent Treatment, to produce a hydrophobic layer for easy polymer detachment. Following polymerisation, gels were removed from the glass slides and left to swell in PBS at room temp for 1 day.

2.2.10. Polymer Functionalisation

Functionalisation of the poly(HEMA-co-EGDMA) hydrogel is necessary for cell attachment.

2.2.10.i. AEMA

AEMA is a primary amine monomer, with the capacity to increase free amine groups at the surface of the gel, therefore increasing its nucleophilicity and reactivity for potential further functionalisation (Figure 2.3).

AEMA was copolymerised with HEMA and EGDMA to produce poly(HEMA-co-EGDMA-co-AEMA) (Figure 2.4). Water soluble AEMA was dissolved in water with 10 mM VA-044, then added to the HEMA and EGDMA mixture as described in Section 2.2.9.ii.

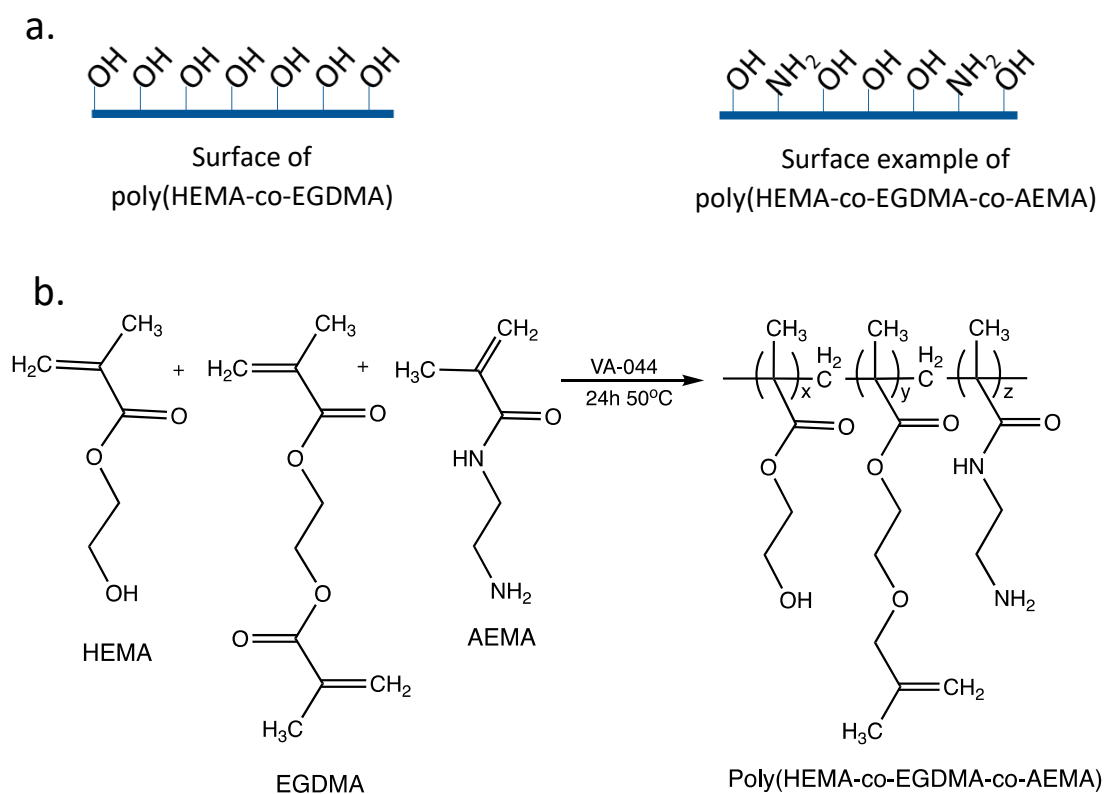


Figure 2. 3. Copolymerisation of HEMA and EGDMA with AEMA. (a) Diagram demonstrating increase of primary amine functional groups at surface of hydrogel through the copolymerisation of HEMA and EGDMA with AEMA. (b) Copolymerisation mechanism to produce poly(HEMA-co-EGDMA-co-AEMA).

2.10.ii. GGGRGD and GGGYIGSR

Cell adhesive peptides GGG-RGD and GGG-YIGSR were bought modified with an N terminal methacrylic acid from GenScript. The three glycine repeats were attached to increase the distance of the peptide at the surface from the hydrogel, based on previous work by Floor Ruiters [141]. The methacrylamide N terminal end group was included to permit free radical initiation, with incorporation of the peptide into the bulk synthesis of the hydrogel. Both peptides were dissolved at a concentration of 10 mg/ml, which was the highest feasible concentration without precipitation. GGGRGD was dissolved in DMSO (ThermoFisher Scientific), and GGGYIGSR was dissolved in acetic acid with a couple of drops of Trifluoroacetic acid (TFA) (Merck, CAS: 76-05-1). These were the highest concentrations permitted for full dissolution. The peptides were then added at different concentrations, to the HEMA/EGDMA solution as outlined in Section 2.2.9.ii, described in Chapter 6.

2.2.10.iii. Resilin-like polypeptides (RLPs)

The RLP-FM was dissolved in PBS at 20 wt % concentration. Dissolution of the initiator, lithium phenyl-2,4,6-trimethylbenzoylphosphinate (LAP), was performed in PBS to create a stock solution with the concentration of 13.4 mg/mL. This solution could be stored at 4°C and used for up to 7 days. A 5% volume was added to the RLP solution, and the sample was vortexed to achieve a final concentration of 2.2×10^{-3} M.

A precursor mixture of HEMA/EGDMA was also formed as described in 2.2.9.ii, using 1% DMPA dissolved directly into HEMA as an initiator. Glass slides were prepared by either coating with RainX, or adding a layer of Teflon tape, to enable gel detachment after curing. 0.5 mM strips of silicone were placed at either end of the slide, and 5 μ L of the HEMA/EGDMA precursor solution was pipetted onto the slide. The sample was then part polymerised by UV irradiation for 2 min (365 nm, ≈ 5 mW/cm²), with the intensity confirmed using a radiometer. 1 μ L of the RLP precursor was then pipetted onto a separate, coated slide, and part-polymerised using UV for 1 min at the same intensity.

Following the part polymerisation of both materials, the two slides were sandwiched together, separated by the silicone spacers, ensuring the two hydrogel solutions came into contact. A further 8 min of UV exposure at the same intensity allowed the two hydrogel materials to cure together. At the interface, it was hypothesised that the free radical reaction would continue with free methyl groups at the surface of each material, consequently binding them together.

2.2.11. Polymer Analytical Techniques

2.2.11.i. Mechanical Testing

To investigate the mechanical properties of hydrogels, samples were evaluated under tensile loading. Tensile testing is where a material is subject to a controlled tension until it fractures, therefore reaching failure. Samples were mechanically cut, using a scalpel, into a dogbone shape (overall length of 115 mm (the gauge length being 25 mm), width of 6 mm, and thickness of 3 mm), with two shoulders that can be easily gripped, and a gauge area with a smaller cross section, so that failure can occur here. During testing, the elongation of the gauge system is measured against the applied force, with data consistently manipulated to be independent of the geometry of the test samples.

Tensile loading occurred at 0.1 mm/sec using an electromechanical universal tester (Instron 50 kN 3342, Canton, MA equipped with Series IX/S software) and a 5 kg load cell. Initial sample dimensions were measured using callipers to calculate the cross-sectional area and applied stress. Young's modulus is the modulus of elasticity of a material, therefore giving information on how easily it can be stretched. Before a material is stretched beyond its limit of proportionality, stress is directly proportional to strain, defined on a stress/strain graph as the linear elastic region. The gradient of this region is the Young's modulus and can be calculated using Equation 2.3.

$$E = \frac{FL}{A\Delta L}$$

Equation 2.3. Where E is the young modulus in pascals (Pa), F is the force in newtons (N), L is the original length of the material in meters (m), A is the area in square meters (m^2) and ΔL is the change in length (m).

2.2.11.ii. Oscillatory Rheology

Rheology is used to assess the deformation and flow behaviour of materials, where molecules and particles put into motion are forced to slide along each other, creating a flow resistance caused by the internal friction [142]. In a dynamic, oscillatory test, a sinusoidal strain or stress is applied to the sample under a certain frequency to assess the viscoelastic properties of the fluid. Like a stretched spring trying to return to its original state, when a force or deformation is applied to a structured fluid, the equilibrium energy state is shifted, resulting in an elastic force that tries to restore the material to the initial microstructure. The applied stress is proportional to the resultant strain, as long as the elastic limit is not surpassed. The G' is the elastic modulus, which refers to the elastic behaviour of a material when deformed, relating the stress to the strain. G'' is the loss modulus, which is a measure of the energy dissipated in material once the oscillatory shear has been imposed. It is the proportion of the total rigidity (complex modulus) of a material due to viscous flow of a material, rather than elastic deformation.

Oscillatory rheology was conducted using an AR-G2 rheometer (TA Instruments, New Castle, DE) with an attached UV Light Guide accessory and UV lamp source (OmniCure S2000 (Excelitas)), with an 8 mm diameter stainless steel parallel plate geometry. In this thesis, rheology was performed both *in situ*, and with pre-formed hydrogels.

For *in situ* rheology, precursor solutions were prepared as described in Section 2.2.9.ii. and 2.2.10.iii. 10 μL of solution was pipetted onto the quartz rheometer stage, with the geometry set to a 200 μm gap. Once the gap was reached, mineral oil was deposited around the side to seal the geometry and prevent sample dehydration. Over the entirety of the measurement, the sample was exposed to UV

light at 365 nm (5 mW/cm² intensity) to induce cross-linking. The mechanical properties of the hydrogel were measured in the viscoelastic range at 1% strain and an angular frequency of 6 rad/s. A frequency sweep was performed from 1 to 100 rad/second at 1% strain and an amplitude sweep from 0.1% to 1000% strain.

For rheological measurements on preformed hydrogels, hydrogels were placed on an 8 mm plate and compressed by the probe until a force of 0.1 Newtons was registered. A frequency and amplitude sweep were performed as previously described. For all experiments, 3 hydrogels were used for each condition, and the shear modulus was reported as the sample mean. Trios software (TA instruments) was used to analyse the data.

2.2.11.iii. Equilibrium Water Content

The equilibrium water content (EWC) is the water content at which the material is neither gaining nor losing moisture. Crosslinker percentage and additional monomers for copolymerisation can affect the swelling capacity of a hydrogel.

8 mm biopsy punch circles were taken from the hydrogels prepared as previously described. Samples were weighed in their wet state and following 72h lyophilisation. EWC was calculated as shown in the below equation.

$$EWC = \frac{(wet\ weight - dry\ weight)}{wet\ weight * 100\%}$$

Equation 2.4. Where EWC is equilibrium water content. Weights were taken of the biopsy punched hydrogels before and after swelling.

2.2.11.iv. Opacity Assay

Optical clarity is an important characteristic in contact lens development. Transparency was assessed through opacity assays, using the CLARIOStar plate reader. Light of a selected wavelength is transmitted through a sample and the absorbance is measured. Absorbance is directly correlated to the opacity of a sample, with no absorbance representing full transparency.

The hydrogels were cut using an 8 mm (Kai Medical) biopsy punch and transferred to a 48 well plate. A well scan was performed as a matrix scan with 10 flashes per scan point. Scan matrix dimension was set to 15 mm x 15 mm with an overall scan width of 2.5 mm. The test was run as 492 nm, with thresholds set between -0.01 and 2.5 relative absorbance units, represented by a gradient from white to black respectively. All values were normalised to a PBS only control by calculation of the fold change in absorbance.

2.2.11.v. Cell attachment to hydrogels

Cell attachment to hydrogels was assessed using CMSCs and BM-MSCs. Cells were cultured as described in Section 2.2.1.ii. and 2.2.1.iii. Hydrogels were prepared as described in 2.2.9.ii. and functionalised using one of the methods described in Section 2.2.10. Following materialisation, hydrogels were soaked in 1% AbAm for 24 h. Samples were then submerged in the corresponding media for a further 24 h. Samples were placed in 96 well plates, and cells were seeded at 2×10^4 cells/cm². Cells were cultured for 5 days with a media change at day 3. On day 5, the hydrogels were submerged in 4% (w/v) formaldehyde (10% (w/v) neutral buffered formalin) and incubated for 10 min at room temperature. All samples were washed 3 times with PBS before and after fixation and left submerged in PBS until further processing.

To assess cell structure, phalloidin and DAPI staining were used, following the same protocol described in Section 2.2.4. For imaging, the samples were transferred cell seeded side down onto a glass slide, a few droplets of PBS were added, and a coverslip was placed on top. The Zeiss CD7 Confocal Microscope (University of Delaware) or The Zeiss LSM710 Confocal Microscope (University of Nottingham) was used for imaging the samples. Further details can be found in Chapter 6.2.8.

2.2.12. Statistical Analysis

Different statistical tests were used throughout this thesis, defined in each results chapter. All statistical analysis was performed using Graphpad Prism (Version 9.4.1), with statistical significance assumed based on a 95% confidence interval ($P < 0.05$).

Levels of statistical significance were symbolised on graphs with asterisks ($P \leq 0.05$ (*), $P \leq 0.01$ (**), $P \leq 0.001$ (***), $P \leq 0.0001$ (****)).

CHAPTER 3: Analysis of corneal mesenchymal stromal cell phenotype over increasing passages

3.1. Introduction

The stroma makes up about 90% of the overall cornea thickness, which predominantly consists of a heterodimeric complex of type 1 and V collagen lamellae with sparsely interspersed keratocytes [143]. These mesenchymal-derived cells are quiescent, with no expression of stress fibres or generation of substantial contractile forces, and have a dendritic morphology, with typical expression of the markers aldehyde dehydrogenase (ALDH), CD133 and CD34 [144]. They play fundamental roles in maintaining the homeostasis of the ocular surface through their extensive intracellular contacts and their capacity to produce and sustain extracellular matrix (ECM) proteins, ensuring the accurate structure and transparency of the cornea.

As described in chapter 1, keratocytes cultured *in vitro* in optimised media shift to corneal mesenchymal stromal cells (CMSCs) and have been demonstrated to obtain a phenotype almost identical to MSCs derived from fetal liver [66]. In accordance with the International Society for Cellular Therapy (ISCT), minimal criteria to define an MSC includes an ability to adhere to plastic; expression of surface molecules CD105, CD73 and CD90 and lack of expression of CD45, CD34, CD14 or CD11b, CD79 or CD19 and HLA-DR; and an aptitude to differentiate into osteoblasts, adipocytes and chondroblasts *in vitro* [25]. CMSCs mainly comply to these guidelines, alongside evidence showing their potent immunomodulatory efficacy when applied to an *in vitro* model of corneal injury, therefore displaying favourable characteristics to combat inflammation in ocular surface disorders [33].

In addition to the therapeutic value of MSCs, other stem cells have been utilised for cell therapies. This includes differentiation of induced pluripotent stem cells (iPSCs) into immune regulating cells, such as regulatory T cells, however their high

tumorigenicity is still a major obstacle to their use in therapy. Nevertheless, characteristic markers of stem/ progenitor cells have been linked to augmented cell properties, including ABCG2 expression correlated to increased multilineage differentiation potential [145]; and CD34 linked to improved cell migration [146]. It could be hypothesised that these advantages may be translated to MSCs displaying the same markers, with potential to increase the potency of therapeutic MSCs.

A major limitation of widespread usage of cell therapies is their autologous nature, where the patient-specific cell product is costly and difficult to manufacture (Figure 3.1). Alternatively, allogenic products are scalable and readily available for point-of-care treatment, however the foreign cell antigens pose an increased risk of rejection. Assessing cell therapies for topical delivery to the ocular surface is advantageous compared to other, internal tissues, due to the immune-privileged status of the cornea. This unique and innate characteristic is responsible for the particularly high success rates of corneal transplantations and is referred to as the Anterior Chamber-Associated Immune Deviation [147]. This was first demonstrated in the 1940s, where skin allografts transplanted in the anterior segment of the eye persisted indefinitely if the blood barrier remained intact, compared to the rapid rejection observed following transplantation into other organs, including the skin. One immunosuppressive mechanism well described is the inhibitory effect of the aqueous humour on the regulation of T cells, which can migrate through the blood barrier to the eye [148]. Furthermore, cells of the cornea express molecules on their membrane surface, including Fas ligand and programmed cell death receptor 1 (PD-1), which can interact with T cells to cause regulatory activity or induce apoptosis. Ultimately, a combination of anatomical factors, soluble factors, membrane associated proteins and alternative antigen presenting cells help to create a microenvironment favourable for the application of an allogenic cell therapy.

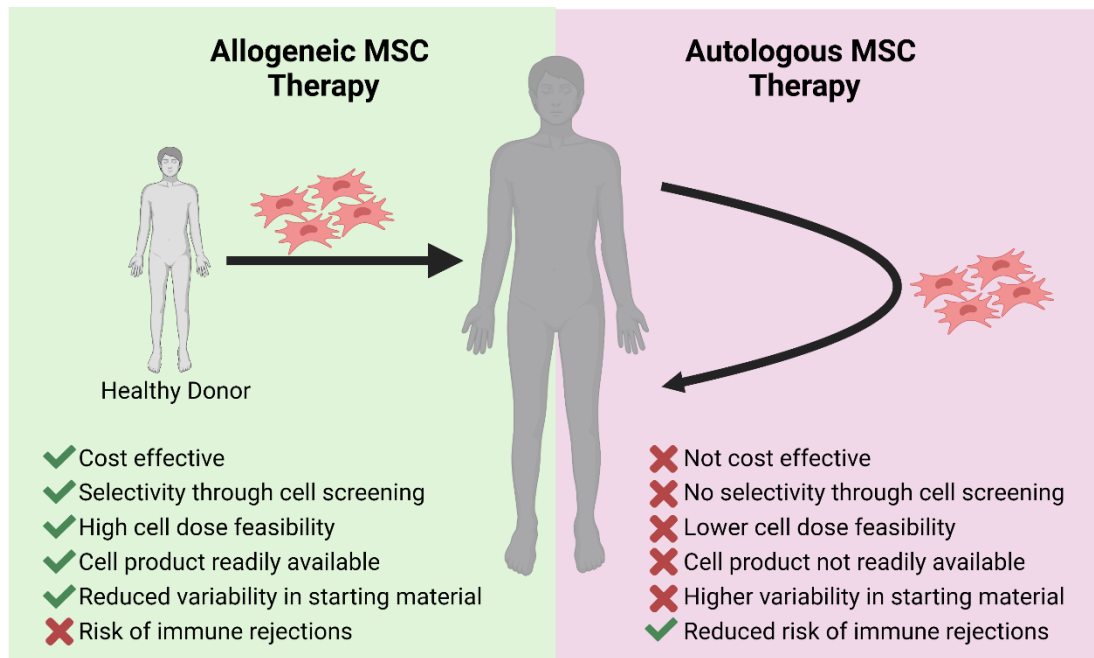


Figure 3. 1. Advantages and limitations of allogeneic and autologous Mesenchymal stem cell (MSC) therapy. Figure adapted from Durand *et al.* (2022) [149].

Scalability is vital for cell therapies, particularly due to the disparity between the very low abundance of cells initially isolated, compared to the quantity required for a cellular product. For example, BM-MSCs account for around 0.001- 0.01% of bone marrow mononuclear cells, necessitating extensive *in vitro* culturing and expansion [150]. Throughout the process of cell manufacture, it is crucial that cells are monitored and characterised, to guarantee minimal change to cell properties and potency (Figure 3.2). For example, Yang *et al.* (2018) found that BM-MSCs changed morphology, increased senescence, reduced doubling rate and showed genetic differences as the cell aged [70]. Higher passages have also been linked to increased genomic instability, likely due to the accumulation of proliferative stress [29] and reduced chemotaxis, potentially caused by the increased percentage of senescent cells in the population [151]. It is important to note that although later passages have been questioned, early ones have also been brought into contention, with BM-MSCs at passage 3 compared to passage 5 showing reduced chondrogenic differentiation; impaired telomerase activity; changes in chromosomal morphology with potential anomalous karyotypes, indicating senescence; downregulation of the

cell cycle, DNA replication and mismatch repair pathways; and increased genomic instability [152].

This highlights the requirement to understand the therapeutic window of the cells, aiming to balance successful scale up with optimal cell characteristics for transplantation. In this chapter, the aim was to develop an insight into the phenotype, genotype, growth kinetics, and secretome of CMSCs over increasing passage when cultured *in vitro*, to identify passages that could be used in clinic, as well as for the continuation of work in this thesis.

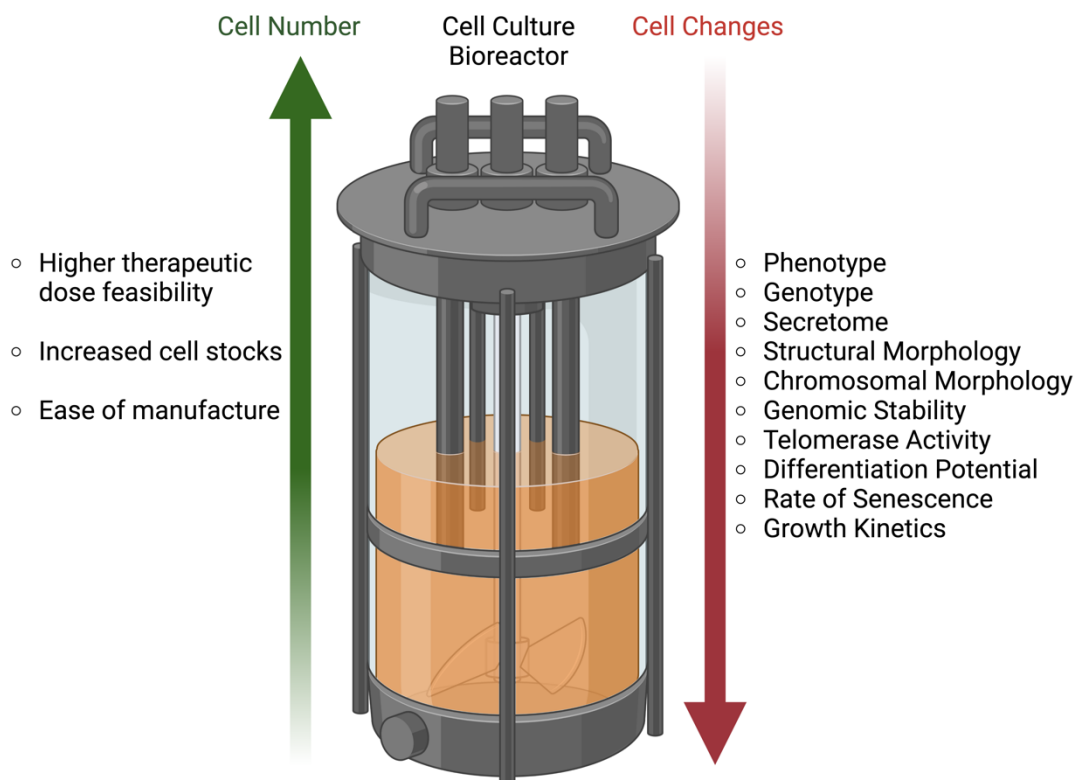


Figure 3. 2. Balance between increasing cell number during cell therapy manufacture and cell changes. Increasing cell number leads to advantages for therapeutic cell product, however this is synonymous with multiple structural and functional changes in the cell.

In addition to scalability, another major limitation for cell therapy manufacture is the donor-to-donor variability. The heterogeneities observed in phenotype and growth kinetics can lead to inconsistent preclinical and clinical outcomes. Consequently, it is vital that donor cell selection is robust, with effective screening methods prior to implementation [153]. For cell phenotyping, functional markers

and structural markers provide different types of information about cells, and having robust information for both is important for a comprehensive understanding of cellular characteristics.

Functional markers provide information about the dynamic activities and behaviour of cells. They encompass various aspects of cellular function, such as enzymatic activity, cytokine secretion, proliferation, differentiation, migration, and response to stimuli. Functional markers reflect the biological activities and physiological state of cells, enabling the assessment of their functional capacity and responsiveness to stimuli or interventions. These markers provide insights into how cells interact with their environment and contribute to specific cellular processes or functions. Non-functional markers, also known as structural markers, are features of cells that provide information about their physical and structural characteristics. They include surface markers, intracellular components, organelles, and molecular structures. Non-functional markers are often used to define cell populations based on specific surface antigens or molecular signatures. They help identify cell types, characterize their differentiation state, and provide information about cell structure, organization, and surface properties. Combining functional and non-functional markers allows a more comprehensive characterization of cell populations. It provides a multi-dimensional understanding of cellular behaviour by integrating information about both the functional capabilities and structural attributes of cells.

In this chapter, a cell surface screening panel was used with CMSCs isolated in-house from five different donors to identify homogeneously and heterogeneously expressed cell surface markers. Here for the first time, extensive characterisation of CMSCs was shown, allowing for the identification of key markers constitutively expressed across CMSC donors, which could be used for cell identification. Furthermore, the discovery of markers with significant changes in expression between donors are useful to utilise as a reference point for future functional investigations, which may discern a link with the antigen expression and cell potency.

CMSC phenotype was investigated between passages 4 and 10, with the main aim to determine any difference in phenotypic expression of CMSCs undergoing increasing doubling numbers, which in turn could aid defining a cell passage postulated to be desirable for a CMSC therapy. Cell phenotype analysis was achieved through flow cytometry and immunocytochemistry; cell viability was measured using a PrestoBlue assay; and growth and doubling rates assessed through cell counts. This work was used to choose a passage to perform future work on, including CMSC phenotyping. Ultimately, this research presents an insight into the maximum number of cells that can be gathered from a single cornea donor without affecting cell phenotype, to inform future manufacture, in addition to identifying some key markers for future therapeutic screening of CMSCs.

3.2. Experimental Design

3.2.1. CMSC Culture

CMSCs were isolated from corneoscleral rings (N = 5) and cultured using serum-free stem cell media (SCM). Cells were cultured at passage 0 until they reached 90% confluency. From passage 1 to 10 cells were passaged every 7 days, with full media exchange every 2-3 days. More detailed methods for CMSC extraction and culture are outlined in Chapter 2.2.1.

This group of experiments aimed to investigate any changes in cell characteristics, especially MSC phenotype, as cell population doubling increased. Analysis was performed at passage 4, 6, 8 and 10. A schematic overview of the experiments performed in this chapter can be found in Figure 3.3.

3.2.2. Immunocytochemistry (ICC)

For immunocytochemistry, cells were seeded in 10 well chamber slides (Cellview cell culture slide; Greiner Bio-one) at day 0 (defined as day of passage) and were fixed following culture on day 7. Cells were stained for CD105, CD90, CD73, CD34, ABCG2, ALDH3A1, SSEA4, OCT4A, phalloidin and vimentin. All information about primary and secondary antibodies, and the methods used for immunocytochemistry can be found in Chapter 2.1.2 and 2.2.3.

3.2.3. Flow Cytometry

Flow cytometry was performed at day 0 of each analysis passage. Cells were stained for CD105, CD90, CD73, CD34, SSEA4 and Ki67. All details regarding antibodies and methodologies are located in Chapter 2.2.4.

3.2.4. PrestoBlue Viability Assay

PrestoBlue assay was performed on day 7 of each analysis passage to assess the viability of the cells. Assay methodology is described in Chapter 2.2.2.

3.2.5. Growth Rate and Population Doublings

Growth rate and population doubling of the cells were calculated based on cell counts and the equations displayed in Section 2.2.5.

3.2.6. RT-qPCR

CMSCs were seeded in 6 well plates on day 0. Cells were lysed for RNA collection on day 7 using 350 μ L of RLT buffer. Cell lysis suspension was stored at -80°C until analysis. Following cDNA synthesis, PCR was performed to analyse GAPDH, *ENG*, THY1, NT5E, CD34, *ACTA2* and *ALDH1*. Details on the probes used and comprehensive methods can be found in Section 2.1.3. and Section 2.2.7 respectively.

3.2.7. Statistical Analysis

GraphPad Prism was used for all statistical analysis. In this chapter, ordinary one-way ANOVA was performed with post hoc Tukey's multiple comparison tests to determine any significance in flow cytometry, growth rate and population doubling data between passages. For PrestoBlue cell viability data, ordinary one-way ANOVA was performed with post hoc Tukey's multiple comparison tests to compare the different passages, with separate tests performed for day 1, 4 and 7. N = number of individual donors or donor groups; n = number of technical repeats. Further information on statistics used can be found in Chapter 2.2.9.

3.2.8. BD Lyoplate Cell Surface Marker Panel

CMSCs were isolated from 3 separate corneoscleral disks using methods previously defined and pooled into one sample (N = 5). Samples were cultured to passage 5-7, before being collected for use with the BD Lyoplate Cell Surface Marker Panel (Section 2.1.2. and 2.2.5) Briefly, 242 separate cell surface markers were stained for, and analysed using the BD FACSCanto II. Experimental layout for this experiment is displayed as a schematic in Figure 3.4.

3.2.9. Lyoplate Data Analysis

Heat maps were created for a visual representation of median fluorescence intensity with respect to the isotype control (MFI FI) and percentage of cells from each CMSC donor expressing each antigen. MFI FI and the coefficient of variation (CV) were then used to determine markers homogeneously expressed across donors. Log₂ transformation of the MFI FI was performed to improve the resolution of low FI values, and low variation was selected for by performing a CV calculation on the log₂ MFI FI, and discounting any values above 0.5 (CV of log₂ MFI FI < 0.5).

Hierarchical clustering (HCL) was performed on the remaining markers by Graziela Figueredo from the University of Nottingham using Python. Box and whisker plots were produced for each of the separate clusters to visualise the markers. MFI values were compared to cell percentage data for a greater understanding of antigen expression across the donors.

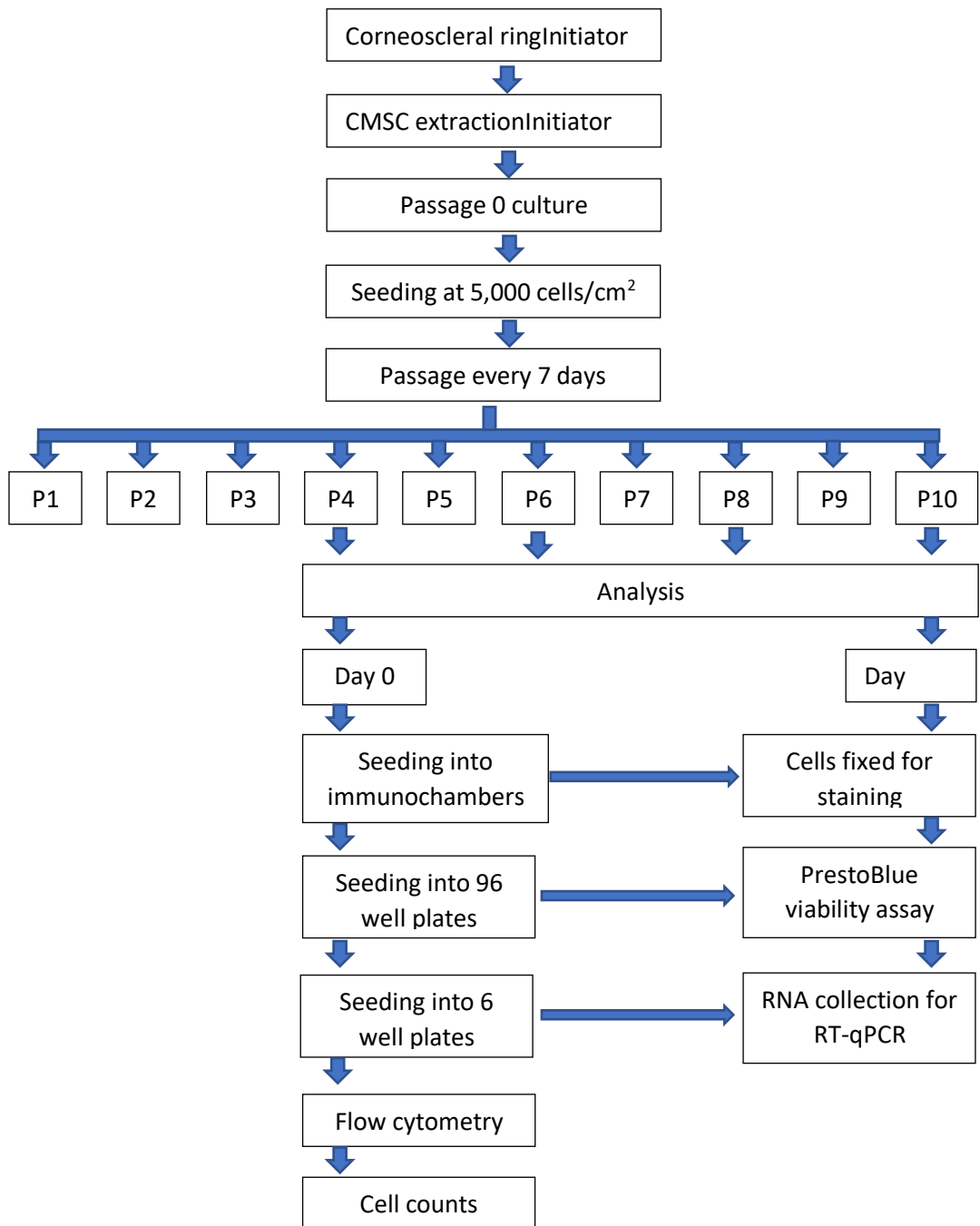


Figure 3. 3. Schematic overview of experiments investigating changes in phenotype, genotype and growth kinetics in CMSCs as passage (P) increases. Schematic shows simplified experimental design for Section 3.2.1.- 3.2.7. Samples were passaged every 7 days, and analysed on passage 4, 6, 8 and 10. The day of passage was referred to as day 0. On day 0 of analysis passages, samples were seeded into immunochambers, 96 well plates, 6 well plates, flow cytometry was performed and cell counts taken. On day 7, cells were fixed for staining, a PrestoBlue viability assay was performed and RNA was collected for qPCR.

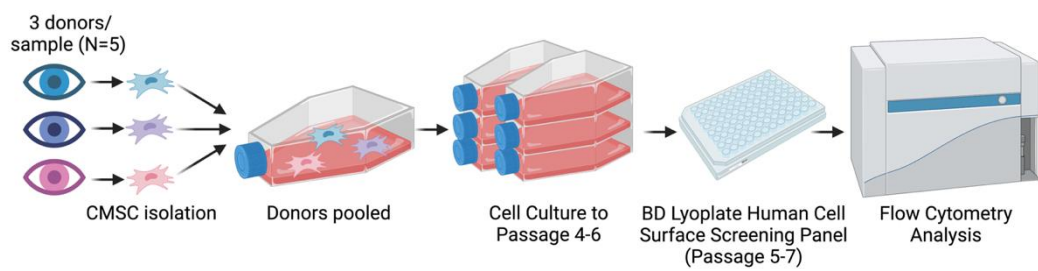


Figure 3. 4. Schematic overview of experiments investigating phenotype of CMSCs to assess donor-donor variation. Schematic shows simplified experimental design for Section 3.2.8. and 3.2.9.

3.3. Results

3.3.1. MSC Marker Expression

To identify any changes in CMSC expression of MSC markers over increasing passage number, CD105, CD90, CD73 and CD34 were assessed phenotypically using flow cytometry and ICC, and genotypically with RT-qPCR (Figure 3.5. - 3.7). MSC markers were constitutively expressed in CMSCs between passages 4 and 10. Flow cytometry and ICC demonstrated expression of MSC markers CD105, CD90 and CD73, in addition to and absence of CD34 (Figure 3.5. and 3.6) ICC figures shown are representative of the whole sample and different donors. Flow cytometry histogram overlays gave a visual representation of equal marker expression at passage 4, 6, 8 and 10 (Figure 3.5.B), with no significant difference detected with any marker, between any passage (Figure 3.5.A) (N = 5, n = 3; CD105, P = 0.9286; CD90, P = 0.7112; CD73, P = 0.148; CD34, P = 0.1827). This data was supported by ICC, where CD105, CD90 and CD73 staining was maintained throughout the passages, with no detection of CD34 (Figure 3.6).

RT-qPCR showed no significant changes in gene expression of *ENG* (CD105), *THY1* (CD90), *NT5E* (CD73) and *CD34*, aligning with the phenotypic results (Figure 3.7).

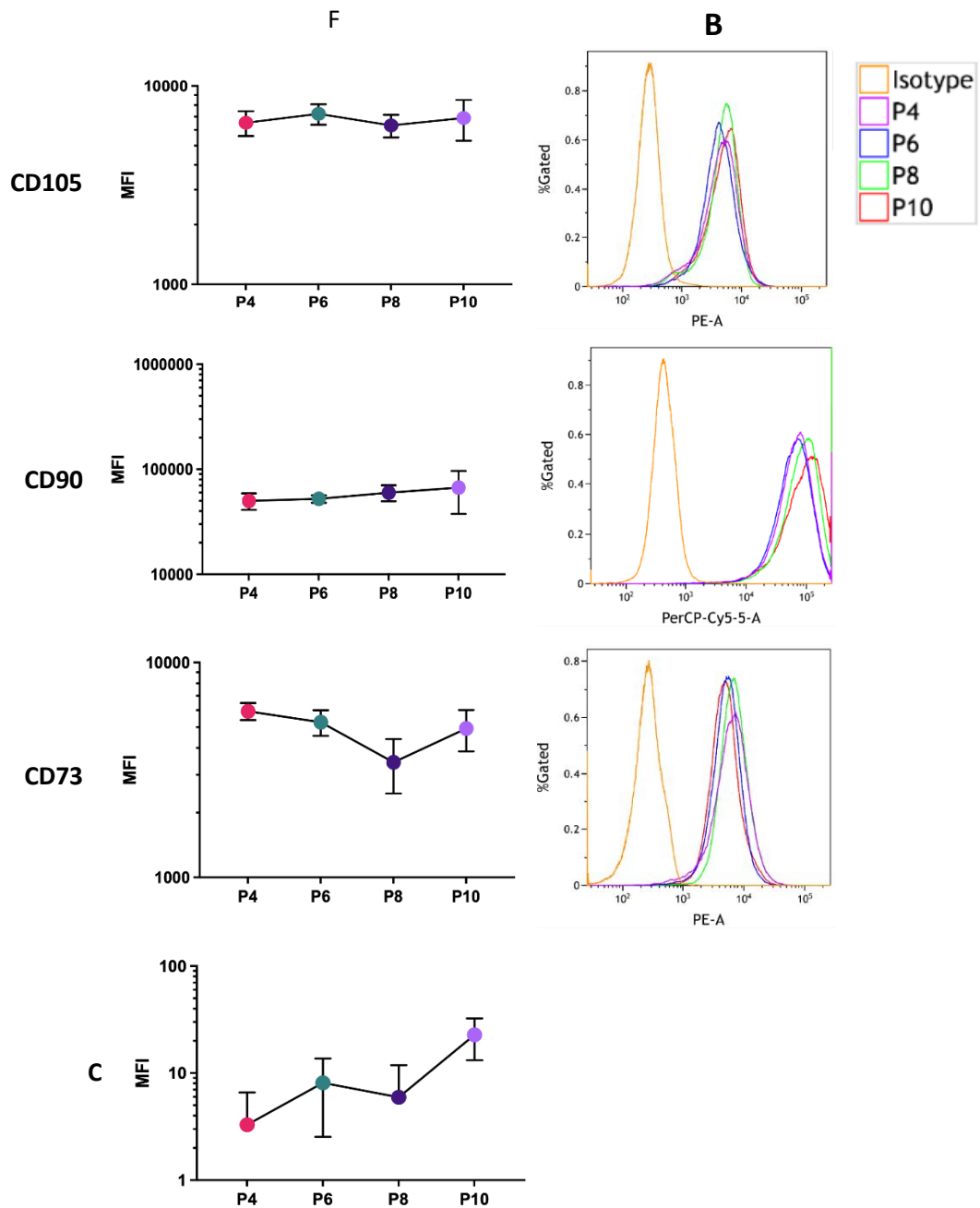


Figure 3. 5. Flow cytometry analysis of MSC markers (CD105, CD90 and CD73) and negative marker (CD34) on CMSCs between passage 4 and 10 (N = 5, n = 3). Column A shows differences in Median Fluorescence Intensity (MFI) over time, with no significant difference in any marker found between passages. Column B shows flow cytometry histogram overlaps of percentage of positive cells in the gated population. The overlays represent the negative isotype control (orange), passage 4 (purple), passage 6 (blue), passage 8 (green) and passage 10 (red). Data shows overlaying of each passage, demonstrating no changes in phenotype. Error bars = \pm SEM.

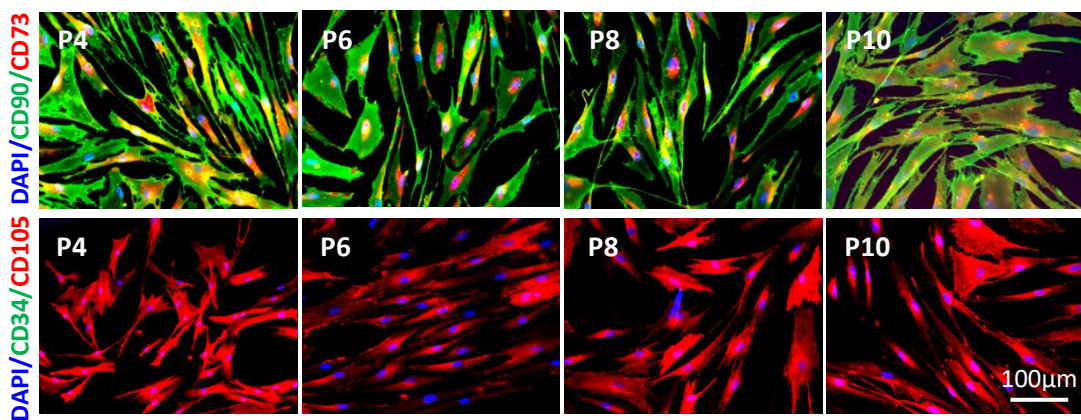


Figure 3. 6. ICC analysis of MSC markers (CD105, CD90 and CD73) and negative marker (CD34) on CMSCs between passage 4 and 10. Data demonstrates constitutive expression of CD73 (red) and CD90 (green) (a) and expression of CD105 (red) but not CD34 (green). Images are representative of whole sample and different donors (N = 5).

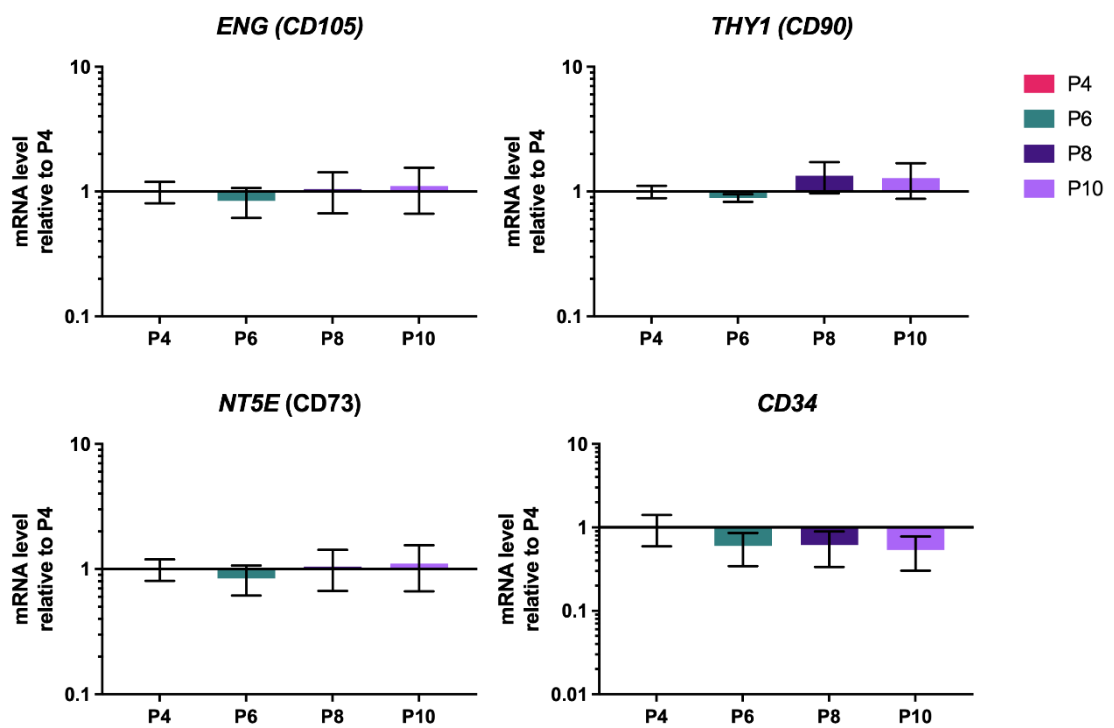


Figure 3. 7. Genotypic analysis using RT-qPCR found no significant difference in gene expression of classical MSC markers (*ENG*, *THY1*, and *NT5E*) and negative MSC marker (*CD34*) in CMSCs between passage 4 and 10 (N = 5, n = 3). All error bars represent sample standard deviation.

3.3.2. Stem Cell and Myfibroblast Marker Expression

To assess changes in CMSC expression of stem cell markers over passages, phenotypic analysis with flow cytometry and ICC investigated SSEA4, ABCG2, OCT4 and ALDH3A1 between passage 4 and 10, and RT-qPCR was performed to determine gene expression of *ALDH* (Figure 3.8 – 3.10). Additionally, to determine if there was dedifferentiation of CMSCs to myofibroblasts over increasing passages, α SMA expression was assessed phenotypically using ICC and genotypically using RT-qPCR.

Positive and negative expression of SSEA4 was detected using flow cytometry (Figure 3.8) and ICC on CMSCs at passage 4, 6, 8 and 10 (Figure 3.9). All ICC images are representative of whole sample and different donors. Most results indicated no significant change in expression ($P > 0.05$), however a significantly higher expression of SSEA4 was observed at passage 8 compared to passage 6 ($P = 0.0273$). This appears to be supported by ICC, where staining is present on a similar ratio of cells but to a lower intensity at passage 6 compared to the other passages (Figure 3.9.a). ABCG2 expression was not detected at any passage by flow cytometry, however ICC indicated low level expression through low intensity staining (Figure 3.8., 3.9.b).

ICC was also utilised to analyse the expression of OCT4A and ALDH3A1, and myofibroblast marker, α SMA (Figure 3.4.c., d). High levels of ALDH3A1 were detected with expression on almost every cell at every passage. This was similar to OCT4A, however here expression appeared to be nonbinary, with varying intensity between cells. No change was observed between the passages. α SMA expression was negative at every passage.

RT-qPCR was used to assess genotypic changes in *ALDH1* (ALDH3A1) and *ACTA2* (α SMA). No significant change was found between passage 4 and 10 (Figure 3.10), supporting the phenotypic data (Figure 3.9).

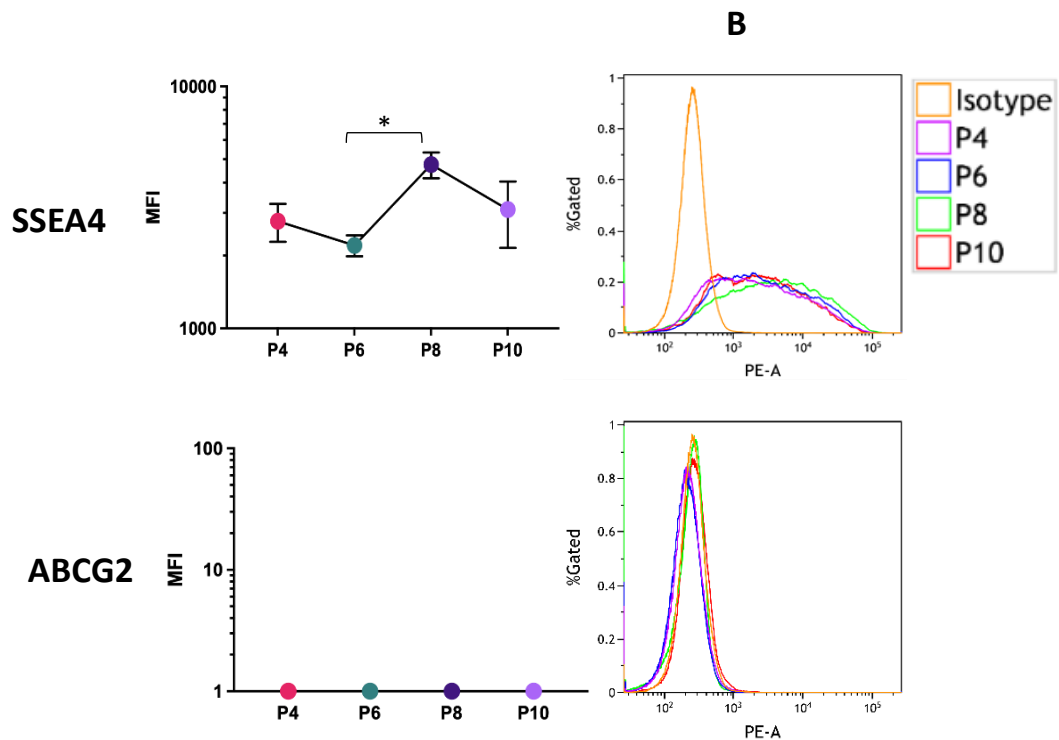


Figure 3. 8. Flow cytometry analysis of stem cell marker expression (SSEA-4 and ABCG2) on CMSCs between passage 4 and 10 (N = 5, n = 3). Column A shows differences in mean MFI over time with standard deviation error bars. No significant difference in any marker found between passages, except SSEA4 expression between passage 6 and 8 (*). Column B shows flow cytometry histogram overlaps of percentage of positive cells in the gated population. The overlays represent the negative isotype control (orange), passage 4 (purple), passage 6 (blue), passage 8 (green) and passage 10 (red). Data shows overlaying of each passage, pointing to no changes in phenotype. Error bars represent SEM.

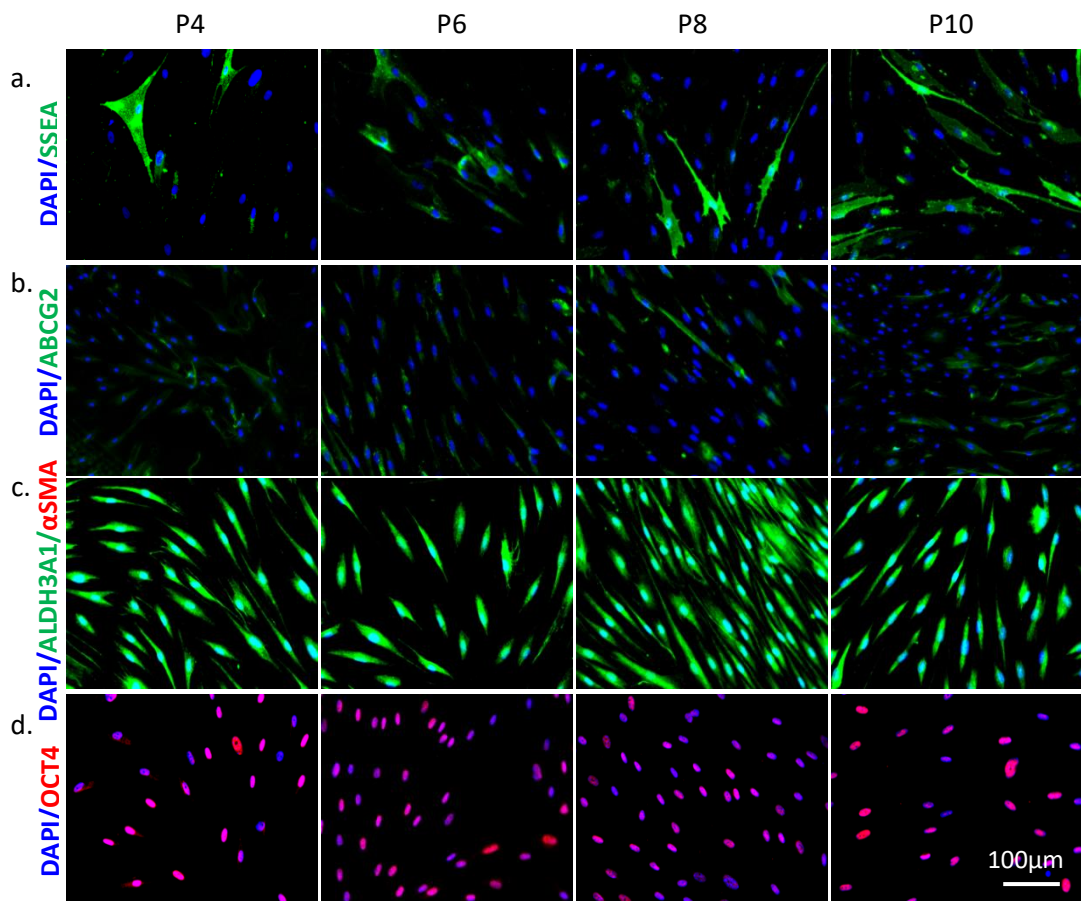


Figure 3. 9. ICC staining of stem cell (SSEA4, ABCG2, ALDH3A1 and OCT4) and fibrotic markers (α SMA) in CMSCs over increasing passages. (a) SSEA4 staining (green) could be detected in a proportion of cells at each passage. (b) Low levels of ABCG2 (green) were observed between passages 4 and 10. (c) ICC shows expression of ALDH3A1 (green) in all CMSCs between passage 4 and 10, but no detection of α SMA (red). (d) OCT4 staining (red) was evident in all passages. ICC images are representative of whole sample and different donors. Scale bars = 100 μ m.

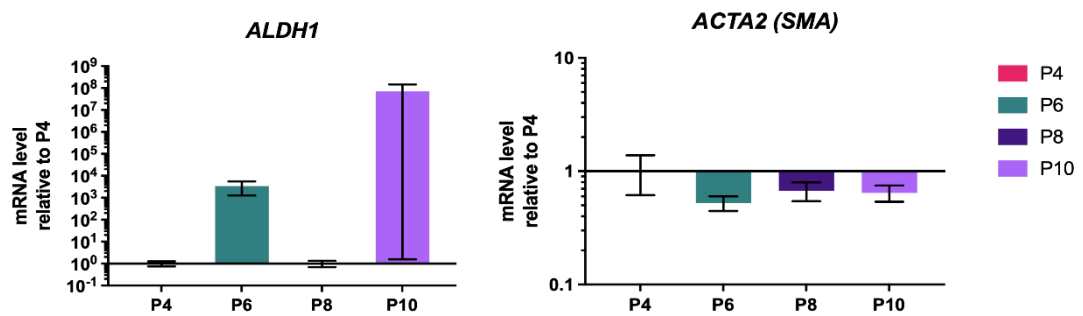


Figure 3. 10. CMSC genotypic analysis of stemness and fibrosis. RT-qPCR demonstrated no significant change from passage 4 to passage 10 in gene expression of ALDH1 (ALDH3A1) and ACTA2 (α SMA) (N = 5, n = 3). All error bars represent StDev.

3.3.4. Cell growth assessment

CMSC growth kinetics were determined through analysis of growth rate, population doubling, cell viability, and CMSC expression of the proliferation marker, Ki67 (Figure 3.11). No significant difference was observed in growth rate (h^{-1}) ($P = 0.4231$) (Figure 3.11.a) or population doubling ($days^{-1}$) ($P = 0.7182$) (Figure 3.11.b) of CMSCs between passages 4 and 10, with average population doubling length (PDL) over all measured passages at 3.31 days (StDev = 0.272). An increasing trend in cell viability was observed between day 1 and day 7 of CMSCs at each passage, which would be expected due to the increased culture time (Figure 3.11.c). However, no significant differences were observed between the passages at day 1, 4 or 7. The proliferation marker Ki67 was also utilised to assess the proliferative capacity of the cells between passages, with no significant difference in marker expression detected ($P = 0.2596$) (Figure 3.11.d,e).

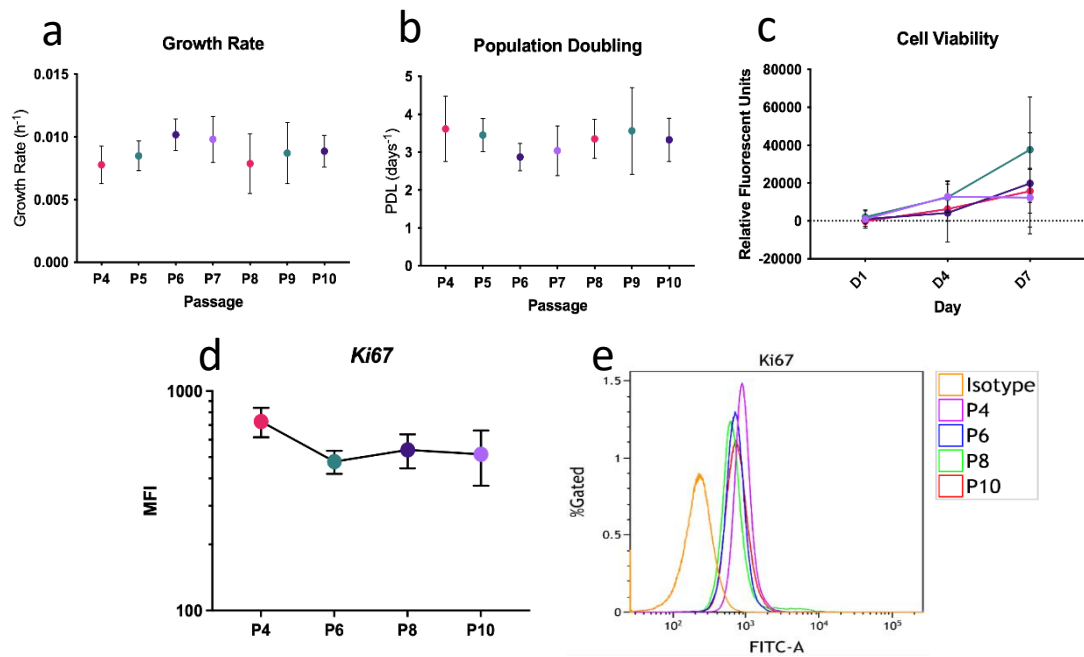


Figure 3. 11. Growth capacity of CMSCs. No significant difference in growth rate (a), population doubling (b), cell viability (c) and expression of proliferation marker, Ki67 (d,e) was detected between passages 4 to 10 (N = 5, n = 3). All graph plots represent sample means with standard deviation.

3.3.4. Structural marker analysis

Vimentin and actin staining were used for structural analysis of CMSCs, including observation of size, morphology and actin cytoskeleton makeup (Figure 3.12). At passage 4 and 6 CMSCs were small and compactly organised, with a spindle-like morphology. At passage 8 and 10, the cells had adopted a larger, more spread out phenotype with lower levels of actin expression, detected by phalloidin.

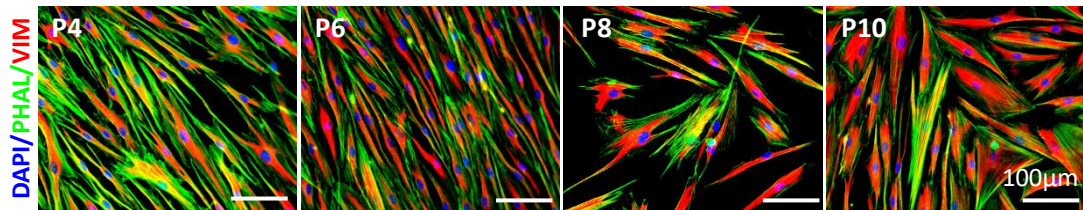


Figure 3. 12. Vimentin and phalloidin staining to assess structure of CMSCs between passages 4 and 10 (P4-10). Cell appear to enlarge by later passages, with actin skeleton breakdown showing signs of aging. Images are representative of whole sample and different donors. Scale bars = 100 μ m.

3.3.5. CMSC Phenotyping

The BD Lyoplate Cell Surface Marker Panel was used to assess expression and donor-to-donor variation of 242 different cell surface markers on 5 donor groups of CMSCs (Figure 3.13). MFI FI for each donor pool was plotted in a heat map against each of the antigens (Figure 3.13). Data was categorized into sections as previously performed by Bear *et al.*, (2012) [154] dependent on the antigen functionality. Results showed that around 60% of the markers are negative for expression on the CMSCs. For example, in the Immune Cell Markers column, CD10 is the only antigen to show a fold increase in MFI (mean: 20.89; StDev: 11.71). Other variable markers of interest included HLA-A2, where only 2 donors showed expression (Figure 3.13, Immune Response Induction/ Immunomodulation). CD99 also has a very low expression in the first donor pool compared to the other 4 (Figure 3.13, Others). The highest MFI FIs can be seen in CD44 (mean: 351.42, StDev: 198.49), CD59 (mean: 271.47, StDev:53.22) and CD81 (mean: 212.69, StDev: 30.12).

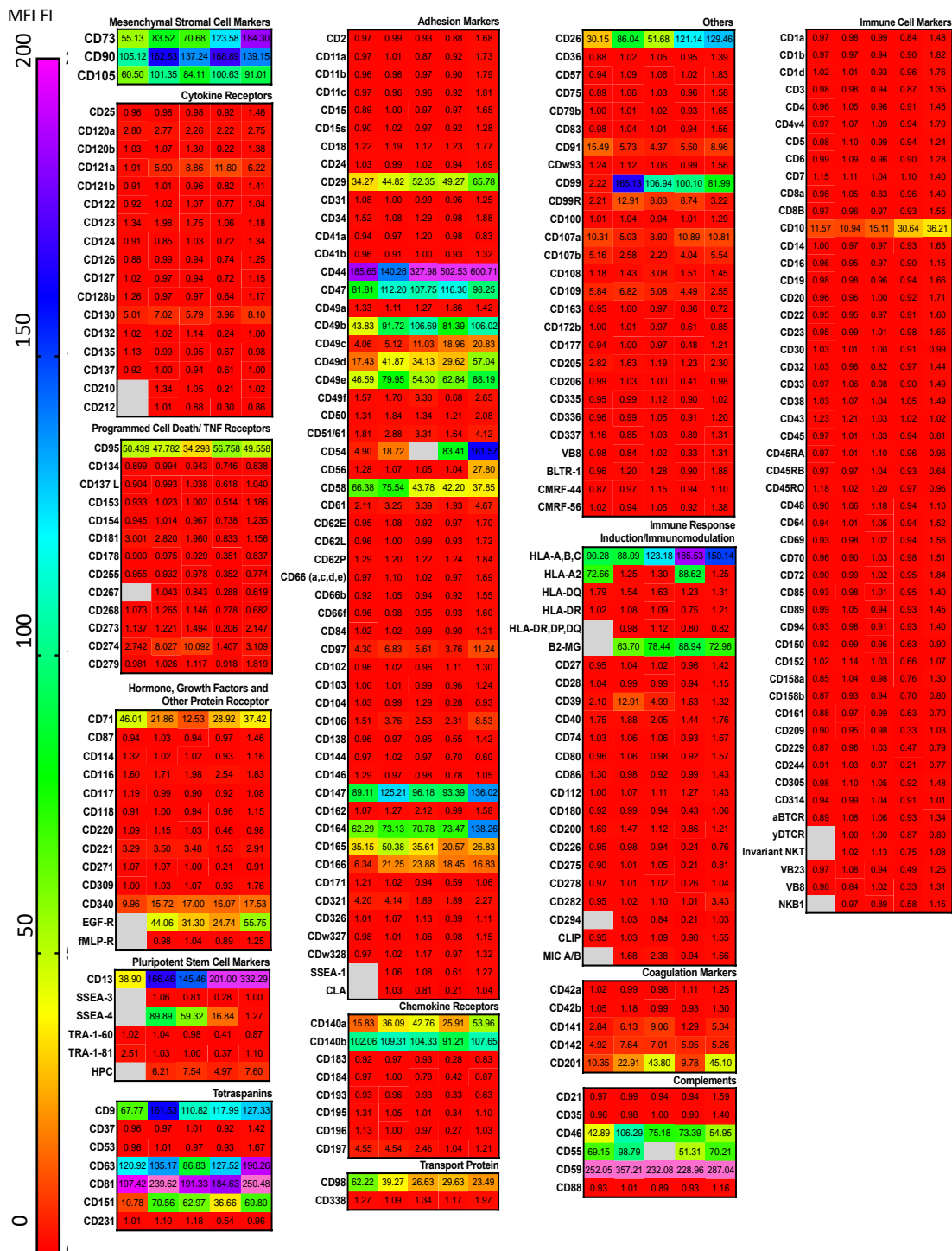


Figure 3. 13. Heat maps showing median fluorescent fold increase (MFI) in expression of different markers on CMSCs compared to the isotype control. Each column represents a different donor group. The BD Lyoplate™ was utilised, which contains 242 purified, monoclonal antibodies and isotype controls. 10,000 CMSCs (N = 5, passage = 5-7) per well were analysed using a BD Canto Flow Cytometer. Colours are representative of MFI FI in the scale on the left, with any values over 200 in pink. Cells were categorized based on previous grouping by Baer *et al.*, (2012) [154]. For mAbclones see Section 2.1.2.ii. and for antigen abbreviation definitions see the Appendix (Table A1.1).

To assess donor-to-donor variation and select markers that are constitutively expressed throughout the samples with little variation, a CV calculation was performed. 55 of the 242 markers reached the selective criteria for low variation, where $CV \log_2 (MFI FI) > 0.5$ (Figure 3.14). Hierarchical clustering was then performed by Graziela Figueredo (University of Nottingham), with 2 main clusters, and 4 closer clusters. Selected antigens were heat mapped for a visual representation of expression (Figure 3.14.b). The two main clusters were categorized based on low expression (Cluster 1) and high expression (Cluster 2). The clusters were plotted separately as box and whisker plots (Figure 3.15), with data demonstrating MFI FI range: cluster 1a: 7.1 to 12.0; cluster 1b: 1.5 to 5.0, cluster 2a: 15.2 to 53.1, and cluster 2b: 66.4 to 351.4. Clusters were therefore defined as: 1a, medium expression; 1b, low expression; 2a, high expression; and 2b, very high expression (Figure 3.14). Key markers of interest were in cluster 2b, due to their constitutively high expression across all the donors. This included 20 markers: CD44, CD59, CD81, CD13, CD90, CD63, HLA-A,B,C, CD9, CD147, CD47, CD73, CD105, CD49b, CD164, B2-MG, CD26, CD55, CD46 and CD49b (Figure 3.15)

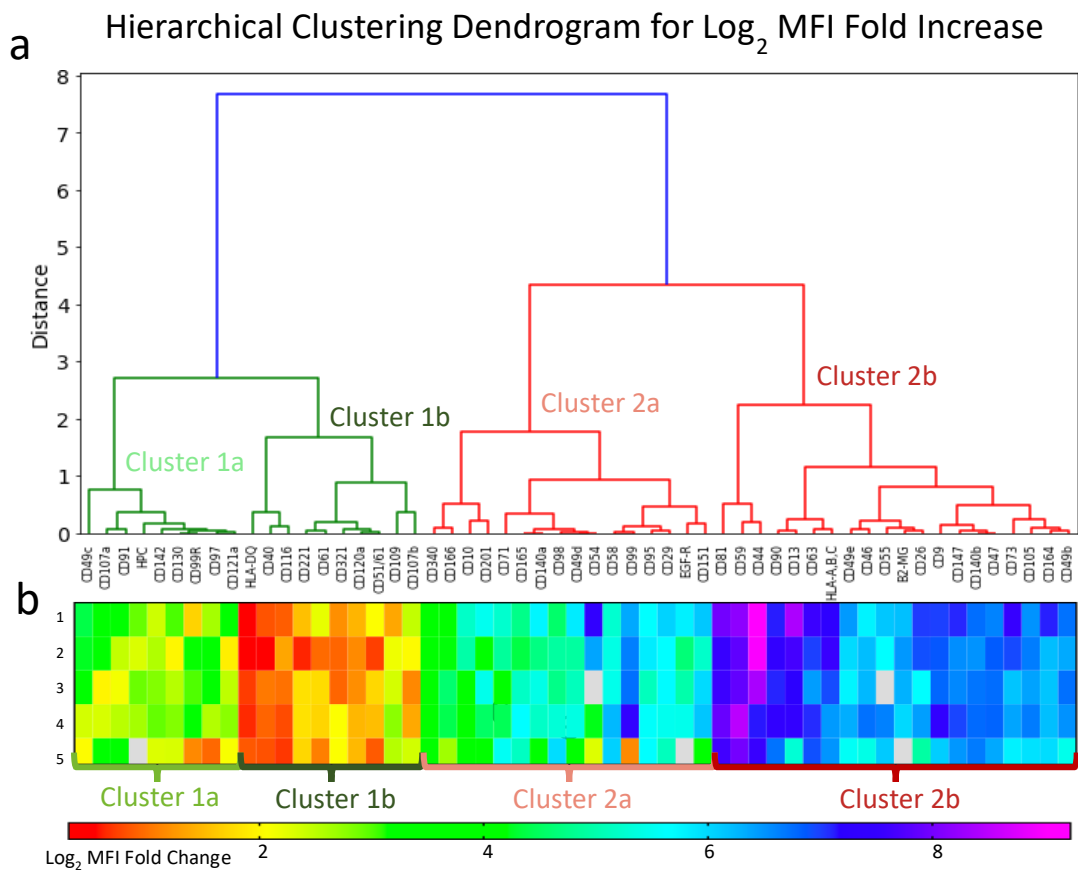


Figure 3. 14. Identification of CMSC markers with the lowest variation between cell donors (N = 5). (a) Marker classification according to unsupervised HCL. Clusters were separated into 1a, 1b, 2a and 2b, based on branching. Data are presented as \log_2 Median Fluorescence Intensity (MFI) fold change compared to the isotype control, with 55 markers selected for by displaying a coefficient of variation (CV) \log_2 MFI > 0.5. (b) Heat map of the 55 selected markers with each row representing a separate donor group and each column in relative position to the antigen in the HCL. Rainbow scale bar from red to purple shows the \log_2 MFI fold change, with highest marker expression seen in Cluster 2b.

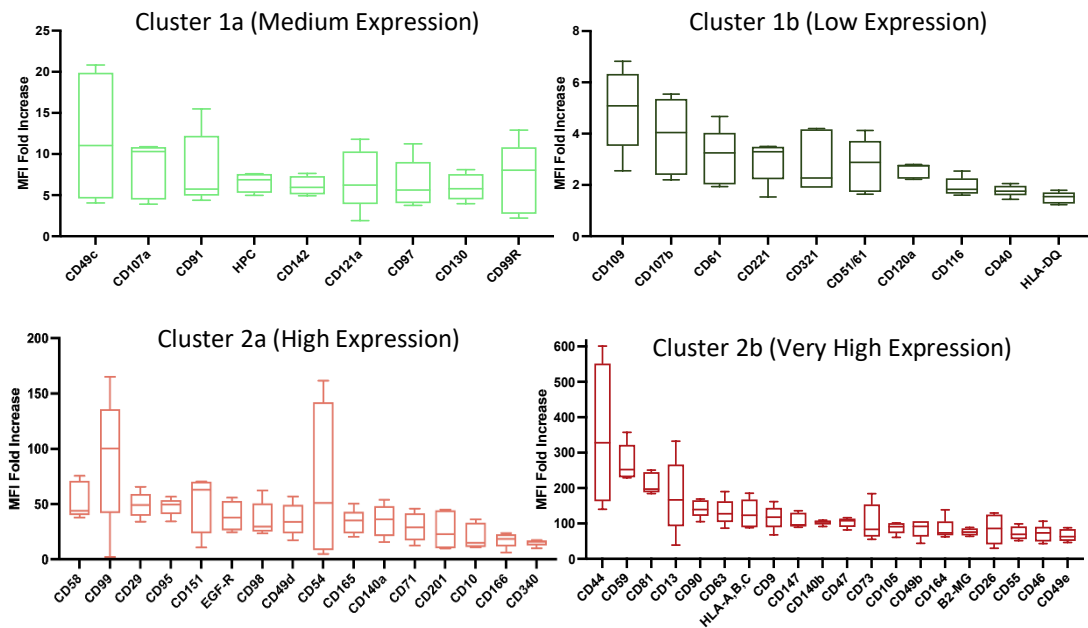


Figure 3. 15. Clusters of markers expressed by CMSCs (N = 5). Positive CMSC markers identified with homogeneous expression across donors, identified through a CV \log_2 (MFI F) < 0.5. Clusters 1a, 1b, 2a and 2b identified through HCL. Boxes in graphs extend from the 25th to 75th percentile, with the center line representing the mean value, and the whiskers showing min and max value Axis differs for each graph to give greater insight into antigen values. Clusters show data categorized as: 1a, medium expression; 1b, low expression; 2a, high expression; and 2b, very high expression.

To develop an insight into screening criteria for CMSC populations with \log_2 (MFI FI) < 0.5, MFI FI was compared to percentage of positive cells (% pos) for the corresponding antigen (Figure 3.16). Data demonstrated a reduction in % pos in order of cluster 2b, 2c, 1a to 1b, with values from 99.2 – 89.6%, 97.9 – 82.4%, 77.5 to 60.9%, and 60.4 – 5.9%, respectively. The decreasing values correlate with the decreasing MFI FI, validating the results.

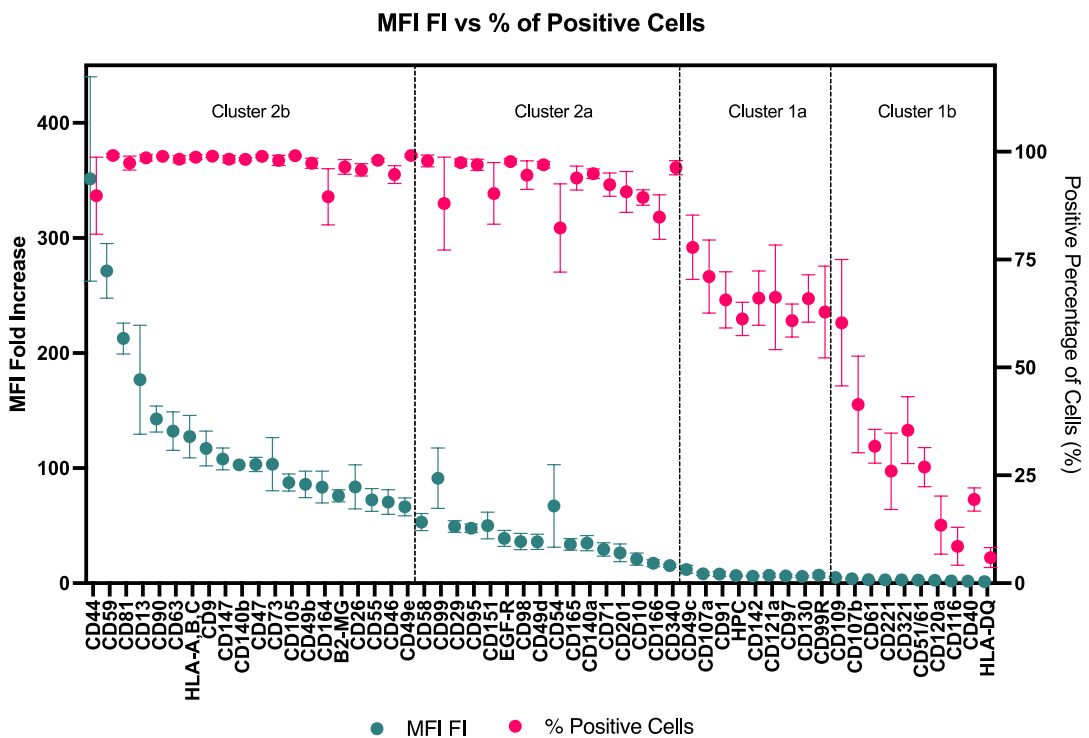


Figure 3. 16. Comparison of MFI FI (turquoise) and percentage of CMSCs expressing each antigen (pink). Markers selected have $CV\text{-}\log_2$ (MFI FI) < 0.5. Antigens were clustered using Hierarchical clustering. Points and error bars represent mean and SEM values of different donor groups (N = 5).

3.4. Discussion

The characteristic profile of CMSCs is growing in accordance with their increasing therapeutic interest. However, the majority of these studies investigate phenotype, genotype and therapeutic efficacy of the cells around passages 4 to 6 [136, 155, 156]. Studies which investigate cells at higher passages could help to develop an increased understanding of the capacity of the cell for clinical translation, giving a greater insight into an optimal therapeutic passage, with higher passages allowing for generation of larger cell numbers during product manufacture.

Prior to determining an optimal therapeutic passage, understanding of the desired cell properties must be defined. With the ultimate goal of utilising the CMSCs as an anti-inflammatory therapy in ocular surface disorders, the cell phenotype with the greatest immunomodulatory capacity would be superior. Due to the well characterised immunomodulatory properties of MSCs, it was hypothesised the highest potency of CMSCs in a therapy for inflammation are likely to correlate with the greatest MSC marker expression.

In this study, with reference to the ISCT MSC marker criteria, MSC phenotype and genotype was assessed between passages 4 and 10 through protein expression analysis of CD105, CD90, CD73 and CD34 cell surface markers, and their corresponding genes; *ENG*, *THY1*, *NT5E* and *CD34*. In line with the ISCT criteria, CD105, CD90 and CD73 were expressed on almost the entire population of cells up to passage 10, with no detection of CD34. As population doubling increased, no phenotypic or genotypic shift was detected, indicating maintenance of MSC phenotype up to 10 passages. With a PDL average of 3.31 days, cells cultured every 7 days, and measurements taken between passage 4 and 10, it can be concluded that the cells maintained this phenotype over 42 population doublings, indicating the ability to continue cell propagation to higher cell numbers for final manufacture.

Although CD34 is predominantly viewed as a haematopoietic stem cell marker, and negative expression is therefore indicative of an MSC phenotype, this is highly debated amongst the literature. Extracted stromal cells from various tissue sources

which did not undergo cell passage and culture have been demonstrated to contain CD34 positive cells [157, 158]. Furthermore previous research has shown that keratocytes *in vivo* express CD34, and when extracted from the corneal stroma and cultured in serum containing media contained populations of CD34+CD105+, CD34+CD73+ and CD34+CD90+ cells [66, 69, 159] concluding that CD34+ expression can be found in CMSC populations. Due to the analysis conducted here starting at passage 4, CD34- expression is fitting with the literature, which points to a CD34 decline over time, and a complete loss of any expression by passage 3 [160].

In addition to MSC phenotype, CMSCs which also display markers associated with progenitor and stem cells may be advantageous, due to the increased plasticity and differentiation potential of the cells. It was hypothesised that this may be an advantageous phenotype based on the self-renewal potential of progenitor cells, and the capacity to modulate the cells to increase efficacy, however it may also present the risk of generating different cells in the cell product. Therefore, it is important to develop an understanding of the stemness of the cells between passages 4 and 10, executed by OCT4-A, SSEA-4, ABCG2 and ALDH3A1 assessment. OCT4-A is an essential transcription factor for pluripotency and self-renewal [161], and SSEA-4 and ALDH, are both common markers for pluripotency [162]. ABCG2 is likely to be involved in the maintenance of stem cells in an undifferentiated state, supported by data demonstrating a reduction of expression in differentiating cells [163]. OCT4-A expression was constitutively expressed between passages, with staining present in almost all cells, however in a non-binary fashion. For SSEA4, a significantly higher expression in passage 8 compared to passage 6 was detected. Although this appears to highlight this population of cells to possess increased plasticity, there is evidence to suggest that unlike OCT4-A, SSEA-4 does not play a critical functional role in the maintenance of pluripotency [164]. High variability was also found between CMSC donors, indicating multiple factors may impact the expression. Truong *et al.* [165] argued that SSEA-4 should be used as a negative marker of stem cells, due to data demonstrating high expression in differentiated corneal epithelial cells, compared to in limbal stem/progenitor cells. The uncertainty surrounding the indicative characteristics of SSEA4 mean that it should

not hold much priority in its influence when choosing an optimal CMSC therapeutic passage, and may not impact the potency of the therapy when selecting a donor. ICC demonstrated ubiquitous staining of ALDH1A3 across all passages, however genotyping revealed significantly higher expression in passage 6 than 4 and 10. Interestingly, ALDH1 isoforms have been identified as important functional markers for stem cell regulation, through the biosynthesis of retinoic acid and other molecular regulators of cellular function [166], providing an argument for cell utilisation at passage 6.

Data obtained investigating ABCG2 proved inconclusive, with no expression detected in flow cytometry but very low signals detected in ICC. It is possible this indicates very weak ABCG2 expression that was amplified with the indirect staining method used for ICC, but not strong enough to be detected by direct staining used for flow cytometry. Keratocytes near the limbus have been shown to positively express ABCG2 [167], and the literature demonstrates that CMSCs cultured in SCM, the medium utilised throughout this study, have higher ABCG2 expression compared to those cultured in serum containing media [160]. This would be expected, due to the knockout serum replacement utilised in place of the FBS possessing advantageous properties for stem/ progenitor cell maintenance, as it eliminates the risk of spontaneous cell differentiation caused by unregulated components in each FBS batch [168]. Furthermore, the supplemented b-FGF and LIF used in SCM are factors essential for the maintenance of pluripotency of human and mouse embryonic stem cells respectively [169] [170]. To develop a greater understanding, cells should be assessed on a genotypic level.

No α -SMA was detected at any passage, indicating the absence of myofibroblasts. This contradicts previous research where small percentages of myofibroblasts have been identified in CMSC culture in serum-free medium. Evidence in the literature suggests that bFGF has the capacity to completely reverse the myofibroblast phenotype in a population of adipose derived MSCs back to the fibroblast phenotype [171]. Therefore, it is possible that by analysis at passage 4, there had been a shift back to a fibroblast phenotype which was conserved through to passage 10.

With an understanding of MSC and stem marker maintenance, structure was also assessed using vimentin and actin staining. Data shows that by passage 8, the cells are larger and have started to adopt a more spread out, less spindle shaped morphology. Furthermore, there is a clear reduction in actin staining, indicating the breakdown of the actin cytoskeleton. This has been linked with cell aging, where collagen fibrils surrounding aging cells become fragmented, less dense and disorganised, and the assembly of the actin cytoskeleton in skin fibroblasts was diminished [172]. These clear signs of aging that manifest at passage 8 are problematic when contemplating use as a therapy, with aged MSCs linked to impaired therapeutic potential [173]. This includes reduced migration ability [174], increased susceptibility to stress-related senescence [175, 176], increased risk of transformation to a form of fibrosarcoma (a soft tissue cancerous tumour) [177], and vitally for an anti-inflammatory therapy, there can be an age-related decrease in several cytokine and chemokine receptors, preventing activation of BM-MSCs and reduced secretion of anti-inflammatory cytokines [174]. It is worth noting that these experiments have been done on cells from older animals or humans, rather than cells subject to long lengths of time in culture, however, could be translated to the CMSCs based on the evident structural signs of ageing. It could be argued that these points add value to the adoption of an allogeneic therapy compared to autologous, as cells can be harvested from young individuals and screened to ensure signs of ageing aren't present before use as a therapeutic agent.

With regards to allogeneic cell therapy manufacture, to avoid waste of resources and therefore reduce cost, it is important to take into consideration the growth rates and proliferative capacities of the cells. Although greater cell number can be achieved through increased population doublings, this is wasteful if there is a significant drop in cell growth at later passages. However, here the data demonstrates no significant difference between passages 4 and 10 of CMSC culture in growth rate, population doublings, cell viability or proliferative marker, Ki67, expression. Consequently, cell growth is not a limiting factor when assessing the optimal CMSC therapeutic passage, permitting the use of allogeneic cell therapy.

The high potential of MSCs as a therapeutic agent and the low success rate of their translation from the bench to clinic, demonstrates a need to determine and tackle the transferability issue [178]. One of the first requirements is to adopt robust characterisation guidelines to accommodate different MSC populations. The ISCT minimal criteria describes plastic adherence, trilineage potential, positive cell expression ($\geq 95\%$) of CD73, CD90 and CD105, and negative cell expression ($\leq 2\%$) for CD45, CD34 and CD14 or CD11b, CD79 α or CD19, and HLA-DR surface antigens [25]. These specifications originated in 2006 and have since been disputed as outdated. Leading to inconsistencies, this criteria does not account for cell passage, cell species or cell source, with the guidelines created surrounding BM-MSCs [178]. Limited characterisation data exists for CMSCs due to their relatively new discovery. Here, medium throughput phenotypic analysis was used as a method to determine markers homogeneously expressed in the notoriously heterogenic MSC population. As expected, the cells positively and negatively expressed the relative markers laid out by the ISCT. However, to expand on the minimal criteria, a group of markers with very high expression, constitutively expressed across the donors, was determined that could be a criterion if screening for CMSCs as a therapeutic cell. These include the key MSC markers CD105, CD90 and CD73, and also demonstrated very high expression of other markers commonly associated with the MSC phenotype, including CD29, CD44, CD164, CD13 and HLA-A,B,C and CD81. These markers expressed a mean percentage of positive cells $\geq 95\%$ except for CD44 and CD164. The high percentages of cells stained provides a threshold for assessment of CMSCs, in line with the 95% value chosen by the ISCT. The mean CD44 and CD164 expression was reduced to 90%, due to one donor pool from each displaying significantly lower values. This may be an anomalous result, due to human or mechanical error, or may indicate a difference in phenotype which needs further assessment for any impact on functionality.

Another marker which showed high variation, with a very small fold change in MFI for just one donor pool compared to the others was CD99 [179, 180]. Interestingly, CD99 has previously been shown to be negative or to show low levels of expression on BM-MSCs, however this marker has been linked to upregulation in an induced

chronic stress model of BM-MSCs, leading to a suppression of autophagy, and therefore an increase in tumorigenicity [181]. This study therefore helped to identify markers of interest for further exploration, for example here, selective screening against CD99 may result in optimal therapeutic results with a reduced safety profile.

In comparison to markers showing high variability between donors, markers constitutively expressed over all donors were of interest, as it can be assumed that they should be present on all CMSCs, and can give an insight into mechanism of the cells. These markers included membrane cofactor protein (CD46), complement decay accelerating factor (CD55) and protectin (CD59), which are all key in protecting cells from complement-mediated lysis [182]. The complement system plays a key role in innate immunity, which can elicit efficient and well-regulated inflammatory and cytolytic immune responses to infectious organisms, damaged tissue, and other foreign organisms. Briefly, complement involves an array of proteins which form a hierarchy of proteolytic cascades. First, there is identification of the pathogenic surface, causing proteolytic cleavage of C3 and C5 to generate the potent proinflammatory mediators, anaphylatoxins (e.g. C3a and C5a). Opsonization, where the pathogenic surface is 'coated' through various complement opsonins, e.g. C3b, leads to pathogenic lysis of the pathogenic surface, through the assembly of membrane-penetrating pores, which is known as the membrane attack complex (MAC). CD46 acts as a cofactor in the cleavage of C3b and C4b, mediated by Factor 1, functioning to protect excessive complement activation [183]. CD55 inhibits complement activation through interfering with the function of C3 and C5 convertases, leading to decreased anaphylatoxins [183]. CD59 binds to complement components C5 and C9, preventing the polymerisation of C9, which is involved in the formation of the MAC complex [184]. The high expression of these three inhibitors on CMSCs provides safety in the knowledge that the cells have a defence against complement phagocytosis, with the potential to survive and tolerate the microenvironment of the ocular surface, where the complement system acts as a primary defence mechanism against pathogenic infection [185]. MSCs genetically modified to express higher levels of the complement inhibitors

demonstrated an improved ability to evade complement lysis [182], highlighting the benefit of these cell surface molecules as key factors for therapeutic screening.

Not all markers demonstrating low variation and high expression (Cluster 2b) are advantageous phenotypes. Human leucocyte antigen class 1 (HLA-1) consists of HLA-A, B and C, and are the molecules responsible for presenting 'non-self' antigens for recognition by CD8⁺ T cells [186]. They are made up of a heavy chain and a light chain which is also known as β 2-microglobulin (B2-MG), and when genotypically deleted, renders HLA-1 non-functional. Consequently, the clustering of B2-MG and HLA-A,B,C expression together is not surprising, as the B2-MG is a necessary part of the HLA-1 complex. Although commonly expressed on MSCs from other sources, categorisation of these markers as homogeneously and highly expressed on CMSCs may raise initial reservations. Controversy surrounds the safety of MSC therapy, with data suggesting that knockdown of B2-MG, and consequent HLA-1 depletion, can evade immune rejection, meaning reduced immunogenicity and improved efficacy. For example, B2-MG knock out in MSCs derived from iPSCs, resulting in no expression of HLA-1, did not affect the phenotype, multipotency or immune suppressive qualities of the cells, however did reduce allogeneic immunogenicity of induced-MSCs to peripheral blood mononuclear cells [187]. Findings demonstrating beneficial responses to HLA-1 depletion appear to be *in vitro* and *in vivo* investigations, compared to evidence from completed and ongoing clinical trials showing that HLA groups which are not matched between allogeneic donor and cell recipients is not a cause for concern, presenting with very low risk of rejection, and literature suggesting no benefit in efficacy of HLA-matched MSCs for treatment of multiple indications [188]. Only a limited number of clinical trials have assessed the generation of potentially harmful anti-HLA antibodies in patients who receive allogeneic MSC therapies. Within this data, discrepancies in outcomes exist, with studies demonstrating no patients developed antibodies specific to the donor [188, 189], and others showing the antibodies could be detected in a proportion of the trial participants [190, 191]. These studies did conclude that regardless of HLA-matching, or the development of donor specific antibodies, there was no clinical relevance in the efficacy of the treatment. Based off the literature, it could be

argued that the high expression of HLA-1 in CMSCs may impact the immunogenicity of MSCs in preclinical investigations, however the complexity and confounding variables *in situ* may offer a protective effect to the cells, with MSCs largely deemed immunoprotected in the clinical setting, regardless of HLA-1 expression.

In addition to potentially lacking necessity, engineering HLA-1 knockdown in therapeutic CMSCs may attenuate the therapeutic capacity of the cells due to the consequent knockdown of HLA-A2 expression. This HLA serotype is the most common HLA-1 molecule [192], interestingly only expressed at relatively high levels in 2 of the 5 markers, showing no expression in the remaining 3 donor pools. HLA-A2 knockdown in umbilical cord derived MSCs (UB-MSCs) demonstrated compromised MSC induced suppression of TNF- α and T cell proliferation, and reduced secretion of anti-inflammatory mediator, prostaglandin E2 (PGE2) [193]. This also resulted in reduced efficacy in a rat model of hyperoxic lung injury, due to reduced survival and impaired functionality for macrophage polarisation. The high discrepancies in CMSC HLA-A2 expression, and the anti-inflammatory, therapeutic properties associated with the antigen make it an ideal candidate for CMSC screening. Future work could explore the functionality of the marker in CMSCs to validate this claim.

Here, any changes in CMSCs over increasing passage was investigated, to determine an optimal therapeutic passage, and to select a passage window for all future work in this thesis. Cells showed limited changes over passages in MSC phenotype and genotype, cell growth, population doublings, cell viability and expression of proliferative marker, Ki67. Although phenotypic analysis and growth characteristics therefore indicated flexibility when choosing an optimal therapeutic passage of CMSCs, the structural analysis demonstrated a change in cell morphology, and breakdown of the actin cytoskeleton pointed towards ageing cells by passage 8, which may impact the therapeutic capacity of the cells. As a result, it can be concluded that future work into the development of a cellular therapy using CMSCs for ocular surface disorders should be performed using cells no later than passage 7, to avoid deleterious effects of older cells, whilst utilising the subset of cells displaying higher levels of stemness. Once an insight into the culture of CMSCs was

developed, medium throughput phenotypic screening of CMSCs between passage 5 and 7 was performed, to provide an overview of cell surface markers with both high and low variation between different donors. HCL was used to identify CD44, CD59, CD81, CD13, CD90, CD63, HLA-A,B,C, CD9, CD147, CD140b, CD47, CD73, CD105, CD49b, CD164, B2-MG, CD26, CD55, CD46 and CD49e as highly expressed with very low variation, with expression in $\geq 95\%$ of cells, except for CD44 and CD164 ($\geq 90\%$). These markers could be used for screening to confirm correct phenotype of CMSCs. Furthermore, markers of interest, including HLA-A2 and CD99, with high levels of variability between donors, were identified which could be used for future functional therapeutic tests for CMSCs.

This is the first time that CMSCs have been assessed in SCM up to passage 10, providing useful information on the cell's characteristics during long term culture. Furthermore, novelty was demonstrated with the extensive characterisation of cell surface markers constitutively and differentially expressed across CMSC donors, which can be used for identifying populations of CMSCs, and as a reference point for future functional investigations. As a continuation of this work, Chapter 4 investigated the phenotype and genotype of CMSCs compared to BM-MSCs, to provide insight into characteristics shared with the 'gold standard' and markers that individuate CMSCs, which could also be assessed for potency in the future.

CHAPTER 4: Medium throughput immunophenotypic and genotypic comparison of CMSCs with BM-MSCs to identify common and differentially expressed markers

4.1. Introduction

Mesenchymal stromal cells (MSCs) present a promising and exciting therapeutic tool for several disorders, with efficacy demonstrated from *in vitro* data, all the way through to their application in hundreds of clinical trials [121]. Extensive characterisation of BM-MSCs compared to those derived from other sources, and consequently their [BM-MSCs] definition as the 'gold standard', is due to their early discovery by Friedenstein and colleagues in 1976 [194]. However, clinical trials using MSCs are exponentially growing, utilising cells from continually increasing sources, including adipose tissue, dental pulp, umbilical cord, amniotic fluid and the cornea [195]. Consequently, the benefits of bone marrow as a primary source compared to other tissues is being challenged [196]. To determine the suitability of cells from other sources, characterisation of the cells for properties including phenotype and genotype, and drawing comparatives to BM-MSCs, can provide a useful insight into the therapeutic potential of the cells.

Currently, flow cytometry is the gold standard tool for assessing the immunophenotype of MSCs expanded *ex vivo*, used as a component of quality assessment for the clinical use of cells in compliance with good manufacturing practices (GMP) standards. Developments in high throughput analysis techniques have also provided an opportunity to screen hundreds of cell surface markers in a single assay, aiding efficient and detailed analysis of the phenotypic profile of MSCs, capable of identifying markers specific to MSCs from each source that could be used for future screening [197]. Comprehensive phenotypic screening of MSCs has

been performed by other groups using this method, for sub-cutaneous fat and visceral fat adipose derived MSCs [198], cord blood derived MSCs [197], adult derived human liver progenitor cells [199], tonsil derived MSCs and BM-MSCs [200].

Flow cytometry is also the key method for identifying the key MSC markers outlined in the International Society for Cellular Therapy (ISCT) guidelines, a commonly used standard in the field of cellular therapy. However, the criteria are regularly challenged for being too narrow and not adequately capturing the diversity of MSCs that exist [201]. This has led to calls for the expansion of the criteria to better reflect the full range of MSCs and their phenotypic 'fingerprint'. Here, the commonalities between BM-MSCs and CMSCs were explored, to identify key markers homogeneously expressed across the two populations of cells. Thorough cell characterisation is necessary to develop a robust and uniform screening panel, aiding the consistent development of a cell product which meets the required safety and efficacy thresholds for clinical success.

In addition to advanced screening techniques in flow cytometry, qPCR can be applied to characterise the genotype of the cell. The Qiagen RT² qPCR profiler for wound healing is a medium-throughput assay, which has been used to assess the wound healing potential and capacity of MSCs from multiple sources including human umbilical cord Wharton's jelly MSCs [202] and pig adipose derived MSCs [203]. The array is made up of genes involved in the key mechanisms of wound healing and fibrosis, including extracellular matrix (ECM) structural constituents, cell adhesion molecules and growth factors. Developing an insight into the wound healing capabilities of MSCs, in addition to phenotypic profiling, helps to build strong characterisation data for the cells prior to therapeutic investigation in addition to highlighting any potential advantageous or limiting markers that may impact the quality of the cells as a therapeutic tool.

The aim of this chapter was to continue the characterisation of CMSCs from Chapter 3, advancing the data by drawing comparisons with the 'gold standard', BM-MSCs. Before molecular or therapeutic comparisons of the cells are assessed, CMSCs display many beneficial practical properties compared to BM-MSCs. In

particular, the harvesting of CMSCs from waste corneal tissue compared to the invasive procedure necessary for BM-MSC isolation provides an opportunity to avoid donor shortages, in addition to allocating a use for tissue that is unsuitable for corneal transplants.

Eye banks are currently responsible for the procurement, processing and distribution of donated eye tissue. Differences in current eye banking methodology exist at a national and international level, employing either hypothermic storage in Optisol, between 2-8°C for graft maintenance of up to 10 days, or organ culture medium at 34-37°C, preserving viable corneas for up to 5 weeks [204]. Both storage methods have shown increased time in organ culture leads to decreases in endothelial and epithelial cell numbers through apoptosis [205], with an endothelial cell reduction of 5% by day 7, increasing to 11-20% by week 3 [206]. However, corneal stromal cells, similar to CMSCs, have been isolated from corneas in organ culture medium stored at ambient temperatures at week 4, providing a use for corneas deemed as unsuitable based on epithelial or endothelial cell characteristics or deficiencies [207] (Figure 4.1). Furthermore, CMSCs are isolated from the stroma of the corneal limbus. During corneal transplants, surgeons will use the centre of the suitable corneal transplant, leaving behind the limbus, which can be repurposed for the harvesting of CMSCs. The potential to produce a therapy from waste tissue provides the motivation to perform further characterisation and deduce the molecular and therapeutic properties of the cells compared to BM-MSCs.

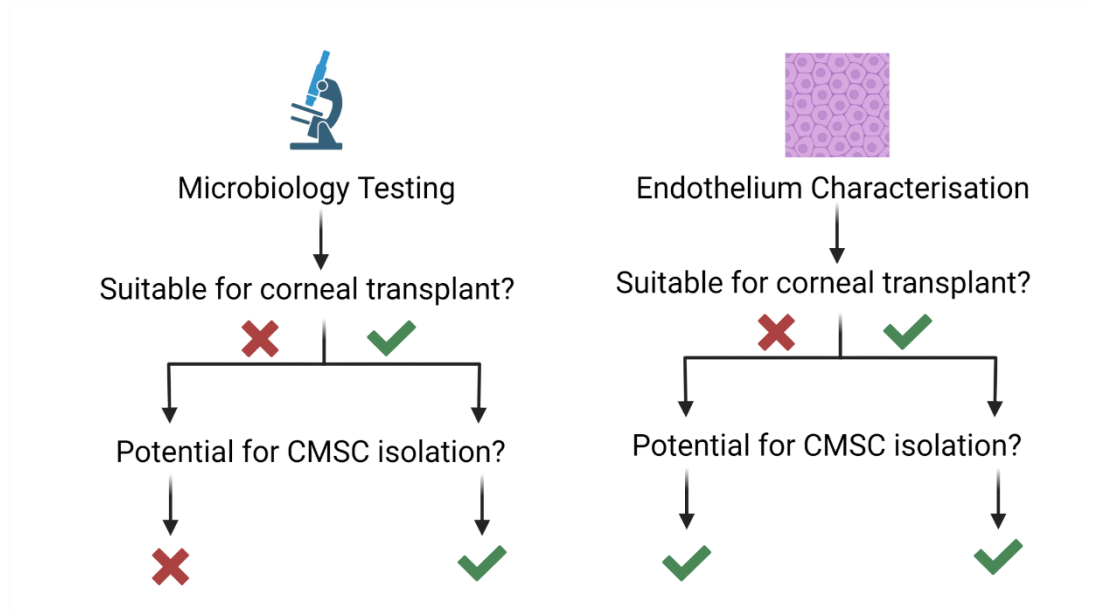


Figure 4. 1. Harvesting of CMSCs from waste tissue in eye banks. Collection could occur using tissue that is suitable and used for corneal transplants, as well as tissue which does not meet the endothelial cell characterisation requirements. Tissue would be unsuitable for cell harvesting if infection was identified during microbiological testing.

In this chapter, medium throughput phenotypic and genotypic characterisation was performed to determine the similar and differentially expressed markers in CMSC and BM-MSC populations. These results form a foundation of robust CMSC characterisation data which can be referred to for future therapeutic testing. Highlighting similarities in cell phenotypic and genotypic profiles provides confidence in the capabilities of CMSCs as a therapeutic tool, and identification of differentially expressed markers gives an insight into potential mechanisms at play, whilst also showing markers specific to the CMSC population.

4.2. Methods

A schematic depicting the experimental flow of the experiments performed in this chapter can be found in Figure 4.2.

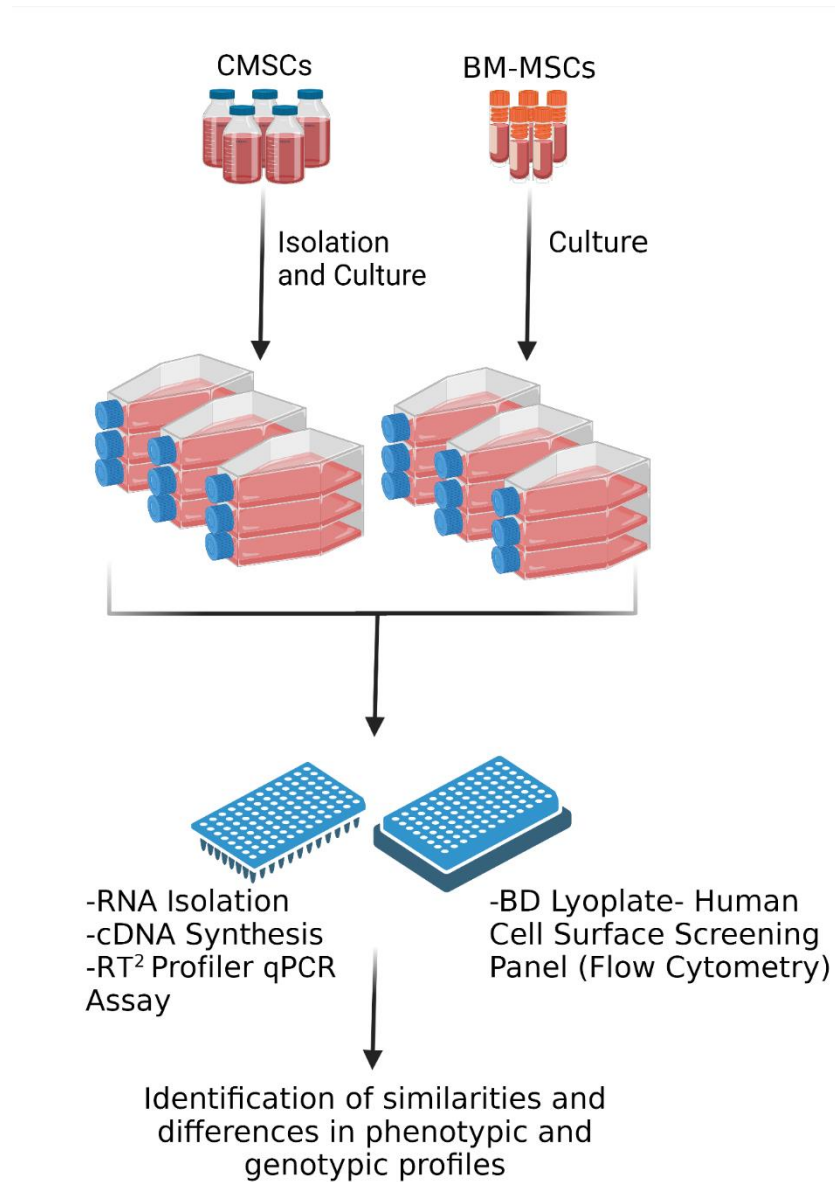


Figure 4. 2. Schematic of experimental procedure, investigating similarities and differences in phenotype and genotype of CMSCs and BM-MSCs.

4.2.1. CMSC Culture

CMSCs were isolated from corneoscleral rings and cultured using serum-free stem cell media. Three donors were pooled at passage 1 to account for variability, creating one repeat. All cell culture details, including extraction and culture are outlined in Chapter 2.2.1. Cells were utilised for experimentation between passage 5 and 7, based on data collected in Chapter 3. Information including age and gender were not collected.

4.2.2. BM-MSC Culture

BM-MSCs were purchased from Lonza (PT-2501) and cultured using serum-free stem cell media. All cell culture details are outlined in Chapter 2.2.1.iii. An experimental passage between 5 and 7 was utilised, to behave as a direct comparison to CMSCs.

4.2.3. BD Lyoplate™ Human Cell Surface Marker Screening Panel

The BD Lyoplate™ Human Cell Surface Marker Screening Panel (BD Biosciences) was used to characterise CMSCs and BM-MSCs. The kit provided detailed phenotypic information for the two cell types. Cells were collected for analysis from untreated CMSCs and BM-MSCs once they had reached 90% confluency. For CMSCs, cells from 5 separate donor pools were analysed (N = 5). For BM-MSCs, cells cultured from 5 separate vials were analysed (N = 5). Detailed methodology of the cell marker kit can be found in Chapter 2.2.5. Median fluorescent intensity fold increase (MFI FI) and percentage of positive cells with respect to the isotype control was used to describe each marker. Unpaired T tests with Welch's correction were used to determine significantly different expression levels.

4.2.4. Hierarchical Clustering

Log₂ transformation of MFI FI was performed to improve the resolution of low values. Average, standard deviation and coefficient of variation (CV) were calculated for Log₂ MFI FI. To define markers common between CMSCs and BM-MSCs, markers across the 2 populations with a CV > 0.5 were eliminated, leaving

the markers with the lowest variance. Unsupervised HCL was performed using Python by Graziela Figuerdo, The University of Nottingham. Following clustering based on MFI, confidence in markers of cluster 1 was classified based on percentage of cell expressing the antigen, with high confidence (85 – 90%), higher confidence (90.01 – 15%), and highest confidence ($\geq 100\%$).

4.2.5. Wound Healing Gene Array Panel

The RT² Profiler PCR Array for wound healing was utilised to provide detailed information of the CMSC genotypic profile compared to BM-MSCs. RNA was collected from pooling of 2 wells of a 6 well plate from untreated CMSCs and BM-MSCs once 90% confluency was achieved. For CMSCs, cells from 3 separate donor pools were analysed. For BM-MSCs, cells cultured from 3 separate vials were analysed (N = 3). Detailed methodology can be found in Chapter 2.2.7. To assess statistically significant genotypic marker expression in CMSCs compared to BM-MSCs, unpaired T tests with Holm-Šídák's multiple comparison test was utilised.

4.2.6. Statistical Analysis

Statistical tests are described in their corresponding method. A 95% confidence level was adopted, represented on graphs as: P = 0.1234 (ns), 0.0332 (*), 0.0021 (**), 0.0002 (***) and < 0.0001 (****). For CMSCs, N = number of donor 'pools', each consisting of 3 donors. For BM-MSCs, N = number of donors cultured from separate, bought vials.

4.3. Results

4.3.1. Phenotypic differences were observed between CMSCs and BM-MSCs.

The BD marker panel allowed high throughput phenotyping of the two cell types in cultured in serum free stem cell media. High expression of MSC markers CD105 and CD90 were observed in both CMSCs and BM-MSCs ($> 90\%$) (Figure 4.3.a), however mean expression of BM-MSCs expressing CD73 was lower at 74.4% compared to 98.0% in CMSCs. Other highly expressed markers across both groups included CD13, (Figure 4.3.b), CD95 (Figure 4.3.e), CD63 (Figure 4.3.h), B2-microglobulin (Figure

4.3.i), CD98 (Figure 4.3.k), CD29, CD58, CD147 (Figure 4.3.g). Correlating MFI heatmaps can be found in the Appendix (Figure A1.1).

Percentage of positive cells was used as a parameter to understand the heterogenous populations, providing a suitable method for comparison between the two cell types. For significant differences between the markers, 8 markers were observed in a significantly higher percentage of BM-MSCs compared to CMSCs (α BTCR, CD8a, CD24, CD49f, CD102, CD108, CD128, CD146, CD273 and CD275) (Figure 4.4). 14 markers were identified with significantly more cells expressing the markers from the CMSC population compared to BM-MSCs (CD107a, CD119, CD121a, CD130, CD141, CD142, CD221, CD321, EGF-R and HPC).

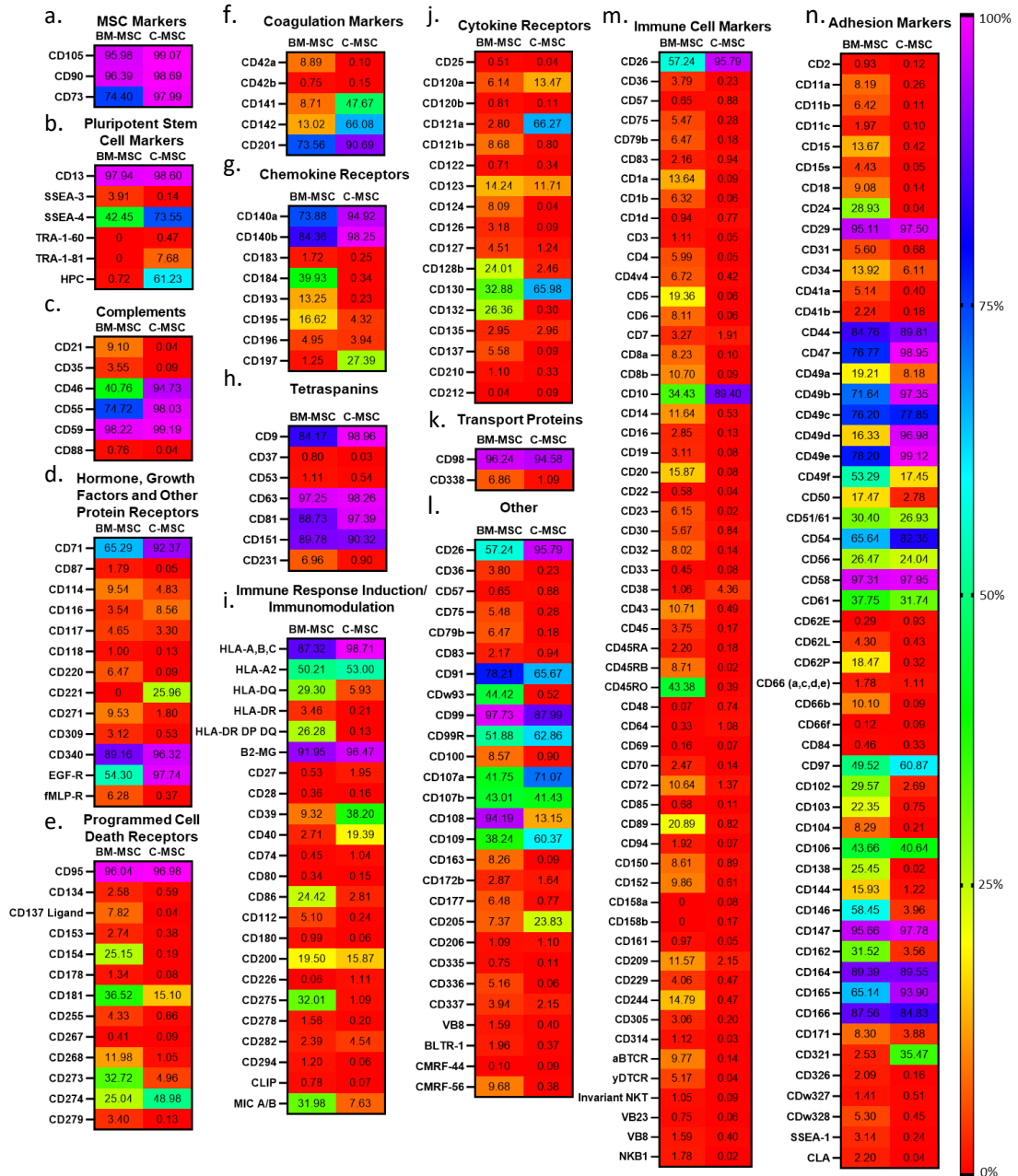
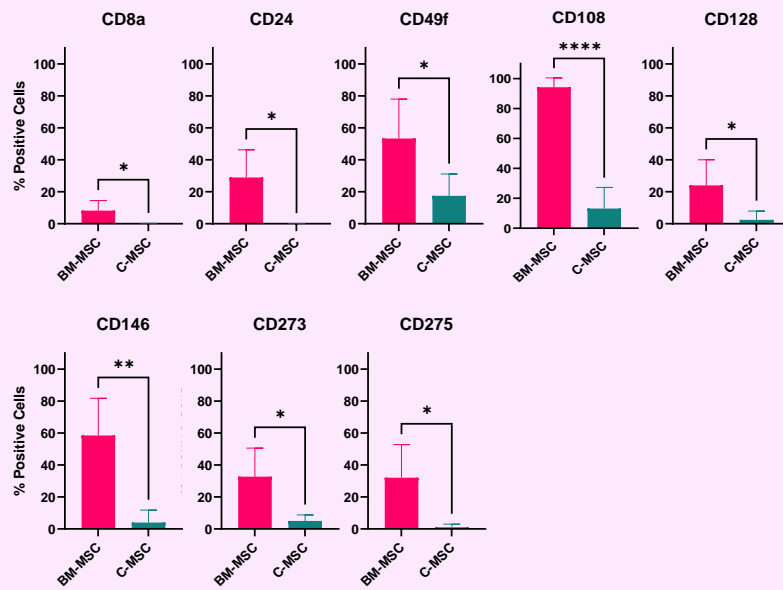


Figure 4. 3. Heat maps showing percentage of positive cells expressing different markers on CMSCs compared to BM-MSCs. The BD Lyoplate™ was utilised (N = 5, passage 5-7)). Colours are representative of percentage in the scale on the left. For mAbClones see Section 2.1.2.ii. and for antigen abbreviation definitions see the Appendix (Table A1.1).

Markers significantly higher in BM-MSCs than C-MSCs



Markers significantly higher in CMSCs than BM-MSCs

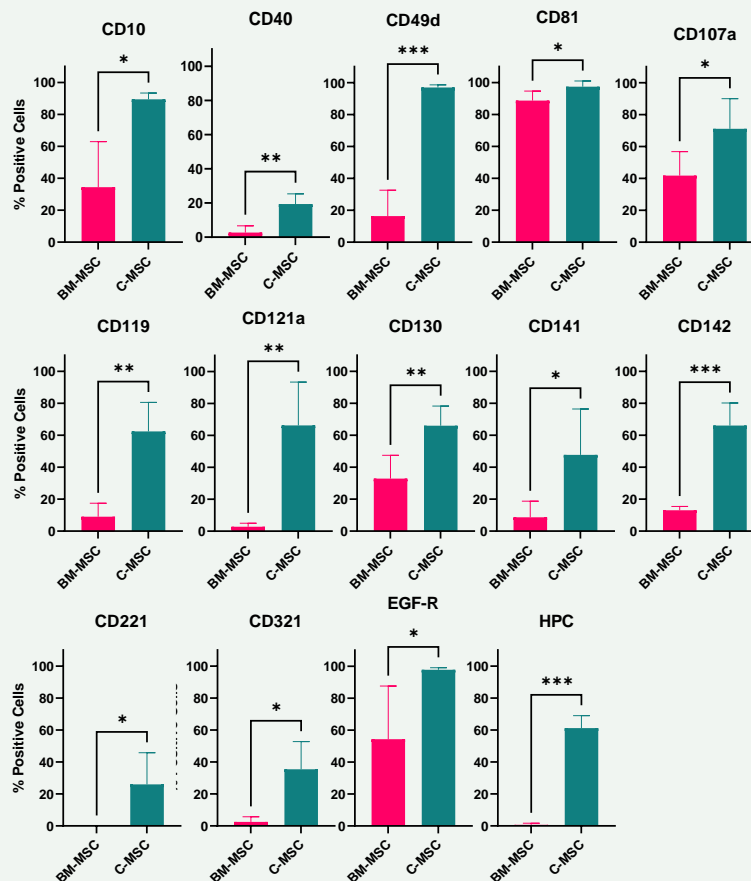


Figure 4. Identification of markers expressed by significantly different proportions of the CMSC and BM-MSC heterogeneous populations based on percentage of cells expressing the marker. Mean values are plotted with error bars for StDev. P = 0.1234 (ns), 0.0332 (*), 0.0021 (**), 0.0002 (***) and < 0.0001 (****). (N = 5).

4.3.2. Identification of cell surface markers specific to CMSCs and BM-MSCs

Markers were filtered for no expression in either the CMSC and BM-MSC population (MFI FI ≥ 1.5 ; percentage of positive cells $< 2\%$) and a Venn diagram was produced based on markers expressed by CMSCs, BM-MSCs or both (Figure 4.5). Of the 242 phenotypic markers originally stained for, 76 were only identified as positive on BM-MSCs, with 6 of these markers displaying a significant difference in expression compared to CMSCs, defining them as specific to BM-MSCs (CD128b, CD146, CD24, CD273, CD275 and CD8a). For CMSCs, 5 markers were classified as positive for this population only, with significance expressed for CD121a, CD40 and HPC, highlighting the expression of these markers as specific to the CMSC population. A further 68 markers were determined to be positive and expressed by cell populations from both sources.

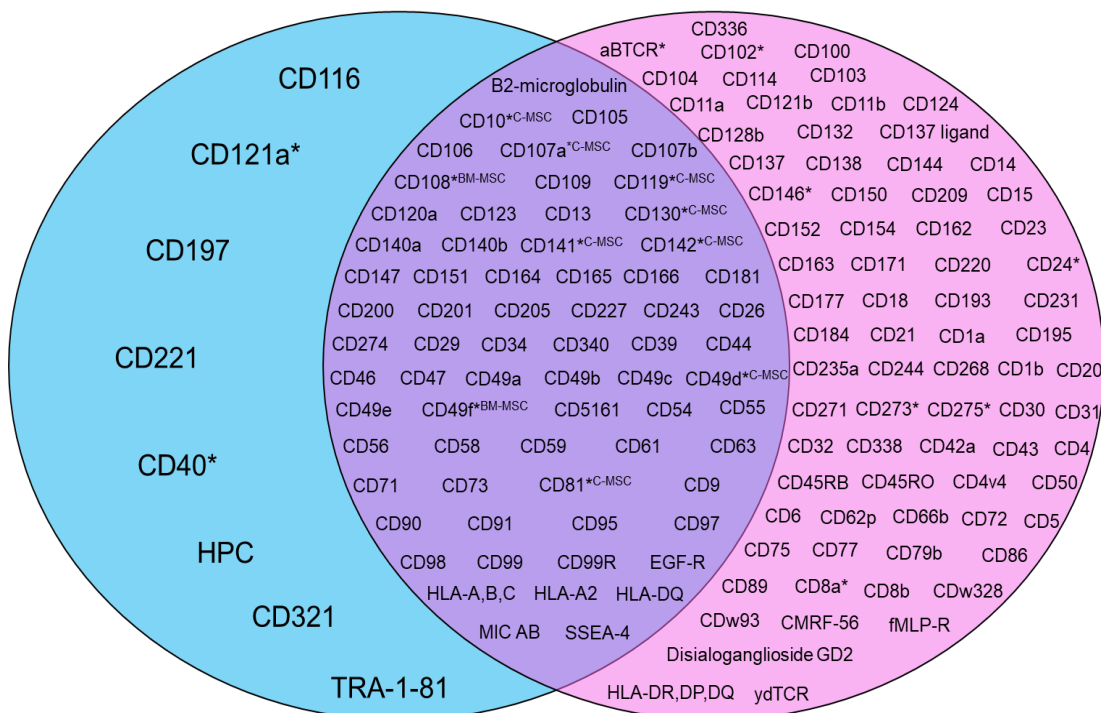


Figure 4. 5. Venn diagram of markers expressed in CMSCs (blue), BM-MSCs (pink) and both (purple). Markers with expression above 2% of each population with MFI ≥ 1.5 were classified as positive. Asterix (*) represent markers with significantly different expression between the two populations. For markers expressed in both CMSC and BM-MSC populations, the Asterix is annotated with C-MSC or BM-MSC, to show the population with the significantly higher expression.

4.3.3. Identification of cell surface markers commonly expressed between CMSCs and BM-MSCs

To assess variation and select markers that are constitutively expressed throughout the samples with little variation, a CV calculation was performed. 30 of the 242 markers reached the selective criteria for low variation, where $CV \log_2 (MFI FI) > 0.5$ (Figure 4.6). Hierarchical clustering was then performed by Graziela Figueredo (University of Nottingham), with 2 main clusters, and 4 closer clusters. Selected antigens were heat mapped for a visual representation of expression (Figure 4.6.b). The two main clusters were categorized based on high expression (Cluster 1) and low expression (Cluster 2). The clusters were plotted separately as box and whisker plots (Figure 4.7), with data demonstrating MFI FI range: cluster 1a: 107.4 to 134.3; cluster 1b: 85.5 to 91.0, cluster 2a: 18.9 to 41.0, and cluster 2b: 6.6. to 11.2.. Clusters were therefore defined as: 1a, very high expression; 1b, high expression; 2a, medium expression; and 2b, low expression. Key markers of interest were in cluster 1, due to their constitutively high expression across all the donors. This included 19 markers: CD147, CD44, CD81, CD13, CD90, CD73, HLA-A,B,C, CD47, CD105, CD63, CD9, CD29, CD151, CD95, CD98, CD49b, CD49e, CD140b and CD99 (Figure 3.15). Of these markers CD49b and CD49e were grouped as high confidence (> 85%), CD81, CD9, CD151, CD140b and CD99 as higher confidence (90.01 – 95%), and highest confidence (> 95%) for CD47, CD147, CD63, CD95 and CD98.

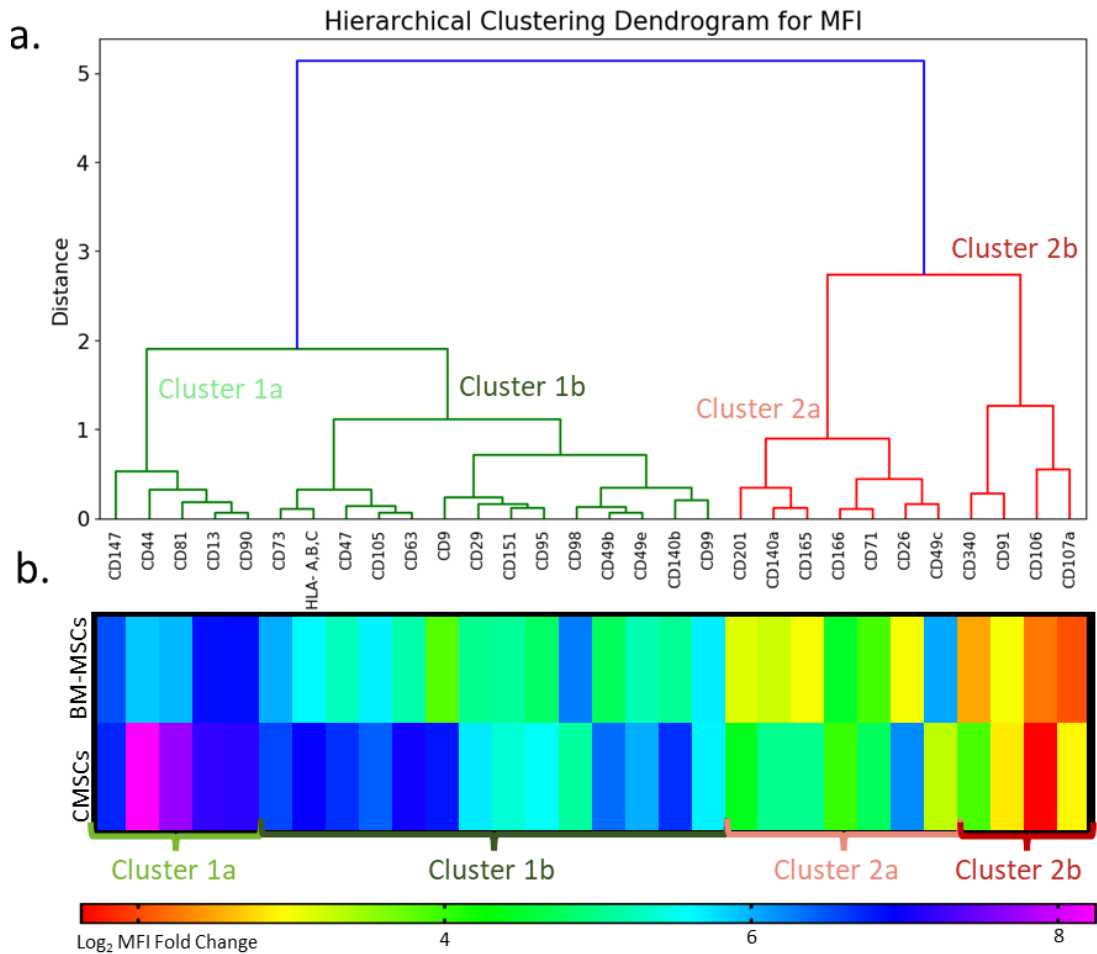


Figure 4. 6. Identification of phenotypic markers with the lowest variation between CMSCs and BM-MSCs (N = 5). (a) Marker classification according to unsupervised HCL. Clusters were separated into 1a, 1b, 2a and 2b, based on branching. Data are presented as log₂ MFI fold change compared to the isotype control, with 30 markers selected for by displaying a CV log₂ MFI > 0.5. (b) Heat map of the 30 selected markers with each row representing BM-MSCs and CMSCs, and each column in relative position to the antigen in the HCL. Rainbow scale bar from red to purple shows the log₂ MFI fold change.

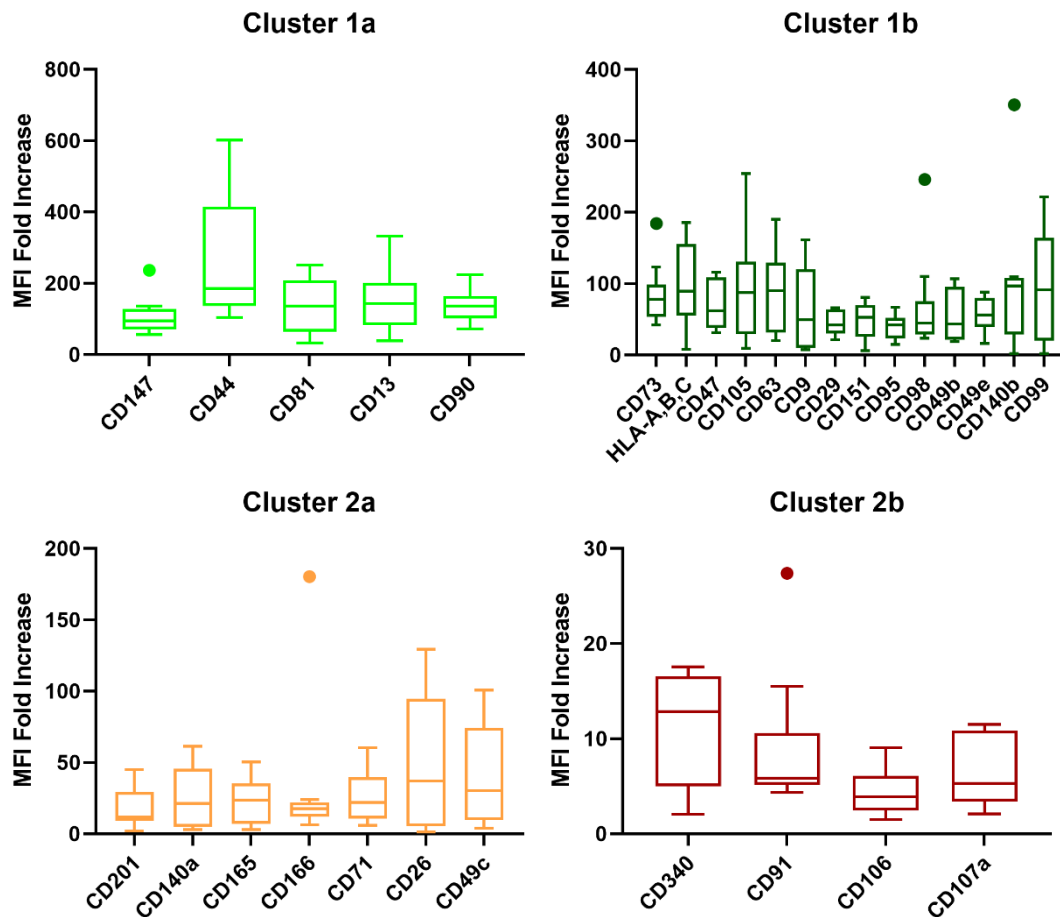


Figure 4. 7. Clusters of markers positively expressed by both CMSCs and BM-MSCs (N = 5). Positive markers identified with homogeneous expression across CMSCs and BM-MSCs, identified through a $CV \log_2$ (MFI FI) < 0.5. Clusters 1a, 1b, 2a and 2b classified through HCL.

Boxes in graphs extend from the 25th to 75th percentile, with the center line representing the mean value, the whiskers showing min and max value, and outliers identified through the Tukey method. Axis differs for each graph to give greater insight into antigen values. Clusters show data categorized as: 1a, very high expression; 1b, high expression; 2a, medium expression; and 2b, low expression.

4.3.4. Comparison of MFI FI against percentage of cell population expressing markers of interest.

To develop an insight into screening criteria for MSC populations with \log_2 (MFI FI) < 0.5, MFI FI was compared to percentage of positive cells (% pos) for the corresponding antigen (Figure 3.16). Data demonstrated a weak trend for decreasing % pos in order of cluster 1a, 1b, 2a to 2b, with values from 87.2-98.5%, 84.4-97.8%, 76.5-87.6%, and 42.1-92.3, respectively. The decreasing values correlated with the decreasing MFI FI, validating the results.

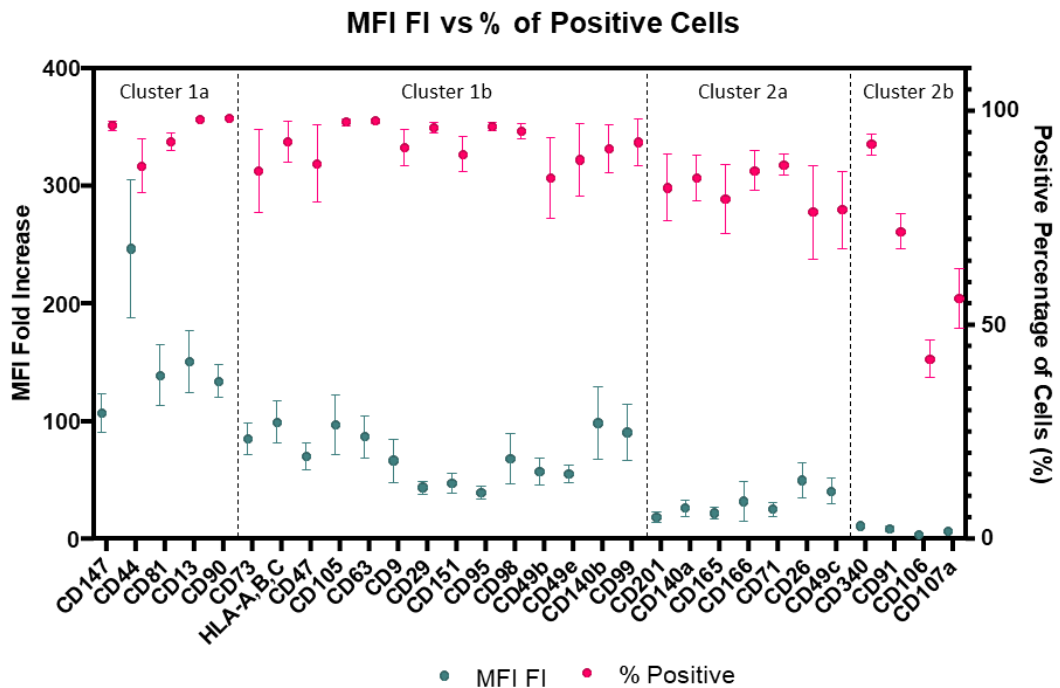


Figure 4. 8. Comparison of MFI FI (turquoise) and percentage of cells expressing each antigen (pink) homogeneously expressed by both CMSCs and BM-MSCs (n = 5). Markers selected have CV- \log_2 (MFI FI) < 0.5. Antigens were clustered using Hierarchical clustering. Points and error bars represent mean and SEM values.

4.3.5. Genotypic differences were observed between BM-MSCs and CMSCs

The Qiagen Human Wound Healing RT² Profiler PCR Array kit was utilized to determine genotypic differences between CMSCs and BM-MSCs (Figure 4.9). Markers were first categorized based on their function, and markers of interest

identified as those which demonstrated significant differences between the two groups.

No significant difference was displayed in any of the markers categorized as ECM structural constituents (Figure 4.9.a). Comparatively, significantly higher expression was observed in the BM-MSC population for cytoskeleton regulators (*ACTA2*, *RAC1*, *RHOA* and *TAGLN*) (Fig 4.9.b); cathepsins and MMPs (*MMP2* and *TIMP1*) (Figure 4.9.c); growth factors (*CTGF*, *EGF*, *FGF2*, *HBEGF*, *PDGFA*, *TGFB1* and *TGFB3*) (Figure 4.9.d); signal transduction receptors, *WNT5A* and *IL6ST*) (Figure 4.9.e); cell adhesion molecules (*ITGA1*, *ITGA2*, *ITGA3*, *ITGA5*, *ITGA6*, *ITGAV*, *ITGB1*, *ITGB3*, *ITGB5* and *ITGB6*) (Figure 4.9.f); inflammatory chemokines (*CCL2*, *CCL7* and *CXCL2*) (Figure 4.9.g); and inflammatory cytokines (*CSF2*, *MF*, *TNF*, *IL10* and *IL6*) (Figure 4.9.h). The only markers showing significantly lower gene expression in BM-MSCs compared to CMSCs were *ACTC1*, *TGFB3*, *IL6ST*, *ITGA4*, *CXCL2*.

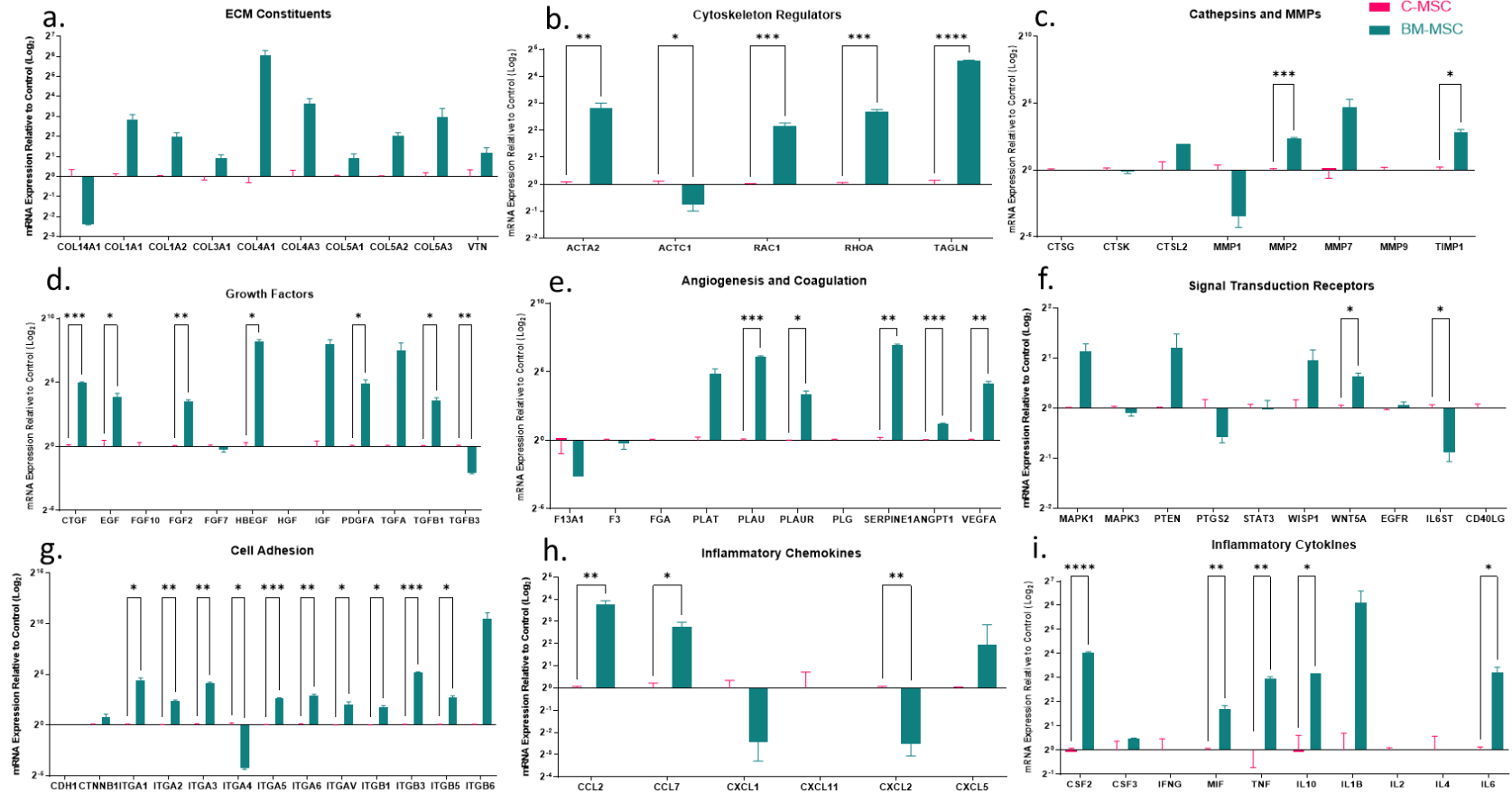


Figure 4. 9. RT² Profiler array to detect the expression of genes associated with wound healing and fibrosis in CMSCs and BM-MSCs (N = 3). Genes were grouped into (a) ECM Structural Constituents, (b) Cytoskeleton Regulators, (c) Cathepsins and MMPs, (d) Growth Factors, (e) Angiogenesis and Coagulation, (f) Signal Transducers and Receptors, (g) Cell Adhesion Molecules (h) Inflammatory Chemokines and (i) Inflammatory Cytokines. Points and error bars represent mean and StDev respectively. P = 0.1234 (ns), 0.0332 (*), 0.0021 (**), 0.0002 (***) and < 0.0001 (****).

4.4. Discussion

Bone marrow has remained the primary source of MSCs destined for clinical applications, despite the invasiveness of the cell harvesting procedure. Consequently, alternative sources are being researched, including CMSCs from waste corneal tissue. In this chapter, a comprehensive characterisation of MSCs isolated and expanded *in vitro* from both the corneal limbus and bone marrow was performed, firstly to identify any markers associated with known functional differences that may impact the therapeutic potential of the cells. In addition, this chapter aimed to identify markers similarly expressed between the two populations, using HCL clustering to provide information on the markers that may be typical to MSC populations, outside of the ISCT criteria (Chapter 3). A medium throughput flow-cytometry and qPCR screening approach was used to investigate the immunophenotype and expression of genes associated with wound healing for both BM-MSCs and CMSCs.

To identify markers commonly expressed across the two cell groups, an unsupervised hierarchical clustering classification was performed using $CV \log_2 MFI < 0.5$, selecting phenotypic markers with the lowest variation across the sample. Currently, no standardisation of release criteria exists for MSC products, with studies mainly using the ISCT guidelines, where great discrepancies in classification have been demonstrated, even in the small number of defined markers, with some studies demonstrating populations of cells expressing the recommended markers in significantly less than 95% of the population, yet still refer to the cells as MSCs [208]. Through phenotypic profiling techniques using flow cytometry, this study identified 19 homogeneous markers which were strongly and consistently expressed by both CMSCs and BM-MSCs. These markers existed in cluster 1 of the HCL analysis, and included the 3 accepted ISCT MSC markers, CD90, CD105 and CD73, and other markers widely accepted to be associated with MSC phenotype but not defined by the ISCT, including CD29, CD44, CD13 and HLA-A,B,C. As an extension to this phenotypic understanding, 12 non-classical markers were also identified. All markers showed a mean expression in over 85% of the population of CMSCs and BM-MSCs, grouped as high confidence ($> 85\%$) for CD49b and CD49e,

higher confidence (90.01 – 95%) for CD81, CD9, CD151, CD140b and CD99, and highest confidence (> 95%) for CD47, CD147, CD63, CD95 and CD98. Identifying these markers with similar expression patterns to ISCT defined MSC markers using CV for the MFI and analysis of percentage of positive cells, represents a stringent method for suitable selection of markers for screening and identifying MSCs. A similar classification method was used by Amati *et al.*, (2018) [197], investigating commonalities between BM-MSCs and cord blood derived MSCs (CB-MSCs). Interestingly, they also demonstrated common expression in high percentages of the population of 7 novel cell surface markers, including CD81, CD47, CD151 and CD98, which were all grouped into cluster 1 (high expression) for CMSCs and BM-MSCs. In addition, markers identified as strongly expressed using cluster analysis of the cell surface proteome of adipose stromal cells correlated with the markers expressed in cluster 1 (high expression) of this study [209]. Synonymity was seen between the strongly expressed markers on the adipose stromal cells and all of cluster 1 (except CD99) for the CMSC and BM-MSC classification. This supporting literature validates these markers as ubiquitously expressed across multiple MSC sources, validating their inclusion for MSC screening. However, it is important to note that a plethora of other cell surface antigens have been identified that weren't represented in this study, perhaps due to the less stringent classification, omitting the CV clearing step that was performed here. The robust phenotyping adds validity to the group of markers identified as commonly expressed by MSCs, regardless of the source, aiding the development of successful screening criteria.

After determining common, highly expressed MSC markers, the second aim was to identify differences in characteristics of CMSCs compared to BM-MSCs. Distinguishing markers specific to MSCs from different sources allows for easier and more accurate isolation of cells, higher confidence in the cell population when applied therapeutically, and aids the understanding of the biology of these cells and their potential for use in a variety of medical applications. The results showed that CD116, CD121a, CD197, CD221, CD40, CD321, TRA-1-81 and HPC were all present in more than 5% of the CMSC population, compared to BM-MSCs which displayed expression less than the 5% threshold employed for identifying positively and

negatively expressed markers. However, only CD40 and CD121a displayed significantly higher expression levels in CMSCs compared to BM-MSCs, substantiating the claim that these markers are specific to the CMSC population compared to BM-MSCs. Interestingly, previous studies have demonstrated nearly undetectable levels of CD40 in BM-MSCs, yet knock out of CD40 from the population resulted in uncontrolled T cell activation at the expense of T regulatory cells, with impaired B cell development [210]. The immunoregulatory properties associated with CD40 expression may point towards an increased potency of CMSCs, even though expression was only found in an average of 19% of the cell population. In addition, gene expression of BM-MSCs demonstrated significantly higher levels of inflammatory chemokines *CCL2* and *CCL7*, and inflammatory cytokines, *CSF2*, *MIF*, *TNF*, *IL10*, *1L1B* and *IL6* compared to CMSCs. Although comparative functional testing and secretomic analysis is required before any potency conclusions can be drawn, the characteristic data proposes that CMSCs have a more suitable profile for an anti-inflammatory therapy, based on their higher expression of the functional antigen, CD40, associated with immunoregulation, and lower expression of inflammatory genes. Different expression levels of key functional markers between sources highlights the benefits of cell characterisation to form new research inquisition pathways.

Expression of CD121a was seen in an average of 66.3% of the CMSC population compared to 2.6% of BM-MSCs. Negative or low expression of CD121a in BM-MSCs is synonymous with previous studies [197], however it has been identified as a key functional marker associated with the high proliferative capacity of synovial fluid derived MSCs [211]. CD121a is also known as the interleukin 1 receptor 1 (IL1-R1), and stimulated proliferation through the ERK signalling pathway following interaction with its ligand, interleukin 1 β (IL-1 β). As with CD40, the expression of CD121a indicates a potential benefit of CMSCs to BM-MSCs through cell surface analysis, highlighting a protein which may increase the sensitivity and therefore paracrine response of CMSCs at an injury site where IL-1 β is likely to be present.

Although CD40 and CD121a were identified to only be present in the CMSC population and not the BM-MSC population, different expression levels of markers in both populations could also be used to distinguish the 2 cell populations from each other. Of the 246 markers, 24 markers were expressed by a significantly different percentage of the population, with 10 of these markers significantly higher in BM-MSCs, and 14 significantly higher in CMSCs. Markers which showed greater significant differences ($P > 0.0002$) were selected to focus on based on the robustness of the data, including CD108, CD49d, CD142 and HPC.

High expression of CD142 in CMSCs (66%) was identified compared to BM-MSCs (13%). Previous studies in BM-MSCs have shown that CD142 expression is donor dependent with high variability in expression, compared to AD-MSCs and WJ-MSCs, which constitutively express the surface antigen [212]. CD142, or tissue factor, is a transmembrane receptor for circulating clotting factor FVII/VIIa expressed in cells surrounding blood vessels. Although the antigen has been identified to increase healing potency of WJ-MSCs, following *in vivo* systemic administration [213], CD142 has been identified as a key trigger for the detrimental instant blood-mediated inflammatory reaction (IBMIR), with major impact on the safety and efficacy of the therapy [214]. The varying levels of CD142 is a concern surrounding the use of cells not routinely in contact with the blood, with calls for cells from non-haematopoietic tissues to be administered in conjunction with anti-coagulants if systemic application is necessary [215]. Topical administration at the ocular surface of CD142+ cells is unlikely to activate IBMIR (due to the lack of a blood supply to the cornea), however it is important to note this as a potential limitation of CMSCs compared to BM-MSCs and should be acknowledged if CMSCs were to be explored as therapeutic options for different tissues, with different administration routes in the future.

An additional marker separating the populations of CMSCs and BM-MSCs was CD49d, noted as an antigen of interest due to its very high expression in CMSCs (97%) compared to BM-MSCs (16%). With expression by almost the whole population of cells, CD49d could be used to assess the purity and consistency of

CMSCs for therapeutic application, in addition to providing a valuable marker for identifying and isolating CMSCs. Low expression of CD49d (α 4-integrin) in BM-MSCs has been previously reported [216], with one study investigating differences between umbilical cord derived MSCs (UB-MSCs) and BM-MSCs, demonstrating comparatively low levels of CD49d in BM-MSCs, however reduced age of the donor (below 20) correlated with higher levels of CD49d and a cell surface more comparable with UB-MSCs [217]. Contradictory to this, the high levels of CD49d observed in CMSCs are likely not related to age, with most corneal tissue harvested from older cadavers, compared to the younger BM-MSC donors. For cell therapies administered systemically, high levels of CD49d have been proposed to be linked with lung clearance of MSCs, impacting the efficacy of the therapy. However, the aim in this thesis was to apply the cells topically through adherence to a functionalised contact lenses (Chapter 6). The higher level of the α 4-integrin (CD49d) in CMSCs may also provide confidence in higher levels of adhesion to functionalised surfaces using fibronectin derived RGD sequences, due to the affinity of the integrin-sequence binding. This would be beneficial, as greater adherence would decrease the risk of cell detachment from the scaffold, where the cells can administer therapeutic effects through paracrine mechanisms [218].

This data was supported at the genotypic level, with significantly higher gene expression of *ITGA4* in CMSCs, (fold increase > 5) suggesting that integrin α 4 is a key cell adhesion molecule expressed by CMSCs, especially when considering the significantly lower gene expression of *ITGA1* (CD49a), *ITGA2* (CD49b), *ITGA3* (CD49c), *ITGA5* (CD49e), *ITGA6* (CD49f), *ITGAV* (CD51), *ITGB1* (CD29), *ITGB3* (CD61) and *ITGB5* in CMSCs compared to BM-MSCs. However, the phenotype data shows that although gene expression may alter for the other integrins, CD49b, CD49c, CD49e and CD29 were found to be common markers expressed over the two cell populations (CV < 0.5), with CD49b, CD49c, CD49e and CD29 expressed by over 95% of the CMSC population. It is important when developing a topical cell therapy where the aim is for cells to remain on the scaffold to behave as wound healing stimulators through paracrine mechanisms, that successful, strong adhesion through integrin-scaffold interaction is achieved, to prevent the integrin/ corneal

ECM interactions. This proposes many challenges, however this data on integrin protein and gene expression provides a useful tool for determining optimal application methods.

A final phenotypic marker of interest was CD108, based on large variability between CMSC and BM-MSC populations. CD108 was expressed by a mean of 13% of the CMSC population compared to 94% of BM-MSCs. Surprisingly, CD108 has previously been identified as a marker which can discriminate between MSCs and non-stem cell MSC cultures [219], implicated with immune regulation, angiogenesis and osteogenic differentiation, features typical of MSCs. However, low CD108 expression in mouse corneas has been demonstrated, likely due to the necessity to maintain low levels of angiogenic factors in the healthy cornea [220]. Increased expression was demonstrated following exposure to angiogenic stimulating factors, including bFGF, however the basal conditions used for this analysis, and the differences in microenvironment and the requirements of the niche BM-MSCs and CMSCs were extracted from, may account for the difference in expression levels observed.

To support this, markers associated with angiogenesis and coagulation (*PLAU* (CD87), *PLAUR*, *SERPINE1*, *ANGPT1* and *VEGFA*) also showed significantly higher expression in BM-MSCs compared to CMSCs. Although vascularisation is a key component for wound healing in many tissues, the primary aim of this thesis was to produce a cell therapy for ocular surface disorders, where it is vital to balance wound healing stimulation and tissue remodelling, whilst avoiding the deleterious effects of corneal neovascularisation. Consequently, the lower expression of angiogenic factors in CMSCs may be advantageous for therapeutic strategies for the cornea over other tissues, once again highlighting the importance of achieving therapeutic efficacy through successful cell characterisation, allowing ease of matching disease or ailment with the correct cell source.

Here, for the first time, a comprehensive, comparative study was performed to investigate the commonalities and differences in phenotype and genotype for BM-MSCs and CMSCs. In addition to the ISCT defined MSC markers, 9 non-classical MSC

markers were identified that were homogeneously expressed by over 85% of the population of cells from both sources (CD49b, CD49e, CD81, CD9, CD151, CD140b, CD99, CD47, CD147, CD63, CD95 and CD98). These markers indicate their specificity to MSCs regardless of their source, potentiating their inclusion in MSC screening criteria, with potential for expanding the current ISCT panel for a more robust selection method and increased safety and efficacy of the therapeutic cell product. Following the observation of similar markers, significantly different markers between the two sources were identified, with CD40, CD121a, CD108, CD49d, CD142 and HPC identified as key markers with higher specificity for CMSCs, based on their expression profile. The functionality of these markers along with genotypic expression, potentiate CMSCs as possessing characteristics associated with increased immunoregulation and reduced expression of inflammatory and angiogenesis factors, however the high expression of CD142 in CMSCs increases their risk of inducing IMBR. Functional tests are required to deduce the true potency and safety implications of each of these markers, but this chapter presents a complex characterisation profile for a relatively novel cell type, providing information on markers similarly and differentially expressed, with potential functional implications. The chapter provides a new depth of understanding the characteristic 'fingerprint' of CMSCs, which can be utilised to determine new investigative pathways.

All of characterisation work to this point has been performed on CMSCs in normal cell culture conditions, using optimised media and without stimulation. Chapter 5 expands on the breadth of data collected in the last Chapter 3 and Chapter 4, by assessing the response of CMSCs to an *in vitro* inflammatory environment, created to mimic the toxic microenvironment of an inflamed ocular surface.

CHAPTER 5: Analysis of corneal mesenchymal stromal cells in an *in vitro*, proinflammatory environment

5.1. Introduction

Anterior corneal injury describes the damage to the corneal epithelium, or the corneal epithelium and the underlying stromal tissue, commonly caused through the modalities of trauma, infection, toxicity, and surgical injury [10]. In response to the injury, damaged corneal cells produce a plethora of pro-inflammatory factors involved in immunomodulation, angiogenesis, chemotaxis, apoptosis and wound healing [221].

When considering a regenerative medicine therapy, it is important to account for how these factors alter the microenvironment of the injury site. Corneal derived mesenchymal stromal cells (CMSCs) have previously been demonstrated to secrete anti-inflammatory factors upon activation in inflammatory environments [33], highlighting their suitability as an anti-inflammatory therapy. Topical application of CMSCs to the ocular surface would be non-invasive, allowing for an easy treatment option, in addition to enhancing therapeutic capacity through direct cell-to-cell contact [113]. However, administration of CMSCs directly into the wound bed exposes them to the plethora of factors released by cells at the injury site, with potential to both decrease viability and increase immunogenicity [222]. It has previously been reported that interferon gamma (IFN- γ) exposure can upregulate the co-stimulatory molecule CD40, adhesion molecule CD54 (ICAM-1), and the major histocompatibility complex-I and -II (MHC-I and -II) [223]. Therefore, not only can this environment increase the stress inside the cell resulting in apoptosis or necrosis, but also increase the risk of exposure to effector cells of the immune system, reducing viability at the injury bed. Exposure to this toxicity is of less importance for other administration routes, including intravenous, where MSCs can remain protected whilst eliciting a response through paracrine function.

Although the factors present at the injury bed can decrease cell viability, they are also capable of enhancing the therapeutic potential of MSCs through cell activation, also referred to as cell priming or licensing. For example, IFN- γ treated MSCs have also shown increased protection against natural killer (NK) cells, in addition to NK cell- MHC-I interaction causing NK inhibition [224]. This idea is where therapeutic cells exposed to inflammatory factors prior to administration have demonstrated increased cell potency, providing an effective tool that can be assessed during the development of cell therapy strategies.

Proinflammatory cytokines previously reported as key mediators in the corneal inflammatory response include interleukin (IL)-1 β , tumor necrosis factor (TNF)- α , and IFN- γ . IL-1 β is a biologically inert pro-peptide, which requires cleavage by caspase-1 following inflammasome activation [225]. Mechanistically, cleavage induced activation of IL-1 β leads to the redistribution of tight junction proteins ZO-1 and occludin, from adjacent corneal epithelial cells (HCECs), causing epithelial barrier disruption [226]. This is similar to the effects of TNF- α on HCECs, with the proinflammatory cytokine also causing disruption to the tight junctions, and increased paracellular permeability [226]. TNF- α is produced by various cell types, and can be found in the epithelium, stroma and endothelium of the ocular surface [226]. Inflammatory and infectious conditions lead to the synthesis and secretion of the cytokine, primarily from macrophages and T lymphocytes, and to a lesser degree, NK cells, neutrophils, dendritic cells, fibroblasts, smooth muscle cells, neurons and keratinocytes [227]. IFN- γ is predominantly secreted from NK cells, T cells and B cells, and enhances inflammation through mechanisms including stimulation of macrophages and dendritic cells, induced maturation of CD4⁺ T cells, and upregulation of MHC molecules, implicated to play a role in the aetiologies of autoimmune diseases including Sjögren Syndrome, and corneal graft rejections [228]. In addition, bacterial lipopolysaccharides (LPS), a cell-wall component of Gram-negative bacteria, has been implicated in many infectious diseases of the cornea, including production of inflammatory cytokines involved in dry eye disease mechanisms [229]. IL-1 β , TNF- α , IFN- γ and LPS have all been implicated in the pathogenesis of inflammation associated ocular surface disorders, including

infection, injury and dry eye [226, 230, 231], and were chosen for use in an inflammatory factor 'cocktail' for this chapter.

The interaction of these pro-inflammatory cytokines and bacterial mitogens with CMSCs, through to secretion of various soluble factors, is likely to involve numerous, complex signaling pathways (Figure 5.1). Although not fully elucidated, previous literature could be used to implicate the activation of nuclear factor kappa-light-chain-enhancer of activated B cells (NF- κ B), and the MAPK pathways; extracellular signal-regulated kinase (ERK), c-Jun N-terminal kinase (JNK) and p38 MAPK [232].

The binding of each factor from the inflammatory cocktail with their corresponding receptors initiates the signaling pathways implicated in the MSC paracrine response, including the activation of p38 MAPK and JNK isoforms (Figure 5.1). NF κ B proteins include NF- κ B2 p52/p100, NF- κ B1 p50/p105, c-Rel, RelA/p65 and RelB, and function as signal-dependent, dimeric transcription factors, regulating genes involved in numerous biological processes, including inflammation. Retained in the cytoplasm by I κ B in an inactive form, activation occurs through three main phases. Firstly, activation of an IKK complex (IKK α and IKK β) leads to phosphorylation of I κ B, resulting in proteasomal degradation and the release of NF κ B. Subsequently, the transcription factor is carried from the cytoplasm, across the nuclear pore into the nuclear membrane by bound importins. In the nucleus, NF κ B then associates with various coactivators to form the transcription complex. The coactivator associations result in the high regulation of NF κ B by different post-translational modifications, for example, phosphorylation and acetylation of NF κ B p65. Phosphate accepting p65 residues behave as downstream targets for upstream kinases, including p38 MAPK, an upstream NF κ B regulatory kinase.

p38 MAPK is one out of the three predominant molecules that comprise the MAPK family, alongside ERK and JNK (Kim and Choi, 2010). These all play a vital role in a variety of biological processes, including cell proliferation, differentiation, apoptosis and inflammation. Each MAPK signaling pathway comprises a MAPK kinase (MAP3K), which mediates phosphorylation and activation of a MAPK kinase

(MAP2K), which in turn phosphorylates and activates a MAPK. The activated MAPKs then have the capacity to phosphorylate a variety of substrate factors including transcription factors, such as NFκB.

The p38 MAPK and JNK isoforms are activated by a variety of cellular stresses and mediators of inflammation, including proinflammatory cytokines, IL-1β and TNF-α, chemoattractants, chemokines and bacterial LPS. ERK 1/2 are predominantly activated by growth factors, but also by ligands for heterotrimeric G protein-coupled receptors (GPCRs), cytokines, osmotic stress, and microtubule disorganization. The implications of the different ligand receptor interactions are summarized below.

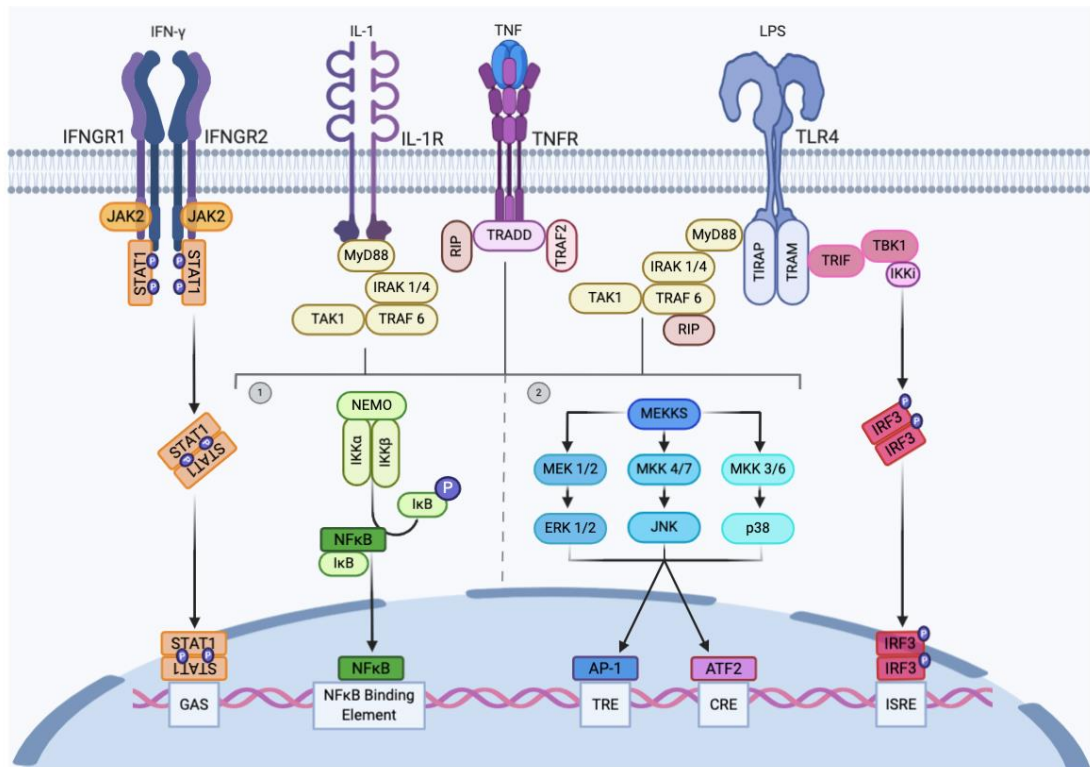


Figure 5. 1. Potential inflammatory signalling pathways following exposure of CMSCs to the inflammatory cocktail (IFN- γ , IL-1 β , TNF- α and LPS). The binding of IFN- γ to IFNGR leads to the dimerization of IFNGR1 and IFNGR2, activating the associated JAKs by autophosphorylation, and providing a docking site for STAT proteins. IFN- γ stimulates the formation of a STAT1-STAT1 homodimer, which undergoes nuclear translocation and binds to the IFN γ -activated site (GAS) elements on target genes. There is crosstalk between IL-1R, TNFR and TLR4 activation. Interleukin (IL)-1 β activates the IL-1 receptor (IL-1R), causing dimerization and downstream signalling via MYD88 and IRAK. This activates multiple downstream pathways, including NF- κ B (1) and p38 MAPK (2). TNF- α binding to TNFR activates IKK via RIP and TRAF2 recruitment by TRADD. IKK activation promotes I κ B phosphorylation and release of NF- κ B, which can then translocate to the nucleus (1). TNF- α binding also activates p38 and MEKK. The activation of MEKK causes JNK to stimulate AP-1, which binds to TPA DNA-response elements (TRE) and ATF2, which binds to cAMP responsive elements (CRE) (2). Activation of TLR by LPS initiates the signalling pathway through MyD88, which recruits IRAK to bind TRAF6 and activate NF- κ B and JNK pathways (1 and 2). Additionally, the LPS/TLR4 MyD88-independent signalling pathway involves the activation of TRIF, TBK1, IKK and IRF3. IRF3 induces binding to interferon-stimulated response elements (ISRE), resulting in IFN-related cytokines, and can potentiate NF- κ B gene transcription [233]. Figure adapted from Hemmati *et al.* (2017) [234].

5.1.1. Receptors

5.1.1.i. Toll-like receptor 4 (TLR4)

TLR4 is a type 1 membrane glycoprotein, with a primary sensory role in determining the presence of pathogens. LPS binds to TLR4 to initiate signal transduction by forming a complex with accessory modules, such as myeloid differentiation-2 (MD-2), LPS-binding protein subunit (LBP) and CD14 [235]. Following activation of the receptor, various cytosolic adapter molecules, including myeloid differentiation primary response gene 88 (MyD88) are recruited, activating various transcription factors, including NFkB, IRF1/3/7 and MAP kinases, responsible for the secretion of multiple pro-inflammatory cytokines.

5.1.1.ii. Tumor necrosis factor receptor 1 (TNFR1)

TNFR1 is expressed in an abundance of tissues, and exists as a component of a TNFR superfamily. TNFR1 can be fully activated through binding of the membrane-bound and soluble, trimeric forms of TNF, including TNF- α . This receptor is linked to several intracellular signaling cascades, including I κ B kinase and MAPK cascades, which modulate the NFkB and AP-1 transcription factors, respectively.

In response to the cytokines, p38 isoforms promote the recruitment of TRAF adapter proteins to the intracellular domains of the receptors, promoting the activation of certain MAPKKs, which in turn activate p38. Interestingly, p38 and ERK are involved in the activation of mitogen- and stress activated kinase (MSK), a MAPK activated kinase which has been implicated as a vital factor in TNF- α mediated transcription of NFkB [236].

5.1.1.iii. Interferon gamma receptor 1 (IFN- γ R1)

The pro-inflammatory factor IFN- γ is recommended by the ISCT as a standard priming method for determining the immunosuppressive capacity of MSCs, with measurement obtained through the quantity of the tryptophan catabolizing enzyme, IDO [30]. Consequently, MSC response to IFN- γ has been the most extensively investigated out of the inflammatory cocktail, and has demonstrated significant increase in IDO from MSCs derived from multiple tissues.

The interferon receptor is split into two subunits, IFNGR1 and IFNGR2, associated with JAK1 and JAK2 respectively [237]. Dimerization of the subunits following ligand interaction activates the associated JAKs by autophosphorylation, providing a docking site for signal transducer and activator of transcription (STAT) proteins. IFN- γ stimulates the formation of a STAT1-STAT1 homodimer, which undergoes nuclear translocation and binds to the IFN γ -activated site (GAS) elements on target genes, thus modulating many factors, including the expression of indoleamine 2,3-dioxygenase (IDO). Alternatively, STAT1 can stimulate the upregulation of IDO through inducing the production of Interferon regulatory factor 1 (IRF-1) [29].

Binding of IFN- γ to IFNGR1 results in an increase in secretion of IDO through the activation of the IFN- γ -Janus kinase (JAK)-signal transducer and activator of the STAT1 pathway [29]. Active STAT1 can then bind directly to the IDO gene regulatory region, or alternatively can stimulate the upregulation of IDO through inducing the production of IRF-1. Additionally, it has recently been shown that PI3Ka is a major novel regulator of IFN γ -induced IDO expression upstream of STAT1 [238]. Complete STAT1 activation through phosphorylation of STAT1 residues, S727 and Y701, is dependent on IFN γ -induced PI3Ka activation, highlighting the complex interplay between the signaling cascades. Interestingly, overexpression of STAT1 induced higher sensitivity in MSCs to IFN- γ , resulting in upregulated secretion of IDO. Comparatively, STAT-1 knockdown lead to complete abrogation of MSC capacity in T cell suppression.

5.1.1.iv. Interleukin 1 receptor type 1 (IL-1 R1)

IL1-R1, required for IL-1B stimulation, is abundantly expressed in MSCs, and similarly to some of the other activation methods previously discussed, results in the activation of the MAPK and ERK pathways, leading to release of the enzyme COX-2, and cytokines IL-6 and IL-8 [239].

5.1.2. Chapter Hypotheses

As each pathway is activated, changes in CMSCs were hypothesised to be observed at both the phenotypic and genotypic level. Here, medium throughput kits were used to assess these changes in inflammatory conditions in addition to assessing

the cell secretome for various proteins including growth factors, wound healing factors, anti-inflammatory cytokines and pro-inflammatory cytokines. The secretome data was compared to corneal epithelial cells in the same conditions to act as a comparative cell type, and it was hypothesized that the CMSCs would secrete more anti-inflammatory and wound healing factors. This characterization data was expected to provide an overview that can be used to set further hypotheses into mechanisms at play, aiding selection of markers of interest, and mechanistic studies in future work. Furthermore, a recovered group was included, where the cells were treated with cytokines and then returned to normal media (not containing cytokines), to give an insight into any potential benefits or limitations of priming the cells within a pro-inflammatory environment. Again, this was performed through the assessment of the phenotype, genotype and secretome of CMSCs.

5.2. Methods

A schematic depicting the experimental set up of the experiments performed in this chapter can be found in Figure 5.2.

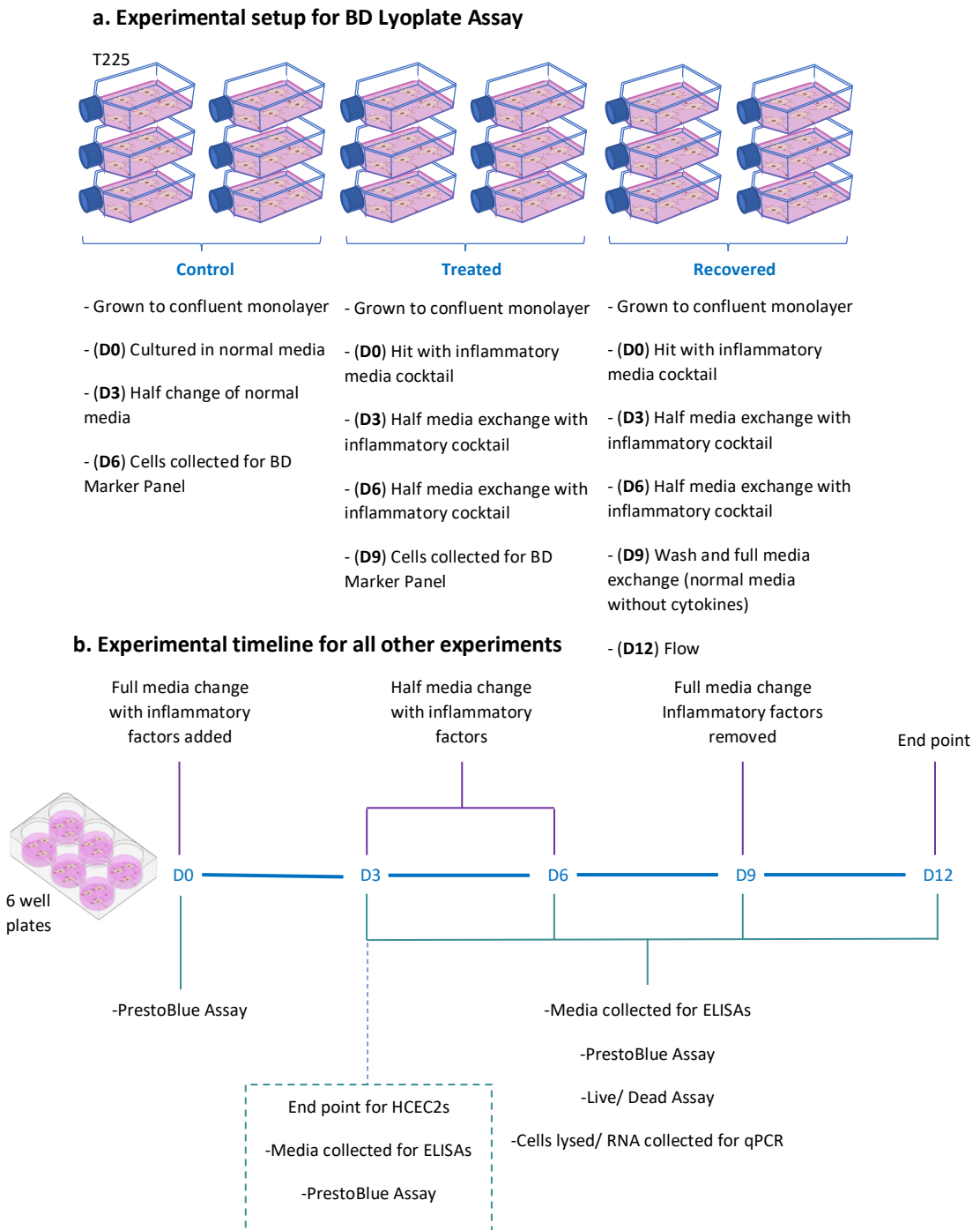


Figure 5. 2. Schematic overview of the inflammatory investigation experimental setup and timeline. (a) Setup of phenotypic investigation of CMSCs in different inflammatory conditions (control, treated and recovered) using a BD Lyoplate. (b) Timeline of all other experiments, from manipulation of conditions at day 0 (D0), to overall endpoint at day 12 (D12).

5.2.1. Inflammatory Cocktail

The inflammatory cocktail defined in Chapter 2, Section 2.1.6, consisting of TNF- α (10 ng/mL), IFN- γ (10 ng/mL), IL-1 β (1 ng/mL) and LPS (1 μ g/mL) in corresponding cell media. Throughout this chapter, conditions defined as control were cells cultured in their media alone, as previously described (Section 2.1.6). The term 'treated' depicts cells treated with an inflammatory cocktail, and 'recovered' describes cells which have been exposed to the inflammatory cocktail, before reversion back to control media.

5.2.2. CMSC Culture

CMSCs were isolated from corneoscleral rings and cultured using serum-free stem cell media. Three donors were pooled at passage 1 to account for variability, creating one repeat, with a total of 9 donors (N = 3). All cell culture details, including extraction and culture are outlined in Chapter 2, Section 2.2.1. Cells were utilised for experimentation between passage 5 and 7, based on data collected in Chapter 3.

CMSCs were the main cell type used for the experiments in this chapter, which aimed to investigate their tolerance, phenotype, genotype and secretome when exposed to inflammatory inducing factors, mimicking an injured ocular surface.

5.2.3. HCEC2 Culture

HCEC2s were cultured in supplemented keratinocyte serum free media and experimented on at 70-80% confluence. Further details on methods and materials for HCEC2 culture can be found in Chapter 2, Section 2.2.1.

HCEC2s were used as a comparative cell type to provide perspective into the levels of each factor secreted by CMSCs when exposed to inflammatory factors (N = 3). This cell type was chosen due to their corneal specificity in addition to their similarity to the corneal primary epithelial cells which would be present at the ocular surface.

5.2.4. PrestoBlue Viability Assay

PrestoBlue was performed to assess CMSC viability in the anti-inflammatory investigation at day 0, day 3, day 6, day 9 and day 12 (N = 3, n = 3). The same assay was performed on HCEC2s at day 0 and day 3. Assay methodology can be found in Chapter 2.2.2.

5.2.5. Live/Dead Staining

Live/Dead fluorescence staining was performed for a qualitative assessment of CMSC viability in the anti-inflammatory investigation at day 3, day 6, day 9 and day 12 (N = 3, n = 3). The stain also provided an insight into cell morphology in the different conditions. Images shown are representative of all cells in the samples, and were taken using the Leica DFC3000 G microscope. Assay methodology can be found in Chapter 2, Section 2.2.3.

5.2.6. BD Lyoplate™ Human Cell Surface Marker Screening Panel

The BD Lyoplate™ Human Cell Surface Marker Screening Panel (BD Biosciences) was used to characterise CMSCs in the inflammatory investigation. The kit provided detailed phenotypic information for CMSCs in different inflammatory environments. Cells were collected for analysis from untreated, control CMSCs at day 9, CMSCs treated with the inflammatory cocktail at day 9, and cells treated with the cocktail for 9 days and left to recover for 3 days, at day 12 (N = 3). Detailed methodology of the cell marker kit can be found in Chapter 2, Section 2.2.5. Brown Forsyth and Welch ANOVA with Dunnetts T3 multiple comparisons test was used to assess statistical significance.

5.2.7. Wound Healing Gene Array Panel

The RT² Profiler PCR Array for wound healing was utilised to provide detailed information of CMSC genotype in the inflammatory investigation. RNA was collected from pooling of 2 wells of a 6 well plate from untreated control CMSCs at day 9, CMSCs treated with the inflammatory cocktail at day 9, and cells treated with the cocktail for 9 days and left to recover for 3 days, at day 12 (N = 3). Detailed

methodology can be found in Chapter 2, Section 2.2.7. RM two-way ANOVA with Tukey's multiple comparisons test was performed for statistical analysis.

5.2.8. ELISAs

ELISAs were performed to investigate quantity of EGF, FGF, HGF, Hya,IDO, IL-10, IL-1ra, IL-6, IL-8, PEDF, PTX-3, TGF- β 1 and TSP-1 in the secretome of CMSCs and HCEC2s in different inflammatory conditions (N = 3, n = 3). ELISAs were performed on cells cultured in 12 well plates. Media was collected from both control and treated CMSCs at day 3, day 6 and day 9, and from control and recovered CMSCs at day 12. Media was collected from control and treated HCEC2s at day 3. ELISA methodology can be found in Chapter 2, Section 2.1.4. To assess statistical significance in CMSCs across the different conditions and time points, RM two-way ANOVA with Sidaks multiple comparisons test was used. To compare CMSC and HCEC2 secretomes at day 3, unpaired T tests with Holm-Šídák's multiple comparison test were performed.

5.2.9. Statical Analysis

Statistical tests are described in their corresponding method. A 95% confidence level was adopted, represented on graphs as: P = 0.1234 (ns), 0.0332 (*), 0.0021 (**), 0.0002 (***) and < 0.0001 (****). N = number of biological repeats and n = number of technical repeats.

5.3. Results

5.3.1. A subset of CMSCs survived the cytokine cocktail, with inhibited proliferation.

Prestobblue viability assay and Live/ Dead staining were used to assess the tolerance and maintenance of CMSCs following exposure to the cytokine cocktail for 9 days, followed by 3 days of recovery, defined by the removal of cytokines and use of normal culture media (Figure 5.3). Data showed that cytokine addition led to a reduction in CMSC viability compared to the control. It appeared the same group of cells remained resistant to the cytokines, as viability was equal at day 3, 6 and 9, supported by Live/ Dead images. When cytokines were removed, Live/ Dead imaging suggested an increase in cell number, however no significant difference was observed in the viability assay.

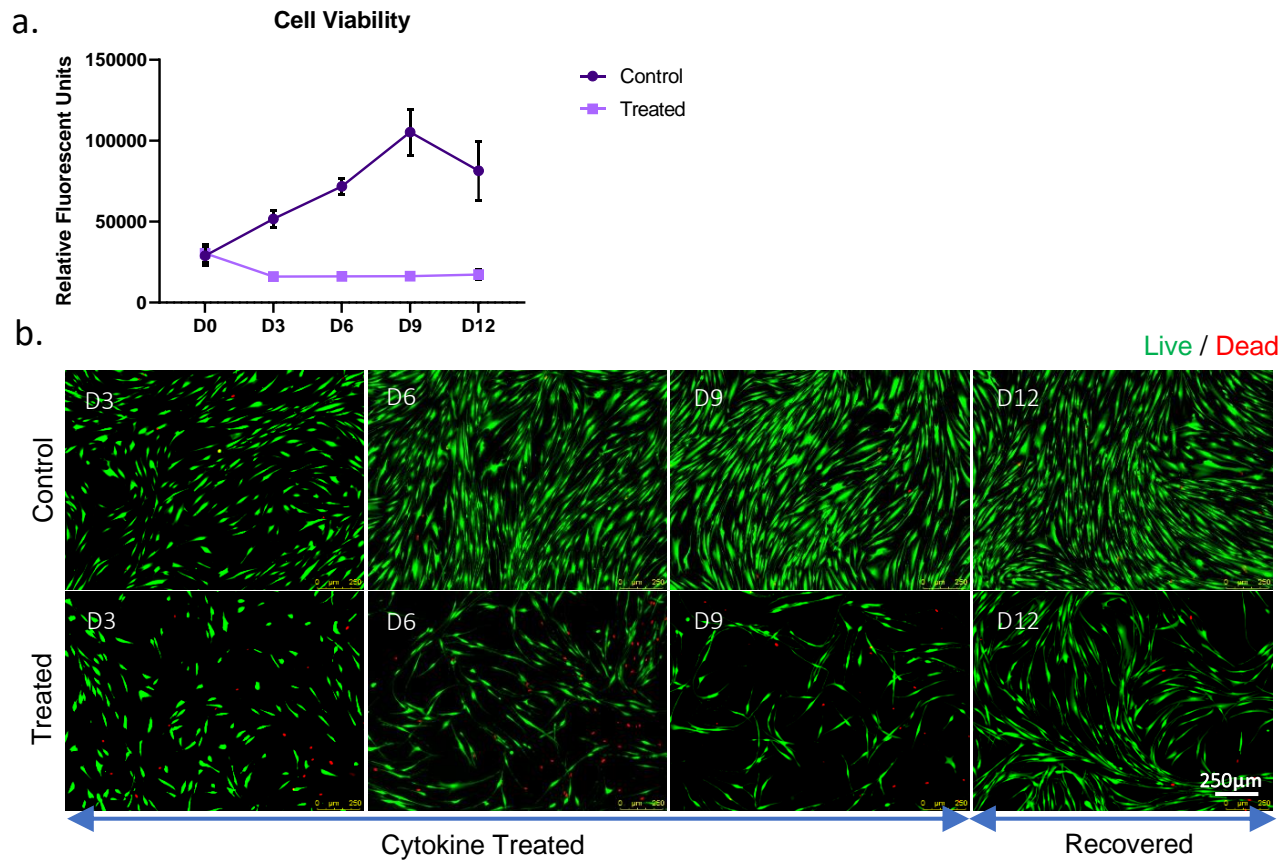


Figure 5. 3. Viability of CMSCs to the inflammatory cytokine cocktail. Cell viability measured in control cells (CMSC media with no exposure to cytokines) compared to CMSCs treated with the inflammatory cocktail for 9 days and left to recover for 3 days in non-cytokine exposed conditions. (a) PrestoBlue was used to measure cell metabolism and visualized in (b) with representative images from Live/Dead staining (Green/Red respectively). Graph shows mean relative fluorescent units measured and error bars represent SEM (N = 3, n = 3) Images are representative of all cells for each condition. Scale bar = 250 µm.

5.3.2. Phenotypic differences were observed between CMSCs in different conditions.

The BD marker panel allowed high throughput phenotyping of CMSCs in non-cytokine-exposed cell culture conditions, following exposure to cytokines, and following addition and removal of cytokines. MSC markers CD73, CD90 and CD105 were highly expressed across all groups (> 90% cells) (Figure 5.4; Mesenchymal Stem Cell Markers); also observed in EGF-R, CD95, CD140b, HLA-A,B,C, β 2-microglobulin, CD98 and CD147 (Figure 5.4). However, a mean reduction in CD105 was observed from 87.5% for the control, to 20.6% and 26.2% for treated and recovered, respectively (Figure 5.5; Mesenchymal Stem Cell Marker). HLA-A2 positive expression in 50-60% of the population was maintained across the three groups, however showed an increase in MFI FI in the treated and recovered group (non-significant) (Figure 5.4 and 5.5; Immune Response Induction/ Immunomodulation). CD44 showed very high expression across the three groups, with an MFI FI from 332.6 to 384.7, with percentage positive ranging from 86.8 to 96.9% (Figure 5.4. and 5.5; Adhesion Molecules).

Markers demonstrating significant changes for percentage positive and MFI FI were identified (Figure 5.6) For percentage positive, the groups were formed from markers significantly reduced in both the treatment and recovered group compared to untreated (CD106 and CD243); markers significantly reduced between untreated and treated only (CD109, CD130 and CD91), markers significantly reduced between treated and recovery only (CD121a, HPC and SSEA4); markers with significantly increased expression between untreated and recovery only (CD10,CD38, CD40 and CD97); and markers with significantly higher expression in the recovered group compared to untreated and treated (MIC A/B) (Figure 5.6). No significant increases of expression in the treated group alone were identified, or significant changes between the treated and recovered group only. For MFI FI, markers significantly reduced in both the treatment and recovered group compared to untreated were CD105, CD109, CD130, CD340 and HPC; markers significantly reduced between untreated and treated only were CD49d, CD63, CD81, CD119, CD165, CD221, CD271 and CD278; markers significantly reduced between treated and recovery only were

CD59, CD140b and B2-microglobulin; and MIC A/B, with significantly higher expression in the treated and recovered groups compared to untreated (MIC A/B) (Figure 5.6). Markers identified in both MFI FI and percentage positive included CD109, CD130, HPC and MIC A/B. Although they mirrored the increase or decrease in expression compared to the untreated control, percentage positive expressed significance in both treated and recovered groups compared to the control, whereas MFI FI only showed significance between the control and either treated or recovered groups (Figure 5.6).

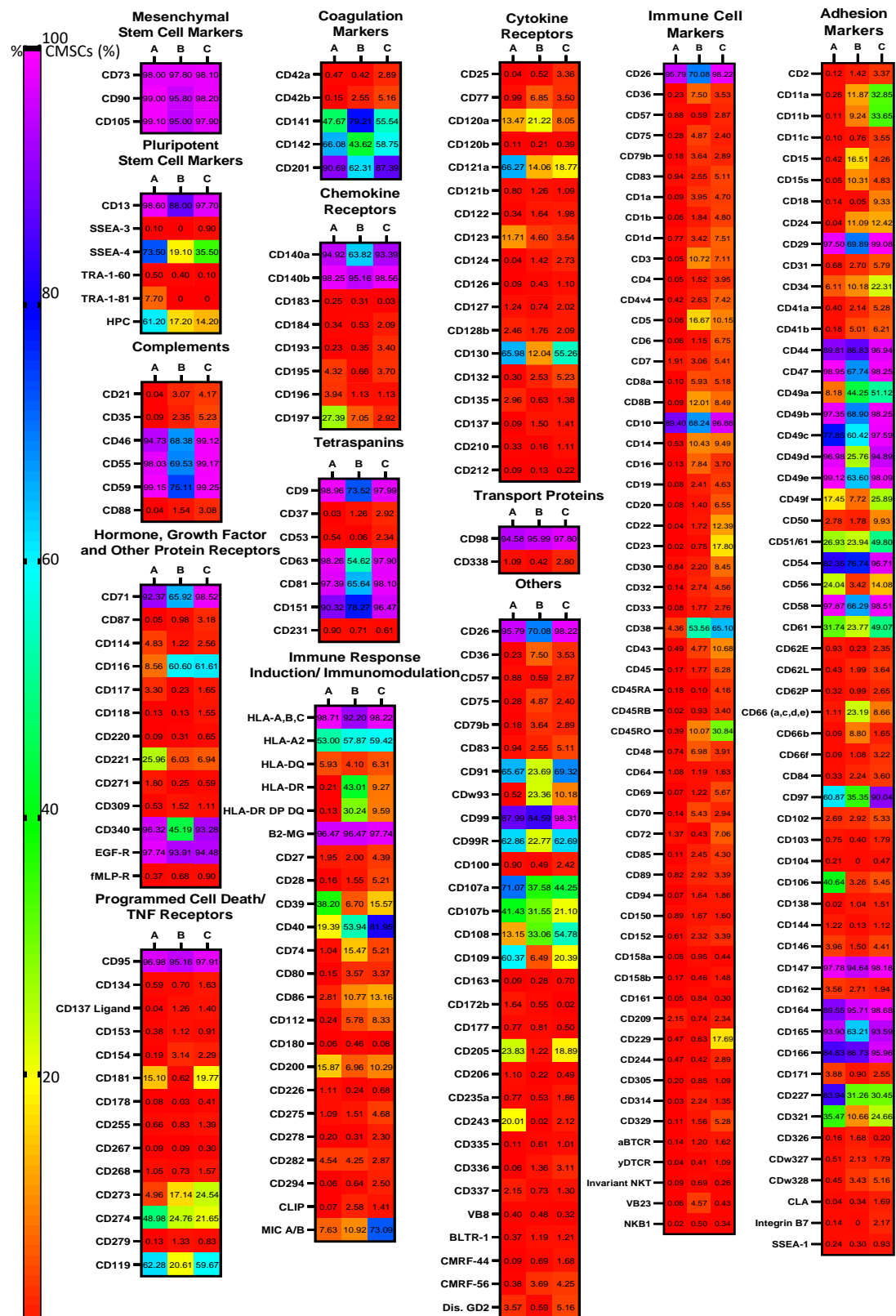


Figure 5. 4. Heat maps showing percentage of positive cells expressing different markers on CMSCs compared to the isotype control. Each column represents readings from different conditions; A: Untreated, B: Treated, C: Recovered. The BD Lyoplate™ was utilised (N = 3, passage = 5-7). Colours are representative of percentage in the scale on the left. Cells were categorised based on a previous grouping by Baer *et al.*, (2012) [154]. For mAbclones see Section 2.1.2.ii. and for antigen abbreviation definitions see the Appendix (Table A1.1).

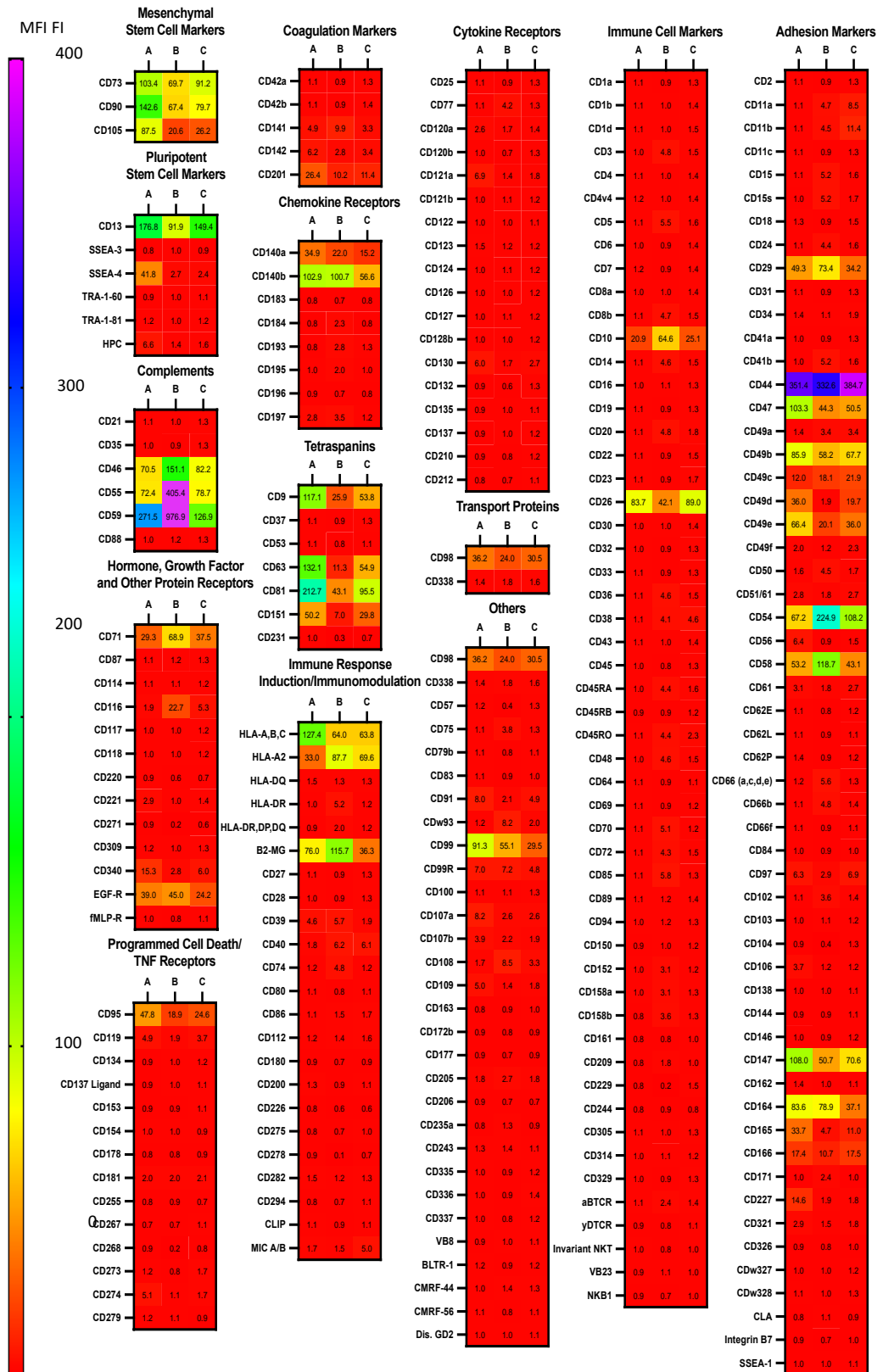
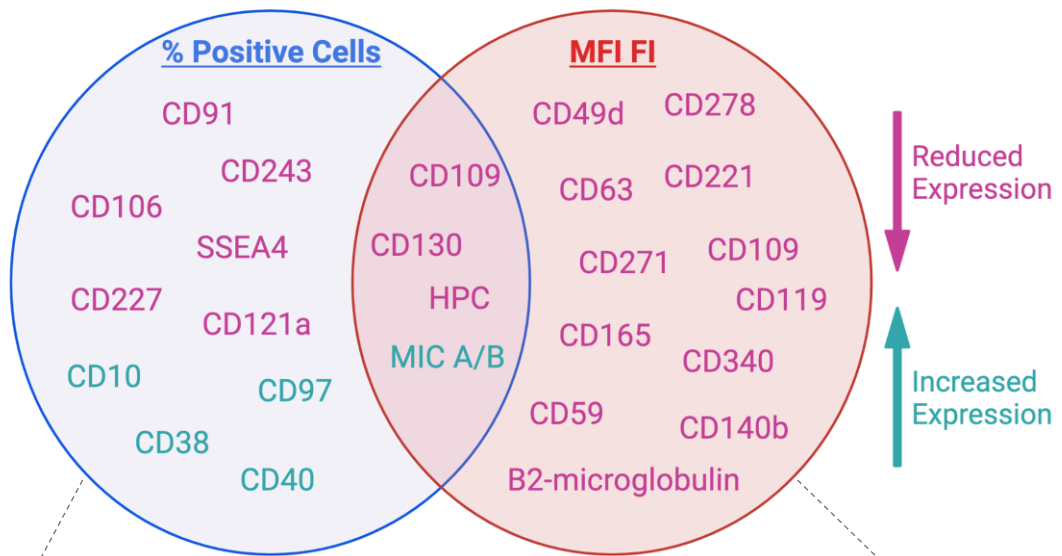


Figure 5. Heat maps showing median fluorescent fold increase (MFI FI) in expression of different markers on CMSCs compared to the isotype control. Each column represents readings from different conditions; A: Untreated, B: Treated, C: Recovered. The BD Lyoplate™ was utilised (N = 3, passage = 5-7). Colours are representative of percentage in the scale on the left. Cells were categorised based on previous grouping by Baer *et al.*, (2012) [154]. For mAbclones see Section 2.1.2.ii. and for antigen abbreviation definitions see the Appendix (Table A1.1).



Key: % Positive Cells, MFI FI, *Both

	Untreated vs Treated	Untreated vs Treated and Untreated vs Recovered	Untreated vs Recovered
Reduced Expression	CD91 CD109* CD130* CD49d CD63 CD81 CD119 CD165 CD221 CD271 CD278	CD106 CD243 CD105 CD109* CD130* CD340 HPC*	SSEA4 CD227 CD121a HPC* CD59 CD140b B2-microglobulin
Increased Expression		MIC A/B*	CD10 CD38 CD40 CD97 MIC A/B*

Figure 5. 6. Diagram summarising markers displaying significant differences between untreated vs treated and recovered groups. (a) Venn diagram with markers showing significantly reduced expression (pink) and increased expression (green) based on percentage of positive cells (blue) and MFI FI (red). (b) Table demonstrating which groups the significance was found between for percentage of positive cells (blue) and MFI FI (red), with a purple Asterix to denote the 4 markers with significance crossover.

5.3.3. Genotypic differences were observed between CMSCs in different conditions.

The Qiagen Human Wound Healing RT² Profiler PCR Array kit was utilized to determine genotypic differences between untreated, treated and recovered CMSCs (Figure 5.8). Markers were first categorized based on their function, and markers of interest identified as those which demonstrated significant changes from the untreated control group (Figure 5.7). Markers categorized as ECM structural constituents were nearly all significantly downregulated in the treated and recovered groups compared to the untreated (*COL1A1*, *COL1A2*, *COL3A1*, *COL4A1*, *COL4A3*, *COL5A1*, *COL5A2*, *COL5A3* and *COL14A1*) (Figure 5.7.a). *VTN* was the only marker of this category which displayed no change between the 3 groups. Other markers significantly downregulated compared to untreated were the cytoskeleton regulators *ACTA2*, *ACTC1* and *TAGLN* (5.7.b). *ACTC1* also demonstrated significantly lower expression in the treated group than the recovered. No other groups contained markers significantly reduced.

Markers significantly upregulated in the treatment and the recovered group compared to the untreated control included *MMP1* (Figure 5.7.c); *HBEGF* (Figure 5.7.d); *VEGFA* and *PLAU* (Figure 5.7.e) and *CSF2* (Figure 5.7.i). Markers significantly upregulated in the treated and recovered compared to untreated, with additional significance between treated and recovered included *ITGB3*, *CSF3*, *IL1B*, *CXCL5*, *PLAUR*, *SERPINE1* and *TGFA* (Figure 5.7. a, e, g, h, i). Genotypic changes are summarized in Figure 5.8.

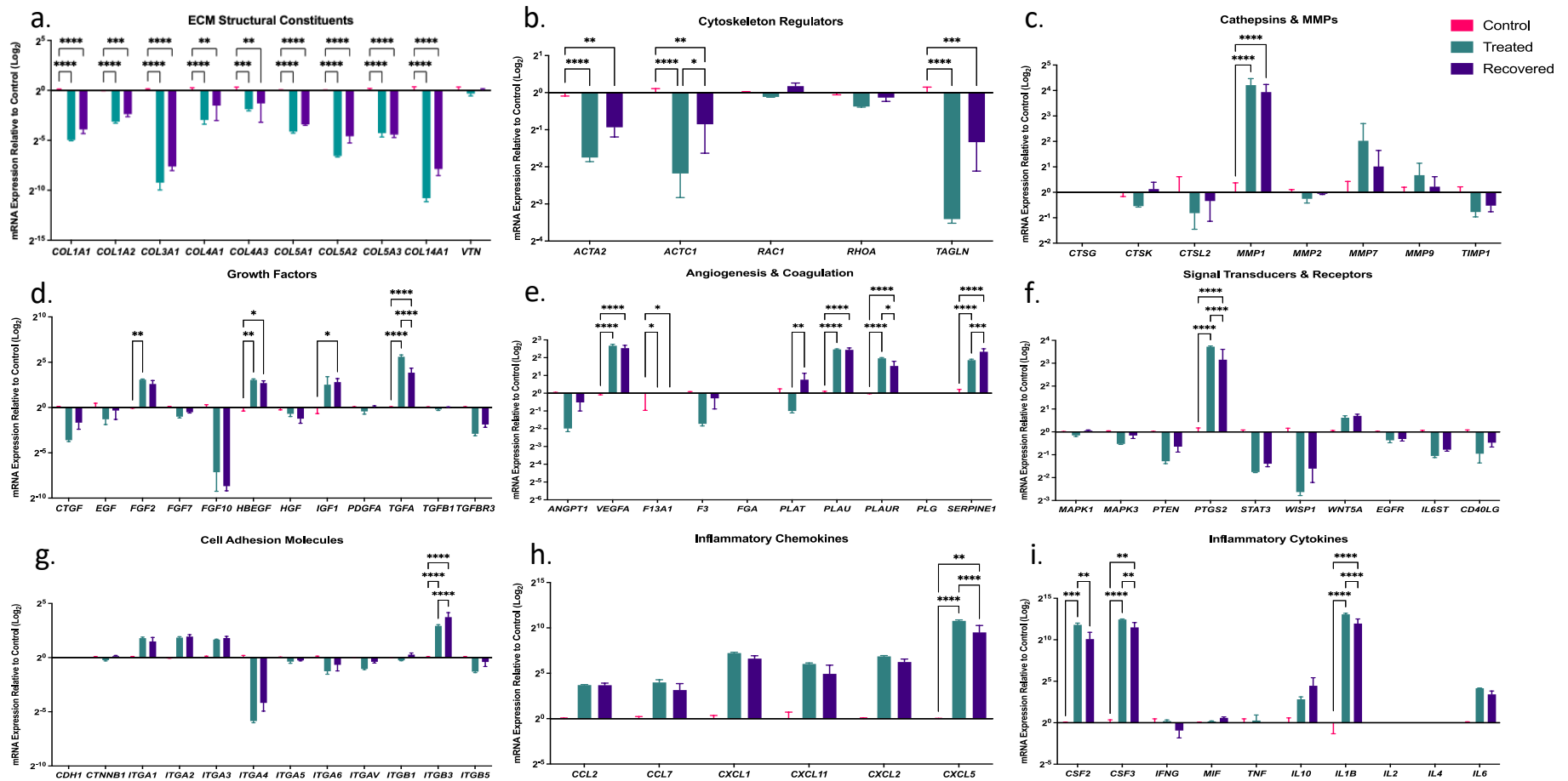


Figure 5. 7. RT² Profiler PCR array to detect the expression of genes associated with wound healing and fibrosis. Genes were grouped into (a) ECM Structural Constituents, (b) Cytoskeleton Regulators, (c) Cathepsins and MMPs, (d) Growth Factors, (e) Angiogenesis and Coagulation, (f) Signal Transducers and Receptors, (g) Cell Adhesion Molecules, (h) Inflammatory Chemokines and (i) Inflammatory Cytokines. The data are presented as the means of fold change of expression in treated and recovered CMSCs compared to untreated controls (N = 3). Points and error bars represent mean and StDev respectively. P = 0.1234 (ns), 0.0332 (*), 0.0021 (**), 0.0002 (***) and < 0.0001 (****).

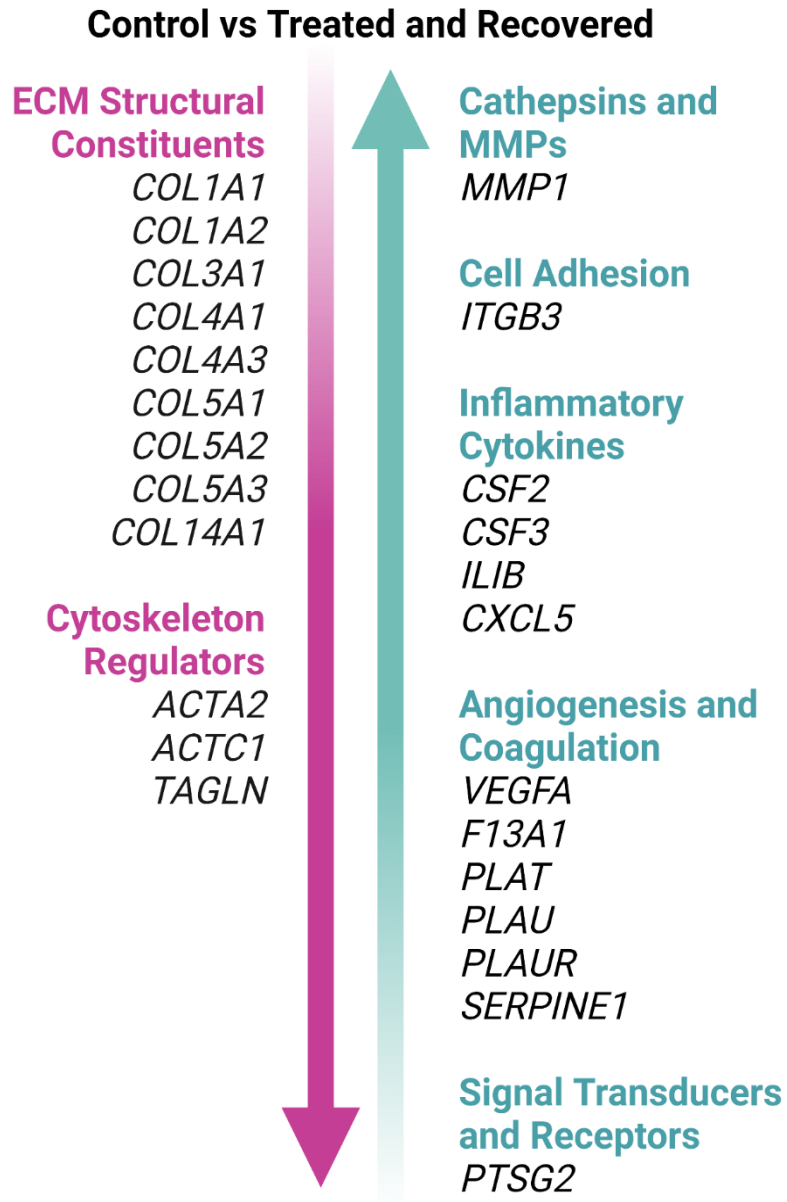


Figure 5. 8. Summary schematic of genes showing significantly lower (pink) and higher (green) expression in the treated and/or recovered group compared to the control, collected using the RT² Profiler.

5.3.4. The cytokine cocktail altered the secretome of CMSCs.

ELISAs were used to assess differences in the secretome of CMSCs following exposure to the inflammatory cocktail compared to an untreated control. The treated group were investigated for 9 days with cytokines present, followed by 3 days returning to media without cytokines for 'recovery'. IL-6, IL-8, TSP-1, Hya and FGF were significantly higher at all time points in the treated group compared to the control, including following recovery (Figure 5.9). Alternatively, significantly more PTX3 was observed in the control group, which appeared to reduce over time (Figure 5.9.d). Significantly higher levels of TGF-B1 were secreted from the treated group at day 3 and day 9 only (Figure 5.9.b). HGF also showed significance between the groups at every time point, with higher levels in the treated group compared to control before recovery (days 3, 6 and 9), which switched to higher levels in the control group following recovery (Figure 5.9.b). Significantly more PEDF was also found in the control group during recovery, compared to the groups before recovery where no difference was observed other than on day 3, with significantly higher levels detected in the secretome of the treated group (Figure 5.9.c). IDO and IL-1ra could both be observed in the treated group only at day 3 and day 6, and day 3, day 6 and day 9 respectively (Figure 5.9.e). Neither protein was observed when no cytokines were present, and IL-1ra appeared to reduce in a time dependent manner. TGF-B2 and TGF-B3 were also tested for but yielded negative results for all conditions (data not shown). Data for the treated cells at day 3, and the recovered cells, compared to the control is summarized in Figure 5.10.

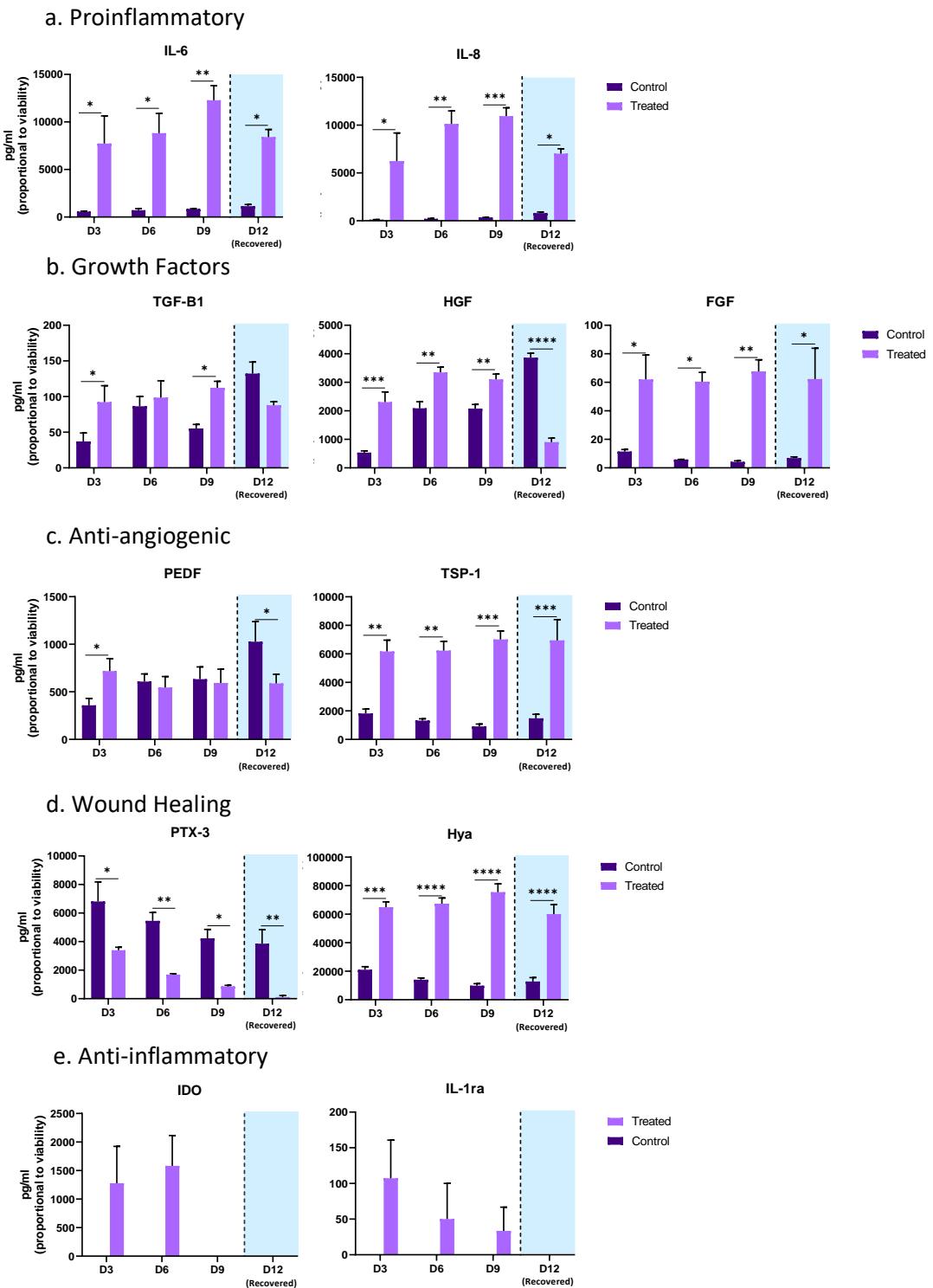


Figure 5. 9. Factors secreted by control (dark purple) vs activated and recovered CMSCs (light purple). Results investigating (a) proinflammatory, (b) growth, (c) anti-angiogenic, (d) wound healing and (e) anti-inflammatory factors secreted from CMSCs stimulated with an inflammatory cocktail for 9 days, with 3 days recovery. Graphs represent mean values with error bars for SEM (N = 3, n = 3).

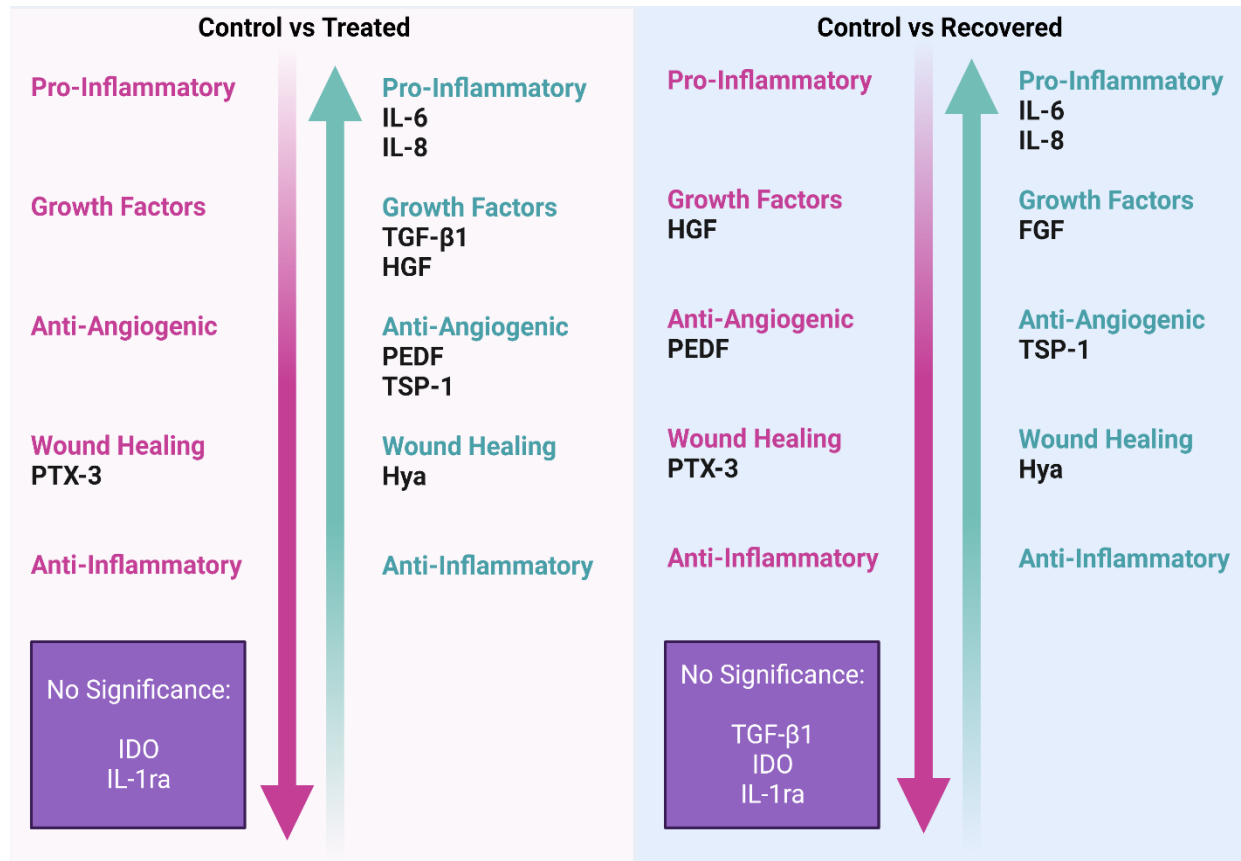


Figure 5. 10. Summary schematic of proteins showing significantly lower (pink) and higher (green) secretion from CMSCs for control cells (no cytokines) compared to cells treated with cytokines for 3 days, and control cells compared to the recovered group (exposure and removal of cytokines). Proteins were detected using ELISAs.

5.3.5. Comparison of the CMSC secretome to corneal epithelial cells demonstrated factors more specific to CMSCs.

The day 3 secretome of HCEC2s were compared to the CMSCs. HCEC2s were utilized as a relative control to understand levels of factors released from CMSCs when exposed to the inflammatory stimuli. Significantly higher levels of Hya and TSP-1 could be found in the HCEC2s compared to the CMSCs for both control and treated (Figure 5.9. c,d). HCEC2s also secreted significantly higher levels of IL-6 and IL-8 in the treated groups only compared to the CMSCs (Figure 5.11.a). Alternatively, growth factors HGF, FGF and TGF-B1 were significantly higher in both the control and treated group of the CMSCs compared to the HCEC2s (Figure 5.11.b). Data for the differences between treated CMSCs and HCEC2s is summarized in Figure 5.12.

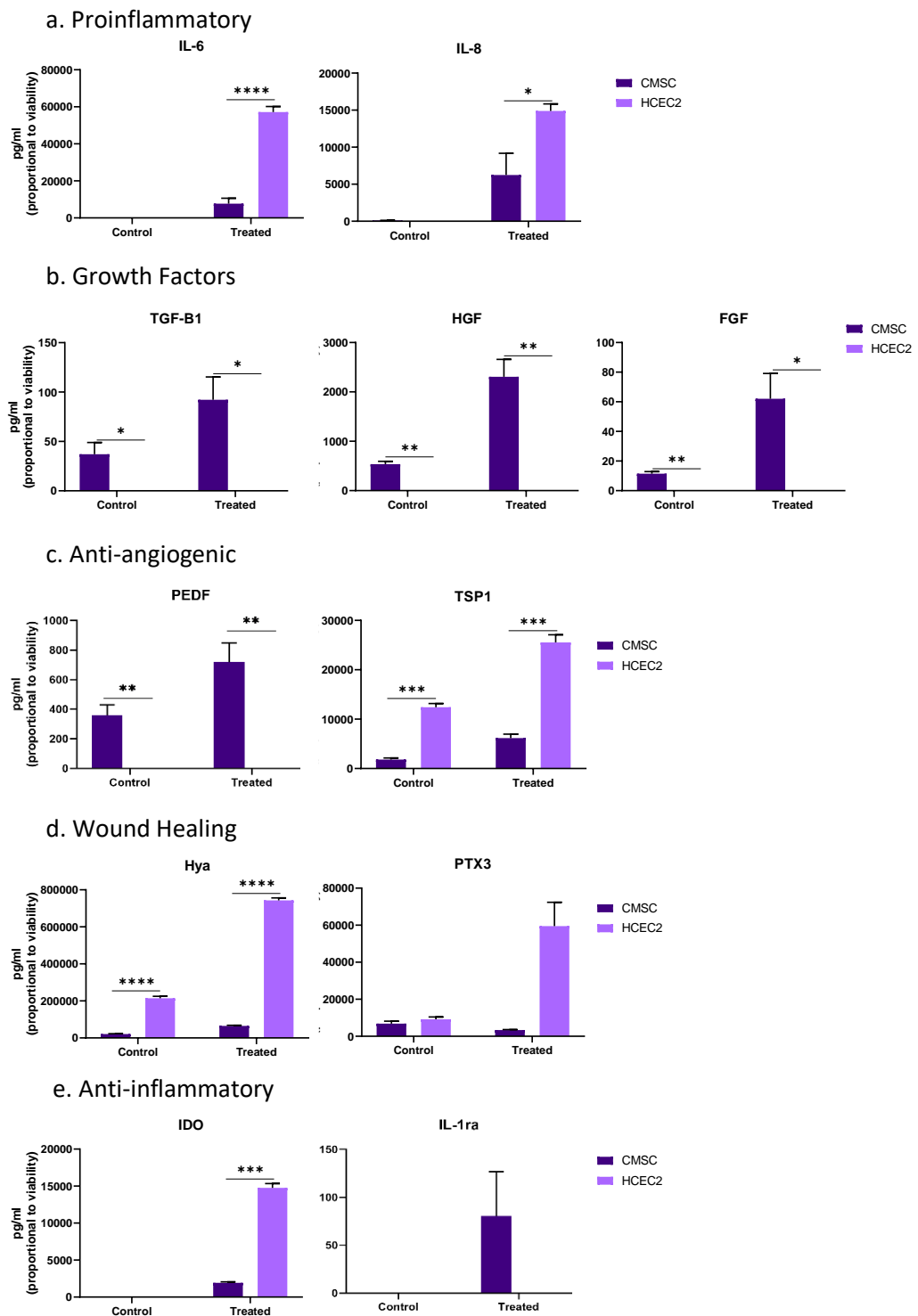


Figure 5. 11. Factors secreted by CMSCs (dark purple) vs HCEC2s (light purple) stimulated with the inflammatory cocktail for 3 days. Results investigating (a) proinflammatory, (b) growth, (c) anti-angiogenic, (d) wound healing and (e) anti-inflammatory factors secreted from CMSCs and HCEC2s. Graphs represent mean values with error bars for SEM (N = 3, n = 3).

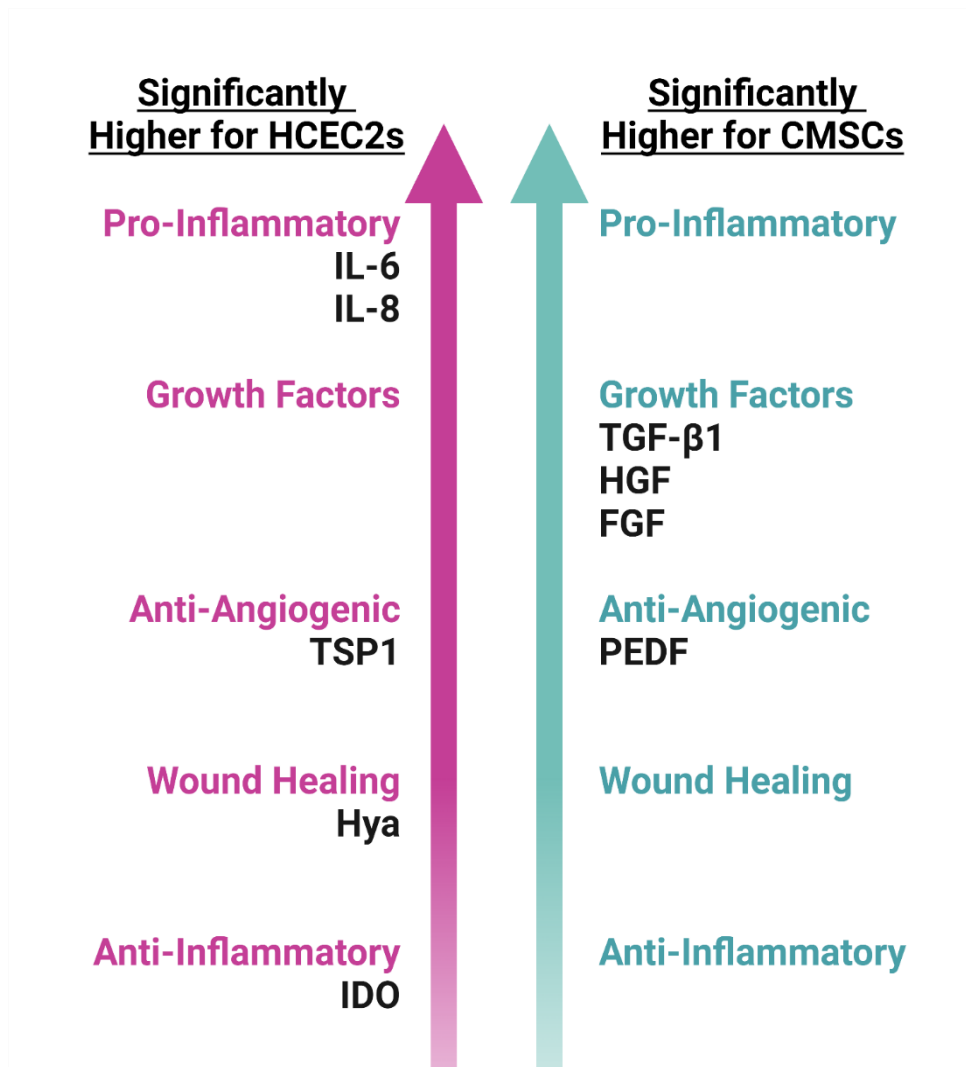


Figure 5. 12. Summary schematic of proteins showing significantly higher secretion from CMSCs (pink) or HCEC2s (green) for cells treated with cytokines for 3 days. Proteins were detected using ELISAs.

5.4. Discussion

This chapter focused on providing a synopsis of how CMSCs respond to an inflammatory environment, designed to mimic the toxicity of an injured ocular surface. Through determining an overall picture of survival, phenotypic, genotypic and secretomic responses, the experiment was able to determine genes and proteins of interest, that could be explored further in future functional investigations.

Initially, the aim was to determine whether CMSCs had a suitable survival rate when exposed to the inflammatory cocktail, comprised of IFN- γ , IL-1B, TNF- α and LPS. High levels of cell death would reduce the therapeutic potential of the therapy, as less viable cells would be present to produce beneficial factors. Here, using PrestoBlue viability assay and Live/Dead staining, a significant reduction in cell metabolism at day 3 compared to day 0, and the control was demonstrated. It has been suggested that increased p38a/B MAPK activity can attenuate the activation of FGFR1 by FGF ligands, in addition to preventing asymmetric division and generation of daughter cells [240]. Although speculative, the inhibited proliferation of CMSCs following addition of cytokines could be an impact of the significant upregulation of the p38a/B MAPK pathway, preventing cell self-renewal. Future work could investigate the restoration of self-renewal in the presence of cytokines through ectopic-ligand activation of FGFR1, which would potentiate the restoration of asymmetric phosph-p38a/B MAPK activation [240]. Furthermore, p38 MAPKs have been implicated in the negative regulation of cell cycle progression at both G1/S and G2/M transitions through mechanisms including the downregulation of cyclins and upregulation of CDK inhibitors, with pro-apoptotic functions linked to the pathway [240].

It appeared that between day 3 and day 9, where cytokines are present in the media, cell viability does not further diminish. In work leading on from this thesis, it may be of interest to address the question of what makes this subset of cells capable of surviving the inflammatory cocktail. Additionally, there appears to be a regrowth of cells following recovery, demonstrated in the Live/Dead staining. This

suggests that the proliferation inhibition is temporary, in addition to providing an argument for priming of the cells. If the subset of cells can survive in environments with high levels of inflammatory cytokines, and proliferate following the removal of cytokines, it potentiates that these cells may be more resistant to the microenvironment when used as a cell therapy. Consequently, this work describes the characteristics of this subset of cells that survived the inflammatory environment, including their genotype, phenotype and secretome.

To determine the similarities and differences between CMSCs treated with cytokines and following recovery compared to an untreated control, the experiments began by using the BD cell marker panel. This flow cytometry kit allowed the investigation of a relatively high number of cell surface proteins, giving a broad phenotypic picture, in addition to identification of markers of interest for future work. Heat maps of the three conditions (control, cytokine treated and recovered) allowed for quick identification of markers with both negative or expressed, in addition to homogeneous and heterogeneous expression throughout the three groups, for both MFI FI and percentage of positive cells. Although highly contended, as described in Chapter 3, the ISCT criteria still provides a guideline for identifying MSCs [30]. Here, the high expression (> 95%) of previously defined MSC markers CD73, CD90 and CD105 is demonstrated, with negative expression maintained in CD34, CD45 and HLA-DR (Figure 5.4.a), showing their phenotypic maintenance as MSCs throughout the 3 conditions. However, MFI FI for CD105 dropped from 87.5 in the control group to 20.6 and 26.2 in the treated and recovered groups, respectively (Figure 5.5.a). The biological function of CD105 on MSCs is widely debated, with variations observed between cell sources and culture conditions, without impacting differentiation of immunological capacity [241]. Consequently, it is likely that this reduction in CD105 MFI FI would not impact the therapeutic quality of CMSCs following exposure to inflammatory factors, however bring into question whether treated cells can still be defined as MSCs.

MHC Class I molecule, β 2-microglobulin (B2M), and transmembrane complex, HLA-A, B and C were both maintained at high levels of expression throughout the three treatment groups. B2M knockout models in MSCs derived from iPSCs have been

demonstrated to reduce immunogenicity to allogeneic peripheral blood mononuclear cells, whilst maintaining their phenotype and immunosuppressive properties [187]. This indicates that B2M is likely not involved in the therapeutic mechanisms of MSCs, presenting its knock out as a potential route for future MSC trials. No significant change in expression of HLA-A, B and C is consistent with work by Mckinniry et al [242], where treatment of AD-MSCs with IFN- γ and TNF- α did not alter their expression levels. Although immunogenic, high expression of B2M has previously been identified in MSCs without concern, with studies highlighting its suitability as a reference gene for qPCR [243]. Additionally, upregulation of MHC-I has demonstrated increased immunomodulatory properties through the inhibition of NK cells following NK-MHC-I interaction [224].

Throughout these investigations, a 'recovered' group was included to provide an insight into any potential advantages or limitations of priming the cells prior to therapeutic application. An additional member of the MHC-I family was MHC-I chain-related protein A/B (MIC A/B), where a significant increase in expression for both percentage positive and MFI was observed in the recovered group compared to the control group. MIC A/B act as ligands for natural killer group 2, member D (NKG2D), an activating receptor expressed on the surface of NK cells and T cell subsets including CD8+ cytotoxic T cells [244]. Consequently, primed CMSCs may be at increased risk of cytolytic activity, which would attenuate their therapeutic capacity through reducing their maintenance at the ocular surface. These results also highlight the benefit of large screening panels, to identify markers which could affect downstream experiments.

The high percentage of cells expressing epithelial growth factor receptor (EGF-R) throughout the three conditions is of particular interest, as ELISA data from previous work from Laura Sidney's group have shown that EGF is not produced by CMSCs (data not yet published). EGF-Rs are situated on both corneal epithelial cells and keratocytes. EGF is released from stressed corneal epithelial cells, which in turn activates keratocytes through the PI-3K pathway, leading to their proliferation, migration and differentiation [245]. A potential risk factor associated with the abundance of EGF-Rs on CMSCs is induced differentiation towards a myofibroblast.

Although implicated in wound healing, the scarring phenotype is important to consider- it is necessary to find an optimal balance between therapeutic links with activation, and risk of scar formation.

Other markers that were constitutively expressed in over 90% of cells of the untreated control, inflammatory factor treated and recovered groups were CD95, CD140b and CD147, suggesting that they are also not key proteins involved in the activation or response of CMSCs in an inflammatory environment. CD95 belongs to the TNF receptor superfamily regulating apoptosis [246]; CD140b is necessary for normal physiological development and cell growth [247]; and CD147 has been implicated as a necessary agent for the migration of MSCs [248]. All these markers demonstrating expression in over 90% of cells have been identified at high levels in MSCs from different sources [197], demonstrating their consistent presence in MSCs, regardless of their origin or processing.

Interestingly in this study, only four of the phenotypic markers were found to be significant for both MFI FI and percentage of positive cells. Percent positive separates cells that have the peptide bound to them versus those that don't, compared to MFI which gives a relative value of peptide bound to the population of cells. Here, CD109, CD130, HPC and MIC A/B were identified as four markers of interest based on the significance observed in both data sets. This also highlights the importance of assessing both metrics, to obtain a full picture of marker expression in the cell population.

In addition to phenotype, the genotype and secretome of CMSCs were also assessed following treatment and recovery, with additional secretome experiments with HCEC2s to behave as comparative cell type. Below, proinflammatory, growth, anti-angiogenic, anti-inflammatory and wound healing factors secreted from CMSCs are discussed, with the information gained from the genotypic and phenotypic pathways used to hypothesise the potential pathways activated and silenced.

5.4.1. Pro-inflammatory Factors

In accordance with the literature on corneal fibroblasts, IL-6R (CD126) was not present on the CMSC surface under any conditions, likely making the cells unresponsive to IL-6 alone [249]. In a co-culture or *in situ* environment, CMSCs can respond to IL6, as corneal epithelial cells can produce soluble IL-6 receptor (sIL-6R) through shedding or translation of alternatively spliced mRNA, which forms an IL-6/sIL-6r complex, and can subsequently bind to gp130 (CD130) on the surface of CMSCs. Interestingly, CD130 expression was found to be significantly decreased following addition of the inflammatory cocktail, with demonstrated significance in both percentage positive and MFI FI groups. This is likely due to IL-1 β or TNF- α activation of the protein kinase p38, leading to MAPK-activated protein kinase 2 (MK2) dependent serine phosphorylation of gp130, and receptor internalisation and degradation [250]. Consequently, IL-6 mediated activation of the STAT-3 pathway is reduced following a negative feedback cycle between IL-6, IL-1 β and TNF- α , and gp130, meaning that when activated, CMSCs are less likely to respond to IL-6 produced by epithelial cells. Although this can ultimately delay the anti-inflammatory effects of IL-6, resulting in CMSCs potentially increasing inflammation, preventing the phosphorylation of STAT-3 could formulate a mechanism to inhibit neovascularisation through inhibition of VEGF release by CMSCs [249]. The significant upregulation of IL-6 in inflammatory conditions compared to untreated for CMSCs, was mirrored with IL-8. However, the quantity released from activated CMSCs was significantly lower than treated HCEC2s, putting the CMSC response into perspective. Furthermore, although an increase was seen in the treated and recovered group in the gene expression of *IL-6*, it was not a significant change.

The cytokine release is likely due to LPS binding to TLR4, initiating signal transduction by forming a complex with accessory modules, such as myeloid differentiation-2 (MD-2), LPS- binding protein subunit (LBP) and CD14 [235] This study demonstrated the upregulation of CD14 in CMSCs following cytokine addition, from a negative population to approximately 10%. In further investigations, it would be interesting to deduce whether this CD14+ population significantly contributes to the increased secretion of IL-6 and IL-8 from CMSCs in

the presence of the inflammatory cocktail. Following the removal of the cytokines and allowing the cells to recover for 3 days resulted in a significant decrease in secretion of both cytokines, however not a full return to baseline. This data alludes to a steady downregulation of the IL-6 and IL-8 producing signaling cascades when the TLR4 stimulator, LPS, was removed.

It should be noted that although the literature indicates the main role of IL-6 and IL-8 in the proinflammatory response, with IL-8 a key factor in neutrophil chemotaxis, the role of TLR4 is multifactorial. Previous studies have demonstrated the capacity of TLR4 activated MSCs to induce immunosuppression via induction of TRegs, using the Notch signaling pathway, with an upregulation in Delta-like 1 [251]. Additionally, there is evidence that TLR4 stimulated BM-MSCs maintain an immunosuppressive phenotype through a strong induction of galectin-9 [252], an additional anti-inflammatory factor not tested for in this investigation.

Furthermore, IL-6 and IL-8 have been shown to play an active role in wound healing. Activation of the IL-6/STAT3 pathway in corneal epithelial cells has been demonstrated to increase cell migration and wound healing *in vitro* and *in vivo*, with McFarland-Mancini *et al* (2010) [253] reporting delayed macrophage infiltration, fibrin clearance and wound contraction in an IL-6^{-/-} mouse model.

Overall, IL-6 and IL-8 were secreted at elevated levels by both corneal epithelial cells and CMSCs, likely through TLR4/CD14 activation. In CMSCs, this resulted in an increased level of gp130 internalization and degradation, preventing the phosphorylation of STAT3 and therefore potentially decreasing the overall effects of IL-6 mediated CMSC anti-inflammatory chemokines. However, the high levels of IL-6 present are also a necessity for improving wound healing and corneal epithelial cell migration.

5.4.2. Growth Factors

In addition to IL-6 and IL-8, growth factors play a vital role in reepithelialisation and wound healing following corneal injury. TNF- α or LPS stimulation has been implicated in the secretion of growth factors by MSCs HGF produced by the CMSCs

is a key mitogen and motility factor for corneal epithelial cells, exerting its effects through binding to the c-Met receptor. Leuning et al. (2017) [254] demonstrated a significant upregulation in HGF secretion in human kidney perivascular stromal cells compared to BM-MSCs, which was found to play a vital role in their increased capacity for epithelial wound healing through aiding epithelial cell proliferation and migration, and inhibition of apoptosis [255]. Furthermore, HGF has been implicated as an anti-fibrotic strategy for restoring transparency in a damaged corneal stroma, through induction of apoptosis in myofibroblasts and blocking of TGF- β 1 induced fibrosis through inhibition of the TGF- β signaling pathway. Similarly to HGF, bFGF plays a major role in wound healing through stimulating granulation tissue formation, matrix remodeling and re-epithelialization, with its efficacy demonstrated through its incorporation into many commercial products for cutaneous wound healing [256]. bFGF and HGF secretion from CMSCs was maintained throughout the 9 days of exposure to treated conditions, however was not secreted by HCEC2s. This, along with the significantly higher gene expression in the treated and recovered groups for multiple growth factors highlights these factors as key players in the therapeutic mechanism of CMSCs at the ocular surface.

The resulting increase of growth factors in the secretome of treated CMSCs may be responsible for the significant increase in gene expression of ITGB3 (Integrin β 3).

5.4.3. Anti-angiogenic Factors

To maintain corneal transparency, tightly monitored homeostasis is required in a healthy cornea between angiogenic and anti-angiogenic factors. In the presence of injury and inflammation, this balance can be distorted, leading to an increase in angiogenic factors, neovascularisation, and subsequently corneal haze. For example, although bFGF is a useful cytokine for epithelial wound healing, it also enhances corneal endothelial cell proliferation [257]. It is therefore vital that the relationship between these factors, and the host epithelial cells and therapeutic CMSCS, is understood.

TSP-1 and PEDF behave as potent anti-angiogenic factors, with their secretion necessary to prevent neovascularization and corneal haze. TSP-1 exerts its effects

through the disruption of CD47 and VEGF receptor (VEGFR)-2 (CD309) signalling, as well as suppressing the VEGF-Akt-eNOS pathway [258]. TSP-1 can also downregulate MMP2, which is a potent, proangiogenic, inflammatory chemokine. PEDF works through selective inhibition of VEGF induced neo-vessels, in part through γ -secretase dependent cleavage of the C terminus of VEGFR1, which inhibits VEGFR2 induced angiogenesis. Furthermore, PEDF secreted from CMSCs has been demonstrated to exhibit anti-inflammatory potency through contributing to the polarisation of macrophages from an M1 to M2 phenotype, which in turn, functions to remove immune cells, granulation tissue and neovasculature [136]. Additionally, CMSCs have been demonstrated to enhance macrophage's secretion of PEDF in co-culture *in vitro* experiments. Ultimately, both of these glycoproteins are highly anti-angiogenic, but also have the capacity to modulate inflammation, making them key factors when assessing the therapeutic potential of CMSCs.

Here, the data demonstrates the significant upregulation of TSP-1 expression in both CMSCs and HCEC2s following addition of the inflammatory cocktail. Expression was maintained at a consistent level from D0 to D12 in CMSCs, regardless of cytokine removal at day 9. The high levels of TSP-1 that are secreted in the presence of the inflammatory cocktail give us an insight into the high levels of the protein that would be present at the ocular surface following use of CMSCs as a therapy for epithelial injury. Furthermore, PEDF was found to be exclusively secreted by CMSCs in this study, Highlighting the molecule as a factor of interest for further exploration.

TSP-1 has also been demonstrated to be rapidly upregulated in the presence of TGF- β 1 [259]. In turn, TGF- β 1, secreted by most cells in the inactive form, termed latent, can be activated by TSP-1. It is possible that this positive feedback cycle is responsible for the maintained levels of TGF- β 1 and TSP-1 following cytokine removal, demonstrated in this study. Active TGF- β 1 is implicated in a plethora of cell mechanisms, including development, differentiation and gene expression. Although previously eluded to as an inducer of fibrosis, inhibited by HGF, TGF- β 1 has been implicated in wound healing and immunomodulation through the induction of macrophages to the M2 phenotype [260]. Yang *et al.* (2016) [53]

reported that orbital fat derived MSCs significantly improved corneal epithelial wound healing *in vitro*, demonstrating significantly attenuated therapeutic capacity with the inhibition of TGF- β 1. Activation of the TGF- β /Smad2 signalling pathway in corneal epithelial cells augments wound healing through the upregulation of integrin β 1, mediating epithelial cell migration from the limbus, across the cornea. This data demonstrated that HCEC2S were negative for TGF- β 1 production, implicating the potential therapeutic crosstalk between the CMSC secretome and the impact on the injured epithelial cells.

CD109 is a co-receptor and potent inhibitor of the TGF- β signalling pathway [261]. CD109 was one of the 4 markers found to show significant reduction in expression between the treated and control group for both MFI FI and % positive, providing validity. The decrease of CD109 phenotypic expression and the significant increase of TGF- β 1 in the secretome of the treated group is synonymous with the literature.

5.4.4. Anti-inflammatory Factors

The pro-inflammatory factor IFN- γ is recommended by the ISCT as a standard priming method for determining the immunosuppressive capacity of MSCs, with measurement obtained through the quantity of the tryptophan catabolizing enzyme, IDO [30]. Consequently, MSC response to IFN- γ has been the most extensively investigated out of the inflammatory cocktail, with an abundance of literature supporting its activation of IDO production in MSCs from different sources [74, 262-264].

The interferon receptor is split into two subunits, IFNGR1 and IFNGR2, associated with JAK1 and JAK2 respectively [265]. Dimerization of the subunits following ligand interaction activates the associated JAKs by autophosphorylation, providing a docking site for STAT proteins. IFN- γ stimulates the formation of a STAT1-STAT1 homodimer, which undergoes nuclear translocation and binds to the GAS elements on target genes, thus modulating many factors, including the expression of IDO. Alternatively, STAT1 can stimulate the upregulation of IDO through inducing the production of IRF-1 [266].

Additionally, it has recently been shown that phosphatidylinositol 3-kinase (PI3Ka) is a major novel regulator of IFN γ -induced IDO expression upstream of STAT1 [238]. Complete STAT1 activation through phosphorylation of STAT1 residues, S727 and Y701, is dependent on IFN γ -induced PI3Ka activation, highlighting the complex interplay between the signaling cascades. Interestingly, overexpression of STAT1 induced higher sensitivity in MSCs to IFN- γ , resulting in upregulated secretion of IDO. Comparatively, STAT-1 knockdown led to complete abrogation of MSC-induced T cell suppression.

Here the data shows a significant decrease in MFI FI of IFNGR1 (CD119) by day 6 following cytokine addition (Figure 5.5.e. and 5.6). This has previously also been reported to occur in T cells, as a safety mechanism to avoid apoptosis [267], potentially also adopted by MSCs. Supporting this hypothesis, receptor abundance returned to baseline following the removal of the cytokines, as the stress stimuli were removed. The reduced occurrence of IFNGR1 may also account for the depletion in secretion of IDO by CMSCs by day 9 of treatment with the inflammatory cocktail. Less receptors for IFN- γ binding at the cell surface is likely to reduce activation of the JAK/STAT1 pathway, ultimately reducing IDO release. It is also important to note that large variability was observed between donors, and the significantly higher IDO secretion by HCEC2s compared to CMSCs suggesting IDO is unlikely to be a key factor for paracrine release from CMSCs.

IL-1ra is an additional factor associated in reducing inflammation, exerting its effects by acting as an antagonist for IL-1 β and IL-1 α receptor proinflammatory signalling [268]. IL-1ra exists as 4 isoforms by alternative RNA splicing and translation initiation, however here, data is shown from the one isoform which can be secreted, termed soluble IL-1ra (sIL-1ra). IL-1ra has been demonstrated to display significant anti-inflammatory properties, including suppressing the influx of bone marrow-derived inflammatory cells following injury [8], inducing macrophage polarisation from M1 to M2 phenotype, and inhibiting B cell differentiation [268]. The success of IL-1ra as a therapeutic agent has been demonstrated *in vivo* and in clinical trials of dry eye disease treatment, inhibiting the pro-inflammatory IL-1 β signalling which acts as one of the main disease pathophysiologies [269].

IL-1ra has also been implicated to play an essential role in corneal wound healing, demonstrated in a diabetic mouse model, where IL-1ra expression was suppressed. This resulted in delayed reepithelialisation, increased cell apoptosis, reduced cell proliferation, and impaired sensory nerve reinnervation. Local administration of recombinant IL-1ra significantly reversed these aetiologies, highlighting the necessity for the correct balance between IL-1 β and IL-1ra signalling for normal wound healing [53].

This Chapter demonstrated the secretion of IL-1ra by CMSCs in the presence of the inflammatory cocktail compared to no secretion in untreated conditions. This supports the utilisation of CMSCs for the therapy of corneal injury, due to the potential capacity to inhibit the pro-inflammatory effects of IL-1 β following secretion by the injured corneal epithelial cells.

5.4.5. Wound Healing Factors

Long pentraxin (PTX3) contributes to the group of humoral pattern recognition molecules, involved in providing defence against infectious agents, and modulation of tissue repair and inflammation [270]. PTX3 can be induced by the pro-inflammatory cytokines IL-1 β , TNF- α and the microbial component, LPS. Multiple *in vivo* injury models have been used to demonstrate the necessity of PTX3 for wound healing, with PTX3 deficiency leading to excessive fibrin accumulation, delayed reepithelialisation and increased collagen deposition [271]. Furthermore, PTX3 has been implicated as a major therapeutic agent for MSC induced wound healing, with administration of PTX3^{-/-} UB-MSCs found to significantly delay wound healing compared to wild type UB-MSCs in a murine model of skin repair [271].

Significantly lower release of PTX3 by CMSCs compared to HCEC2s was shown. Additionally, significantly reduced levels were detected in treated CMSCs compared to treated. This is contradictory to the literature and the HCEC2s, where significantly higher levels of PTX3 were detected in the treated group, with an upward trend over time. It could be speculated that this is an outcome of the reduced occurrence of IL1R1 (CD121a) in the MSC population, or a complex negative feedback loop between the MSCs and other soluble factors present. Further research is required

to determine the mechanisms underlying the reduced secretion of PTX3 in treated CMSCs.

The significant decrease in CD121a expression following addition of cytokines, and the maintenance of low levels detected following removal of the cytokines, is indicative of a disadvantage to priming the CMSCs prior to therapeutic administration. The presence of inflammatory cytokine receptors may be key for the immunosuppressive response from CMSCs, and further work should investigate the therapeutic potency of CMSCs following licensing.

An additional factor recognised as important for the therapeutic capacity of MSCs is hyaluronan (Hya), a member of a family of glycosaminoglycans. Hyaluronan exists in humans as 3 isoforms and is synthesised by hyaluronan synthases (HAS's). Heavy molecular weight Hya has been evidenced to be synthesised by HAS-1 and HAS-2, eliciting anti-inflammatory and immunosuppressive properties, compared to HAS-3, which produces various sized chain lengths of Hya, with light, fragmented chains documented as potent pro-inflammatory molecules. It has previously been reported that BM-MSCs produce high amounts of Hya, with abundant HAS-1 mRNA expression, indicating the synthesis of the anti-inflammatory form of the molecule [272].

Hya is mainly known for its key role in maintaining ECM structure through interacting with water to dilate the ECM, however its potential for the augmentation of wound healing and immunomodulation have also been shown. Hya possesses a range of biological and protective properties which are responsible for its efficacy in increasing tear film stability, reducing the evaporation rate, and providing relief for dry eye symptoms, with Hya eye drops commercially available as a tear substitute [273]. Furthermore, these tear drops have been demonstrated to augment wound healing, increasing the migration potential of epithelial cells *in vitro* [273], reducing wound closure time *in vivo* [274], and evidenced to be efficacious in a clinical trial investigating superficial corneal abrasion caused by mechanical injury [134]. The efficacy of Hya alone is therefore well documented, however an additive therapeutic effect of the MSC secretome and a Hya scaffold on

corneal wound healing *in vivo* has been shown [86], demonstrating the potential of high levels of Hya present in therapies for ocular epithelial injury. With the significantly increased concentrations of Hya in the CMSC treated group compared to untreated CMSCs and treated and untreated HCEC2s, it can be hypothesised that Hya plays a useful role in the CMSC secretome for the treatment of epithelial ocular injury.

Interestingly, high percentages of cells and MFI expression were also found in CMSCs of the principal receptor for Hya binding, CD44, over all of the treatment groups. Although found on most haemopoietic cells, CD44 has also been identified as a marker upregulated from no expression during cell culture of MSCs. It has been suggested that CD44-Hya interactions are a key mechanism for MSC homing and migration to injury sites, demonstrated by no localisation of CD44^{-/-} MSCs at the injury site of an *in vivo* mouse kidney injury model [275]. It would be interesting to investigate whether inhibition of CD44 on CMSCs altered cell adherence to the scaffold used for cell application to the ocular surface.

The genotype panel demonstrated a reduction in CMSC collagen expression following exposure to the inflammatory cocktail, that was maintained following removal of the cytokines, with significantly lower mRNA expression of *COL1A1*, *COL1A3*, *COL3A1*, *COL4A1*, *COL4A3*, *COL5A1*, *COL5A2*, *COL5A3*, and *COL14A1* between control and treated, and control and recovered groups, as well as a significant reduction of expression of profibrotic genes, *ACTA2* and *TAGLN* [276]. It has previously been demonstrated that cytokines, in particular TNF- α and IL-1 respectively act at a transcriptional level to inhibit collagen synthesis and inhibit translational regulation in dermal fibroblasts [277]. Overproduction of collagen and ECM deposition by fibroblasts converting to myofibroblasts have been shown in inflammatory conditions, in particular with TGF- β , resulting in fibrosis [278]. The reduction in collagen mRNA levels shown here may help to prevent fibrosis, however also may impact the adhesion of CMSCs to their therapeutic scaffold. Taylor *et al.*, (2015) [279] observed reduced attachment of mouse primary osteoblasts to a cell secreted matrix. Furthermore, the decrease in expression of *TAGLN* and the increase of *MMP1* in treated conditions may lead to increased

migration of MSCs, limiting the possibility of the cells remaining on the scaffold following application [280, 281]. Separate investigations would have to be performed to assess the impact of cytokines on the scaffold- cell interactions. This also may provide an argument against priming the cells, if cell adhesion is a necessary component of the therapeutic method.

5.5. Conclusion

Overall, this chapter provided a vast overview into the hypothetical mechanisms at play following CMSC exposure to inflammatory stimuli. Using factors to mimic an inflamed ocular surface, it was shown that a subset of CMSCs appear to be resistant to the inflammatory cocktail, displaying inhibited proliferation. This subset of cells responds to the environment by increasing the secretion of a plethora of factors, including growth factors HGF, FGF2 and TGF β . These proteins are of particular interest due to their secretion from CMSCs but not HCEC2s, highlighting a more cell specific benefit. Phenotype and genotype were also assessed of CMSCs in the different environment, to gain a better understanding of potential pathways being activated. Interestingly, gene expression of ECM structural constituents and cytoskeleton regulators were significantly reduced in the treatment group, potentially beneficial to avoid fibrosis but also increasing the risk of poor cell adhesion to the cell scaffold of choice. Finally, phenotype and genotype of cells with a three-day recovery period following cytokine addition were assessed, to provide an insight into the phenotypic, genotypic and secretomic response of CMSCs to priming. An increase in expression of MIC A/B was highlighted as a factor to further investigate, based on the risk of increased immunogenicity, providing an argument against cell licensing. This work provides a vast characterization of CMSCs, that can be utilized as an overview for future, more specific, mechanistic experiments.

To accompany the large body of CMSC characterization data obtained in Chapters 3-5, the next chapter aimed to identify methods to aid topical application of the cells to the ocular surface. This would potentiate quicker translation to the clinic, as the administration route is also vital for the safety and efficacy of a therapy.

CHAPTER 6: Optimisation steps for the functionalisation of poly(HEMA-co-EGDMA) hydrogels for corneal mesenchymal stromal cell attachment

6.1. Introduction

Hydrogels are defined as hydrophilic, cross-linked three-dimensional polymeric networks, produced by the simple reaction of one or more monomers [282]. They hold the capacity to swell extensively and retain a significant fraction but are resistant to dissolution. These properties are due to hydrophilic functional groups attached to the polymeric backbone for water absorbance, with crosslinking for maintenance of structure [283].

In the early 1960s, Otto Wichterle created the first soft contact lens using free radical initiation to produce a poly(HEMA-co-EGDMA) hydrogel [104]. Although primarily made for vision correction, these have now also been used as a biological bandage to provide aid to trauma at the ocular surface, and for drug and protein delivery [284, 285]. Poly(HEMA-co-EGDMA) is also suited to stem cell applications due to the abundance of surface primary hydroxyls, which can be used for activation and coupling of affinity ligands [113]. The material is therefore ideal for functionalisation for stem cell attachment.

An appropriate therapeutic soft contact lens is defined as possessing good mechanical strength, durability, wettability and capacity for oxygen permeabilization [113]. Oxygen permeabilization requires good swelling capacity, which can be assessed through determination of equilibrium water content (EWC) [286], previously found to be around 40% water by weight in poly(HEMA-co-EGDMA) hydrogels.

For characterising the mechanical properties of contact lens hydrogels, the Young's modulus provides the most relevant information [287]. The Young's modulus,

generally defined as the ratio of tensile stress (σ) to tensile strain (ϵ), is a description of the material stiffness which determines how well the contact lens would resist deformation or stretching. *In situ*, the contact lens material is subject to external forces from the eyelids, in addition to stress from handling. However, for wearer comfort, the material must be flexible and drape easily over the cornea. Consequently, a material with an optimal Young's modulus which provides balance between stability and comfort must be manufactured.

Varying the cross-linking density and incorporating different chemistries through copolymerisation can be utilised to alter the mechanical properties of poly(HEMA-co-EGDMA), including the swelling, stiffness and elasticity [286]. Reduction in the crosslinker produces a softer hydrogel with higher malleability, and greater capacity for use in soft tissue regeneration. In addition to impact on mechanical properties, copolymerisation with reagents such as methylmethacrylate or inclusion of dextran can reduce the material hydrophilicity and improve cellular adhesion *in vivo* [288].

Copolymerisation can also be used to enhance the reactivity of the material. For example, primary amine monomers, such as 2-aminoethyl methacrylate hydrochloride (AEMA), have been identified as cell adhesion motifs, through the addition of charge to the material surface. It has been shown that both $-NH_2$ and $-COOH$ terminal groups caused increased attachment of ovarian cancer cells, however those cultured on the amino substrates had a higher proliferative capacity and increased cell spreading over a greater area [289]. This is due to the positive charge of the amino group, which enhances the generation and stretch of filopodia, compared to the negative charge of the carboxyl terminus. Cells immobilized on positively-charged biointerfaces have been shown to display a larger area of focal adhesion, in addition to longer and more numerous actin filaments, which are likely a result in the synergistic effect of electrostatic attraction and topographic interaction [290]. The functionality of the pendant primary amine can also be utilised as a handle to immobilise cell attachment motifs through peptide bonding [291]. These peptides include arginine-aspartic acid (RGD) and tyrosine-isoleucine-glycine-serine-arginine (YIGSR) peptide sequences, which have been demonstrated to increase cell adsorption to a material surface [292]. Alternatively, these peptides

can be modified to include an N- terminal methacrylic acid group for incorporation into bulk synthesis, omitting the need for the AEMA handle.

These cell adhesive peptides are short amino acid sequences, which are the minimal motif necessary for the specific binding of a cellular receptor involved in cell adhesion [293]. Through incorporation into synthetic scaffolds, it is possible to replicate the cell binding mechanisms of animal-based macromolecules of the extracellular matrix (ECM). RGD and YIGSR are isolated from fibronectin and laminin, respectively [294] and were chosen for inclusion in this study due to the abundance of cell adhesion data that exists, and previous work which demonstrated attachment of CMSCs to peptide-modified polymer fibres [112].

These motifs can also be easily incorporated into protein-based polymeric materials, for example, their adoption into elastin-like polypeptides, which are utilised as elastomeric substrates for cell culture [295]. In addition, resilin has been modified with peptide motifs, with the same goal to improve cell adhesion. Natural resilin is a rubber-like protein that exists in specialised compartments of most arthropods, with useful mechanical features similar to the elastins, including low stiffness, high resilience, large strain, and reversible extensibility. Resilin like polypeptide (RLP) hydrogels were chosen for investigation in this chapter due to their beneficial properties for creating a cell adhesive substrate. These include biocompatibility, with application employed widely for biomedical applications. They have low immunogenicity and are well-tolerated by living tissues, making them suitable for interactions with target tissues without triggering adverse immune responses [296]. In addition, the elasticity and flexibility possessed by resilin allows RLP-based coatings to stretch and conform to the contours of the contact lens and the ocular surface, minimizing mechanical stress on both the cells and the lens. The physical and chemical properties of RLPs can be tailored by modifying their sequence, length, and cross-linking density [297]. This versatility allows for fine-tuning the mechanical properties and surface characteristics of RLP-functionalized contact lenses to optimize the attachment and behaviour of MSCs. RLP-based coatings also exhibit good stability and durability, enabling long-term functionality of the functionalized contact lenses [295]. This is important for

maintaining the attachment of MSCs during wear and minimizing the risk of detachment or loss of functionality over time. Finally, RLP hydrogels have been synthesised using free radical initiation, allowing straight forward co-polymerisation with poly(HEMA-co-EGDMA) using the same polymerisation method.

Ultimately, the work described in this chapter aimed to develop a poly(HEMA-co-EGDMA) hydrogel with optimal mechanical, optical and swelling characteristics for its use as a contact lens. This was achieved through the investigation of manufacture, cross linker density and HEMA percentage. Additionally, these properties were assessed following functionalisation of the hydrogel through copolymerisation with AEMA, to investigate any effect of the primary amine monomer on the bulk properties of the gel. This was measured by tensile testing, opacity assays and equilibrium water content (EWC) investigations. It was hypothesised that CMSCs would adhere to the contact lens following functionalisation with a cell adhesive motif. Following the failure of cell attachment to the hydrogel using AEMA, other methods were attempted, including copolymerisation with RGD, YIGSR and RLPs. Overall, this work aimed to develop a base scaffold material for CMSC adhesion, to act as a therapy for ocular surface disorders.

6.2.1. Experimental Plan

Optimisation of the poly(HEMA-co-EGDMA) hydrogel followed the workflow highlighted in Figure 6.1, in order of analysis of HEMA concentration, cross linker density, manufacturing methods, and functionalisation with AEMA, methylated cell adhesive peptides, and RLPs. Detailed practical polymer synthesis and analysis methods can be found in Chapter 2.2.6.

6.2.2. Optimisation of HEMA concentration

Increasing weight percentages of water included in the initial monomer solution were investigated to determine the maximum water content for the production of a transparent gel. Transparency and hydrogel gelation were also assessed using *in situ* rheology, as described in Chapter 2.2.11.ii. All gels were made with 1% molar concentration EGDMA based on previous literature. Original transparency images were taken following thermal free radical polymerisation using VA-044, and all rheology was performed using photo-initiation via DMPA. Monomer to water concentrations were based on volume. The concentrations are shown in Table 6.1.

Table 6. 1. Volumetric percentages of monomer and water used for optimisation of water solvent in initial solution.

HEMA/EGDMA (%)	H2O (%)
100	0
80	20
60	40
40	60
20	80
10	90

6.2.3. Manufacture optimisation

Hydrogels were cast in 96 well plates on normal, treated tissue plastic; between glass slides; or using the SureCast Gel Handcast system, using both thermal and photo initiation, as described in Chapter 2.2.9. Optimal manufacturing method was determined through observation, identifying the hydrogels which appeared transparent and uniformed.

6.2.4. Optimisation of EGDMA concentration

Varied concentrations of EGDMA were incorporated into the gel, calculated via molar percentage (Table 6.2), to understand the impact of cross linker density on the mechanical properties of the hydrogel. Young's Modulus and EWC were calculated for the different hydrogels using methods laid out in Chapter 2.2.11.i. and 2.2.11.iii.

Table 6. 2. Molar percentages of HEMA and EGDMA used for optimisation of crosslinker concentration.

HEMA (mol %)	EGDMA (mol %)
99.5	0.5
99	1
98	2
96	4

6.2.5. Synthesis of poly(HEMA-co-EGDMA-co-AEMA) with increasing AEMA concentration

Various concentrations of AEMA calculated through molar percentage (Table 6.3) were assessed to determine any effects on the bulk properties of the gel. All AEMA assessment was performed with 20% (v/v) H₂O solvent and 1 mol % EGDMA using thermal free radical initiation with VA-044. Mechanical properties for each hydrogel were calculated, including Youngs modulus, max stress and strain using methods in Chapter 2.2.11.i. EWC and opacity testing were also determined using methods in Chapter 2.2.11.iii. and 2.2.11.iv.

Table 6. 3. Molar percentage of HEMA, EGDMA and AEMA utilised for initial functionalisation of the hydrogels.

HEMA (mol %)	EGDMA (mol %)	AEMA (mol %)
93	1	6
95	1	4
97	1	2
99	1	0

6.2.6. Functionalisation with peptides

Functionalisation of poly(HEMA-co-EGDMA) hydrogels using 0.4% (Mw) GGGYIGSR and GGGRGD with methacrylic acid N terminals was attempted through bulk synthesis, as described in Chapter 2.2.10.ii. 0.4% was selected deduced from the maximum dissolution of the peptides in solvent. The polymerisation took place using DMPA and photoinitiation in chamber slides.

6.2.7 Functionalisation with RLP

Optimisation of co-polymerisation of poly(HEMA-co-EGDMA) hydrogels with RLPs was achieved through assessing different part-polymerisation times (Table 6.4). *In situ* rheology experiments can be performed, with frequency sweep tests to investigate the transition of a polymer from a liquid to a solid state. Frequency sweep, also known as dynamic frequency sweep or oscillatory frequency sweep, involves subjecting the material to a range of frequencies while measuring its response. In a frequency sweep test, the viscoelastic properties of the polymer, such as storage modulus (G') and loss modulus (G''), are measured as a function of frequency. These moduli provide information about the material's elastic (solid-like) and viscous (liquid-like) behaviour. When a polymer transitions from a liquid to a solid, there is typically an increase in the storage modulus (G') and a decrease in the loss modulus (G''), revealing the 'gel point' of the material.

Samples were prepared as described in Chapter 2.2.10.iii, DMPA and LAP for photoinitiation of the 60% poly(HEMA-co-EGDMA) and 20% RLP hydrogels, respectively. Samples were sandwiched between glass slides with a silicone spacer

(Figure 6.2). All RLPs were synthesised by Cristobal Garcia and Sai Patkar at the University of Delaware.

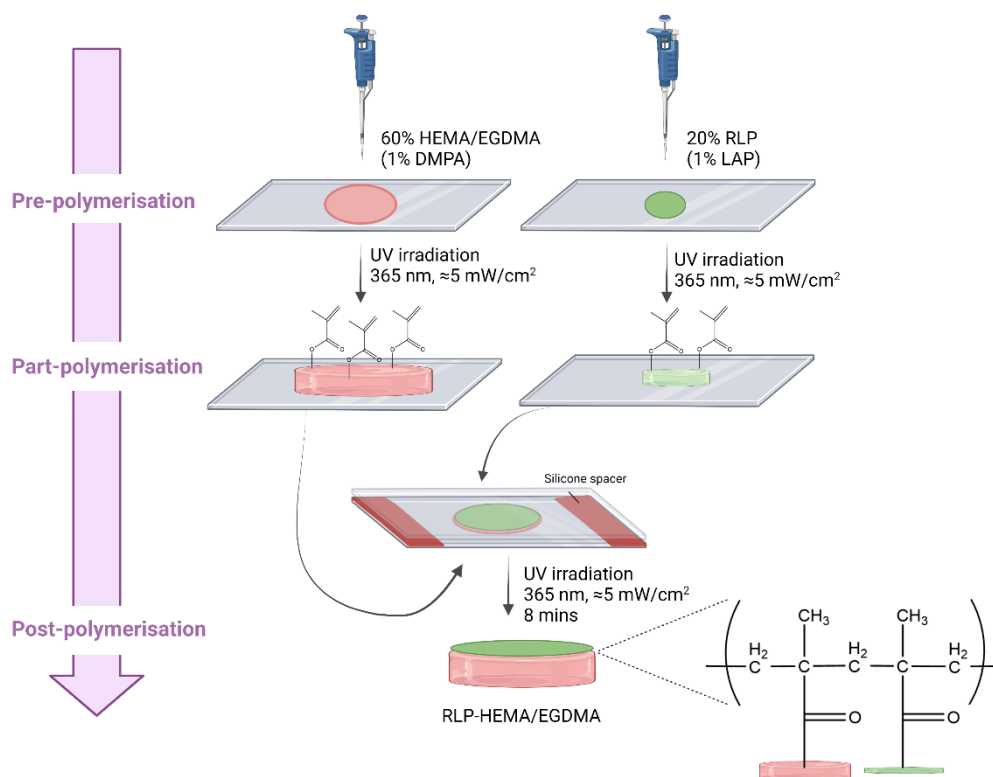


Figure 6. 2. Schematic illustration of methods for functionalising 60% poly(HEMA-co-EGDMA) with 20% RLP hydrogel using free radical polymerisation.

Table 6. 4. Optimisation strategy for functionalisation of poly(HEMA-co-EGDMA) with RLP.

	HEMA	RLP
Part-polymerisation	No	No
Part-polymerisation	Yes (160 s)	No
Part-polymerisation	Yes (160 s)	Yes (60 s)

6.2.8. Cell Culture and Seeding on Hydrogels

6.2.8.i. BM-MSCs

BM-MSCs were cultured as described in Chapter 2.2.1.iii. Cells between passage 4 and 6 were seeded onto functionalised hydrogels, using the serum containing media MSCGM™ Mesenchymal Stem Cell Growth Medium BulletKit™. Cells were seeded on hydrogels placed in a 96 well plate, at 2×10^4 cells/cm² and cultured for 3 days. Cell seeded hydrogels were then washed, fixed and permeabilised using methods described in Chapter 2.2.4.i. and 2.2.4.ii. Staining was performed using Phalloidin AlexaFluor 594 (ThermoFisher Scientific, A12381) and nuclear stain, Hoechst 33342 Solution (ThermoFisher Scientific, 62249), using the same methods described for Phalloidin AlexaFluor 488 and DAPI respectively, outlined in Chapter 2.2.4.iii.

6.2.8.ii. CMSCs

CMSCs were cultured as described in Chapter 2.2.1.ii., in either serum containing M199 or SCM (Chapter 2.2.1.i). CMSCs were seeded as described in Chapter 6.2.5.i., and cultured for 7 days with a media change at day 3, to try to achieve a confluent monolayer. Cells and hydrogels were fixed, permeabilised and stained using DAPI and Phalloidin as described in Chapter 2.2.4.

6.2.9. Confocal imaging of MSC seeded hydrogels

For imaging hydrogels were placed between glass slides, immersed in a few drops of PBS. ZEN Microscopy Software from Zeiss was used for all image acquisition and analysis. Fluorescent imaging of BM-MSCs on hydrogels was performed using the Zeiss Celldiscoverer7, with detection wavelengths between 540 - 570 and 370 - 400. For snapshot imaging, tile images were taken at the 4x/0.35 objective. Z-stack imaging was performed using a 20x/0.7 objective and viewed as a maximum intensity projection or stitched maximum intensity projection.

Imaging of CMSCs seeded on hydrogels was performed using the Zeiss LSM710 Confocal Microscope. Fluorescent images were taken using two channels with detection wavelengths between 495 - 630 and 410 - 490, with snapshot overviews

and Z-stacks taken at an objective of 10x/0.45, with Z-stacks either converted to a maximum intensity projection tiff, the Z-stack tiles stitched and converted to a maximum intensity projection tiff, or snapshot overview images stitched and converted to a tiff.

6.3. Results

6.3.1. Analysis of optimal HEMA concentration

Poly(HEMA-co-EGDMA) hydrogels were assessed for an optimal monomer to water ratio. Hydrogels began to show features of opacity when 60% (vol:vol) H₂O was included in the reaction mixture (Figure 6.3.4), with hydrogels containing 80% (Figure 6.3.5) and 90% H₂O (Figure 6.2.6) displaying complete opacity. Hydrogels containing 100% monomer/ 0% H₂O (Figure 6.3.1), 80% monomer/ 20% H₂O (Figure 6.3.2) and 60% monomer/ 40% H₂O (Figure 6.3.3) formed transparent gels. *In situ* rheology using DMPA and photoinitiation demonstrated increases in storage (G') and loss (G'') modulus with increasing HEMA concentration, with respective values ranging from 0.01 MPa and 0.00 MPa in 20% HEMA hydrogels, to 12.1 MPa and 4.0 MPa in 80% HEMA hydrogels (Figure 6.4). Optical properties were the same in both the thermal and photo-initiated hydrogels.

All further experiments were done at 60% HEMA concentration, to ensure the formation of an optically clear gel, with suitable mechanical properties and water content.

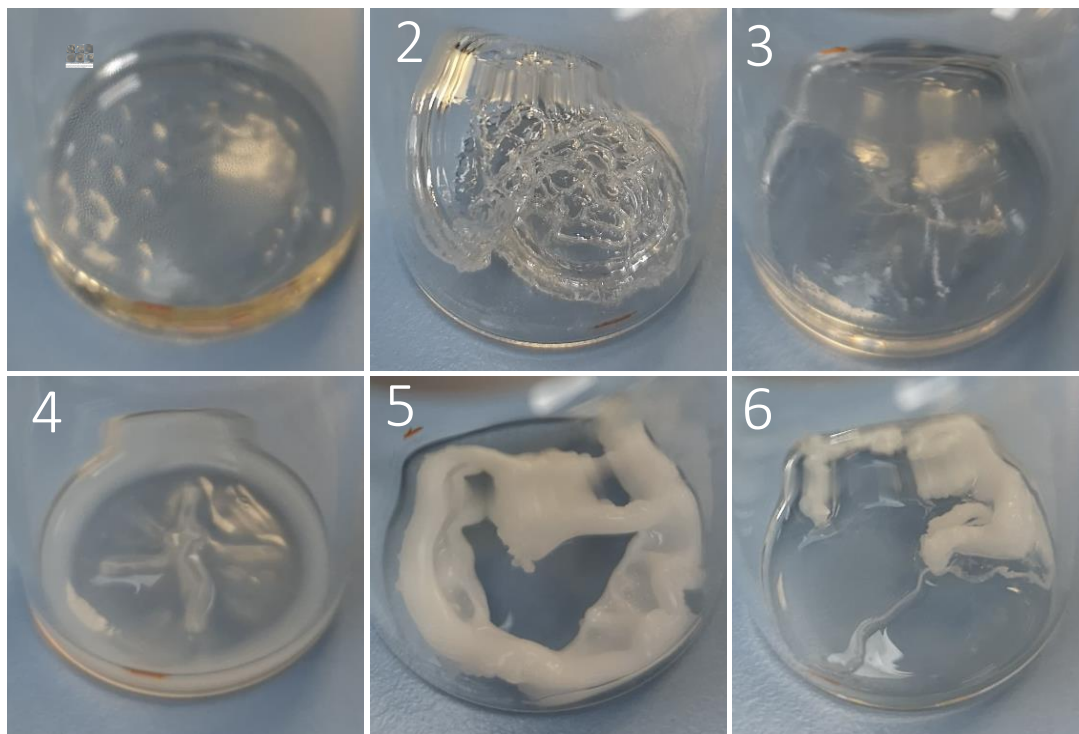


Figure 6. 3. Poly-HEMA-co-EGDMA hydrogels with increasing vol/vol % water. (1) 100% monomer/ 0% H₂O; (2) 80% monomer/ 20% H₂O; (3) 60% monomer/ 40% H₂O; (4) 40% monomer/ 60% H₂O; (5) 20% monomer/ 80% H₂O; (6) 10% monomer/ 90% H₂O. Polymerised using AIBN for thermal free radical initiation and 1% EGDMA crosslinker. Phase separation occurred with the addition of $\geq 40\%$ H₂O, resulting in an opaque gel.

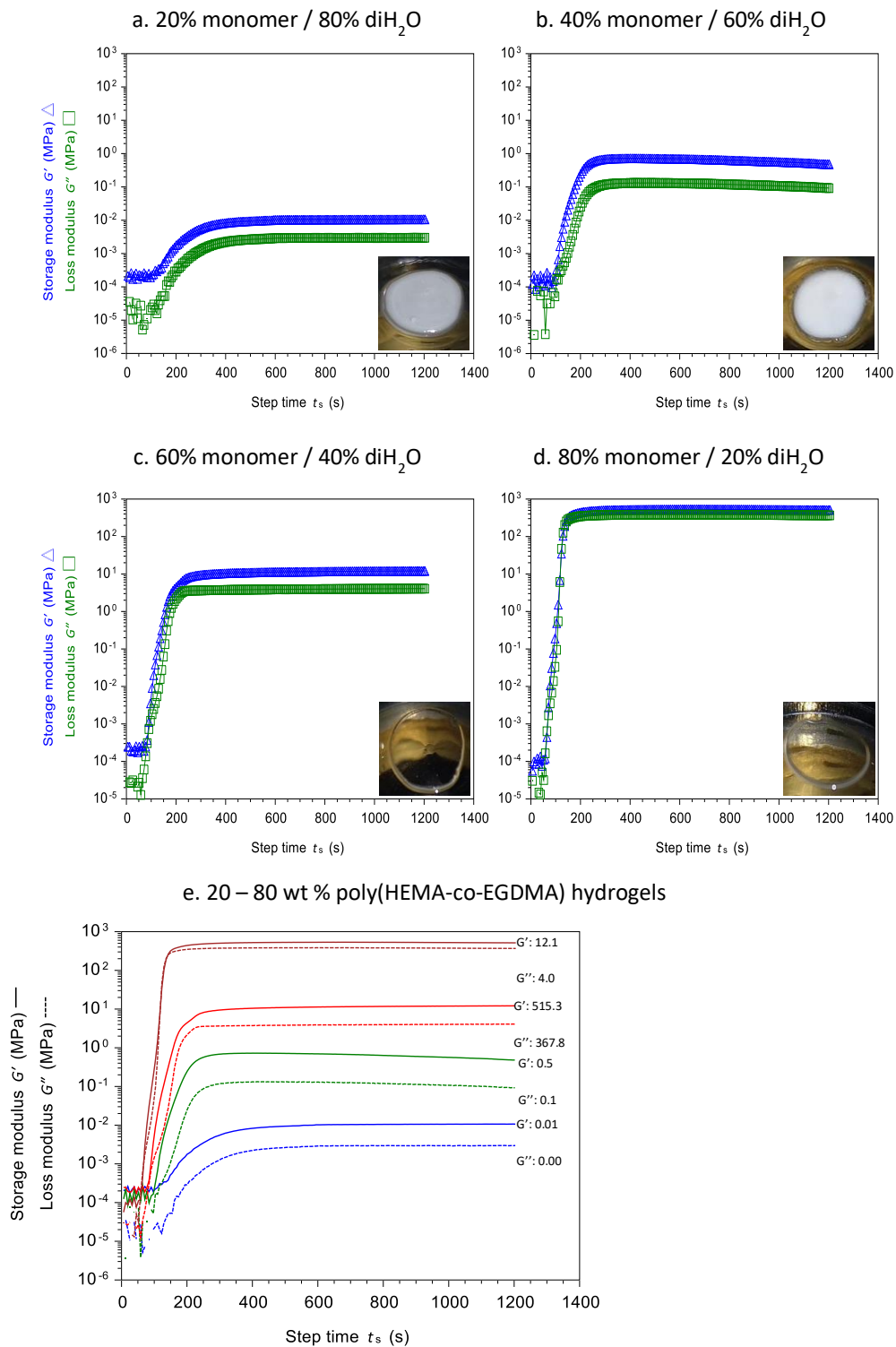


Figure 6. 4. Frequency sweeps from *in situ* rheology to demonstrate changes in storage (G') and loss (G'') modulus of Poly-HEMA-co-EGDMA hydrogels with increasing vol/vol % water, and corresponding images to show transparency. (1) 100% monomer/ 0% H₂O; (2) 80% monomer/ 20% H₂O; (3) 60% monomer/ 40% H₂O; (4) 40% monomer/ 60% H₂O; (5) 20% monomer/ 80% H₂O; (6) 10% monomer/ 90% H₂O. Polymerised using DMPA for photo free radical initiation and 1% EGDMA crosslinker.

6.3.2. Methods of manufacture to achieve consistently well formed, clear hydrogels

Poly(HEMA-co-EGDMA) hydrogels were initially cast in tissue culture plates (Figure 6.5.a), with the main goal for easy methods and analysis of future cell attachment to functionalised gels. Hydrogels displayed inconsistent properties, with areas of reduced transparency and an appearance of air bubbles. Hydrogels manufactured between two glass slides separated by a silicone spacer and held together with bulldog clips (6.5.b) were consistently optically transparent with no air bubbles. This could be replicated to produce larger hydrogels with less experimental variation using the SureCast Gel Handcast System (Figure 6.5.c).

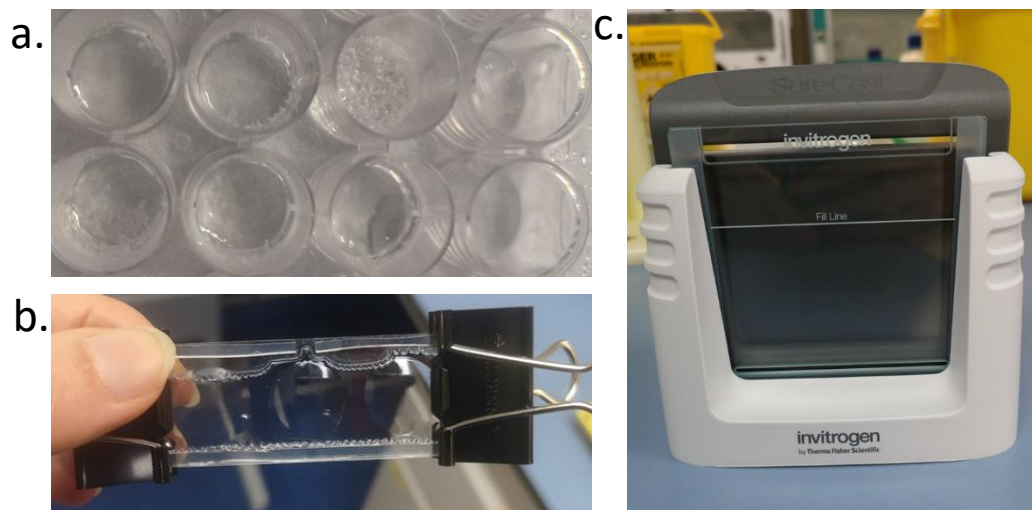


Figure 6. 5. Manufacture of poly-HEMA-co-EGDMA hydrogels in cell culture plates (a) produced inconsistent gels with areas of reduced transparency. Production of gels between 2 glass slides (b) separated with a silicone spacer and held in place with bulldog clips consistently produced well formed, optically transparent hydrogels. This could be replicated for accuracy using the Invitrogen SureCast Gel Handcast System (c).

6.3.3. Effect of different EGDMA densities on properties of poly(HEMA-co-EGDMA) hydrogels

EWC and Young's Modulus were assessed to determine difference in poly(HEMA-co-EGDMA) hydrogel properties with increasing EGDMA concentrations (Figure 6.6). Increasing the molar concentration of EGDMA caused a significant decrease in EWC of the hydrogels ($n = 8$; $P < 0.0001$) with significant reductions shown between 0.5% and 2% EGDMA ($P = 0.0003$), 0.5% and 4% EGDMA ($P = < 0.0001$), 1% and 4%

EGDMA ($P < 0.0001$) and 2% and 4% EGDMA ($P < 0.0001$) (Figure 6.6.a). No significant difference was found in EWC between 0.5% and 1% EGDMA, and 1% and 2% EGDMA.

Increasing concentrations of EGDMA also resulted in a significant increase in Young's Modulus ($P = 0.003$), with significance detected between 0.5% and 2% EGDMA ($P = 0.0025$) and 1% and 2% EGDMA ($P = 0.0282$) (Figure 6.6.b). No significance was found in Young's Modulus between 0.5% and 1% EGDMA.

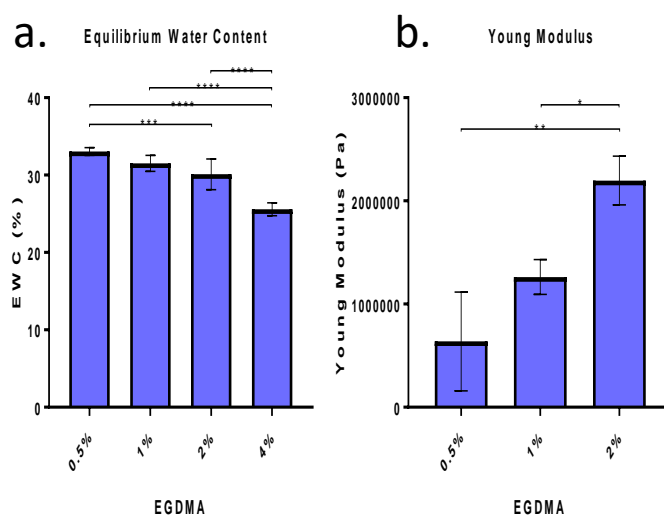


Figure 6. 6. (a) Equilibrium water content (%) and (b) Young Modulus of varying EGDMA densities (mol %) in poly-HEMA-co-EGDMA hydrogels ($n=5$). Graphs are plotted as mean values with \pm SD represented by the error bars. Significance is shown as $P \leq 0.05$ (*), $P \leq 0.01$ (**), $P \leq 0.001$ (***), $P \leq 0.0001$ (****). Data demonstrates a decrease in EWC and an increase in Young Modulus with increasing EGDMA concentration.

6.3.4. Effect of different AEMA concentrations on properties of poly(HEMA-co-EGDMA-co-AEMA) hydrogels

EWC as well as Young's Modulus, max stress and max strain were assessed to determine the difference in swelling capacity and mechanical properties of poly(HEMA-co-EGDMA) hydrogels with increasing AEMA concentrations (Figure 6.7). Results demonstrate a significant increase in EWC (%) as AEMA concentration (mol %) increased ($n = 8$; $P < 0.0001$), with significance detected between every sample ($P < 0.0001$) (Figure 6.7).

No significant difference in Young's Modulus was detected in poly(HEMA-co-EGDMA-co-AEMA) hydrogels with increasing concentrations of AEMA ($n = 3$), however Young's Modulus appeared lower in samples containing 4% and 6% AEMA compared to 0% and 2% (Figure 6.7.b). Standard deviations in samples containing 4% and 6% AEMA were also higher than the 0% and 2% AEMA hydrogels (SD; 0% 169158.439, 2% 7703.585, 4% 464196.438, 6% 253562).

There was a significant reduction in maximum stress of the poly(HEMA-co-EGDMA-co-AEMA) hydrogels with increasing AEMA concentrations ($n = 3$; $P = 0.0006$) (Figure 6.7.c). This decrease was shown between the hydrogels containing 0% and 4% AEMA ($P = 0.0019$), 0% and 6% AEMA (0.0023), 2% and 4% AEMA ($P = 0.0053$) and 2% and 6% AEMA ($P = 0.0063$). No significance was detected between 0% and 2% AEMA concentrations, and 4% and 6% AEMA concentrations.

Increasing concentrations of AEMA% in poly(HEMA-co-EGDMA-co-AEMA) resulted in a significant decrease in the maximum strain of the hydrogels ($n = 3$; $P = 0.0003$), with significant reductions between all samples (0% vs. 2%, $P = 0.0263$; 0% vs. 4%, $P = 0.0006$; 0% vs. 6%, $P = 0.0004$; 2% vs. 4%, $P = 0.0469$, 2% vs. 6%; $P = 0.0287$), except 4% and 6% AEMA, where no significance was drawn (Figure 6.7.d).

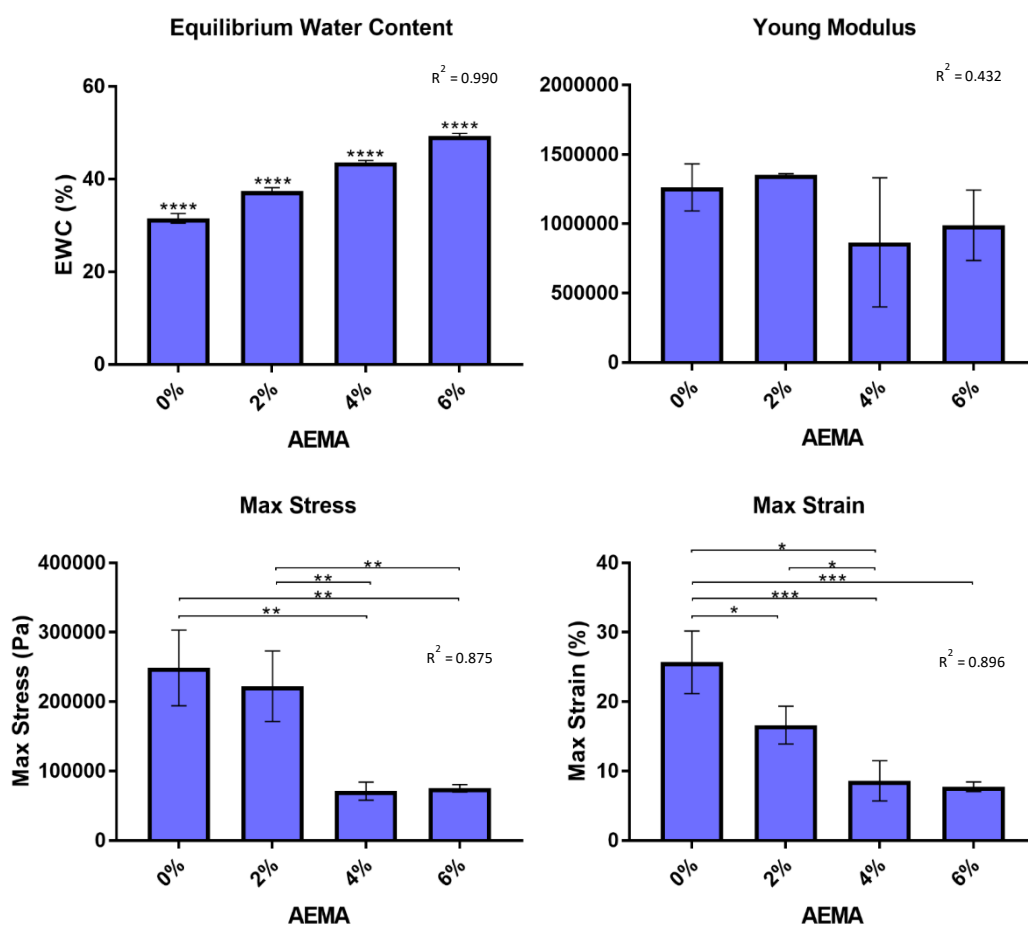


Figure 6. 7. (a) Equilibrium water content (%), (b) Young Modulus, (c) max stress and (d) max strain of varying AEMA densities in poly(HEMA-co-EGDMA-co-AEMA) hydrogels. Graphs are plotted as mean values with \pm SD represented by the error bars. Significance is shown as $P \leq 0.05$ (*), $P \leq 0.01$ (**), $P \leq 0.001$ (***), $P \leq 0.0001$ (****). Data demonstrates a significant increase in EWC, decrease in max stress and decrease in max strain as AEMA (%) increases. No correlation was found between Young Modulus and AEMA concentration.

6.3.5 Transparency of hydrogels with varied EGDMA and AEMA concentrations

Opacity assays were performed on hydrogels containing varying concentrations of EGDMA and AEMA to deduce the transparency of the gels. The higher the absorbance the lower the transparency. Data demonstrates significance in absorbance fold change of hydrogels containing differing concentrations of EGDMA ($P = 0.0002$) and AEMA ($P = 0.0147$) in comparison to a PBS control (Figure 6.8). Hydrogels containing 2% EGDMA had a significantly higher absorbance than those made up with 0.5% EGDMA ($P = 0.0057$), 1% EGDMA ($P = 0.0339$) and 4% EGDMA ($P < 0.0001$) (Figure 6.8.a). No significant difference was found between gels containing 0.5%, 1% and 4% EGDMA.

In poly(HEMA-co-EGDMA) hydrogels made up with varying concentrations of AEMA, significance was only detected in the increase in absorbance between 2% and 6% AEMA concentrations ($P = 0.0135$) (Figure 6.8.b).

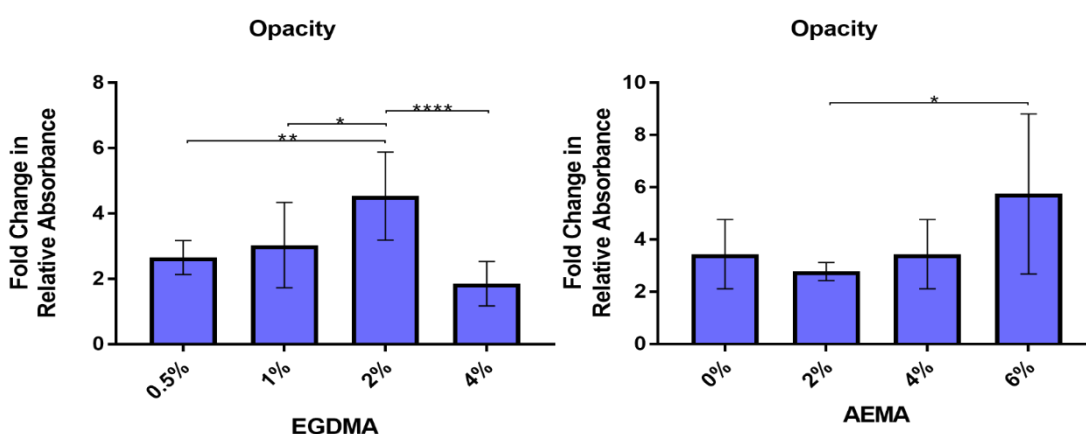


Figure 6. 8. Opacity assay demonstrating fold change in absorbance compared to PBS control. Graphs are plotted as mean values with \pm SD represented by the error bars. Significance is shown as $P \leq 0.05$ (*), $P \leq 0.01$ (**), $P \leq 0.001$ (***), $P \leq 0.0001$ (****). (a) Data demonstrates a significant affect of EGDMA (mol %) and (b) AEMA (mol %) on absorbance of light from the hydrogels, and therefore on the transparency.

6.3.6. CMSC attachment to hydrogels functionalised through bulk synthesis.

CMSCs did not adhere to AEMA functionalised poly-HEMA-co-EGDMA hydrogels (Data not shown). Cell attachment was observed on poly-HEMA-co-EGDMA functionalised with Meth-GGG-YIGSR and Meth-GGG-RGD (Figure 6.9), however cells remained rounded, with no cell spreading on the surface of the gel, compared to the spindle-like morphology of CMSCs cultured on tissue culture plastic (control). Cells appeared larger in RGD functionalised hydrogels, suggesting higher levels of cell stress. YIGSR and RGD functionalised hydrogels were not optically clear and maintained the phenol red from the media.

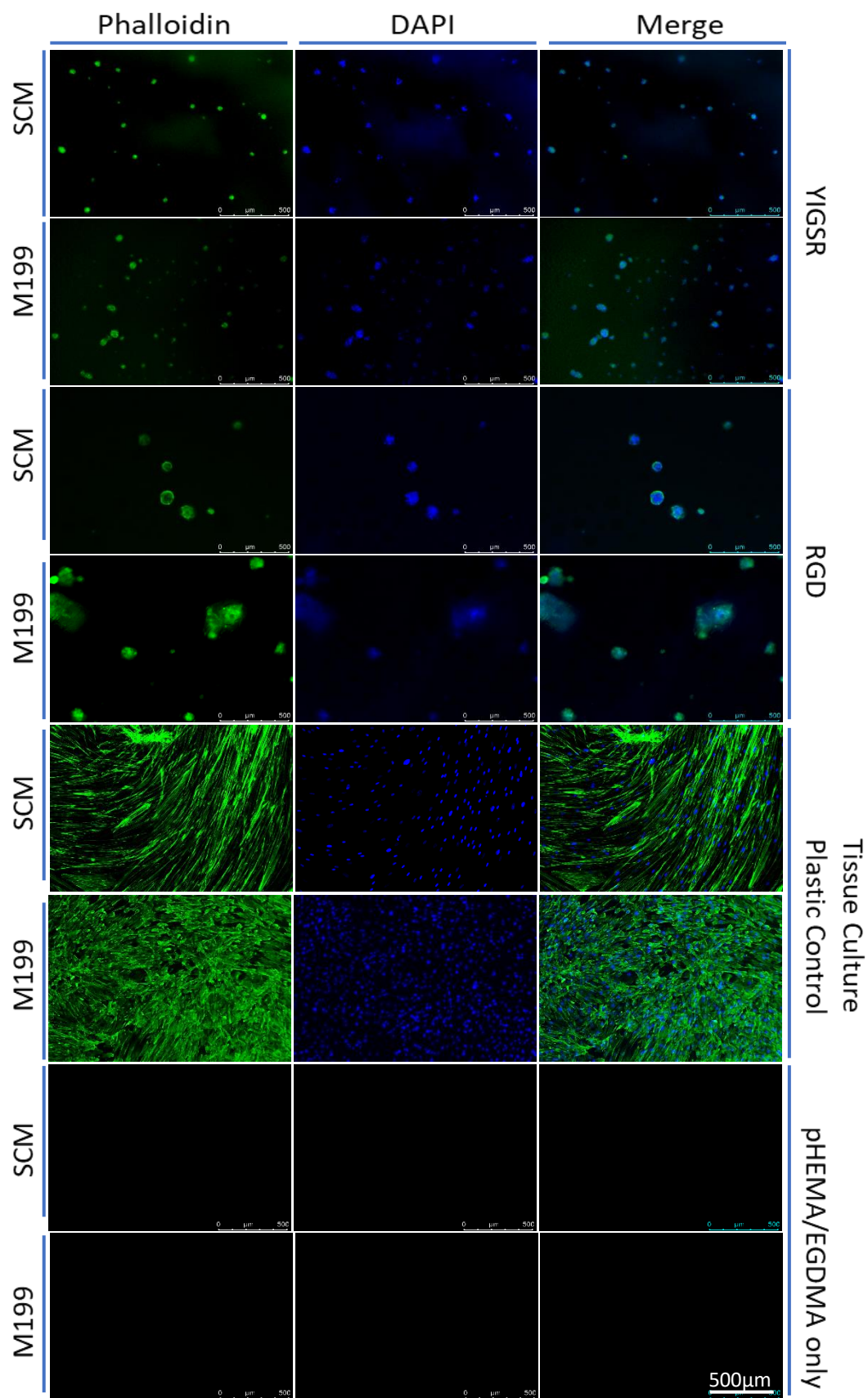
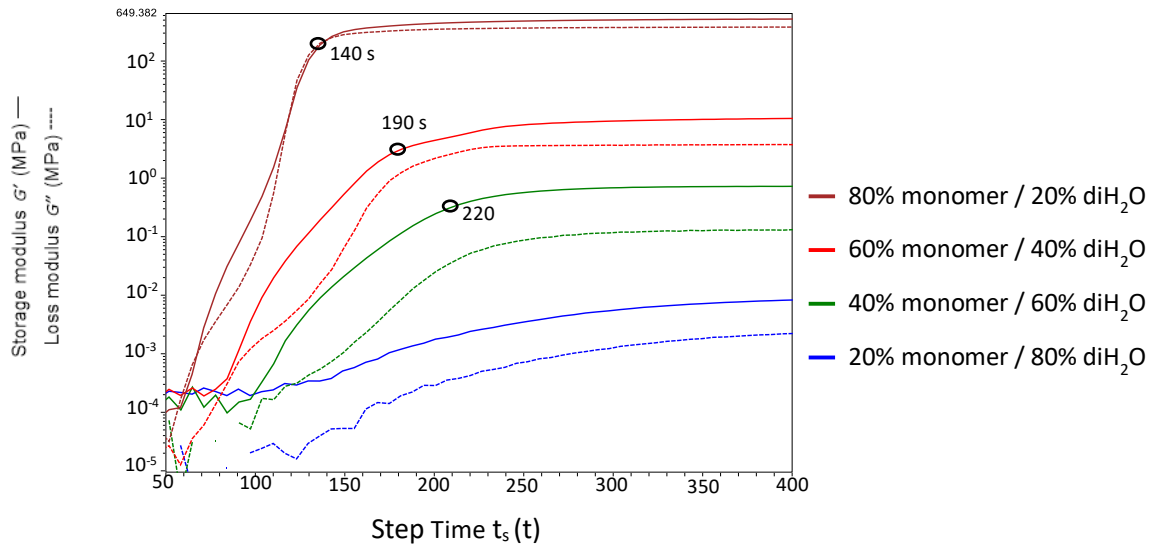


Figure 6. 9. (a) Phalloidin (green) and DAPI (blue) staining of CMSCs seeded on poly-HEMA-co-EGDMA hydrogels functionalised with 0.4% (Mw) YIGSR and RGD. Cells supplemented with either M199 or SCM media. Control cells grown on tissue culture plastic. Images representative of all cells in each sample. Scale bars = 500 μ m.

6.3.7. Gelation time of poly-HEMA-co-EGDMA) hydrogels

In situ rheology was used to estimate the gelation time of poly(HEMA-co-EGDMA) hydrogels, for future surface functionalisation following part-polymerisation (Figure 6.10.a). 80%, 60%, 40% and 20% wt poly(HEMA-co-EGDMA) hydrogels appeared to be fully polymerised at 140 s, 190 s, 220 s and incomplete, respectively. To ensure cross-linking stopped following the removal of UV light, *in situ* rheology was performed using 60 % wt poly(HEMA-co-EGDMA) hydrogels, with removal of the stimulus at different time points (160 – 320) seconds. Polymerisation stopped following the removal of UV light was demonstrated, where hydrogels with low exposure times showed reduced loss and storage modulus. Higher timepoints displayed a reduced difference in mechanical properties compare to the proximity of lower time points. 160 seconds was chosen as a base point for future functionalisation studies, as the hydrogel had started to polymerise, aiding handling, however there would still be methacrylate groups available for free radical synthesis.

a. Overlay assessing gelation times of different % wt poly(HEMA-co-EGDMA) hydrogels



b. Overlay assessing different UV exposure times in 60 % wt poly(HEMA-co-EGDMA)

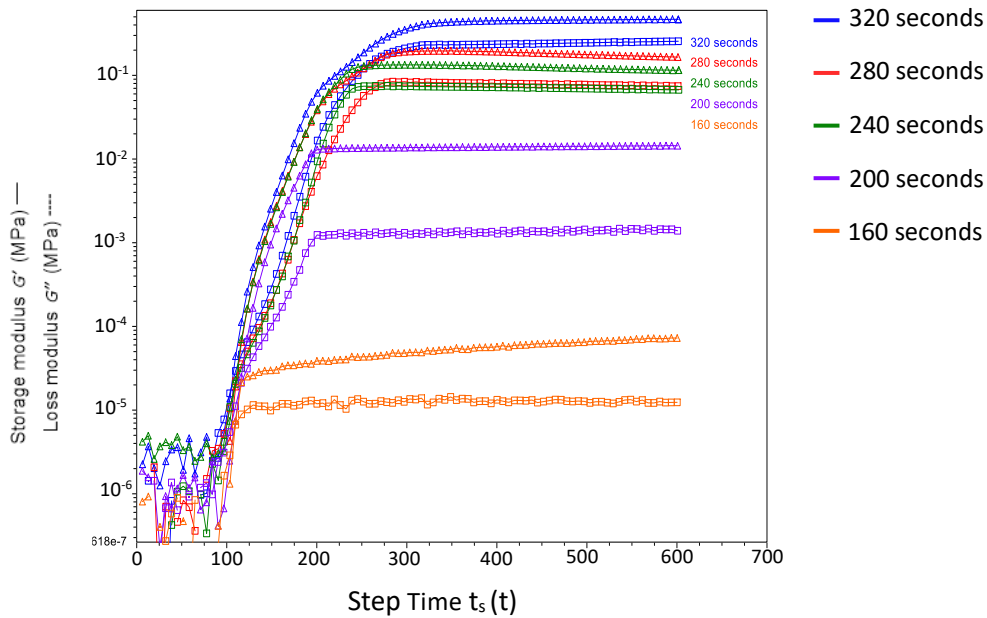


Figure 6. 10. *In situ* rheology of poly(HEMA-co-EGDMA) hydrogels. (a) Frequency sweeps from *in situ* rheology of varying water/monomer concentrations to provide basis of gelation time. (b) Removal of UV light at different timepoints (160 – 320 seconds) to confirm that crosslinking stops when the photo stimulator is removed. Hydrogels made using 1% EGDMA and 1% DMPA.

6.3.8. Optimisation of RLP layer addition

To optimise the functionalisation of poly(HEMA-co-EGDMA) with RLP, time and method were assessed. Combining the 2 monomers prior to polymerisation led to phase separation and an opaque hydrogel (Figure 6.11.a). Part-polymerisation of poly(HEMA-co-EGDMA) for 160 seconds before placement onto RLP solution and further polymerisation lead to a cloudy layer present on the surface of the hydrogel (Figure 6.11.b). Part-polymerisation of the poly(HEMA-co-EGDMA) for 160 seconds and RLP for 60 seconds, before sandwiching together to complete polymerisation, resulted in a clear hydrogel, with excess RLP pushed to the side of the gel, observed as white residue (Figure 6.11.c and d).

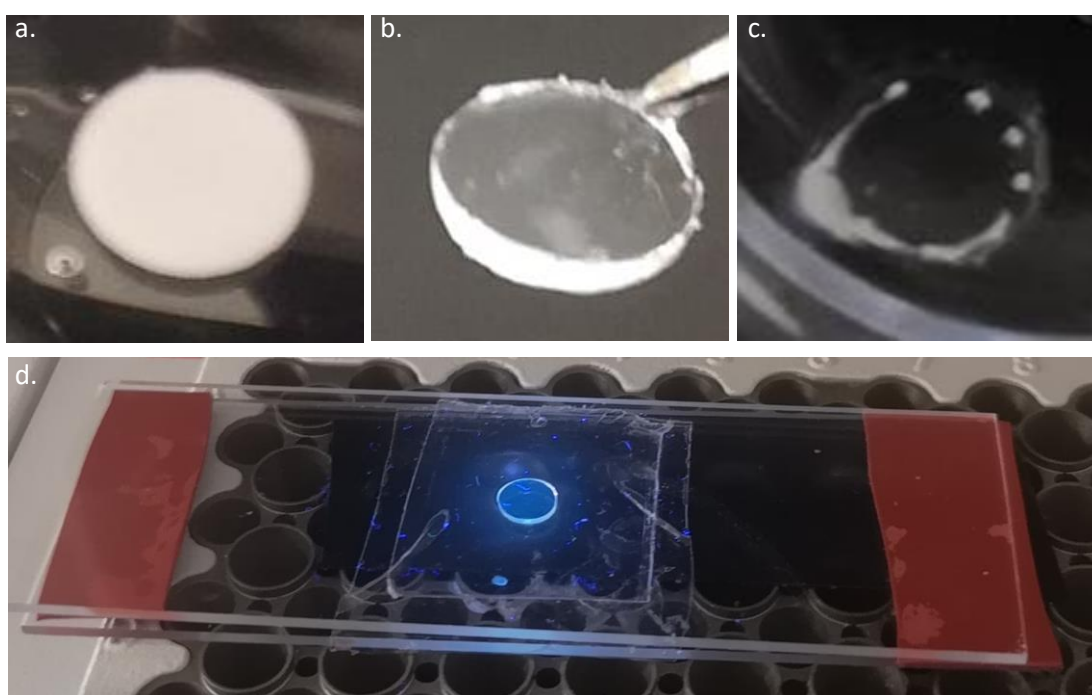


Figure 6. 11. Optimisation of poly(HEMA-co-EGDMA) hydrogels with RLP. 2 μ L of 10 wt% RLP-FM monomer solution with 10 μ L of 60 wt% HEMA monomer solution. (a) Solutions mixed prior to polymerisation. (b) HEMA/EGDMA part-polymerised for 160 seconds before being placed on RLP solution and polymerised for a further 5 mins. (c) HEMA/EGDMA and RLP hydrogels part-polymerised for 160 seconds and 60 seconds respectively, before being sandwiched together and polymerised for a further 5 mins.

6.3.9. Attachment of BM-MSCs to HEMA/RLP hydrogels

As proof of concept, BM-MSCs were seeded on HEMA/RLP in serum containing media, where both layers underwent part-polymerisation, to assess cell attachment. Staining of the nuclei and actin filaments using Hoechst and Phalloidin respectively showed attachment of BM-MSCs to the RLP functionalised hydrogel, but not poly(HEMA-co-EGDMA) alone (Figure 6.12). The cells had not formed a confluent monolayer, however could be observed throughout the entirety of the gel surface. Confocal imaging displayed a spread-out morphology, as expected of MSCs.

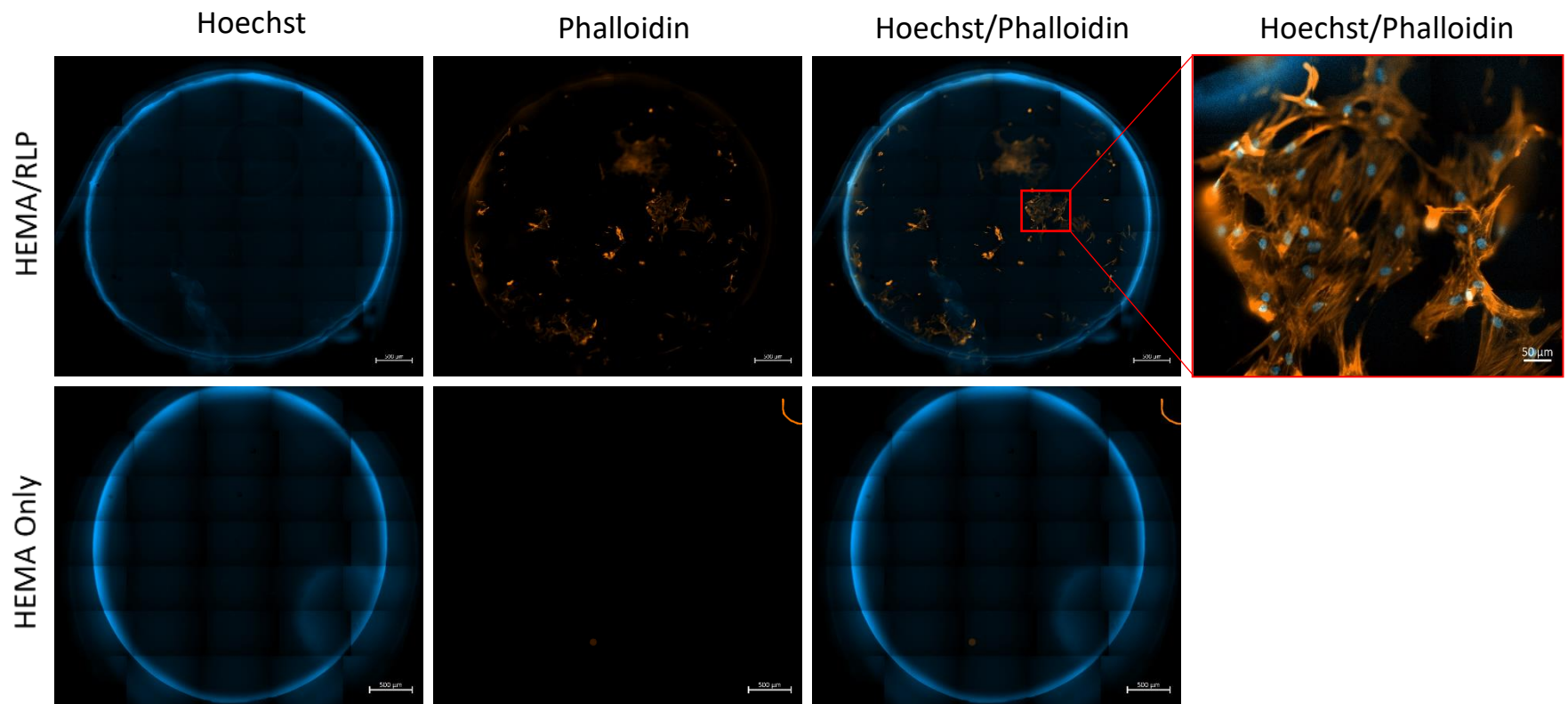


Figure 6. 12. Confocal imaging of BM-MS-C cell attachment to RLP functionalised poly(HEMA-co-EGDMA) hydrogels compared to no functionalisation. Hoechst (blue) and Phalloidin (orange) stains were used to detect cell nuclei and actin filaments, respectively. Images are representative of all samples. Scale bars = 500 μm .

6.3.10. Attachment of CMSCs to HEMA/RLP hydrogels

CMSCs were seeded on RLP functionalised hydrogels and cultured using serum free media. Adherence was assessed using confocal imaging of DAPI and Phalloidin stain for the nucleus and actin filaments respectively. An overview snapshot showed that CMSCs were present and had attached to the RLP layer (Figure 6.13.a). Stitched confocal imaging of the area demonstrated that a confluent monolayer was present over the entire hydrogel (6.13.b). Confluency was confirmed with a higher magnification image. No cells adhered to the poly(HEMA-co-EGDMA) alone.

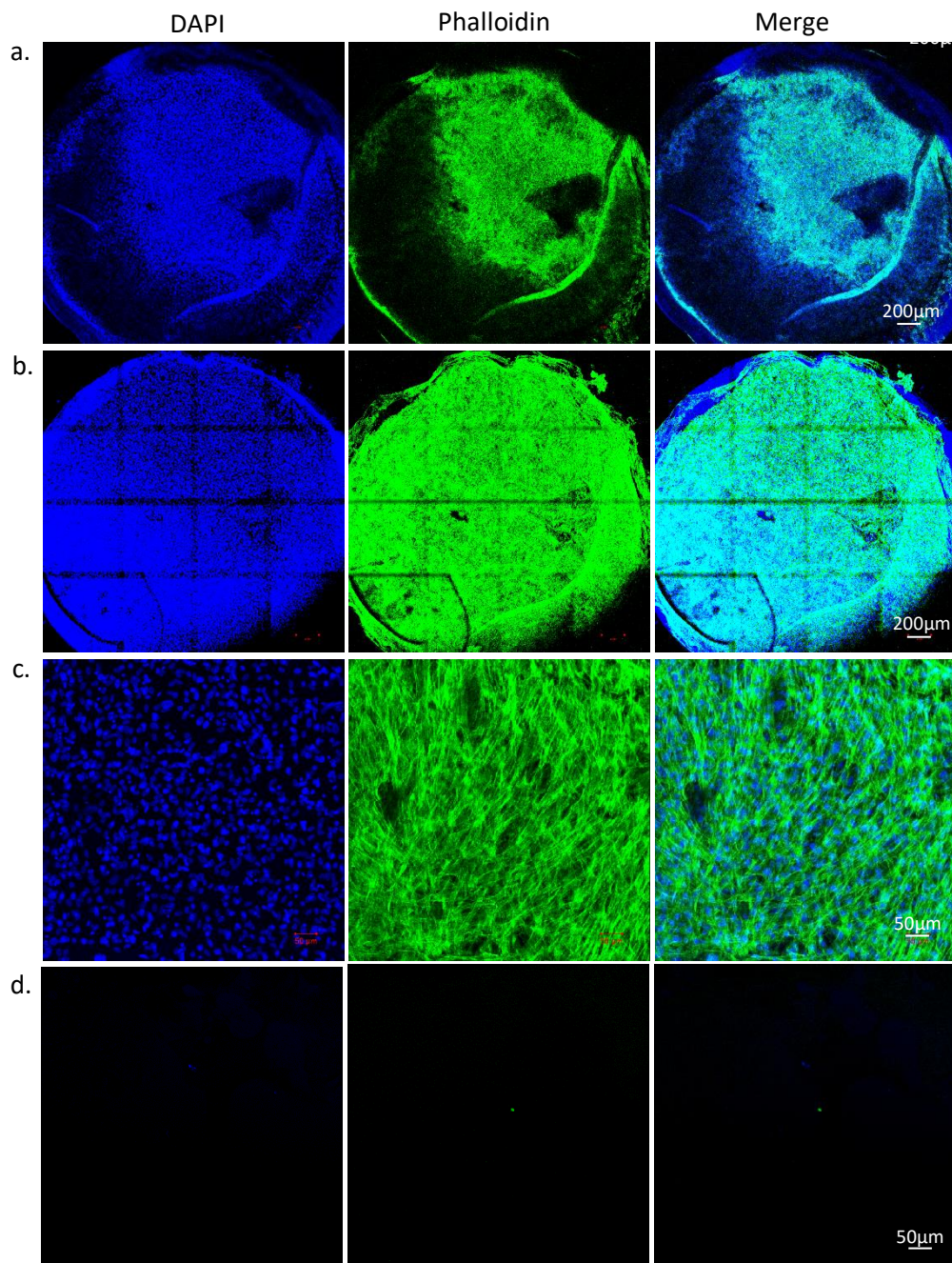


Figure 6. 13. Confocal images of CMSCs adhered to RLP functionalised poly(HEMA-co-EGDMA) hydrogels, with DAPI nuclear stain (blue) and Phalloidin to stain actin filaments (green). (a) Snapshot overview, (b) stitched maximum intensity Z-projection tiles, (c) and maximum intensity Z-projection of CMSCs seeded on RLP functionalised hydrogels, and (d) control CMSCs seeded on poly(HEMA-co-EGDMA) hydrogels alone control. Images are representative of all samples. Scale bars = 200 µm (a and b) and 50 µm (c and d).

6.3.11. Overconfluence of CMSCs on RLP/HEMA hydrogels

CMSCs were also seeded on RLP/HEMA hydrogels in serum containing media. An overview, fluorescent image of CMSC nuclei and actin staining showed that cells were absent from the centre of the gel (Figure 6.14.a). Confocal imaging demonstrated that in some areas of the gel, CMSCs had layered on top of each other (Figure 6.14.b), however it appeared cells had begun to shed, likely due to overconfluency (Figure 6.14.c).

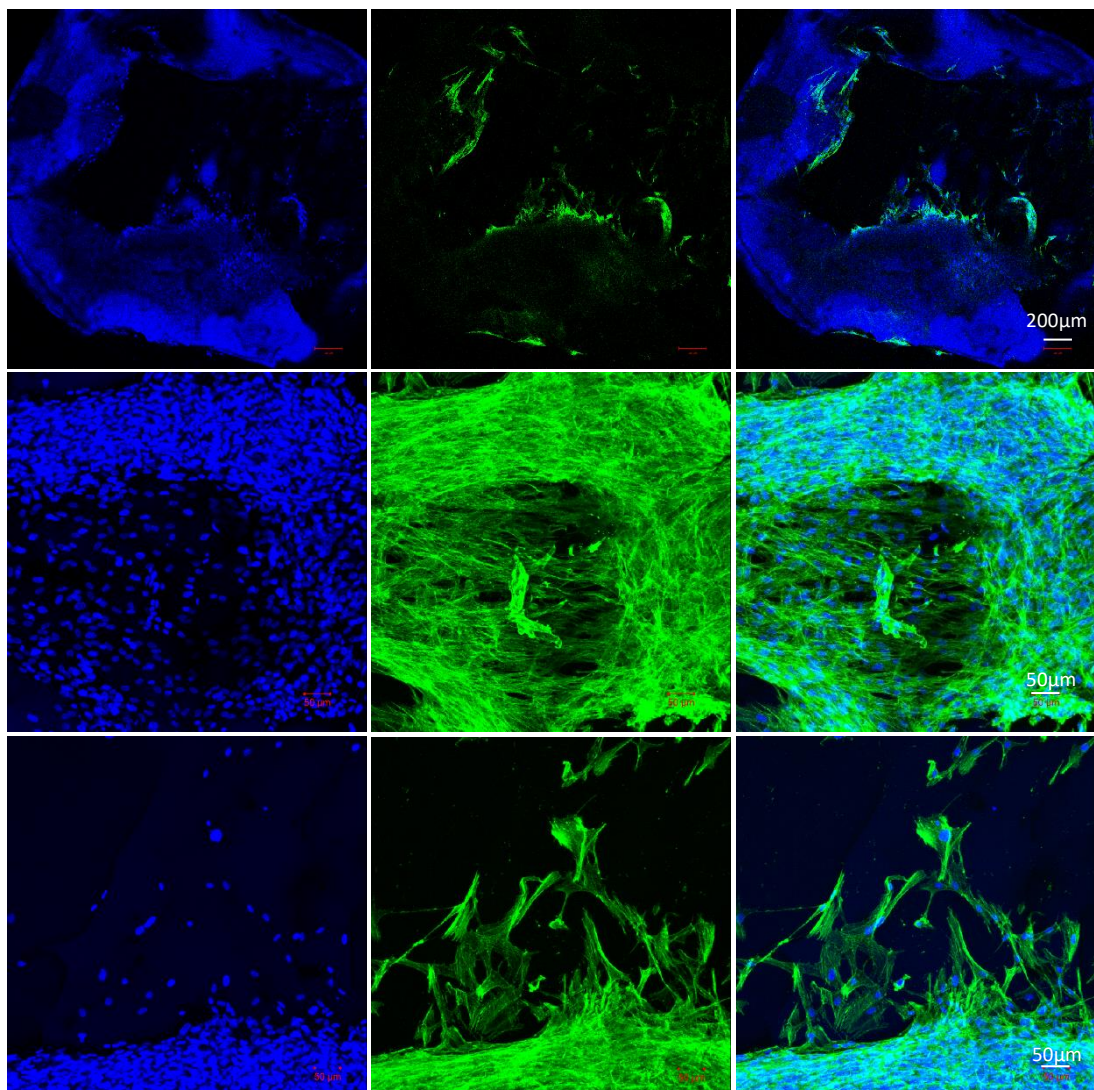


Figure 6. 14. Confocal images of CMSCs adhered to RLP functionalised poly(HEMA-co-EGDMA) hydrogels) in serum containing media. DAPI nuclear stain (blue) and Phalloidin to stain actin filaments (green). (a) Snapshot overview, (b) stitched confocal tiles, (c) single confocal image. Images are representative of all samples. Scale bars = 200 μm (a and b) and 50 μm (c).

6.4. Discussion

Poly(HEMA-co-EGDMA) is a well characterised, highly utilised material, particularly in ophthalmology. Nevertheless, in the development of a novel regenerative medicine strategy, it is important that all components of the therapy are fully characterised. Here we performed optimisation investigations for the development of a base hydrogel, in addition to functionalisation techniques including co-polymerisation with AEMA, methylated cell adhesion motifs and RLP hydrogels. Ultimately, the aim was to produce a hydrogel with good mechanical properties, which aided CMSC attachment, allowing for a novel, regenerative medicine strategy for ocular surface disorders.

Examples of many thermally-activated free radical initiators are cited throughout the literature [298, 299]. At the start of the investigations outlined in this chapter, a thermally-active initiator was used as these are widely available and easy to use. VA-044 was chosen first due to its relatively low degradation temperature of 54°C, which is below the 67°C boiling point of HEMA (values obtained from product information). This eliminated the risk of monomer evaporation, especially in the process of trying to produce consistently well-formed hydrogels. VA-044 is a water soluble initiator, with previous investigations demonstrating poly(HEMA-co-EGDMA) hydrogels to exhibit differential properties in the presence of varying water-to-monomer ratios [300]. Phase separation during copolymerisation is predominantly due to the amount of water in the initial reaction mix, with formation of homogeneous, microporous and macroporous hydrogels with a water percentage of less than 50%, 50-70% and over 70% respectively [301]. The micro and macroporosity in poly(HEMA-co-EGDMA) hydrogel matrix can be visually revealed as gel opacity. This correlates with the findings in this chapter, where a change in transparency can be observed with 60% water, with reaction mixtures containing 80% and 90% visually displaying opaque and physically altered properties. Transparency results were the same with the use of the photo-initiator DMPA, which was implemented for subsequent functionalisation investigations following the decision to co-polymerise using peptides. Although the porous, spongy gels are advantageous in some biological applications, homogeneous

hydrogels and their optical clarity are optimal for contact lens development. The rheology data also showed reduced storage and loss modulus in the 60% compared to 80% HEMA hydrogels, with values indicating the higher flexibility that would be expected with a soft contact lens. Consequently, a 60:40 monomer-to-water ratio was selected for future polymer synthesis investigations, due to the evidence of good miscibility, and viscoelastic properties.

Initially, hydrogels were cast in tissue culture plates, due to the potential for easy cell culture and analysis with the gel systems. However, regardless of crosslinker density or functionalisation monomers present, fully transparent hydrogels were not consistently prepared, with many displaying the appearance of bubbles throughout the structure. Tissue culture plastic often undergoes oxygen plasma treatment [302], so the bubbles present may have been oxygen molecules rising through the hydrogels. However, regular, planer hydrogel sheets were consistently achieved when cast between two glass slides separated with a silicone spacer and held together with bulldog clips. Gel casting kits predominantly used for SDS page and gel electrophoresis provide the same closed system with glass at the material interface, and could also be used to produce bigger gels, with reduced human error variables from constructing the cast.

Low level cross-linking exists throughout the majority of current soft contact lens materials, with manipulation of crosslinking densities capable of altering the hydrogel properties, including pore size, swelling, stiffness and surface hardness [140]. Vast numbers of studies have been performed investigating the swelling behaviours of hydrogels prepared by free radical copolymerisation [303-305]. One key limitation of using poly(HEMA-co-EGDMA) as a soft contact lens material is the relatively low oxygen permeability in comparison to its silicone containing alternatives [113]. The EWC of a non-silicone hydrogel is known to govern its oxygen permeability, with the oxygen permeability coefficient of the hydrogel material increasing exponentially with water content, with a hypothetical oxygen permeability limit of pure water [306]. Furthermore, in general, mechanical properties of hydrogel materials are also governed by EWC, with hydrogels containing a higher water content usually displaying a lower Young's Modulus than

those with a lower water content [283]. Here, It was shown that increasing crosslinker concentration significantly reduces EWC yet increases Young's Modulus in poly(HEMA-co-EGDMA) hydrogels. This result is fairly common across a range of hydrogels [307] and may be due to the increased number of crosslinks leading to a restrained mobility of the macromolecular chains, therefore inhibiting water penetration and reducing the swelling ratio of the hydrogels [308]. Another explanation is that the increased crosslinking reduces the free volumes between the macromolecular chains, so less water molecules can infiltrate the gel [309]. Restrained mobility of the macromolecular chains and reduced spaces between them also explains the increase in mechanical stability of the gels. This allows the structures to possess a higher resistance to deformation, and therefore an increased Young's Modulus.

Although the highest EWC is optimal for oxygen diffusion, a very high Young's Modulus can lead to mechanically induced complications at the ocular surface, including superior epithelial accurate lesions. However if the value is too low, the lens would be difficult to handle for the wearer, and would provide insufficient movement during blinking, leading to poor tear exchange [287]. The modulus of commercial contact lenses is often found within the range from 0.3 to 1.9 MPa. Taking these factors into consideration, it could be argued that 1% EGDMA is an optimal crosslinking concentration, as the EWC was not significantly different to the lowest crosslinker percentage measured (0.5%) and has a Young's Modulus in the central region of available commercial contact lenses, suggesting an acceptable balance between comfort and easy handling.

With regard to functionalisation of the hydrogels with AEMA, the highest obtainable percentage without causing significant detriment to the bulk properties of poly(HEMA-co-EGDMA) hydrogels would be advantageous for the intended application, due to the subsequent increase of positively charged amino groups on the material surface for cell attachment or immobilisation of cell adhesion peptides. In this chapter, it was demonstrated that increasing concentrations of AEMA are significantly correlated to higher EWC. Although the primary amine moiety of AEMA is less electronegative than the hydroxyl group of HEMA [310], AEMA has a shorter

hydrophobic carbon chain, which may result in overall increased hydrophilicity of the monomer [311]. In turn, this would result in a greater swelling ratio and therefore an increased EWC.

As seen with EGDMA, it would be expected that an increased EWC would be related to a reduction in mechanical strength of the hydrogel. This is demonstrated for maximum stress and maximum strain, where a higher resilience to terminal stretching deformation and potential to undergo higher strain forces in hydrogels with lower AEMA concentrations were found. Interestingly, the samples could be split into 2 different groups, with 0% and 2% AEMA showing similar max stress and strain properties, which were significantly higher than those made with 4% and 6% AEMA.

Furthermore, lower Young's modulus values obtained from hydrogels containing 4% and 6% AEMA demonstrate a similar trend in values to the max stress and strain measurements, however no significance could be drawn from the results. The standard deviations of the Young's modulus data for 4% and 6% AEMA hydrogels were large, potentially demonstrating that increased AEMA concentrations leads to the production of polymers with higher structural variability and reduced reliability. Along with the stress and strain data, these results demonstrate that 2% AEMA was the highest applicable concentration to produce uniform hydrogels, with no significant impact on the bulk properties of the gel.

In addition to characterising water content and mechanical properties of the poly(HEMA-co-EGDMA) and poly(HEMA-co-EGDMA-co-AEMA) hydrogels, opacity was assessed to determine if the different monomer compositions had an effect on transparency. Although transparency is a vital property of contact lenses for vision, it could be argued that it is of reduced importance when used for a stem cell scaffold. It is likely that this therapy would be utilised in severe cases of ocular surface damage with vision already compromised. Nevertheless, transparency of the hydrogel lenses would be a beneficial feature, as it could provide potential for wider application to other ocular surface complications. Opacity data for varying EGDMA and AEMA concentrations did not appear to fit a trend. 2% EGDMA was

found to have significantly higher transparency than all other concentrations. The reason for this is unclear and may have been due to inconsistencies in the hydrogel synthesis across batches – for example varying polymerisation rates and extent of phase separation due to variable oxygen permeation into the forming gels. For increasing AEMA concentrations, 0%, 2% and 4% appeared to display similar levels of opacity with 6% slightly higher. It is important to note that these fold changes are still all very small, and the hydrogels still appeared optically clear to the naked eye.

To test whether a poly(HEMA-co-EGDMA) hydrogel functionalised with AEMA would be suitable for therapeutic application, CMSCs were seeded on the hydrogels. However, no cell attachment was observed at any of the AEMA concentrations, including 2% (data not shown). Further studies could be performed to further functionalise the hydrogels through cell adhesion peptide immobilisation to the amino group, however here, predominantly due to the major changes in mechanical properties following inclusion of AEMA, it was decided to go in the direction of direct functionalisation of the poly(HEMA-co-EGDMA) hydrogels with alternative cell adhesive motifs, omitting the AEMA.

Cell adhesive peptides, RGD and YIGSR, were synthesised to include a three repeat, glycine spacer (GGG-YIGSR and GGG-RGD) to increase the distance of the peptide from the surface, creating access of the peptide for cell attachment [112]. Longer glycine spacers have been implicated in increasing the peptide degrees of freedom, contributing to structural stability and increasing the effectiveness of functionalisation for cell attachment [312]. RGD has previously been synthesised to contain an N-terminal methacrylate for multiple regenerative medicine applications, including encapsulation of BM-MSCs and AD-MSCs, using photo-polymerisation of meth-RGD with meth-glycol chitosan hydrogels [313, 314]. Here, it was hypothesised that although bulk synthesis would lead to cell adhesive motifs spread throughout the structure of the gel, permitting encapsulation, it would also provide surface motifs for surface attachment of CMSCs. Following CMSC seeding, a small number of cells were present, however their round structure, absence of cell spreading, and low abundance compared to the control, deemed the scaffold as unsuitable as a therapeutic vehicle. These altered morphologies were observed in

both serum and serum-free conditions, denoting that the integrin attachment sites in serum, including fibronectin, vitronectin and collagen, were not well displayed by the hydrogel and not satisfactory for integrin binding [315].

The next attempt to achieve cell attachment was utilisation of RLPs for copolymerisation. BM-MSC attachment has previously been demonstrated to RLP hydrogels alone [316], highlighting the suitability of the peptide hydrogel structures. The aim was to attach a thin layer of RLP hydrogel to poly(HEMA-co-EGDMA) through free radical polymerisation. To achieve this, it was hypothesised that part-polymerisation of the poly(HEMA-co-EGDMA) would leave free methacrylate groups, without crosslinking, available for RLP photocoupling. This hydrogel coating methodology, using free radical macromolecular polymerisation grafting, has previously been demonstrated with coating of polyurethanes with polyvinylpyrrolidone to increase hydrophilicity [317]. To gain an understanding of gelation time, *in situ* rheology was performed. Results demonstrated that 60 wt % HEMA hydrogels reached complete polymerisation around 190 seconds. To ensure cross-linking stopped following removal of UV light, *in situ* rheology was performed, removing the UV source at different time points, with data showing an inhibition of gelation following the removal of UV, identified through a plateau of storage and loss modulus at the specific time points. This information provided more time flexibility for applying the RLP layer, increasing the feasibility of the method. Additionally, it showed that complete polymerisation is likely to occur between 200 and 240 seconds, as hydrogel oscillatory properties were maintained for UV removal past 240 seconds. 160 seconds was deduced as a guideline for part polymerisation of poly(HEMA-co-EGDMA) hydrogel.

Once an understanding of poly(HEMA-co-EGDMA) gelation times were generated, the next aim was to optimise the methods of hydrogel functionalisation with RLP. It was observed that the RLP and HEMA precursor solutions combined prior to polymerisation resulted in an opaque hydrogel, part polymerisation of poly(HEMA-co-EGDMA) only led to RLP residue on the surface of the hydrogel and part polymerisation of both solutions produced a clear surface, however excess RLP were seen at the sides of the hydrogel surface. For a 'manufacturing' protocol, part

polymerisation of each hydrogel was performed on an open glass slide, which was then sandwiched together with a silicone spacer to complete polymerisation. Although further optimisation could be performed to deduce volume of RLP necessary to coat the surface of the hydrogel without excess build up at the sides, this is a novel method for free radical macromolecular copolymerisation. It is also highly advantageous compared to the previous bulk synthesis attempts, as the material core should not be affected, reducing concerns around mechanical properties. Furthermore, a smaller quantity of RLP can be used to a higher efficiency, as the cell adhesive motifs are concentrated to the surface and not wasted throughout the bulk of the hydrogel. This is highly advantageous for therapies looking at surface attachment but does provide limitations for investigating cell encapsulation [318].

To ensure the surface was coated in RLP, BMMSCs were seeded on the hydrogels. Compared to the control, cell attachment could be seen across the surface, providing proof of concept that RLP functionalisation is a suitable, novel way to adhere cells to poly(HEMA-co-EGDMA). CMSCs were then cultured on the hydrogels for longer in serum containing and serum free media. In the serum free media, the cells spread as a confluent monolayer across the entire surface of the hydrogel, indicating the attachment sites were from the RLP alone. For the serum containing media, it appeared the cells had started to peel away from the hydrogel. This is likely due to overconfluency but is an important finding to highlight the necessity of optimising methods to produce repeatable cell culture conditions for therapeutic applications.

Overall, this chapter has presented optimisation steps for producing a novel coating of poly(HEMA-co-EGDMA) for CMSC attachment, with success in providing a surface for CMSC attachment and growth using RLPs. Further work is required to determine the mechanical properties of the functionalised hydrogel, however the data in this chapter is an excellent basis for exploration of therapeutic potential of the cells delivered to the ocular surface using a contact lens vehicle.

CHAPTER 7: Summary

7.1. Summary

The overarching aim of this thesis was to contribute towards the development of a topical cell therapy for ocular surface disorders, utilising CMSCs as a therapeutic agent, adhered to a contact lens for administration. This aim was based on previous characterisation of CMSCs, where secretion of anti-inflammatory factors were identified following stimulation with inflammatory agents [40]. It was also hypothesised that CMSCs may offer a better alternative to MSCs from other sources for ocular surface therapeutics, based on the harvesting of cells from an abundance of waste tissue, and the familiarity of the cells with the microenvironment they would be returned to. Ultimately, this thesis provided novel insight into the characteristics of CMSCs, potential mechanisms at play for future elucidation, and a method for applying the cells topically to the ocular surface, using resilin-like polypeptide (RLP) functionalised poly(HEMA-co-EGDMA) hydrogels.

It was first hypothesized that CMSCs in *in vitro* culture would show signs of ageing which would have a detrimental impact on their potency and scale up potential as a therapeutic. Based on this hypothesis, one aim of Chapter 3 was to determine a passage window for use of CMSCs for further investigation. Phenotypic, genotypic and secretomic analysis was performed to assess changes in the CMSC population, investigating markers and proteins synonymous with MSCs, between passage 4 and 10. Cell growth was analysed to determine the impact of time in culture on rate of proliferation, and immunocytochemistry was utilised to assess any changes in cell morphology synonymous with aging. It was found that CMSCs showed limited changes in their phenotype and genotype, cell growth, population doublings, and viability, as well as the expression of the proliferative marker Ki67. However, structural analysis revealed a change in cell morphology and breakdown of the actin cytoskeleton by passage 8, suggesting that the cells were ageing, which may impact their therapeutic capacity. Based on these findings, it was concluded that future work on the use of CMSCs for ocular surface disorders should use cells no older than passage 7 to avoid the potential negative effects of older cells.

Once an understanding of how CMSCs behaved in culture was established, it was hypothesised that donor-to-donor variations would exist for CMSCs, which would impact the final cell product. To address this hypothesis, the second aim of Chapter 3 was to expand on the phenotypic analysis of CMSCs, identifying key markers differentially and homogeneously expressed across 5 donors. This was achieved using the BD Human Cell Surface Lyoplate to perform medium-throughput phenotypic screening of CMSCs between passages 5 and 7. Cell surface antigens CD59, CD81, CD13, CD90, CD63, HLA-A,B,C, CD9, CD147, CD140b, CD47, CD73, CD105, CD49b, B2-MG, CD26, CD55, CD46, and CD49e were homogeneously expressed in over 95% of CMSCs, and CD44 and CD164 expressed in over 90% of cells. These markers could be incorporated into screening protocols for CMSCs, to confirm the correct phenotype for a therapeutic product. Additionally, markers with high levels of variability between donors were identified, including HLA-A2 and CD99. HLA-A2 knockdown has been linked to reduced immunomodulatory potency [196], and CD99 has been associated with increased tumorigenicity [184], highlighting an argument for screening to select donors which are positive and negative for specific cell surface markers that may have advantageous or deleterious clinical results. This was the first time donor-to-donor variation in CMSCs had been assessed using a medium throughput phenotypic panel to identify these markers of interest.

After characterisation of the CMSC population alone had been performed, the subsequent step carried out in Chapter 4, was to compare CMSCs to BM-MSCs, which are classified as the current 'gold standard' for MSC therapies. It was hypothesised that CMSCs would have phenotypic and genotypic markers both commonly and differentially expressed compared to BM-MSCs. The BD Human Cell Surface Lyoplate and the Qiagen RT² Profiler PCR Array for wound healing markers were utilised to deduce the feasibility of using CMSCs, as well as to determine markers of interest which may lead to functional advantages or limitations of CMSCs compared to BM-MSCs. In addition to the MSC markers defined by the ISCT, 9 non-classical MSC markers were identified that were homogeneously expressed by over 85% of the population of cells from both CMSCs and BM-MSCs (CD49b,

CD49e, CD81, CD9, CD151, CD140b, CD99, CD47, CD147, CD63, CD95 and CD98). These markers suggest a specificity to MSCs, regardless of their source, potentiating their inclusion in MSC screening criteria. Screening panel expansion would allow for a more robust selection method, leading to increased safety and efficacy of the therapeutic cell product. Following the identification of similar markers, significantly different markers between the two sources were identified, with CD40, CD121a, CD108, CD49d, CD142 and HPC shown as key markers with higher specificity for CMSCs, based on their expression profile. The functionality of these markers along with genotypic expression, potentiate CMSCs as possessing characteristics associated with increased immunoregulation and reduced expression of inflammatory and angiogenic factors, however the high expression of CD142 in CMSCs increases their risk of inducing instant blood-mediated inflammatory reaction. In addition, genotyping provided information that BM-MSCs presented significantly higher expression for many genes associated with wound healing processes. Although linked to higher levels of potentially beneficial groups including growth factors and cytoskeleton regulators, BM-MSCs also expressed significantly higher expression levels of potentially detrimental factors for an ocular surface therapy, including those involved in angiogenesis, inflammation and fibrosis. The work provided a new depth of understanding the characteristic 'fingerprint' of CMSCs, which can be utilised to determine new investigative pathways.

All work to this point was performed on cells in cytokine-free cell culture conditions, however this was not indicative of the toxic microenvironment that exists at an inflamed ocular surface. To mimic this environment, an 'inflammatory cocktail' was incorporated into the media (TNF α , IL-1 β , IFN- γ and LPS) in Chapter 5, and it was hypothesised that survival, properties, and behaviour of CMSCs would change. A 'recovered' group was also included, where the cells were returned to normal conditions before analysis, to determine any insights into benefits and limitations of priming the cells prior to therapeutic application. To address the hypothesis, cell viability and secretomic analysis were undertaken using a live/dead assay and ELISAs, respectively. The BD Human Cell Surface Lyoplate and the Qiagen

RT² Profiler PCR Array for wound healing markers were also used to perform medium throughput phenotypic and genotypic profiling of CMSCs in the normal, inflammatory and recovered conditions. It was demonstrated that following exposure to the inflammatory cocktail, a subset of CMSCs survived, but had inhibited proliferation. This subset of cells responded to the environment by increasing the secretion of factors, including growth factors HGF, FGF2 and TGF β . These proteins were of particular interest due to their secretion from CMSCs but not corneal epithelial cells (HCE2s), highlighting a more cell specific benefit. Phenotype and genotype of CMSCs were also assessed in the inflammatory environment, allowing the cultivation of hypotheses of different pathways being activated. Interestingly, gene expression of ECM structural constituents and cytoskeleton regulators were significantly reduced in the treatment group, potentially beneficial to avoid fibrosis but also increasing the risk of poor cell adhesion to the cell scaffold of choice. In addition, during the 'recovery' period, an increase in expression of MIC A/B was highlighted, which may increase the risk of immunogenicity, providing an argument against cell licensing.

For successful translation of a cell therapy, it is vital the administration route is successfully developed. The final hypothesis was that CMSCs would adhere to a contact lens functionalised with cell adhesive motifs. Consequently, the aim of Chapter 6 was to develop a peptide-functionalised poly(HEMA-co-EGDMA) soft contact lens for CMSC attachment, with potential for future directions as a cell delivery vehicle to an injured ocular surface. Functionalisation through bulk synthesis with a primary amine monomer and methylated cell adhesive peptides (RGD and YIGSR) were found unsuitable for cell attachment, where the very small density of cells that adhered showed a round morphology, with no spreading. Success was achieved through surface attachment of resilin-like polypeptide (RLP) hydrogel, containing cell adhesive motifs, to poly(HEMA-co-EGDMA) through free radical polymerisation. Attachment of BM-MSCs and CMSCs were observed, and the capacity for CMSCs to form a confluent monolayer over the entirety of the hydrogel surface in serum free media was demonstrated. Novel and exciting work was presented in this chapter, with RLP functionalisation of poly(HEMA-co-EGDMA)

and attachment of CMSCs both shown for the first time, with potential future implications as a scaffold for topical therapeutic cell administration to the ocular surface.

To conclude, this thesis contains comprehensive CMSC characterisation information, which is a useful addition to the relatively small repertoire of data that exists compared to MSCs from other sources. Changes of CMSCs over passages, and information on homogeneously and differentially expressed phenotypic markers between different donors provided insight into markers that should be expected in a CMSC population, in addition to those which may be used to identify a donor selection criteria. Comparing these phenotypic results and the genotypic profile to BM-MSCs identified markers which may be standard to MSCs, and differences in gene and cell surface antigen expression that should be further investigated to determine any advantageous or deleterious effects of each source on cell potency. CMSCs were then subject to inflammatory conditions, where a subset of cells which survived secreted an increase in multiple factors, including growth factors and anti-inflammatory cytokines. Phenotypic and genotypic markers which changed when activated were also used to draw hypotheses for potential molecular mechanisms at play in different conditions, helping to broaden the understanding of CMSC biology. Finally, topical administration options for the ocular surface were investigated, with successful cell attachment on poly(HEMA-co-EGDMA) hydrogels functionalised with a RLP layer. Ultimately, this thesis provides an extensive template of cell surface protein and gene expression in CMSCs, with key markers of interest that can be selected for future mechanistic and functional investigations.

7.2. Discussion and Future Directions

The literature contains a plethora of studies investigating the characteristics of MSCs from different sources over passages, however to my knowledge, only one study assessing the longevity of CMSCs in culture [322], where cells were cultured in fibroblast growth medium supplemented with serum. Here, CMSCs were cultured in stem cell media using a serum knockout replacement. This media was selected due to the issues surrounding animal related products, including batch-to-batch variation, viral transmission, and increased immunogenicity [323]. This allowed for

the collection of characterisation data on a cell product that could be more readily and feasibly translated to clinic. The differences in media highlighted here identifies a limitation of the study, as CMSCs were only investigated in one media, with all work performed on 2D tissue culture plastic. Although it has previously been demonstrated that SCM is a suitable candidate for CMSC culture [163], large scale up of MSC therapies is most successful using techniques including stirred or mixed bioreactor systems. These incorporate microcarrier culture systems, where densities of 10^6 to 10^7 cells / mL have been achieved, at significantly quicker propagation rates [324]. It would be interesting to determine the growth potential and corresponding characteristics of CMSCs cultivated using optimised cell culture techniques for large scale manufacture.

Additionally, to expand on all conclusions, including identification of markers associated with MSCs regardless of source, or antigens specific to CMSCs, future work could validate their consistent expression in conditions known to affect cell phenotype. These include culture media, levels of confluency, donor age, and cryopreservation. Accounting for CMSCs in multiple conditions would demonstrate stringent methods to confirm that certain markers are characteristic of CMSCs and can be used for cell screening.

The literature contains investigations which have used the BD Cell Surface Marker Panel to compare MSCs from multiple sources, including sub-cutaneous fat and visceral fat adipose derived MSCs [5], cord blood derived MSCs [4], adult derived human liver progenitor cells [6], tonsil derived MSCs and BM-MSCs [7], and the Qiagen RT2 qPCR profiler for wound healing to assess the wound healing potential of MSCs from sources including human umbilical cord Wharton's jelly MSCs [9] and pig adipose derived MSCs [10]. However, here is the first time these assays have been used to determine the phenotypic and genotypic profile of CMSCs alone, and as a comparative study of CMSCs and BM-MSCs. Commonly expressed antigens in the 2 cell populations were identified as specific to MSCs, with potential for enhancing the ISCT minimal criteria for MSC classification. For future work, a meta-analysis of literature investigating MSC markers would be useful to substantiate this claim, however the different methods employed for data analysis across the studies

provides challenges when defining conclusions. Alternatively, MSCs from other sources could be tested for expression of the common markers identified in this study, to validate or challenge their definition as MSC antigens.

One of the main limitations of the work performed using the BD cell surface lyoplate was the flow cytometry data was not fully validated by additional studies, for example immunocytochemistry or gene expression profiling for the specific correlating gene. Future studies could select markers of interest to perform validating analysis on, which would be more economically feasible than investigating the whole panel of proteins, yet is vital to corroborate any conclusions. In addition to data validation, functional studies are necessary to provide insight into whether the markers with high variation between donors, or antigens differentially expressed on CMSCs and BM-MSCs, impact the potency or safety of the therapeutic CMSCs, e.g. HLA-A2 and CD99. These tests could be carried out through FACS sorting of cells with high and low expression of markers of interest, or through knock out investigations, and assessment of a plethora of parameters. For example, the secretome, effects of co-culture with immune cells including macrophages and therapeutic potency assays on *in vitro* and *ex vivo* injury models could be investigated. However, what this work did achieve, was to present a template to discern markers to incorporate into future studies utilising CMSCs.

Previous literature exists demonstrating anti-inflammatory properties of CMSCs activated with IL-1 β [40], however this was the first time that medium-throughput analysis of CMSC phenotype and genotype had been assessed, alongside viability and changes in cell secretome. One limitation of this study is that it only investigated the inflammatory factors in combination, not as individual entities, so conclusions about the specific impact of each factor could not be drawn. Furthermore, the RT-qPCR assay was designed to assess genes primarily involved in wound healing. This still gave great insight into areas of interest for CMSC paracrine therapy development, including fibrotic potential and growth factor expression, however future investigations could look at gene expression specific to the phenotypic markers, and secretomic proteins of interest.

The large panels of characteristic data collected simultaneously in this chapter, with survival and behaviour information, enabled the formation of hypotheses about different pathways that might be undergoing activation or silencing following exposure to inflammatory cytokines. It would be interesting for future investigations to prove or disprove the presented ideas. For example, investigation into whether the small subset (10%) of CMSCs which expressed CD14 following cytokine exposure are responsible for the increased secretion of pro-inflammatory cytokines IL-6 and IL-8. If this hypothesis was validated, it could be further suggested that priming the cells and screening against the CD14+ cells could reduce the pro-inflammatory response of CMSCs.

A second hypothesis presented was the increased secretion of TGF- β 1 by CMSCs in the inflammatory conditions could form an immunomodulatory positive feedback loop, where the increased cytokine levels potentially led to increased activation of the Smad2/3 signalling pathway, consequently augmenting the immunosuppressive capacity of the cells. Mechanistic investigations specific to TGF- β 1 and the Smad2/3 signalling pathway, followed by therapeutic assays with Smad2/3 inhibition could be performed to provide evidence.

Furthermore, it was possible to draw hypotheses acknowledging the contact lens scaffold and CMSC interactions that should be explored further. High percentages of cells and MFI expression were demonstrated in CMSCs of the principal receptor for Hya binding, CD44, over all the treatment groups (no cytokines, cytokines, and recovered). It has been suggested that CD44-Hya interactions are a key mechanism for MSC homing and migration to injury sites [280]. Considering the original aim to maintain cells on the lens scaffold, preventing migration onto the ocular surface, it would be useful to investigate the inhibition of CD44 on CMSCs as a method for maintaining cell adherence to the scaffold used for cell application to the ocular surface.

Another concern surrounding maintenance of the cells on the scaffold was the significantly reduced collagen and *TAGLN* mRNA levels, and the upregulation of MMP1 in the inflammatory conditions compared to the control (no cytokines). These genes have been collectively linked to reduced cell attachment and increased

migration of MSCs [284] [285, 286]. Separate investigations would have to be performed to assess the impact of cytokines on the scaffold- cell interactions.

It is also important that future studies address the questions raised about potential immunogenicity linked to the increase of MIC A/B in the recovered group (cytokine exposure followed by return to cytokine-free culture), to determine the safety profile of primed cells. Furthermore, the next step would be to investigate the therapeutic potential of CMSCs both with and without priming on *in vitro* and *ex vivo* inflammatory injury models. This would give information on whether cell licencing should be included in future work and therapeutic translation, or CMSCs without activation should be used.

Previous literature shows that RLPs can be used to functionalise polyethylene glycol, and enables cell attachment, including for BM-MSCs [319]. However, this was the first time that an RLP layer had been used to functionalise poly(HEMA-co-EGDMA), and CMSCs have been shown to attach to the hydrogel. This has helped expand the current literature, by increasing the usage potential of RLPs, including their first use as a therapeutic tool for ocular surface disorders. This study provides an exciting basis for multiple avenues of future work. In terms of material characterisation, investigations could be performed to determine the impact of the RLP functionalisation on the characteristics of the contact lens and its suitability, including mechanical testing, swelling content, oxygen transmission and transparency data. In addition, here we demonstrated that it was possible to achieve a monolayer of CMSCs on the hydrogel, however additional work is required to optimise the conditions for consistent results. Furthermore, all the characterisation work of CMSCs in this chapter has been performed on CMSCs on tissue culture plastic. It is known that cell characteristics can change based on the substrate [325, 326], so it would be important to determine the impact of the material change on the CMSCs, either through genotyping and phenotyping, and vitally through assessing the secretome and assessment of the paracrine activity of the cells.

In this thesis, complex characterisation data on CMSCs, in addition to a potential therapeutic administration option were explored. A final future avenue that would

be necessary to investigate for the translation to clinic is the therapeutic potential of CMSCs and the pHEMA/RLP hydrogel combined. This could be achieved using *in vitro* and *ex vivo* injury models, in addition to immunomodulation potency assessment through determining effects of co-culture with immune cells, including macrophages. Ultimately, this would endeavour to amalgamate the information in this thesis, to advance the development of a cell therapy using CMSCs for ocular surface disorders.

7.3. Limitations

Although each chapter was initiated with a solid hypothesis, the data collected using the large screening panels may also have been described as discovery lead research. This is the concept that the cell is placed in different environments, and through assessing a large number of genetic or phenotypic markers, a subset of proteins and genes can be selected for further research. The overarching limitation of this data is the lack of corroborating studies to support the discussions made. Throughout the thesis, potential cellular pathways and mechanisms were described, however with the lack of follow up functional studies, it is impossible to determine what is truly happening in the cell. As well as functional studies, timing prevented investigation into the therapeutic use of the cells, with no informative data presented using *in vitro* or *ex vivo* injury models. Consequently, although this thesis, including the initial hypothesis, has focussed on developing a therapy for ocular surface disorders, it is perhaps more suitable to define the work as purely cell characterisation. This is not to say that CMSCs could not be investigated at a later time point for ocular surface disorder research, however the research presented here is more indicated towards a biological rather than therapeutic understanding of CMSCs.

CHAPTER 8: References

1. Meek, K.M. and C. Knupp, *Corneal structure and transparency*. Prog Retin Eye Res, 2015. **49**: p. 1-16.
2. Dartt, D.A. and M.D. Willcox, *Complexity of the tear film: importance in homeostasis and dysfunction during disease*. Exp Eye Res, 2013. **117**: p. 1-3.
3. Stern, M.E., et al., *Autoimmunity at the ocular surface: pathogenesis and regulation*. Mucosal Immunol, 2010. **3**(5): p. 425-42.
4. Rhee, M.K. and F.S. Mah, *Inflammation in Dry Eye Disease: How Do We Break the Cycle?* Ophthalmology, 2017. **124**(11s): p. S14-s19.
5. Craig, J.P., et al., *TFOS DEWS II Report Executive Summary*. Ocul Surf, 2017. **15**(4): p. 802-812.
6. Chhadva, P., R. Goldhardt, and A. Galor, *Meibomian Gland Disease: The Role of Gland Dysfunction in Dry Eye Disease*. Ophthalmology, 2017. **124**(11s): p. S20-s26.
7. Ting, D. and S. Ghosh, *Acute corneal perforation 1 week following uncomplicated cataract surgery: the implication of undiagnosed dry eye disease and topical NSAIDs*. Therapeutic Advances in Ophthalmology, 2019. **11**: p. 251584141986950.
8. Green, M., A. Apel, and F. Stapleton, *Risk factors and causative organisms in microbial keratitis*. Cornea, 2008. **27**(1): p. 22-7.
9. *The management of dry eye*. Bmj, 2016. **354**: p. i4463.
10. Torricelli, A.A., et al., *The corneal fibrosis response to epithelial-stromal injury*. Exp Eye Res, 2016. **142**: p. 110-8.
11. McDonald, M., et al., *Economic and Humanistic Burden of Dry Eye Disease in Europe, North America, and Asia: A Systematic Literature Review*. Ocul Surf, 2016. **14**(2): p. 144-67.
12. Phulke, S., et al., *Steroid-induced Glaucoma: An Avoidable Irreversible Blindness*. J Curr Glaucoma Pract, 2017. **11**(2): p. 67-72.
13. van der Meulen, I.J., et al., *Age-related risk factors, culture outcomes, and prognosis in patients admitted with infectious keratitis to two Dutch tertiary referral centers*. Cornea, 2008. **27**(5): p. 539-44.
14. Boboridis, K.G. and A.G.P. Konstas, *Evaluating the novel application of cyclosporine 0.1% in ocular surface disease*. Expert Opin Pharmacother, 2018. **19**(9): p. 1027-1039.
15. White, D.E., et al., *Treatment Satisfaction Among Patients Using Anti-Inflammatory Topical Medications for Dry Eye Disease*. Clin Ophthalmol, 2020. **14**: p. 875-883.
16. Wilson, S.E., et al., *The Corneal Wound Healing Response:: Cytokine-mediated Interaction of the Epithelium, Stroma, and Inflammatory Cells*. Progress in Retinal and Eye Research, 2001. **20**(5): p. 625-637.
17. Arya, S.K., et al., *Simple Limbal Epithelial Transplantation in Acid Injury and Severe Dry Eye*. J Clin Diagn Res, 2016. **10**(6): p. Nd06-7.
18. Ma, D.H., et al., *Matrix revolution: molecular mechanism for inflammatory corneal neovascularization and restoration of corneal avascularity by epithelial stem cell transplantation*. Ocul Surf, 2009. **7**(3): p. 128-44.
19. Pellegrini, G., et al., *Concise Review: Hurdles in a Successful Example of Limbal Stem Cell-based Regenerative Medicine*. STEM CELLS, 2014. **32**(1): p. 26-34.
20. Haque, M., et al., *Stem cell-derived tissue-associated regulatory T cells ameliorate the development of autoimmunity*. Sci Rep, 2016. **6**: p. 20588.
21. Cao, S., et al., *Overcoming barriers to the clinical utilization of iPSCs: reprogramming efficiency, safety and quality*. Protein Cell, 2012. **3**(11): p. 834-45.

22. Ghannam, S., et al., *Immunosuppression by mesenchymal stem cells: mechanisms and clinical applications*. Stem Cell Res Ther, 2010. **1**(1): p. 2.
23. Giordano, A., U. Galderisi, and I.R. Marino, *From the laboratory bench to the patient's bedside: an update on clinical trials with mesenchymal stem cells*. J Cell Physiol, 2007. **211**(1): p. 27-35.
24. Wang, M., Q. Yuan, and L. Xie, *Mesenchymal Stem Cell-Based Immunomodulation: Properties and Clinical Application*. Stem Cells Int, 2018. **2018**: p. 3057624.
25. Dominici, M., et al., *Minimal criteria for defining multipotent mesenchymal stromal cells. The International Society for Cellular Therapy position statement*. Cytotherapy, 2006. **8**(4): p. 315-7.
26. Han, J., et al., *Iron oxide nanoparticle-mediated development of cellular gap junction crosstalk to improve mesenchymal stem cells' therapeutic efficacy for myocardial infarction*. ACS Nano, 2015. **9**(3): p. 2805-19.
27. Fischer, U.M., et al., *Pulmonary passage is a major obstacle for intravenous stem cell delivery: the pulmonary first-pass effect*. Stem Cells Dev, 2009. **18**(5): p. 683-92.
28. Madrigal, M., K.S. Rao, and N.H. Riordan, *A review of therapeutic effects of mesenchymal stem cell secretions and induction of secretory modification by different culture methods*. J Transl Med, 2014. **12**: p. 260.
29. Kim, D.S., et al., *Enhanced Immunosuppressive Properties of Human Mesenchymal Stem Cells Primed by Interferon-gamma*. EBioMedicine, 2018. **28**: p. 261-273.
30. Krampera, M., et al., *Immunological characterization of multipotent mesenchymal stromal cells--The International Society for Cellular Therapy (ISCT) working proposal*. Cytotherapy, 2013. **15**(9): p. 1054-61.
31. Kean, T.J., et al., *MSCs: Delivery Routes and Engraftment, Cell-Targeting Strategies, and Immune Modulation*. Stem Cells Int, 2013. **2013**: p. 732742.
32. Omoto, M., et al., *Mesenchymal stem cells home to inflamed ocular surface and suppress allosensitization in corneal transplantation*. Invest Ophthalmol Vis Sci, 2014. **55**(10): p. 6631-8.
33. Orozco Morales, M.L., et al., *Anti-inflammatory potential of human corneal stroma-derived stem cells determined by a novel in vitro corneal epithelial injury model*. World J Stem Cells, 2019. **11**(2): p. 84-99.
34. Su, W., et al., *Culture medium from TNF- α -stimulated mesenchymal stem cells attenuates allergic conjunctivitis through multiple antiallergic mechanisms*. Journal of Allergy and Clinical Immunology, 2015. **136**(2): p. 423-432.e8.
35. Lee, E.Y., et al., *Hypoxia-enhanced wound-healing function of adipose-derived stem cells: increase in stem cell proliferation and up-regulation of VEGF and bFGF*. Wound Repair Regen, 2009. **17**(4): p. 540-7.
36. Sulaiman, R.S., H.D. Basavarajappa, and T.W. Corson, *Natural product inhibitors of ocular angiogenesis*. Exp Eye Res, 2014. **129**: p. 161-71.
37. Yao, L., et al., *Role of mesenchymal stem cells on cornea wound healing induced by acute alkali burn*. PLoS One, 2012. **7**(2): p. e30842.
38. Oh, J.Y., et al., *The anti-inflammatory and anti-angiogenic role of mesenchymal stem cells in corneal wound healing following chemical injury*. Stem Cells, 2008. **26**(4): p. 1047-55.
39. Zhao, Q., H. Ren, and Z. Han, *Mesenchymal stem cells: Immunomodulatory capability and clinical potential in immune diseases*. Journal of Cellular Immunotherapy, 2016. **2**(1): p. 3-20.
40. Mittal, S.K., et al., *Mesenchymal Stromal Cells Modulate Corneal Alloimmunity via Secretion of Hepatocyte Growth Factor*. STEM CELLS Translational Medicine, 2019. **8**(10): p. 1030-1040.

41. Mittal, S.K., et al., *Restoration of Corneal Transparency by Mesenchymal Stem Cells*. Stem Cell Reports, 2016. **7**(4): p. 583-590.
42. Song, H.B., et al., *Mesenchymal Stromal Cells Inhibit Inflammatory Lymphangiogenesis in the Cornea by Suppressing Macrophage in a TSG-6-Dependent Manner*. Molecular therapy : the journal of the American Society of Gene Therapy, 2018. **26**(1): p. 162-172.
43. Oh, J.Y., et al., *Anti-inflammatory protein TSG-6 reduces inflammatory damage to the cornea following chemical and mechanical injury*. Proceedings of the National Academy of Sciences, 2010. **107**(39): p. 16875-16880.
44. Gomzikova, M.O., V. James, and A.A. Rizvanov, *Therapeutic Application of Mesenchymal Stem Cells Derived Extracellular Vesicles for Immunomodulation*. Frontiers in Immunology, 2019. **10**(2663).
45. Samaeekia, R., et al., *Effect of Human Corneal Mesenchymal Stromal Cell-derived Exosomes on Corneal Epithelial Wound Healing*. Invest Ophthalmol Vis Sci, 2018. **59**(12): p. 5194-5200.
46. Karantalis, V., et al., *Allogeneic cell therapy: a new paradigm in therapeutics*. Circulation research, 2015. **116**(1): p. 12-15.
47. Chen, L., et al., *Analysis of Allogenicity of Mesenchymal Stem Cells in Engraftment and Wound Healing in Mice*. PLOS ONE, 2009. **4**(9): p. e7119.
48. Medawar, P.B., *Immunity to homologous grafted skin; the fate of skin homografts transplanted to the brain, to subcutaneous tissue, and to the anterior chamber of the eye*. Br J Exp Pathol, 1948. **29**(1): p. 58-69.
49. Nassiri, N., et al., *Ocular graft versus host disease following allogeneic stem cell transplantation: a review of current knowledge and recommendations*. Journal of ophthalmic & vision research, 2013. **8**(4): p. 351-358.
50. Sato, K., et al., *Mesenchymal stromal cells for graft-versus-host disease : basic aspects and clinical outcomes*. J Clin Exp Hematop, 2010. **50**(2): p. 79-89.
51. Kyurkchiev, D., et al., *Secretion of immunoregulatory cytokines by mesenchymal stem cells*. World journal of stem cells, 2014. **6**(5): p. 552-570.
52. Cejka, C., et al., *The Favorable Effect of Mesenchymal Stem Cell Treatment on the Antioxidant Protective Mechanism in the Corneal Epithelium and Renewal of Corneal Optical Properties Changed after Alkali Burns*. Oxid Med Cell Longev, 2016. **2016**: p. 5843809.
53. Lee, M.J., et al., *Mesenchymal stem/stromal cells protect the ocular surface by suppressing inflammation in an experimental dry eye*. Mol Ther, 2015. **23**(1): p. 139-46.
54. Jin, H.J., et al., *Comparative analysis of human mesenchymal stem cells from bone marrow, adipose tissue, and umbilical cord blood as sources of cell therapy*. Int J Mol Sci, 2013. **14**(9): p. 17986-8001.
55. Fuentes-Julian, S., et al., *Adipose-derived mesenchymal stem cell administration does not improve corneal graft survival outcome*. PLoS One, 2015. **10**(3): p. e0117945.
56. Lam, P.K., et al., *Transplantation of mesenchymal stem cells to the brain by topical application in an experimental traumatic brain injury model*. J Clin Neurosci, 2013. **20**(2): p. 306-9.
57. Lam, P.K., et al., *Topical Application of Mesenchymal Stromal Cells Ameliorated Liver Parenchyma Damage After Ischemia-Reperfusion Injury in an Animal Model*. Transplant Direct, 2017. **3**(6): p. e160.
58. Nieto-Nicolau, N., et al., *In vitro potential of human mesenchymal stem cells for corneal epithelial regeneration*. Regenerative Medicine. **0**(0): p. null.

59. Møller-Hansen, M., et al., *Safety and feasibility of mesenchymal stem cell therapy in patients with aqueous deficient dry eye disease*. *The Ocular Surface*, 2021. **19**: p. 43-52.
60. Kuriyan, A.E., et al., *Vision Loss after Intravitreal Injection of Autologous "Stem Cells" for AMD*. *N Engl J Med*, 2017. **376**(11): p. 1047-1053.
61. Gomes, J.A., et al., *Corneal reconstruction with tissue-engineered cell sheets composed of human immature dental pulp stem cells*. *Invest Ophthalmol Vis Sci*, 2010. **51**(3): p. 1408-14.
62. Joyce, N.C., et al., *Potential of human umbilical cord blood mesenchymal stem cells to heal damaged corneal endothelium*. *Mol Vis*, 2012. **18**: p. 547-64.
63. Azmi, S.M., et al., *Human umbilical cord-mesenchymal stem cells: a promising strategy for corneal epithelial regeneration*. *Regenerative Medicine*, 2020. **15**(3): p. 1381-1397.
64. Sidney, L.E. and A. Hopkinson, *Corneal keratocyte transition to mesenchymal stem cell phenotype and reversal using serum-free medium supplemented with fibroblast growth factor-2, transforming growth factor-beta3 and retinoic acid*. *J Tissue Eng Regen Med*, 2018. **12**(1): p. e203-e215.
65. Polisetty, N., et al., *Mesenchymal cells from limbal stroma of human eye*. *Molecular vision*, 2008. **14**: p. 431-442.
66. Branch, M.J., et al., *Mesenchymal stem cells in the human corneal limbal stroma*. *Invest Ophthalmol Vis Sci*, 2012. **53**(9): p. 5109-16.
67. Hertsenberg, A.J., et al., *Corneal stromal stem cells reduce corneal scarring by mediating neutrophil infiltration after wounding*. *PLOS ONE*, 2017. **12**(3): p. e0171712.
68. Sidney, L.E., O.D. McIntosh, and A. Hopkinson, *Phenotypic Change and Induction of Cytokeratin Expression During In Vitro Culture of Corneal Stromal Cells*. *Invest Ophthalmol Vis Sci*, 2015. **56**(12): p. 7225-35.
69. Hashmani, K., et al., *Characterization of corneal stromal stem cells with the potential for epithelial transdifferentiation*. *Stem Cell Res Ther*, 2013. **4**(3): p. 75.
70. Yang, Y.-H.K., et al., *Changes in phenotype and differentiation potential of human mesenchymal stem cells aging in vitro*. *Stem Cell Research & Therapy*, 2018. **9**(1): p. 131.
71. Liu, H., et al., *Soluble molecules are key in maintaining the immunomodulatory activity of murine mesenchymal stromal cells*. *J Cell Sci*, 2012. **125**(Pt 1): p. 200-8.
72. Mennan, C., et al., *A comprehensive characterisation of large-scale expanded human bone marrow and umbilical cord mesenchymal stem cells*. *Stem Cell Research & Therapy*, 2019. **10**(1): p. 99.
73. Burand, A.J., et al., *Function of Cryopreserved Mesenchymal Stromal Cells With and Without Interferon- γ Prelicensing is Context Dependent*. *Stem cells (Dayton, Ohio)*, 2017. **35**(5): p. 1437-1439.
74. Chinnadurai, R., et al., *IDO-Independent Suppression of T Cell Effector Function by IFN- γ -Licensed Human Mesenchymal Stromal Cells*. *The Journal of Immunology*, 2014. **192**(4): p. 1491-1501.
75. De Witte, S.F.H., et al., *Epigenetic changes in umbilical cord mesenchymal stromal cells upon stimulation and culture expansion*. *Cytotherapy*, 2018. **20**(7): p. 919-929.
76. Ti, D., et al., *LPS-preconditioned mesenchymal stromal cells modify macrophage polarization for resolution of chronic inflammation via exosome-shuttled let-7b*. *J Transl Med*, 2015. **13**: p. 308.
77. Lee, S.C., et al., *Lipopolysaccharide preconditioning of adipose-derived stem cells improves liver-regenerating activity of the secretome*. *Stem Cell Research & Therapy*, 2015. **6**(1): p. 75.

78. Kurte, M., et al., *Time-dependent LPS exposure commands MSC immunoplasticity through TLR4 activation leading to opposite therapeutic outcome in EAE*. Stem Cell Research & Therapy, 2020. **11**(1): p. 416.
79. Kim, N. and S.-G. Cho, *Overcoming immunoregulatory plasticity of mesenchymal stem cells for accelerated clinical applications*. International Journal of Hematology, 2016. **103**(2): p. 129-137.
80. Sorrell, J. and A.I. Caplan, *Topical delivery of mesenchymal stem cells and their function in wounds*. Stem Cell Research & Therapy, 2010. **1**(4): p. 30.
81. Chu, G.-Y., et al., *Stem cell therapy on skin: Mechanisms, recent advances and drug reviewing issues*. Journal of Food and Drug Analysis, 2018. **26**(1): p. 14-20.
82. Xu, G., et al., *Immunosuppressive properties of cloned bone marrow mesenchymal stem cells*. Cell Res, 2007. **17**(3): p. 240-8.
83. Sherman, A.B., et al., *Effect of bone marrow-derived mesenchymal stem cells and stem cell supernatant on equine corneal wound healing in vitro*. Stem Cell Research & Therapy, 2017. **8**(1): p. 120.
84. Martinez-Carrasco, R., et al., *Subconjunctival injection of mesenchymal stromal cells protects the cornea in an experimental model of GVHD*. Ocul Surf, 2019. **17**(2): p. 285-294.
85. Shukla, S., et al., *Therapeutic efficacy of different routes of mesenchymal stem cell administration in corneal injury*. Ocul Surf, 2019. **17**(4): p. 729-736.
86. Carter, K., et al., *Characterizing the impact of 2D and 3D culture conditions on the therapeutic effects of human mesenchymal stem cell secretome on corneal wound healing in vitro and ex vivo*. Acta Biomater, 2019. **99**: p. 247-257.
87. Parolini, O., et al., *Amniotic membrane and amniotic fluid-derived cells: potential tools for regenerative medicine?* Regen Med, 2009. **4**(2): p. 275-91.
88. Bauer, D., et al., *Amniotic membrane transplantation induces apoptosis in T lymphocytes in murine corneas with experimental herpetic stromal keratitis*. Invest Ophthalmol Vis Sci, 2009. **50**(7): p. 3188-98.
89. Marsit, N.M., et al., *Validation and assessment of an antibiotic-based, aseptic decontamination manufacturing protocol for therapeutic, vacuum-dried human amniotic membrane*. Scientific Reports, 2019. **9**(1): p. 12854.
90. Rahman, I., et al., *Amniotic membrane in ophthalmology: indications and limitations*. Eye (Lond), 2009. **23**(10): p. 1954-61.
91. Sheha, H., et al., *Sutureless amniotic membrane transplantation for severe bacterial keratitis*. Cornea, 2009. **28**(10): p. 1118-23.
92. Abu-Ain, M.S. and S.K. Webber, *The biological bandage contact lens: a novel technique for using the amniotic membrane in the treatment of persistent corneal epithelial defects*. Eye (Lond), 2010. **24**(7): p. 1306-7; author reply 1307.
93. Ma, Y., et al., *Reconstruction of chemically burned rat corneal surface by bone marrow-derived human mesenchymal stem cells*. Stem Cells, 2006. **24**(2): p. 315-21.
94. Kamata, H., et al., *Design of Hydrogels for Biomedical Applications*. Adv Healthc Mater, 2015. **4**(16): p. 2360-74.
95. Majee, S.B. *Emerging Concepts in Analysis and Applications of Hydrogels*. 2016.
96. Lace, R., et al., *Characterization of Tunable Poly-ε-Lysine-Based Hydrogels for Corneal Tissue Engineering*. Macromol Biosci, 2021. **21**(7): p. e2100036.
97. Kennedy, S., et al., *Poly-ε-lysine based hydrogels as synthetic substrates for the expansion of corneal endothelial cells for transplantation*. Journal of Materials Science: Materials in Medicine, 2019. **30**(9): p. 102.
98. Kennedy, S.M., et al., *Amoebicidal Activity of Poly-Epsilon-Lysine Functionalized Hydrogels*. Invest Ophthalmol Vis Sci, 2022. **63**(1): p. 11.

99. Gallagher, A.G., et al., *A Novel Peptide Hydrogel for an Antimicrobial Bandage Contact Lens*. *Adv Healthc Mater*, 2016. **5**(16): p. 2013-8.
100. Gu, S., et al., *Differentiation of rabbit bone marrow mesenchymal stem cells into corneal epithelial cells in vivo and ex vivo*. *Mol Vis*, 2009. **15**: p. 99-107.
101. Yates, C.C., et al., *Multipotent stromal cells/mesenchymal stem cells and fibroblasts combine to minimize skin hypertrophic scarring*. *Stem Cell Res Ther*, 2017. **8**(1): p. 193.
102. Ke, Y., et al., *Polysaccharide hydrogel combined with mesenchymal stem cells promotes the healing of corneal alkali burn in rats*. *PLoS One*, 2015. **10**(3): p. e0119725.
103. Maulvi, F.A., T.G. Soni, and D.O. Shah, *A review on therapeutic contact lenses for ocular drug delivery*. *Drug Delivery*, 2016. **23**(8): p. 3017-3026.
104. Nicolson, P.C. and J. Vogt, *Soft contact lens polymers: an evolution*. *Biomaterials*, 2001. **22**(24): p. 3273-83.
105. Feng, Y., et al., *Review of alternative carrier materials for ocular surface reconstruction*. *Curr Eye Res*, 2014. **39**(6): p. 541-52.
106. Di Girolamo, N., et al., *A contact lens-based technique for expansion and transplantation of autologous epithelial progenitors for ocular surface reconstruction*. *Transplantation*, 2009. **87**(10): p. 1571-8.
107. Brown, K.D., et al., *Plasma polymer-coated contact lenses for the culture and transfer of corneal epithelial cells in the treatment of limbal stem cell deficiency*. *Tissue Eng Part A*, 2014. **20**(3-4): p. 646-55.
108. Gore, A., et al., *Cultivation and characterization of limbal epithelial stem cells on contact lenses with a feeder layer: toward the treatment of limbal stem cell deficiency*. *Cornea*, 2014. **33**(1): p. 65-71.
109. Zajicova, A., et al., *Treatment of ocular surface injuries by limbal and mesenchymal stem cells growing on nanofiber scaffolds*. *Cell Transplant*, 2010. **19**(10): p. 1281-90.
110. Bosworth, L.A., et al., *Melt electro-written scaffolds with box-architecture support orthogonally oriented collagen*. *Biofabrication*, 2021. **14**(1): p. 015015.
111. Aladdad, A.M., et al., *A thermoresponsive three-dimensional fibrous cell culture platform for enzyme-free expansion of mammalian cells*. *Acta Biomater*, 2019. **95**: p. 427-438.
112. Ruiter, F.A.A., et al., *The electrospinning of a thermo-responsive polymer with peptide conjugates for phenotype support and extracellular matrix production of therapeutically relevant mammalian cells*. *Biomater Sci*, 2020. **8**(9): p. 2611-2626.
113. Musgrave, C.S.A. and F. Fang, *Contact Lens Materials: A Materials Science Perspective*. *Materials* (Basel), 2019. **12**(2).
114. Passos, M.F., et al., *PHEMA Hydrogels Obtained by Infrared Radiation for Cartilage Tissue Engineering*. *International Journal of Chemical Engineering*, 2019. **2019**: p. 4249581.
115. Alvarez-Lorenzo, C., H. Hiratani, and A. Concheiro, *Contact lenses for drug delivery*. *American Journal of Drug Delivery*, 2006. **4**(3): p. 131-151.
116. Achilias, D.S. and P.I. Siafaka, *Polymerization Kinetics of Poly(2-Hydroxyethyl Methacrylate) Hydrogels and Nanocomposite Materials*. *Processes*, 2017. **5**(2): p. 21.
117. Aljubailah, A., et al., *Copolymer Involving 2-Hydroxyethyl Methacrylate and 2-Chloroquinyl Methacrylate: Synthesis, Characterization and In Vitro 2-Hydroxychloroquine Delivery Application*. *Polymers* (Basel), 2021. **13**(23).
118. Moghadam, M.N. and D.P. Pioletti, *Biodegradable HEMA-based hydrogels with enhanced mechanical properties*. *J Biomed Mater Res B Appl Biomater*, 2016. **104**(6): p. 1161-9.

119. Purcell, B.P., et al., *Incorporation of Sulfated Hyaluronic Acid Macromers into Degradable Hydrogel Scaffolds for Sustained Molecule Delivery*. *Biomaterials science*, 2014. **2**: p. 693-702.
120. Dovedytis, M., Z.J. Liu, and S. Bartlett, *Hyaluronic acid and its biomedical applications: A review*. *Engineered Regeneration*, 2020. **1**: p. 102-113.
121. Galderisi, U., G. Peluso, and G. Di Bernardo, *Clinical Trials Based on Mesenchymal Stromal Cells are Exponentially Increasing: Where are We in Recent Years?* *Stem Cell Reviews and Reports*, 2022. **18**(1): p. 23-36.
122. Levy, O., et al., *Shattering barriers toward clinically meaningful MSC therapies*. *Sci Adv*, 2020. **6**(30): p. eaba6884.
123. Galindo, S., et al., *Therapeutic Effect of Human Adipose Tissue-Derived Mesenchymal Stem Cells in Experimental Corneal Failure Due to Limbal Stem Cell Niche Damage*. *Stem Cells*, 2017. **35**(10): p. 2160-2174.
124. Espandar, L., et al., *Application of adipose-derived stem cells on scleral contact lens carrier in an animal model of severe acute alkaline burn*. *Eye Contact Lens*, 2014. **40**(4): p. 243-7.
125. Eslani, M., et al., *Cornea-Derived Mesenchymal Stromal Cells Therapeutically Modulate Macrophage Immunophenotype and Angiogenic Function*. *STEM CELLS*, 2018. **36**(5): p. 775-784.
126. Nili, E., et al., *The Impact of Limbal Mesenchymal Stromal Cells on Healing of Acute Ocular Surface Wounds Is Improved by Pre-cultivation and Implantation in the Presence of Limbal Epithelial Cells*. *Cell Transplant*, 2019. **28**(9-10): p. 1257-1270.
127. Sharma, J., et al., *Corneal reconstruction in chemically damaged cornea using temperature responsive surface assisted mesenchymal stem cell transplantation in rabbits*. *Graefe's Archive for Clinical and Experimental Ophthalmology*, 2021. **259**(7): p. 1859-1870.
128. Mittal, S.K., et al., *Mesenchymal stem cells augment regulatory T cell function via CD80-mediated interactions and promote allograft survival*. *American Journal of Transplantation*, 2022. **22**(6): p. 1564-1577.
129. Lohan, P., et al., *Third-Party Allogeneic Mesenchymal Stromal Cells Prevent Rejection in a Pre-sensitized High-Risk Model of Corneal Transplantation*. *Front Immunol*, 2018. **9**: p. 2666.
130. Shadmani, A., et al., *Autologous Activated Omental versus Allogeneic Adipose Tissue-Derived Mesenchymal Stem Cells in Corneal Alkaline Injury: An Experimental Study*. *J Curr Ophthalmol*, 2021. **33**(2): p. 136-142.
131. Zhang, N., et al., *Subconjunctival injection of tumor necrosis factor- α pre-stimulated bone marrow-derived mesenchymal stem cells enhances anti-inflammation and anti-fibrosis in ocular alkali burns*. *Graefe's Archive for Clinical and Experimental Ophthalmology*, 2021. **259**(4): p. 929-940.
132. Almaliotis, D., et al., *Evaluation of Clinical and Histological Outcomes of Adipose-Derived Mesenchymal Stem Cells in a Rabbit Corneal Alkali Burn Model*. *Stem Cells International*, 2021. **2021**: p. 6610023.
133. Call, M., et al., *Therapeutic efficacy of mesenchymal stem cells for the treatment of congenital and acquired corneal opacity*. *Mol Vis*, 2019. **25**: p. 415-426.
134. Almaliotis, D., et al., *Mesenchymal stem cells improve healing of the cornea after alkali injury*. *Graefes Arch Clin Exp Ophthalmol*, 2015. **253**(7): p. 1121-35.
135. Veréb, Z., et al., *Role of Human Corneal Stroma-Derived Mesenchymal-Like Stem Cells in Corneal Immunity and Wound Healing*. *Scientific Reports*, 2016. **6**(1): p. 26227.

136. Eslani, M., et al., *Corneal Mesenchymal Stromal Cells Are Directly Antiangiogenic via PEDF and sFLT-1*. Investigative Ophthalmology & Visual Science, 2017. **58**(12): p. 5507-5517.
137. Araki-Sasaki, K., et al., *An SV40-immortalized human corneal epithelial cell line and its characterization*. Invest Ophthalmol Vis Sci, 1995. **36**(3): p. 614-21.
138. Kopeček, J., *HYDROGELS FROM SOFT CONTACT LENSES AND IMPLANTS TO SELF-ASSEMBLED NANOMATERIALS*. J Polym Sci A Polym Chem, 2009. **47**(22): p. 5929-5946.
139. Tsuji, K., et al., *Effects of Different Cell-Detaching Methods on the Viability and Cell Surface Antigen Expression of Synovial Mesenchymal Stem Cells*. Cell Transplant, 2017. **26**(6): p. 1089-1102.
140. Zhao, S. and R.D. Fernald, *Comprehensive algorithm for quantitative real-time polymerase chain reaction*. J Comput Biol, 2005. **12**(8): p. 1047-64.
141. Ruitter, F., et al., *The electrospinning of a thermo-responsive polymer with peptide conjugates for phenotype support and extracellular matrix production of therapeutically relevant mammalian cells*. Biomaterials science, 2020. **8**(9): p. 2611-2626.
142. Mezger, T., *Basics of Rheology Workshop 2011*. 2011. **21**(5): p. 303-304.
143. Sridhar, M.S., *Anatomy of cornea and ocular surface*. Indian J Ophthalmol, 2018. **66**(2): p. 190-194.
144. Perrella, G., et al., *Expression of haematopoietic stem cell markers, CD133 and CD34 on human corneal keratocytes*. Br J Ophthalmol, 2007. **91**(1): p. 94-9.
145. Szepesi, Á., et al., *ABCG2 is a selectable marker for enhanced multilineage differentiation potential in periodontal ligament stem cells*. Stem Cells and Development, 2015. **24**(2): p. 244-252.
146. Kadekar, D., V. Kale, and L. Limaye, *Differential ability of MSCs isolated from placenta and cord as feeders for supporting ex vivo expansion of umbilical cord blood derived CD34+ cells*. Stem Cell Research and Therapy, 2015. **6**.
147. Subbannayya, Y., et al., *What Makes Cornea Immunologically Unique and Privileged? Mechanistic Clues from a High-Resolution Proteomic Landscape of the Human Cornea*. Omics, 2020. **24**(3): p. 129-139.
148. Taylor, A.W., *Ocular Immune Privilege and Transplantation*. Front Immunol, 2016. **7**: p. 37.
149. Durand, N. and A.C. Zubair, *Autologous versus allogeneic mesenchymal stem cell therapy: The pros and cons*. Surgery, 2022. **171**(5): p. 1440-1442.
150. Bhat, S., et al., *Expansion and characterization of bone marrow derived human mesenchymal stromal cells in serum-free conditions*. Sci Rep, 2021. **11**(1): p. 3403.
151. Hong, S.H., et al., *Stem cell passage affects directional migration of stem cells in electrotaxis*. Stem Cell Research, 2019. **38**: p. 101475.
152. Jiang, T., et al., *In vitro expansion impaired the stemness of early passage mesenchymal stem cells for treatment of cartilage defects*. Cell Death & Disease, 2017. **8**(6): p. e2851-e2851.
153. Trivedi, A., et al., *Bone marrow donor selection and characterization of MSCs is critical for pre-clinical and clinical cell dose production*. Journal of Translational Medicine, 2019. **17**(1): p. 128.
154. Baer, P.C., et al., *Comprehensive phenotypic characterization of human adipose-derived stromal/stem cells and their subsets by a high throughput technology*. Stem Cells Dev, 2013. **22**(2): p. 330-9.
155. Choong, P.-F., et al., *Mesenchymal stromal cell-like characteristics of corneal keratocytes*. Cytotherapy, 2007. **9**(3): p. 252-258.

156. Yao, L., et al., *Role of mesenchymal stem cells on cornea wound healing induced by acute alkali burn*. PLoS one, 2012. **7**(2): p. e30842.
157. Ferraro, G.A., et al., *Human adipose CD34+ CD90+ stem cells and collagen scaffold constructs grafted in vivo fabricate loose connective and adipose tissues*. Journal of cellular biochemistry, 2013. **114**(5): p. 1039-1049.
158. Simmons, P.J. and B. Torok-Storb, *CD34 expression by stromal precursors in normal human adult bone marrow*. 1991.
159. Sidney, L.E., et al., *Concise review: evidence for CD34 as a common marker for diverse progenitors*. Stem cells (Dayton, Ohio), 2014. **32**(6): p. 1380-1389.
160. Sidney, L.E., et al., *Effect of culture medium on propagation and phenotype of corneal stroma-derived stem cells*. Cytotherapy, 2015. **17**(12): p. 1706-1722.
161. Han, S.-M., et al., *Enhanced proliferation and differentiation of Oct4-and Sox2-overexpressing human adipose tissue mesenchymal stem cells*. Experimental & molecular medicine, 2014. **46**(6): p. e101-e101.
162. Gang, E.J., et al., *SSEA-4 identifies mesenchymal stem cells from bone marrow*. Blood, 2007. **109**(4): p. 1743-1751.
163. Ding, X.-w., J.-h. Wu, and C.-p. Jiang, *ABCG2: a potential marker of stem cells and novel target in stem cell and cancer therapy*. Life sciences, 2010. **86**(17-18): p. 631-637.
164. Brimble, S.N., et al., *The Cell Surface Glycosphingolipids SSEA-3 and SSEA-4 Are Not Essential for Human ESC Pluripotency*. STEM CELLS, 2007. **25**(1): p. 54-62.
165. Truong, T.T., et al., *SSEA4 Is a Potential Negative Marker for the Enrichment of Human Corneal Epithelial Stem/Progenitor Cells*. Investigative Ophthalmology & Visual Science, 2011. **52**(9): p. 6315-6320.
166. Vassalli, G., *Aldehyde Dehydrogenases: Not Just Markers, but Functional Regulators of Stem Cells*. Stem Cells Int, 2019. **2019**: p. 3904645.
167. Du, Y., et al., *Multipotent stem cells in human corneal stroma*. Stem Cells, 2005. **23**(9): p. 1266-75.
168. Amit, M. and J. Itskovitz-Eldor, *Derivation and spontaneous differentiation of human embryonic stem cells*. Journal of anatomy, 2002. **200**(3): p. 225-232.
169. Levenstein, M.E., et al., *Basic fibroblast growth factor support of human embryonic stem cell self-renewal*. Stem Cells, 2006. **24**(3): p. 568-74.
170. Hirai, H., P. Karian, and N. Kikyo, *Regulation of embryonic stem cell self-renewal and pluripotency by leukaemia inhibitory factor*. Biochem J, 2011. **438**(1): p. 11-23.
171. Desai, V., H. Hsia, and J. Schwarzbauer, *Reversible Modulation of Myofibroblast Differentiation in Adipose-Derived Mesenchymal Stem Cells*. PloS one, 2014. **9**: p. e86865.
172. Qin, Z., et al., *Actin cytoskeleton assembly regulates collagen production via TGF- β type II receptor in human skin fibroblasts*. J Cell Mol Med, 2018. **22**(9): p. 4085-4096.
173. Duscher, D., et al., *Aging disrupts cell subpopulation dynamics and diminishes the function of mesenchymal stem cells*. Scientific reports, 2014. **4**(1): p. 1-9.
174. Bustos, M.L., et al., *Aging mesenchymal stem cells fail to protect because of impaired migration and antiinflammatory response*. American journal of respiratory and critical care medicine, 2014. **189**(7): p. 787-798.
175. Kasper, G., et al., *Insights into Mesenchymal Stem Cell Aging: Involvement of Antioxidant Defense and Actin Cytoskeleton*. Stem Cells, 2009. **27**(6): p. 1288-1297.
176. Liu, J., et al., *Senescence in Mesenchymal Stem Cells: Functional Alterations, Molecular Mechanisms, and Rejuvenation Strategies*. Frontiers in Cell and Developmental Biology, 2020. **8**.

177. Li, H., et al., *Spontaneous expression of embryonic factors and p53 point mutations in aged mesenchymal stem cells: a model of age-related tumorigenesis in mice*. Cancer Research, 2007. **67**(22): p. 10889-10898.
178. Wright, A., M.L. Arthaud-Day, and M.L. Weiss, *Therapeutic Use of Mesenchymal Stromal Cells: The Need for Inclusive Characterization Guidelines to Accommodate All Tissue Sources and Species*. Front Cell Dev Biol, 2021. **9**: p. 632717.
179. Husak, Z. and M.N. Dworzak, *CD99 ligation upregulates HSP70 on acute lymphoblastic leukemia cells and concomitantly increases NK cytotoxicity*. Cell Death Dis, 2012. **3**(11): p. e425.
180. Lin, C.-S., et al., *Commonly used mesenchymal stem cell markers and tracking labels: Limitations and challenges*. Histology and histopathology, 2013. **28**(9): p. 1109-1116.
181. Husak, Z. and M.N. Dworzak, *Chronic stress induces CD99, suppresses autophagy, and affects spontaneous adipogenesis in human bone marrow stromal cells*. Stem Cell Research & Therapy, 2017. **8**(1): p. 83.
182. Soland, M.A., et al., *Mesenchymal stem cells engineered to inhibit complement-mediated damage*. PLoS One, 2013. **8**(3): p. e60461.
183. Geller, A. and J. Yan, *The role of membrane bound complement regulatory proteins in tumor development and cancer immunotherapy*. Frontiers in immunology, 2019. **10**: p. 1074.
184. Weinstock, C., M. Anliker, and I. von Zabern, *CD59: A long-known complement inhibitor has advanced to a blood group system*. Immunohematology, 2015. **31**(4): p. 145-51.
185. Bora, N.S., P. Jha, and P.S. Bora, *The role of complement in ocular pathology*. Semin Immunopathol, 2008. **30**(2): p. 85-95.
186. Zhang, Y., et al., *Knockout of beta-2 microglobulin reduces stem cell-induced immune rejection and enhances ischaemic hindlimb repair via exosome/miR-24/Bim pathway*. Journal of cellular and molecular medicine, 2020. **24**(1): p. 695-710.
187. Zha, S., et al., *Generation of Mesenchymal Stromal Cells with Low Immunogenicity from Human PBMC-Derived β 2 Microglobulin Knockout Induced Pluripotent Stem Cells*. Cell Transplantation, 2020. **29**: p. 0963689720965529.
188. García-Sancho, J., et al., *Influence of HLA Matching on the Efficacy of Allogeneic Mesenchymal Stromal Cell Therapies for Osteoarthritis and Degenerative Disc Disease*. Transplant Direct, 2017. **3**(9): p. e205.
189. Panés, J., et al., *Expanded allogeneic adipose-derived mesenchymal stem cells (Cx601) for complex perianal fistulas in Crohn's disease: a phase 3 randomised, double-blind controlled trial*. The Lancet, 2016. **388**(10051): p. 1281-1290.
190. Skyler, J.S., et al., *Allogeneic mesenchymal precursor cells in type 2 diabetes: a randomized, placebo-controlled, dose-escalation safety and tolerability pilot study*. Diabetes care, 2015. **38**(9): p. 1742-1749.
191. Packham, D.K., et al., *Allogeneic mesenchymal precursor cells (MPC) in diabetic nephropathy: a randomized, placebo-controlled, dose escalation study*. EBioMedicine, 2016. **12**: p. 263-269.
192. Rensing, M.E., et al., *Differential binding of viral peptides to HLA-A2 alleles. Implications for human papillomavirus type 16 E7 peptide-based vaccination against cervical carcinoma*. European journal of immunology, 1999. **29**(4): p. 1292-1303.
193. Kwak, J., et al., *HLA-A2 Promotes the Therapeutic Effect of Umbilical Cord Blood-Derived Mesenchymal Stem Cells in Hyperoxic Lung Injury*. Bioengineering (Basel), 2022. **9**(4).

194. Friedenstein, A.J., R.K. Chailakhjan, and K.S. Lalykina, *The development of fibroblast colonies in monolayer cultures of guinea-pig bone marrow and spleen cells*. Cell Tissue Kinet, 1970. **3**(4): p. 393-403.
195. Berebichez-Fridman, R. and P.R. Montero-Olvera, *Sources and Clinical Applications of Mesenchymal Stem Cells: State-of-the-art review*. Sultan Qaboos Univ Med J, 2018. **18**(3): p. e264-e277.
196. Rodríguez-Fuentes, D.E., et al., *Mesenchymal Stem Cells Current Clinical Applications: A Systematic Review*. Archives of Medical Research, 2021. **52**(1): p. 93-101.
197. Amati, E., et al., *High-throughput immunophenotypic characterization of bone marrow- and cord blood-derived mesenchymal stromal cells reveals common and differentially expressed markers: identification of angiotensin-converting enzyme (CD143) as a marker differentially expressed between adult and perinatal tissue sources*. Stem Cell Res Ther, 2018. **9**(1): p. 10.
198. Ong, Wee K., et al., *Identification of Specific Cell-Surface Markers of Adipose-Derived Stem Cells from Subcutaneous and Visceral Fat Depots*. Stem Cell Reports, 2014. **2**(2): p. 171-179.
199. Dollet, P.-E., et al., *Comprehensive screening of cell surface markers expressed by adult-derived human liver stem/progenitor cells harvested at passage 5: potential implications for engraftment*. Stem Cells International, 2016. **2016**.
200. Cho, K.-A., et al., *RNA sequencing reveals a transcriptomic portrait of human mesenchymal stem cells from bone marrow, adipose tissue, and palatine tonsils*. Scientific Reports, 2017. **7**(1): p. 17114.
201. Galipeau, J., et al., *International Society for Cellular Therapy perspective on immune functional assays for mesenchymal stromal cells as potency release criterion for advanced phase clinical trials*. Cytotherapy, 2016. **18**(2): p. 151-9.
202. Himlal, I., U. Goyal, and M. Ta, *Evaluating Wharton's jelly-derived mesenchymal stem cell's survival, migration, and expression of wound repair markers under conditions of ischemia-like stress*. Stem cells international, 2017. **2017**.
203. Pan, H., et al., *Mesenchymal stem cells combined with tissue fusion technology promoted wound healing in porcine bowel anastomosis*. Stem cells international, 2020. **2020**.
204. Pels, L., *Organ culture: the method of choice for preservation of human donor corneas*. British Journal of Ophthalmology, 1997. **81**(7): p. 523.
205. Crewe, J.M. and W.J. Armitage, *Integrity of Epithelium and Endothelium in Organ-Cultured Human Corneas*. Investigative Ophthalmology & Visual Science, 2001. **42**(8): p. 1757-1761.
206. Møller-Pedersen, T., et al., *Evaluation of potential organ culture media for eye banking using human donor corneas*. The British journal of ophthalmology, 2001. **85**(9): p. 1075-1079.
207. Kureshi, A.K., J.L. Funderburgh, and J.T. Daniels, *Human corneal stromal stem cells exhibit survival capacity following isolation from stored organ-culture corneas*. Invest Ophthalmol Vis Sci, 2014. **55**(11): p. 7583-8.
208. Horwitz, E.M., et al., *Clarification of the nomenclature for MSC: The International Society for Cellular Therapy position statement*. Cytotherapy, 2005. **7**(5): p. 393-5.
209. Donnenberg, A.D., et al., *The cell-surface proteome of cultured adipose stromal cells*. Cytometry Part A, 2015. **87**(7): p. 665-674.
210. Bassani, B., et al., *CD40 Activity on Mesenchymal Cells Negatively Regulates OX40L to Maintain Bone Marrow Immune Homeostasis Under Stress Conditions*. Front Immunol, 2021. **12**: p. 662048.

211. Tang, G., et al., *Short cytoplasmic isoform of IL1R1/CD121a mediates IL1 β induced proliferation of synovium-derived mesenchymal stem/stromal cells through ERK1/2 pathway*. *Heliyon*, 2022. **8**(5): p. e09476.
212. Christy, B.A., et al., *Procoagulant activity of human mesenchymal stem cells*. *Journal of Trauma and Acute Care Surgery*, 2017. **83**(1): p. S164-S169.
213. Chen, J., et al., *Mesenchymal Stromal Cell-Mediated Immune Regulation: A Promising Remedy in the Therapy of Type 2 Diabetes Mellitus*. *Stem Cells*, 2021. **39**(7): p. 838-852.
214. O'Rourke, B., et al., *Mesenchymal stromal cell delivery via an ex vivo bioreactor preclinical test system attenuates clot formation for intravascular application*. *Stem Cells Translational Medicine*, 2021. **10**(6): p. 883-894.
215. Moll, G., et al., *Improved MSC Minimal Criteria to Maximize Patient Safety: A Call to Embrace Tissue Factor and Hemocompatibility Assessment of MSC Products*. *Stem Cells Translational Medicine*, 2022. **11**(1): p. 2-13.
216. Majumdar, M.K., et al., *Characterization and functionality of cell surface molecules on human mesenchymal stem cells*. *J Biomed Sci*, 2003. **10**(2): p. 228-41.
217. Nystedt, J., et al., *Cell Surface Structures Influence Lung Clearance Rate of Systemically Infused Mesenchymal Stromal Cells*. *Stem Cells*, 2013. **31**(2): p. 317-326.
218. Sánchez-Aparicio, P., C. Dominguez-Jiménez, and A. Garcia-Pardo, *Activation of the alpha 4 beta 1 integrin through the beta 1 subunit induces recognition of the RGDS sequence in fibronectin*. *J Cell Biol*, 1994. **126**(1): p. 271-9.
219. Subramanian, A., et al., *Comparative Characterization of Cells from the Various Compartments of the Human Umbilical Cord Shows that the Wharton's Jelly Compartment Provides the Best Source of Clinically Utilizable Mesenchymal Stem Cells*. *PLoS One*, 2015. **10**(6): p. e0127992.
220. Ghanem, R.C., et al., *Semaphorin 7A promotes angiogenesis in an experimental corneal neovascularization model*. *Curr Eye Res*, 2011. **36**(11): p. 989-96.
221. Kempuraj, D. and R.R. Mohan, *Autophagy in Extracellular Matrix and Wound Healing Modulation in the Cornea*. *Biomedicines*, 2022. **10**(2): p. 339.
222. Barrachina, L., et al., *Priming Equine Bone Marrow-Derived Mesenchymal Stem Cells with Proinflammatory Cytokines: Implications in Immunomodulation-Immunogenicity Balance, Cell Viability, and Differentiation Potential*. *Stem Cells Dev*, 2017. **26**(1): p. 15-24.
223. de Witte, S.F.H., et al., *Toward Development of iMesenchymal Stem Cells for Immunomodulatory Therapy*. *Frontiers in Immunology*, 2016. **6**.
224. Spaggiari, G.M., et al., *Mesenchymal stem cell-natural killer cell interactions: evidence that activated NK cells are capable of killing MSCs, whereas MSCs can inhibit IL-2-induced NK-cell proliferation*. *Blood*, 2006. **107**(4): p. 1484-90.
225. Wilson, S.E., *Interleukin-1 and Transforming Growth Factor Beta: Commonly Opposing, but Sometimes Supporting, Master Regulators of the Corneal Wound Healing Response to Injury*. *Investigative Ophthalmology & Visual Science*, 2021. **62**(4): p. 8-8.
226. Kimura, K., S. Teranishi, and T. Nishida, *Interleukin-1 β -Induced Disruption of Barrier Function in Cultured Human Corneal Epithelial Cells*. *Investigative Ophthalmology & Visual Science*, 2009. **50**(2): p. 597-603.
227. Schottelius, A.J.G., et al., *Biology of tumor necrosis factor- α —implications for psoriasis*. *Experimental Dermatology*, 2004. **13**(4): p. 193-222.
228. Ogawa, Y., E. Shimizu, and K. Tsubota, *Interferons and Dry Eye in Sjögren's Syndrome*. *Int J Mol Sci*, 2018. **19**(11).

229. Simmons, K.T., et al., *Inflammatory Response to Lipopolysaccharide on the Ocular Surface in a Murine Dry Eye Model*. Invest Ophthalmol Vis Sci, 2016. **57**(6): p. 2443-51.
230. Jackson, D.C., et al., *Tear Interferon-Gamma as a Biomarker for Evaporative Dry Eye Disease*. Invest Ophthalmol Vis Sci, 2016. **57**(11): p. 4824-4830.
231. Kimura, K., et al., *Delayed disruption of barrier function in cultured human corneal epithelial cells induced by tumor necrosis factor-alpha in a manner dependent on NF-kappaB*. Invest Ophthalmol Vis Sci, 2008. **49**(2): p. 565-71.
232. Kim, S.-C., et al., *Inhibition of c-Jun N-terminal kinase and nuclear factor κ B pathways mediates fisetin-exerted anti-inflammatory activity in lipopolysaccharide-treated RAW264.7 cells*. Immunopharmacology and Immunotoxicology, 2012. **34**(4): p. 645-650.
233. Doyle, S.E., et al., *IRF3 Mediates a TLR3/TLR4-Specific Antiviral Gene Program*. Immunity, 2002. **17**(3): p. 251-263.
234. Hemmati, S., T. Haque, and K. Gritsman, *Inflammatory signaling pathways in preleukemic and leukemic stem cells*. Frontiers in oncology, 2017. **7**: p. 265.
235. Najar, M., et al., *Mesenchymal Stromal Cells and Toll-Like Receptor Priming: A Critical Review*. Immune Netw, 2017. **17**(2): p. 89-102.
236. Hayden, M.S. and S. Ghosh, *Regulation of NF- κ B by TNF family cytokines*. Semin Immunol, 2014. **26**(3): p. 253-66.
237. Walter, M.R., *The Role of Structure in the Biology of Interferon Signaling*. Frontiers in Immunology, 2020. **11**.
238. Mounayar, M., et al., *PI3ka and STAT1 Interplay Regulates Human Mesenchymal Stem Cell Immune Polarization*. Stem Cells, 2015. **33**(6): p. 1892-901.
239. Fan, H., et al., *Pre-treatment with IL-1 β enhances the efficacy of MSC transplantation in DSS-induced colitis*. Cellular & Molecular Immunology, 2012. **9**(6): p. 473-481.
240. Bernet, J.D., et al., *p38 MAPK signaling underlies a cell-autonomous loss of stem cell self-renewal in skeletal muscle of aged mice*. Nat Med, 2014. **20**(3): p. 265-71.
241. Wang, D., et al., *Different culture method changing CD105 expression in amniotic fluid MSCs without affecting differentiation ability or immune function*. J Cell Mol Med, 2020. **24**(7): p. 4212-4222.
242. McKinnirey, F., et al., *Immune modulation via adipose derived Mesenchymal Stem cells is driven by donor sex in vitro*. Scientific Reports, 2021. **11**(1): p. 12454.
243. Li, X., et al., *Identification of optimal reference genes for quantitative PCR studies on human mesenchymal stem cells*. Mol Med Rep, 2015. **11**(2): p. 1304-1311.
244. Cho, H., et al., *MICA/B and ULBP1 NKG2D ligands are independent predictors of good prognosis in cervical cancer*. BMC Cancer, 2014. **14**: p. 957.
245. He, J. and H.E. Bazan, *Epidermal growth factor synergism with TGF-beta1 via PI-3 kinase activity in corneal keratocyte differentiation*. Invest Ophthalmol Vis Sci, 2008. **49**(7): p. 2936-45.
246. Hippe, D., et al., *Fas/CD95-mediated apoptosis of type II cells is blocked by Toxoplasma gondii primarily via interference with the mitochondrial amplification loop*. Infect Immun, 2008. **76**(7): p. 2905-12.
247. Periasamy, R., S.L. Elshaer, and R. Gangaraju, *CD140b (PDGFR β) signaling in adipose-derived stem cells mediates angiogenic behavior of retinal endothelial cells*. Regen Eng Transl Med, 2019. **5**(1): p. 1-9.
248. Lin, S.-Y., et al., *The isolation of novel mesenchymal stromal cell chemotactic factors from the conditioned medium of tumor cells*. Experimental Cell Research, 2008. **314**(17): p. 3107-3117.

249. Ebihara, N., et al., *Role of the IL-6 classic- and trans-signaling pathways in corneal sterile inflammation and wound healing*. Invest Ophthalmol Vis Sci, 2011. **52**(12): p. 8549-57.
250. Radtke, S., et al., *Cross-regulation of cytokine signalling: pro-inflammatory cytokines restrict IL-6 signalling through receptor internalisation and degradation*. J Cell Sci, 2010. **123**(Pt 6): p. 947-59.
251. Rashedi, I., et al., *TLR3 or TLR4 Activation Enhances Mesenchymal Stromal Cell-Mediated Treg Induction via Notch Signaling*. Stem Cells, 2016. **35**(1): p. 265-275.
252. Gieseke, F., et al., *Proinflammatory stimuli induce galectin-9 in human mesenchymal stromal cells to suppress T-cell proliferation*. European Journal of Immunology, 2013. **43**(10): p. 2741-2749.
253. McFarland-Mancini, M.M., et al., *Differences in wound healing in mice with deficiency of IL-6 versus IL-6 receptor*. J Immunol, 2010. **184**(12): p. 7219-28.
254. Leuning, D.G., et al., *Clinical-Grade Isolated Human Kidney Perivascular Stromal Cells as an Organotypic Cell Source for Kidney Regenerative Medicine*. Stem Cells Transl Med, 2017. **6**(2): p. 405-418.
255. Miyagi, H., et al., *The role of hepatocyte growth factor in corneal wound healing*. Exp Eye Res, 2018. **166**: p. 49-55.
256. Park, J.W., S.R. Hwang, and I.S. Yoon, *Advanced Growth Factor Delivery Systems in Wound Management and Skin Regeneration*. Molecules, 2017. **22**(8).
257. Chen, M., et al., *Progress in Research on the Role of FGF in the Formation and Treatment of Corneal Neovascularization*. Frontiers in pharmacology, 2020. **11**: p. 111-111.
258. Bazzazi, H., et al., *Computer Simulation of TSP1 Inhibition of VEGF–Akt–eNOS: An Angiogenesis Triple Threat*. Frontiers in Physiology, 2018. **9**.
259. Murphy-Ullrich, J.E. and M. Poczatek, *Activation of latent TGF- β by thrombospondin-1: mechanisms and physiology*. Cytokine & Growth Factor Reviews, 2000. **11**(1): p. 59-69.
260. de Araújo Farias, V., et al., *TGF- β and mesenchymal stromal cells in regenerative medicine, autoimmunity and cancer*. Cytokine & Growth Factor Reviews, 2018. **43**: p. 25-37.
261. Zhou, S., R. Cecere, and A. Philip, *CD109 released from human bone marrow mesenchymal stem cells attenuates TGF- β -induced epithelial to mesenchymal transition and stemness of squamous cell carcinoma*. Oncotarget, 2017. **8**(56): p. 95632-95647.
262. Boyt, D.T., et al., *Dose and duration of interferon γ pre-licensing interact with donor characteristics to influence the expression and function of indoleamine-2,3-dioxygenase in mesenchymal stromal cells*. Journal of The Royal Society Interface, 2020. **17**(167): p. 20190815.
263. Kim, D.S., et al., *Enhanced Immunosuppressive Properties of Human Mesenchymal Stem Cells Primed by Interferon- γ* . EBioMedicine, 2018. **28**: p. 261-273.
264. Lim, J.-Y., et al., *The therapeutic efficacy of mesenchymal stromal cells on experimental colitis was improved by the IFN- γ and poly(I:C) priming through promoting the expression of indoleamine 2,3-dioxygenase*. Stem Cell Research & Therapy, 2021. **12**(1): p. 37.
265. Satoh, J. and H. Tabunoki, *A Comprehensive Profile of ChIP-Seq-Based STAT1 Target Genes Suggests the Complexity of STAT1-Mediated Gene Regulatory Mechanisms*. Gene Regul Syst Bio, 2013. **7**: p. 41-56.
266. Kim, S.B., et al., *Blockage of indoleamine 2,3-dioxygenase regulates Japanese encephalitis via enhancement of type I/II IFN innate and adaptive T-cell responses*. Journal of Neuroinflammation, 2016. **13**(1): p. 79.

267. Bach, E.A., et al., *Ligand-induced autoregulation of IFN-gamma receptor beta chain expression in T helper cell subsets*. Science, 1995. **270**(5239): p. 1215-8.
268. Luz-Crawford, P., et al., *Mesenchymal Stem Cell-Derived Interleukin 1 Receptor Antagonist Promotes Macrophage Polarization and Inhibits B Cell Differentiation*. Stem Cells, 2016. **34**(2): p. 483-92.
269. Vijmasi, T., et al., *Topical administration of interleukin-1 receptor antagonist as a therapy for aqueous-deficient dry eye in autoimmune disease*. Mol Vis, 2013. **19**: p. 1957-65.
270. Doni, A., et al., *The Long Pentraxin PTX3 as a Link Between Innate Immunity, Tissue Remodeling, and Cancer*. Frontiers in Immunology, 2019. **10**(712).
271. Cappuzzello, C., et al., *Mesenchymal Stromal Cell-Derived PTX3 Promotes Wound Healing via Fibrin Remodeling*. Journal of Investigative Dermatology, 2016. **136**(1): p. 293-300.
272. Antonioli, E., et al., *Modulation of Hyaluronan Synthesis by the Interaction between Mesenchymal Stem Cells and Osteoarthritic Chondrocytes*. Stem Cells International, 2015. **2015**: p. 640218.
273. Sugiyama, T., et al., *The effect of sodium hyaluronate on the migration of rabbit corneal epithelium. II. The effect of topical administration*. J Ocul Pharmacol, 1991. **7**(1): p. 53-64.
274. Nishida, T., et al., *Hyaluronan stimulates corneal epithelial migration*. Experimental eye research, 1991. **53** 6: p. 753-8.
275. Herrera, M.B., et al., *Exogenous mesenchymal stem cells localize to the kidney by means of CD44 following acute tubular injury*. Kidney Int, 2007. **72**(4): p. 430-41.
276. Popova, A.P., *Mesenchymal cells and bronchopulmonary dysplasia: new insights about the dark side of oxygen*. 2019, American Thoracic Society. p. 501-502.
277. Mia, M.M., M. Boersema, and R. Bank, *Interleukin-1 β Attenuates Myofibroblast Formation and Extracellular Matrix Production in Dermal and Lung Fibroblasts Exposed to Transforming Growth Factor- β 1*. PloS one, 2014. **9**: p. e91559.
278. Mauviel, A., et al., *Comparative effects of interleukin-1 and tumor necrosis factor-alpha on collagen production and corresponding procollagen mRNA levels in human dermal fibroblasts*. J Invest Dermatol, 1991. **96**(2): p. 243-9.
279. Taylor, A.J., et al., *Revealing cytokine-induced changes in the extracellular matrix with secondary ion mass spectrometry*. Acta Biomaterialia, 2015. **14**: p. 70-83.
280. Elsafadi, M., et al., *Transgelin is a TGF β -inducible gene that regulates osteoblastic and adipogenic differentiation of human skeletal stem cells through actin cytoskeleton organization*. Cell Death Dis, 2016. **7**(8): p. e2321.
281. Almalki, S.G. and D.K. Agrawal, *Effects of matrix metalloproteinases on the fate of mesenchymal stem cells*. Stem Cell Research & Therapy, 2016. **7**(1): p. 129.
282. Son, Y.-K., et al., *Preparation and properties of PEG-modified PHEMA hydrogel and the morphological effect*. Macromolecular Research, 2006. **14**(3): p. 394-399.
283. Gun'ko, V.M., I.N. Savina, and S.V. Mikhalovsky, *Properties of Water Bound in Hydrogels*. Gels, 2017. **3**(4).
284. dos Santos, J.F., et al., *Soft contact lenses functionalized with pendant cyclodextrins for controlled drug delivery*. Biomaterials, 2009. **30**(7): p. 1348-55.
285. Pratoomsoot, C., et al., *A thermoreversible hydrogel as a biosynthetic bandage for corneal wound repair*. Biomaterials, 2008. **29**(3): p. 272-81.
286. Boazak, E.M., V.K. Greene, Jr., and D.T. Auguste, *The effect of heterobifunctional crosslinkers on HEMA hydrogel modulus and toughness*. PLoS One, 2019. **14**(5): p. e0215895.
287. Horst, C.R., et al., *Measuring the modulus of silicone hydrogel contact lenses*. Optom Vis Sci, 2012. **89**(10): p. 1468-76.

288. Vladkova, T.G., *Surface Engineered Polymeric Biomaterials with Improved Biocontact Properties*. International Journal of Polymer Science, 2010. **2010**: p. 296094.
289. Hsin, I.C. and W. Yiwei, *Cell Responses to Surface and Architecture of Tissue Engineering Scaffolds*, in *Regenerative Medicine and Tissue Engineering*, E. Daniel, Editor. 2011, IntechOpen: Rijeka. p. Ch. 27.
290. Xu, L.-P., et al., *Amplified effect of surface charge on cell adhesion by nanostructures*. Nanoscale, 2016. **8**(25): p. 12540-12543.
291. Kubinová, Š., et al., *The use of new surface-modified poly (2-hydroxyethyl methacrylate) hydrogels in tissue engineering: Treatment of the surface with fibronectin subunits versus Ac-CGGASIKVAVS-OH, cysteine, and 2-mercaptoethanol modification*. Journal of biomedical materials research Part A, 2014. **102**(7): p. 2315-2323.
292. Gouveia, R.M., et al., *The bioactivity of composite Fmoc-RGDS-collagen gels*. Biomaterials science, 2014. **2**(9): p. 1222-1229.
293. Huettner, N., T.R. Dargaville, and A. Forget, *Discovering Cell-Adhesion Peptides in Tissue Engineering: Beyond RGD*. Trends in Biotechnology, 2018. **36**(4): p. 372-383.
294. Boateng, S.Y., et al., *RGD and YIGSR synthetic peptides facilitate cellular adhesion identical to that of laminin and fibronectin but alter the physiology of neonatal cardiac myocytes*. American Journal of Physiology-Cell Physiology, 2005. **288**(1): p. C30-C38.
295. Li, L., et al., *Resilin-like polypeptide hydrogels engineered for versatile biological function*. Soft Matter, 2013. **9**(3): p. 665-673.
296. Li, L., et al., *Biocompatibility of injectable resilin-based hydrogels*. J Biomed Mater Res A, 2018. **106**(8): p. 2229-2242.
297. Balu, R., et al., *Tuning the hierarchical structure and resilience of resilin-like polypeptide hydrogels using graphene oxide*. ACS Applied Bio Materials, 2020. **3**(12): p. 8688-8697.
298. Sun, Y., et al., *Thermal Self-Initiation in Stable Free-Radical Polymerization of Styrene*. Polymer journal, 2009. **41**(11): p. 954-960.
299. Braun, D., *Origins and development of initiation of free radical polymerization processes*. International Journal of Polymer Science, 2009. **2009**.
300. Karpushkin, E., et al., *Rheological properties of homogeneous and heterogeneous poly (2-hydroxyethyl methacrylate) hydrogels*. Polymer international, 2012. **61**(2): p. 328-336.
301. Kopeček, J. and J. Yang, *Hydrogels as smart biomaterials*. Polymer international, 2007. **56**(9): p. 1078-1098.
302. Lerman, M.J., et al., *The evolution of polystyrene as a cell culture material*. Tissue Engineering Part B: Reviews, 2018. **24**(5): p. 359-372.
303. Shen, J., et al., *Mechanical, thermal and swelling properties of poly (acrylic acid)–graphene oxide composite hydrogels*. Soft Matter, 2012. **8**(6): p. 1831-1836.
304. Abd Alla, S.G., H.M.N. El-Din, and A.W.M. El-Naggar, *Structure and swelling-release behaviour of poly (vinyl pyrrolidone)(PVP) and acrylic acid (AAc) copolymer hydrogels prepared by gamma irradiation*. European polymer journal, 2007. **43**(7): p. 2987-2998.
305. Karadağ, E., Ö.B. Üzümlü, and D. Saraydın, *Water uptake in chemically crosslinked poly (acrylamide-co-crotonic acid) hydrogels*. Materials & design, 2005. **26**(4): p. 265-270.
306. Ratner, B.D., et al., *Biomaterials science: an introduction to materials in medicine*. San Diego, California, 2004: p. 162-4.

307. Mohammed, A.H., et al., *Effect of crosslinking concentration on properties of 3-(trimethoxysilyl) propyl methacrylate/N-vinyl pyrrolidone gels*. Chemistry Central Journal, 2018. **12**(1): p. 1-9.
308. Ismail, A. and P. Lai, *Development of defect-free asymmetric polysulfone membranes for gas separation using response surface methodology*. Separation and purification technology, 2004. **40**(2): p. 191-207.
309. Dogu, Y. and O. Okay, *Swelling–deswelling kinetics of poly (N-isopropylacrylamide) hydrogels formed in PEG solutions*. Journal of applied polymer science, 2006. **99**(1): p. 37-44.
310. Boyd, R.J. and S.L. Boyd, *Group electronegativities from the bond critical point model*. Journal of the American Chemical Society, 1992. **114**(5): p. 1652-1655.
311. Brahim, S., D. Narinesingh, and A. Guiseppi-Elie, *Synthesis and hydration properties of pH-sensitive p (HEMA)-based hydrogels containing 3-(trimethoxysilyl) propyl methacrylate*. Biomacromolecules, 2003. **4**(3): p. 497-503.
312. Taraballi, F., et al., *Glycine-spacers influence functional motifs exposure and self-assembling propensity of functionalized substrates tailored for neural stem cell cultures*. Front Neuroeng, 2010. **3**: p. 1.
313. Kim, S., et al., *Photocrosslinkable chitosan hydrogels functionalized with the RGD peptide and phosphoserine to enhance osteogenesis*. J Mater Chem B, 2016. **4**(31): p. 5289-5298.
314. Dhillon, J., et al., *Peptide-modified methacrylated glycol chitosan hydrogels as a cell-viability supporting pro-angiogenic cell delivery platform for human adipose-derived stem/stromal cells*. J Biomed Mater Res A, 2019. **107**(3): p. 571-585.
315. La, W.-G., et al., *3,4-dihydroxy-L-phenylalanine as a cell adhesion molecule in serum-free cell culture*. Biotechnology Progress, 2012. **28**(4): p. 1055-1060.
316. King, R.E., et al., *Biocompatibility and Viscoelastic Properties of Injectable Resilin-Like Polypeptide and Hyaluronan Hybrid Hydrogels in Rabbit Vocal Folds*. Regen Eng Transl Med, 2019. **5**(4): p. 373-386.
317. Butruk-Raszeja, B., M. Trzaskowski, and T. Ciach, *Polyvinylpyrrolidone-Based Coatings for Polyurethanes – The Effect of Reagent Concentration on Their Chosen Physical Properties*. Inzynieria Chemiczna i Procesowa, 2012. **33**: p. 563-571.
318. Chow, C., *Surface and Bulk Modifications of Biomaterials Used in Bone Regeneration*.

Appendix

Table A1.1. List of definitions for the BD Human Cell Surface Marker Panel.

Antigen	Definition
aBTCR	Alpha/ Beta T Cell Receptor
B2-micro	Beta-2-Microglobulin
BLTR-1	Leukotriene B4 Receptor 1
CD1a	T-Cell Surface Glycoprotein CD1a
CD1b	T-Cell Surface Glycoprotein CD1b
CD1d	T-Cell Surface Glycoprotein CD1d
CD2	T-Cell Surface Antigen CD2
CD3	CD3 Gamma Subunit Of T-Cell Receptor Complex
CD4	T-Cell Surface Glycoprotein CD4
CD5	T-Cell Surface Glycoprotein CD5
CD7	T-Cell Surface Antigen Leu-9
CD8a	T-Cell Surface Glycoprotein CD8 Alpha Chain
CD8b	T-Cell Surface Glycoprotein CD8 Beta Chain
CD9	Tetraspanin-29
CD10	Membrane Metalloendopeptidase
CD11a	Integrin Subunit Alpha L
CD11b	Integrin Subunit Alpha M
CD11c	Integrin Subunit Alpha X

Antigen	Definition
CD112	Nectin Cell Adhesion Molecule 2
CD114	Colony Stimulating Factor 3 Receptor
CD116	Colony Stimulating Factor 2 Receptor Subunit Alpha
CD117	KIT Proto-Oncogene, Receptor Tyrosine Kinase
CD118	Leukemia Inhibitory Factor Receptor Subunit Alpha
CD119	Interferon Gamma Receptor 1
CD120a	Tumor Necrosis Factor Receptor Superfamily Member 1A
CD120b	Tumor Necrosis Factor Receptor Superfamily Member 1B
CD121a	Interleukin-1 Receptor, Type I
CD121b	Interleukin-1 Receptor, Type 2
CD122	Interleukin 2 Receptor Subunit Beta
CD123	Interleukin 3 Receptor Subunit Alpha
CD124	Interleukin 4 Receptor
CD126	Interleukin 6 Receptor
CD127	Interleukin 7 Receptor
CD128b	Selectin L
CD130	Interleukin 6 Cytokine Family Signal Transducer
CD132	Interleukin 2 Receptor Subunit Gamma

CD13	Membrane Alanyl Aminopeptidase
CD14	Myeloid Cell-Specific Leucine-Rich Glycoprotein
CD15	Fucosyltransferase 4
CD15s	Fucosyltransferase 4
CD16	Fc Gamma Receptor IIIa
CD18	Integrin Subunit Beta 2
CD19	B-Lymphocyte Surface Antigen B4
CD20	Membrane Spanning 4-Domains A1
CD21	Complement C3d Receptor 2
CD22	Sialic Acid-Binding Ig-Like Lectin
CD23	Fc Epsilon Receptor II
CD24	Small Cell Lung Carcinoma Cluster 4 Antigen
CD25	Interleukin 2 Receptor Subunit Alpha
CD26	Dipeptidyl Peptidase 4
CD27	Tumor Necrosis Factor Receptor Superfamily Member 7
CD28	T-Cell-Specific Surface Glycoprotein
CD29	Integrin Subunit Beta 1
CD30	Tumor Necrosis Factor Receptor Superfamily Member 8
CD31	Platelet And Endothelial Cell Adhesion Molecule 1
CD32	Fc Gamma Receptor IIa

CD134	Tumor Necrosis Factor Receptor Superfamily Member 4
CD135	Fms Related Receptor Tyrosine Kinase 3
CD137	Tumor Necrosis Factor Receptor Superfamily Member 9
CD137 ligand	Tumor Necrosis Factor Receptor Superfamily Member 9 Ligand
CD138	Syndecan 1
CD140a	Platelet Derived Growth Factor Receptor Alpha
CD140b	Platelet Derived Growth Factor Receptor Beta
CD141	Thrombomodulin
CD142	Coagulation Factor III, Tissue Factor
CD144	Cadherin 5
CD146	Melanoma Cell Adhesion Molecule
CD147	Basigin
CD150	Signaling Lymphocytic Activation Molecule Family Member 1
CD151	Platelet-Endothelial Tetraspan Antigen 3
CD152	Cytotoxic T-Lymphocyte Associated Protein 4
CD153	Tumor Necrosis Factor Ligand Superfamily Member 8
CD154	Tumor Necrosis Factor Ligand Superfamily Member 5
CD158a	Killer Cell Immunoglobulin Like Receptor, Two Ig Domains And Long Cytoplasmic Tail 1
CD158b	Killer Cell Immunoglobulin Like Receptor, Two Ig Domains And Long Cytoplasmic Tail 3
CD161	Killer Cell Lectin Like Receptor B1

CD33	Sialic Acid-Binding Ig-Like Lectin 3
CD34	Hematopoietic Progenitor Cell Antigen CD34
CD35	Complement C3b/C4b Receptor 1 (Knops Blood Group)
CD36	Platelet Glycoprotein 4
CD37	Tetraspanin-26
CD38	ADP-Ribosyl Cyclase 1
CD39	Ectonucleoside Triphosphate Diphosphohydrolase 1
CD40	Tumor Necrosis Factor Receptor Superfamily Member 5
CD41a	Selectin P
CD41b	Integrin Subunit Alpha 2b
CD42a	Glycoprotein IX Platelet
CD42b	Glycoprotein Ib Platelet Subunit Alpha
CD43	Sialophorin
CD44	Hematopoietic Cell E- And L-Selectin Ligand
CD45	Protein Tyrosine Phosphatase Receptor Type C
CD45RA	Protein Tyrosine Phosphatase Receptor Type C (1 Exon)
CD45RB	Protein Tyrosine Phosphatase Receptor Type C (1 Exon)
CD45RO	Protein Tyrosine Phosphatase Receptor Type C (0 Exons)
CD46	Trophoblast-Lymphocyte Cross-Reactive Antigen
CD47	Integrin Associated Protein
CD48	Signaling Lymphocytic Activation Molecule 2
CD49a	Integrin Subunit Alpha 1
CD49b	Integrin Subunit Alpha 2
CD49c	Integrin Subunit Alpha 3
CD49d	Integrin Subunit Alpha 4

CD162	Selectin P Ligand
CD163	Scavenger Receptor Cysteine-Rich Type 1 Protein M130
CD164	Multi-Glycosylated Core Protein 24
CD165	AD2
CD166	Activated Leukocyte Cell Adhesion Molecule
CD171	L1 Cell Adhesion Molecule
CD172b	Signal Regulatory Protein Beta 1
CD177	Polycythemia Rubra Vera Protein 1
CD178	Fas Ligand
CD180	Radioprotective 105 KDa Protein
CD181	C-X-C Motif Chemokine Receptor 1
CD183	C-X-C Motif Chemokine Receptor 3
CD184	C-X-C Motif Chemokine Receptor 4
CD193	C-C Motif Chemokine Receptor 3
CD195	C-C Motif Chemokine Receptor 5
CD196	C-C Motif Chemokine Receptor 6
CD197	C-C Motif Chemokine Receptor 7
CD200	OX-2
CD201	Protein C Receptor
CD205	Lymphocyte Antigen 75
CD206	Mannose Receptor C-Type 1
CD209	Dendritic Cell-Specific ICAM-3-Grabbing Non-Integrin 1
CD210	Interleukin 10 Receptor Subunit Alpha
CD212	Interleukin 12 Receptor Subunit Beta 1
CD220	Insulin Receptor

CD49e	Integrin Subunit Alpha 5
CD49f	Integrin Subunit Alpha 6
CD4v4	CD4v4
CD50	Intercellular Adhesion Molecule 3
CD51/61	Integrin Subunit Alpha V / Beta 3
CD53	Tetraspanin-25
CD54	Intercellular Adhesion Molecule 1
CD55	Complement Decay-Accelerating Factor
CD56	Neural Cell Adhesion Molecule 1
CD57	Beta-1,3-Glucuronyltransferase 1
CD58	Lymphocyte Function-Associated Antigen 3
CD59	Membrane Attack Complex Inhibition Factor
CD6	T-Cell Differentiation Antigen CD6
CD61	Integrin Subunit Beta 3
CD62e	Selectin E
CD62l	Selectin L
CD62p	Selectin P
CD63	Tetraspanin-30
CD64	Fc Gamma Receptor Ia
CD66 (a,c,d,e)	Carcinoembryonic Antigen-Related Cell Adhesion Molecules
CD66b	Carcinoembryonic Antigen-Related Cell Adhesion Molecule 8
CD66f	Pregnancy Specific Beta-1-Glycoprotein
CD69	C-Type Lectin Domain Family 2, Member C
CD70	Tumor Necrosis Factor Ligand Superfamily Member 7

CD221	Insulin Like Growth Factor 1 Receptor
CD226	DNAX Accessory Molecule-1
CD227	Mucin 1, Cell Surface Associated
CD229	Lymphocyte Antigen 9
CD231	Tetraspanin 7
CD235a	Glycophorin-A
CD243	ATP Binding Cassette Subfamily B Member 1
CD244	Natural Killer Cell Receptor 2B4
CD255	Receptor Interacting Serine/Threonine Kinase 1
CD267	Tumor Necrosis Factor Receptor Superfamily Member 13B
CD268	Tumor Necrosis Factor Receptor Superfamily Member 13C
CD271	Nerve Growth Factor Receptor
CD273	Programmed Cell Death 1 Ligand 2
CD274	Programmed Cell Death 1 Ligand 1
CD275	Inducible T Cell Costimulator Ligand
CD278	Inducible T Cell Costimulator
CD279	Programmed Cell Death 1
CD282	Toll Like Receptor 2
CD294	Prostaglandin D2 Receptor 2
CD305	Leukocyte Associated Immunoglobulin Like Receptor 1
CD309	Kinase Insert Domain Receptor
CD314	Killer Cell Lectin Like Receptor K1
CD321	F11 Receptor
CD326	Epithelial Cell Adhesion Molecule

CD71	Transferrin Receptor
CD72	B-Cell Differentiation Antigen CD72
CD73	5'-Nucleotidase Ecto
CD74	Invariant Polypeptide Of Major Histocompatibility Complex, Class II Antigen-Associated
CD75	ST6 Beta-Galactoside Alpha-2,6-Sialyltransferase 1
CD77	Alpha 1,4-Galactosyltransferase (P Blood Group)
CD79b	B-Cell Antigen Receptor Complex-Associated Protein Beta Chain
CD80	CD28 Antigen Ligand 1, B7-1 Antigen
CD81	Tetraspanin-28
CD83	B-Cell Activation Protein
CD84	Signaling Lymphocytic Activation Molecule 5
CD85	Leukocyte Immunoglobulin Like Receptor B1
CD86	T-Lymphocyte Activation Antigen CD86
CD87	Plasminogen Activator, Urokinase Receptor
CD88	Complement C5a Receptor 1
CD89	Fc Alpha Receptor
CD90	Thy-1 Cell Surface Antigen
CD91	Low Density Lipoprotein Receptor-Related Protein 1
CD94	Killer Cell Lectin Like Receptor D1
CD95	Fas Cell Surface Death Receptor
CD97	Adhesion G Protein-Coupled Receptor E5
CD98	Solute Carrier Family 3 Member 2

CD329	Sialic Acid Binding Ig Like Lectin 9
CD335	Natural Cytotoxicity Triggering Receptor 1
CD336	Natural Cytotoxicity Triggering Receptor 2
CD337	Natural Cytotoxicity Triggering Receptor 3
CD338	ATP Binding Cassette Subfamily G Member 2 (Junior Blood Group)
CD340	Erb-B2 Receptor Tyrosine Kinase 2
CDw327	Sialic Acid Binding Ig Like Lectin 6
CDw328	Sialic Acid Binding Ig Like Lectin 7
CDw93	Complement Component 1 Q Subcomponent Receptor 1
CLA	Scavenger Receptor Class B
CLIP	CAP-Gly Domain Containing Linker Protein 1
CMRF-44	CMRF-44
CMRF-56	CMRF-56
Disialoganglioside GD2	Disialoganglioside Beta-1,4-N-Acetyl-Galactosaminyltransferase 1
EGF-R	Epidermal Growth Factor Receptor
fMLP-R	fMet-Leu-Phe Receptor 1
HLA-A,B,C	Human Leukocyte Antigen A,B,C
HLA-A2	Human Leukocyte Antigen A2
HLA-DQ	Human Leukocyte Antigen DQ
HLA-DR	Human Leukocyte Antigen DR
HLA-DR,DP,DQ	Human Leukocyte Antigen DR, CP, DQ
HPC	Syntaxin

CD99	MIC2
CD99R	MIC2 (Isoform)
CD100	Semaphorin 4D
CD102	Intercellular Adhesion Molecule 2
CD103	Integrin Subunit Alpha E
CD104	Integrin Subunit Beta 4
CD105	Endoglin
CD106	Vascular Cell Adhesion Molecule 1
CD107a	Lysosomal Associated Membrane Protein 1
CD107a	Lysosomal Associated Membrane Protein 1
CD107b	Lysosomal Associated Membrane Protein 2
CD108	Semaphorin 7A
CD109	C3 And PZP-Like Alpha-2-Macroglobulin Domain-Containing Protein

Integrin B7	Integrin Beta 7
Invariant NK T	Invariant Natural Killer T Cell Antigen
MIC A/B	MHC Class I Polypeptide-Related Sequence A/ B
NKB1	Killer Cell Immunoglobulin Like Receptor, Three Ig Domains And Long Cytoplasmic Tail 1
SSEA-1	Stage-Specific Embryonic Antigen 1
SSEA-3	Stage-Specific Embryonic Antigen 3
SSEA-4	Stage-Specific Embryonic Antigen 4
TRA-1-60	T Cell Receptor Alpha Locus 1-60
TRA-1-81	T Cell Receptor Alpha Locus 1-81
V β 23	T Cell Receptor Variable Beta Chain 23
V β 8	T Cell Receptor Variable Beta Chain 24
ydTCR	T Cell Receptor Gamma Delta Chain

Table A1.2. List of definitions for the RT² Profiler PCR Array

Gene	Definition	Gene	Definition
ACTA2	Actin, alpha 2, smooth muscle, aorta	ITGA2	Integrin, alpha 2 (CD49B, alpha 2 subunit of VLA-2 receptor)
ACTC1	Actin, alpha, cardiac muscle 1	ITGA3	Integrin, alpha 3 (antigen CD49C, alpha 3 subunit of VLA-3 receptor)
ANGPT1	Angiopoietin 1	ITGA4	Integrin, alpha 4 (antigen CD49D, alpha 4 subunit of VLA-4 receptor)
CCL2	Chemokine (C-C motif) ligand 2	ITGA5	Integrin, alpha 5 (fibronectin receptor, alpha polypeptide)
CCL7	Chemokine (C-C motif) ligand 7	ITGA6	Integrin, alpha 6
CD40LG	CD40 ligand	ITGAV	Integrin, alpha V (vitronectin receptor, alpha polypeptide, antigen CD51)
CDH1	Cadherin 1, type 1, E-cadherin (epithelial)	ITGB1	Integrin, beta 1 (fibronectin receptor, beta polypeptide, antigen CD29 includes MDF2, MSK12)
COL14A1	Collagen, type XIV, alpha 1	ITGB3	Integrin, beta 3 (platelet glycoprotein IIIa, antigen CD61)
COL1A1	Collagen, type I, alpha 1	ITGB5	Integrin, beta 5
COL1A2	Collagen, type I, alpha 2	ITGB6	Integrin, beta 6
COL3A1	Collagen, type III, alpha 1	MAPK1	Mitogen-activated protein kinase 1
COL4A1	Collagen, type IV, alpha 1	MAPK3	MAPK3 Mitogen-activated protein kinase 3
COL4A3	Collagen, type IV, alpha 3 (Goodpasture antigen)	MIF	MIF Macrophage migration inhibitory factor (glycosylation-inhibiting factor)
COL5A1	Collagen, type V, alpha 1	MMP1	Matrix metalloproteinase 1 (interstitial collagenase)
COL5A2	Collagen, type V, alpha 2	MMP2	Matrix metalloproteinase 2 (gelatinase A, 72kDa gelatinase, 72kDa type IV collagenase)
COL5A3	Collagen, type V, alpha 3	MMP7	Matrix metalloproteinase 7 (matrilysin, uterine)
CSF2	Colony stimulating factor 2 (granulocyte-macrophage)	MMP9	Matrix metalloproteinase 9 (gelatinase B, 92kDa gelatinase, 92kDa type IV collagenase)

CSF3	Colony stimulating factor 3 (granulocyte)	PDGFA	Platelet-derived growth factor alpha polypeptide
CTGF	Connective tissue growth factor	PLAT	Plasminogen activator, tissue
CTNNB1	Catenin (cadherin-associated protein), beta 1, 88kDa	PLAU	Plasminogen activator, urokinase
CTSG	Cathepsin G	PLAUR	Plasminogen activator, urokinase receptor
CTSK	Cathepsin K	PLG	Plasminogen
CTSL2	Cathepsin L2	PTEN	Phosphatase and tensin homolog
CXCL1	Chemokine (C-X-C motif) ligand 1 (melanoma growth stimulating activity, alpha)	PTGS2	Prostaglandin-endoperoxide synthase 2 (prostaglandin G/H synthase and cyclooxygenase)
CXCL11	Chemokine (C-X-C motif) ligand 11	RAC1	Ras-related C3 botulinum toxin substrate 1 (rho family, small GTP binding protein Rac1)
CXCL2	Chemokine (C-X-C motif) ligand 2	RHOA	Ras homolog gene family, member A
CXCL5	Chemokine (C-X-C motif) ligand 5	SERPINE1	Serpin peptidase inhibitor, clade E (nexin, plasminogen activator inhibitor type 1), member 1
EGF	Epidermal growth factor	STAT3	Signal transducer and activator of transcription 3 (acute-phase response factor)
EGFR	Epidermal growth factor receptor	TAGLN	Transgelin
F13A1	Coagulation factor XIII, A1 polypeptide	TGFA	Transforming growth factor, alpha
F3	Coagulation factor III (thromboplastin, tissue factor)	TGFB1	Transforming growth factor, beta 1
FGA	Fibrinogen alpha chain	TGFBR3	Transforming growth factor, beta receptor III
FGF10	Fibroblast growth factor 10	TIMP1	TIMP metalloproteinase inhibitor 1
FGF2	Fibroblast growth factor 2 (basic)	TNF	Tumor necrosis factor
FGF7	Fibroblast growth factor 7	VEGFA	Vascular endothelial growth factor A
HBEGF	Heparin-binding EGF-like growth factor	VTN	Vitronectin

HGF	Hepatocyte growth factor (hepatopoietin A; scatter factor)		WNT1 inducible signaling pathway protein 1
IFNG	Interferon, gamma	WISP1	Wingless-type MMTV integration site family, member 5A
IGF1	Insulin-like growth factor 1 (somatomedin C)	WNT5A	
IL10	Interleukin 10	ACTB	Actin, beta
IL1B	Interleukin 1, beta	B2M	Beta-2-microglobulin
IL2	Interleukin 2	GAPDH	Glyceraldehyde-3-phosphate dehydrogenase
IL4	Interleukin 4	HPRT1	Hypoxanthine phosphoribosyltransferase 1
IL6	Interleukin 6 (interferon, beta 2)	RPLP0	Ribosomal protein, large, P0
IL6ST	Interleukin 6 signal transducer (gp130, oncostatin M receptor)	HGDC	Human Genomic DNA Contamination
ITGA1	Integrin, alpha 1	RTC	Reverse Transcription Control
		PPC	Positive PCR Control

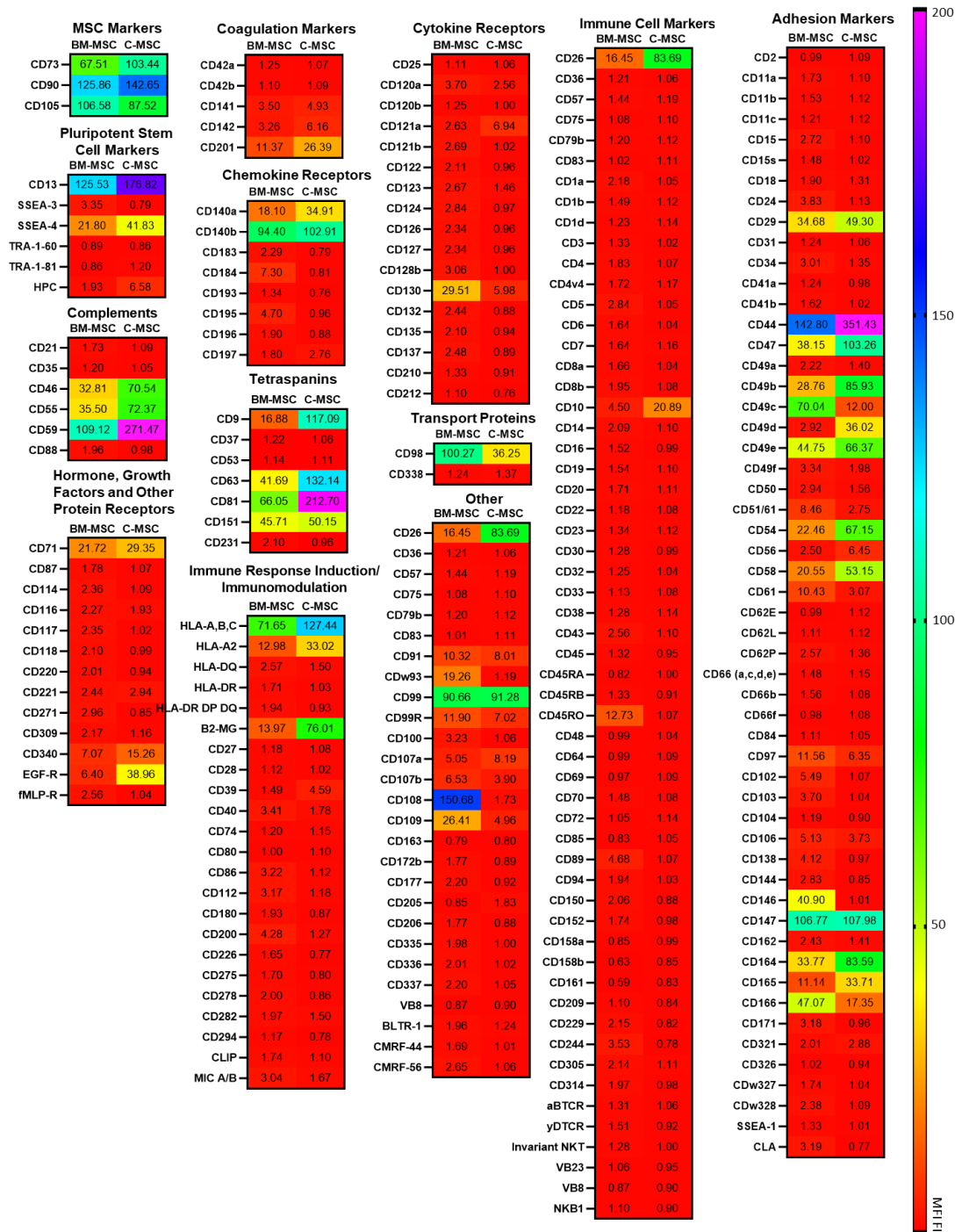


Figure A1.1. Heat maps showing mean Median Fluorescence Intensity Fold Increase (MFI) for different markers on CMSCs compared to BM-MSCs (N = 5). Each column represents readings from BM-MSCs (left) and CMSCs (right). The BD Lyoplate™ was utilised. Colours are representative of percentage in the scale on the left. Cells were categorised based on previous grouping by Baer *et al.*, (2012) [154]. For mAbclones see Section 2.1.2.ii. and for antigen abbreviation definitions see the Appendix (Table A1.1).